Lucerne University of
Applied Sciences and Arts
HOCHSCHULE
LUZERN
Technik & Architektur

Analysis of Existing Rockfall Embankments of Switzerland (AERES)

Commissioned by the Federal Office for the Environment (FOEN)

July 2017

Imprint

Commissioned by
Federal Office for the Environment (FOEN), Hazard Prevention Division, CH-3003 Bern.
The FOEN is an agency of the Federal Department of the Environment, Transport, Energy and Communications (DETEC).

Contractors
Lucerne University of Applied Sciences and Arts, CH-6048 Horw
Irstea, F-38402 Saint Martin d'Hères

Authors
Bernd Kister
Stéphane Lambert

FOEN support
Bernard Loup, Hazard Prevention Division
Arthur Sandri, Hazard Prevention Division

Notes
The AERES report consists of three parts:
- Part A: State of knowledge
- Part B: Analysis of the collected data and comparison with up-to-date knowledge
- Part C: Small-scale experiments

Suggested form of citation for the complete report
Kister B., Lambert S. 2017: Analysis of Existing Rockfall Embankments of Switzerland (AERES). Federal Office for the Environment, Bern, 166 p.

Lucerne University of
Applied Sciences and Arts

HOCHSCHULE
LUZERN

Technik & Architektur

Analysis of Existing Rockfall Embankments of Switzerland (AERES)

Part A: State of Knowledge

Stéphane LAMBERT[1] and Bernd KISTER[2]

[1] Irstea, 2 rue de la papeterie, 38402 Saint Martin d'Hères cedex, France, + 33 4 76 76 27 94, stephane.lambert@irtsea.fr

[2] Lucerne University of Applied Sciences and Arts, Technikumstrasse 21, CH – 6048 Horw, Switzerland. Current position: kister - geotechnical engineering & research, Neckarsteinacher Str. 4 B, D – Neckargemünd, +49 6223 71363, kister-ger@t-online.de

Commissioned by the Federal Office for the Environment (FOEN)

July 2017

Imprint

Commissioned by
Federal Office for the Environment (FOEN), Hazard Prevention Division, CH-3003 Bern.
The FOEN is an agency of the Federal Department of the Environment, Transport, Energy and Communications (DETEC).

Contractors
Lucerne University of Applied Sciences and Arts, CH-6048 Horw
Irstea, F-38402 Saint Martin d'Hères

Authors
Bernd Kister
Stéphane Lambert

FOEN support
Bernard Loup, Hazard Prevention Division
Arthur Sandri, Hazard Prevention Division

Notes
The AERES report consists of three parts:
- Part A: State of knowledge
- Part B: Analysis of the collected data and comparison with up-to-date knowledge
- Part C: Small-scale experiments

This study/report was prepared under contract to the Federal Office for the Environment (FOEN). The contractor bears sole responsibility for the content.

Suggested form of citation for Part A
Lambert S., Kister B. 2017: Analysis of Existing Rockfall Embankments of Switzerland (AERES); Part A: State of Knowledge. Federal Office for the Environment, Bern, 55 p.

Foreword

The aim of this document is to provide the reader with an up-dated and exhaustive vision of the worldwide knowledge concerning the design of rockfall protection embankments (RPE). As a definition, any structure in elevation of at least 2 m with respect to the ground, mostly made of granular materials (soil, gravel, …) and built with the aim of intercepting falling blocks are considered as RPE, whatever their cross sectional shape.

This state of the knowledge is based on different types of publicly available documents:

- National guidelines, recommendations and standards;
- Books;
- Journal articles, presenting a new approach, theoretically or applied to a case study;
- Conference communications, either presenting a new design approach or presenting a case study.

The document is intended for anyone with an interest in the design of RPE, whatever its level of expertise (contracting authority, owner, designer…). It is organized accordingly: the successive sections go from the basics to a discussion on the limitations of the available methods. The different design methods and previous research works are mentioned, making frequent references to existing documents for further reading.

Content

1. General context

As a definition, any structure in elevation of at least 2m with respect to the ground, mostly made of granular materials (soil, gravel, …) and built with the aim of intercepting falling blocks are considered as rockfall protection embankment[1] (RPE), whatever their cross sectional shape[2].

The very first references to RPE in the literature date back from the end of the 80's, even though the very first structures were built more than 50 years ago. Originally, RPE were mainly made from compacted natural soil and were designed for rather low-impact-energy events. Most often, their cross-sectional shape was trapezoidal. Sometimes, the uphill face was steepened for example with rockery or a concrete wall, gabions or prefabricated concrete components with the aim of increasing its steepness (Paronuzzi et al., 1989). At the end of the 1980s, ground-reinforced structures were developed to reach higher protection energies, higher than 100 MJ (Corté et al., 1989; Mathieu and Maréchal, 1989; Morino and Grassi, 1990).

Figure 1 Different types of RPEs (for authors, see Lambert and Bourrier, 2013)

[1] Also defined as rockfall control embankment in Austria (ONR, 2013)
[2] It thus also includes bunds and walls mentioned in CCC (2013) for example.

The variety of these structures has considerably increased over the last two decades, employing different types of construction materials (Figure 1). A descriptive comparison of some of these structures is given in Peila (2011). Many of these structures are presented in technical publications (Mathieu and Marchal, 1989; Morino and Grasso, 1990; Lazzari et al., 1996; Gerbert and Hespel, 1999; Mannsbart, 2002; Cargnel and Nössing, 2004; Coulon and Bruhier, 2006; Jaecklin, 2006; Rimoldi et al., 2008; Interreg III A, 2008; Brunet et al., 2009; Simmons et al., 2009; Hara et al., 2009; Lorentz et al., 2010; Broccolato et al., 2010; Grimod and Segor, 2014; Frenez et al., 2014…).

Table 1 lists the possible materials for the structure's uphill face, core and downhill face. Various combinations can be found between these three lists, some extremely rare and others common worldwide or found only in certain countries. For instance, in France interconnected soil-filled recycled tires are used as face material only or as both core and face materials. On the contrary, earth-dams with a rockery front face are frequently used in various countries (France, Switzerland…). Most often, the RPE is associated to a ditch, aiming in particular at collecting the blocks and fallen material volumes.

Most of the developments over the last decades concern soil-reinforced structures, using horizontal inclusions such as geosynthetics with the aim of increasing the RPE capacity and increasing the steepness of its uphill face while substantially reducing the volume of the structure as well as its footprint and visual impact.

Table 1 . Possible constitutive materials of rockfall protection embankments.

Uphill face	Core	Downhill face
Interconnected tires	Soil reinforced with GSY[1]	Gabion[2]
GSY[1]	Soil reinforced with interconnected tires	Soil
Metallic wire mesh	Soil reinforced with metallic wire mesh	GSY[1]
Cast iron panel	Soil reinforced with wood and steel	Tires
Gabion[2]	Soil bag[3]	Timber
Soil bag[3]	Gabion[2]	Rockery/rip-rap
Soil	Compacted soil	
Timber		
Concrete		
Rockery/rip-rap		

1. Geosynthetics, such as geotextiles or geogrids
2. Woven wire mesh (hexagonal) or welded wire mesh cages filled with either coarse or fine granular materials.
3. Typically a sand-filled geotextile sock.

RPE are appropriate when medium- to very-high-kinetic-energy events are expected, from a few hundred kilojoules to tens of megajoules. They are preferred over net fences when the design impact is higher than 5000 kJ (Descoeudres, 1997). The other declared advantages are low maintenance costs and reduced visual impact (Brunet et al., 2009). Nevertheless, they are not appropriate on steeper slopes and their construction generally requires extensive space and accessibility for heavy vehicles. For large structures, designed for high-kinetic-energy blocks, the ditch is dug in the slope uphill of the structure and the cut materials are generally used to erect the embankment.

In some cases, RPE are not intended to control the trajectory of medium to large kinetic energy single blocks, but to stop and contain frequent and limited kinetic energy rockfall or rockslides. In such cases, the accumulation of debris in the ditch dictates the structure design and requires planning debris removal when the maximum permissible volume is reached. Also, some embankments are designed to divert rockfall (Calvino et al., 2001; Interreg III A, 2006). These structures may either be dam-like or stem-like.
These cases are rather rare and not detailed in the literature.

The design of RPE addresses different issues, some being specific while others are more classical in the field of geotechnical engineering. These later are:

- Global stability of the slope: the slope stability may be altered as a result of an excessive RPE mass, or of the cut in the talus;
- Internal stability of the RPE, under static and seismic loadings;
- Interaction of the RPE with natural flows (surface run-off, torrent, debris flow, water source, snow avalanche), that may accumulate in the ditch, with possible detrimental influence on the RPE stability. (e. g., Gondo, Valais, in Jaecklin, 2006).

On the contrary, the design with respect to the block's trajectory and the structure's stability under impact are highly specific. These two facets of RPE design are referred to as the functional and the structural design, respectively. These two facets are developed in detail in the following, considering that classical facets are developed elsewhere.

2. Functional design

2.1. Introduction

As for any type of passive countermeasure against rockfall aiming at controlling the block trajectory, the functional design of RPE is based on trajectory analysis, which can provide a statistical distribution for the blocks passing height[3] and velocity in the vicinity of the RPE.

The ability of the RPE to act as a barrier against rockfall depends on its dimensions. It also depends on the ditch width: the larger the ditch the smaller the impact energy and passing height of the blocks reaching the embankment. As a consequence, there basically exist two

[3] Also refered to as jump height, flying height or bounce height in the literatue.

strategies concerning the design approach for the ditch-RPE system: (1) a catchment ditch made of loose material intended to dissipate the block's energy before it reaches the embankment (Peckover and Kerr, 1977; Hoek, 2007; Maegawa et al., 2011) or (2) a ditch made of a dust road allowing the circulation of heavy vehicles for fallen block removal, particularly in areas where frequent or large-volume events are expected. In the former strategy, the embankment, which represents the completion of the dissipative ditch, has a limited importance on the system efficiency as the ditch dissipates most of the incident kinetic block energy, with consequences on the impact conditions on the structure. Design charts have been proposed for the design of such ditch-RPE systems. For example, Figure 2 gives the values of ditch width (L) and ditch depth (D) with respect to the RPE crest for pairs of values of talus slope inclination (α) and block vertical travelling distance (H). In this example, the ditch width may be twice the height of the embankment, which may be less than 2 meters in height. For example, in case of a 30 m. in height slope with a 60° inclination, the ditch should be 4 m in width and 2 m in depth, approximately. This strategy will not be detailed in the following. Instead of that focus will be on large dimension structures exposed to severe loadings (later strategy).

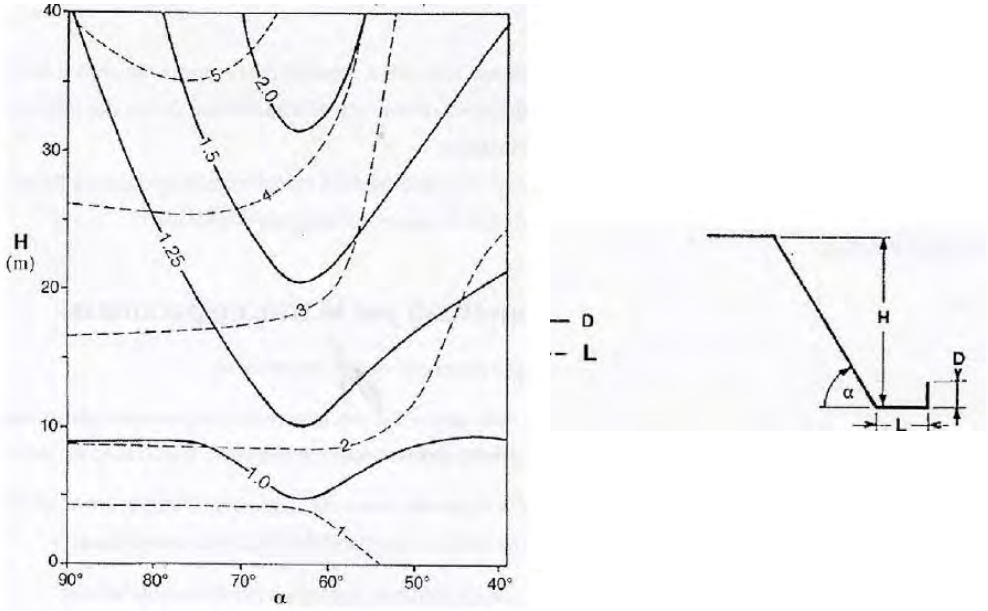

Figure 2. Example of design chart for catching ditches (Whiteside, 1986)

The functional design of a RPE aims at defining the structure geometry, which allows intercepting the blocks. This design is based on trajectory simulation data and aims at reducing the percentage of passing blocks below a targeted value. In general, this design is conducted after the RPE is positioned along the slope, after considering topographical or land-use constraints. Occasionally, the position of the embankment along the slope is defined with the aim of minimizing the block passing height and kinetic energy in the RPE vicinity, with positive consequences on the RPE dimensions.

The scientific and technical literature on the efficiency of RPE in controlling the block's trajectory is rather reduced. Some references address the efficiency of existing embankments in stopping the blocks, but with minimum details on the functional design method and criteria (e.g. Masuya et al., 2009, Agliardi and Crosta, 2003; Agliardi et al., 2009). Besides, some recommendations have been proposed in France (Calvino et al., 2001), Italy (UNI, 2012) and Austria (ONR, 2013). In such a context, the state of knowledge is presented considering successively the two main parameters governing the RPE ability in controlling the block trajectory, namely the structure height (section 2.2) and the uphill face inclination (section 2.3). Then, limitations of the proposed recommendations are discussed.

2.2. Structure height

The structure height is here defined as the distance along the vertical axis from the toe of the uphill face to the crest of the RPE (Fig. 3 a). This definition is consistent with most of the references, even if in some cases the height is referred to the direction perpendicular to the slope, to the structure face or to the vertical distance to the natural ground (resp. H', H'' and H''' in Figure 3 b). The definition for H' results from the fact, that the block passing height, provided by some trajectory simulation tools, is measured along the perpendicular to the soil surface.

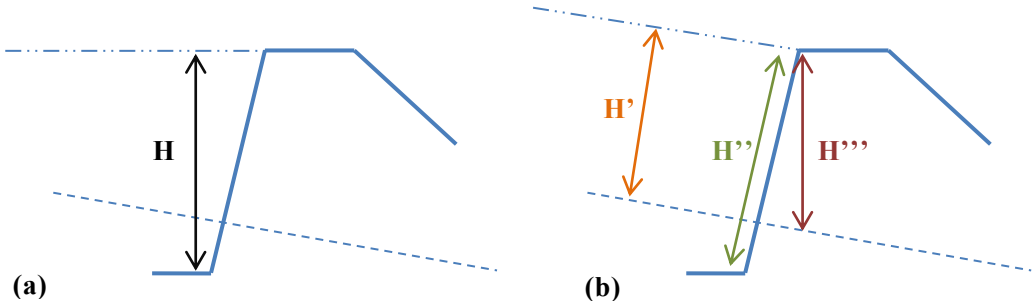

Figure 3 Structure height definitions: (a) as considered in this report and (b) other existing ones.

The RPE height should be determined based on the reference block's passing height increased by a freeboard.

In the majority of cases the reference block's passing height is defined based on statistics associated to the trajectory simulation results. In Italy and Austria, it is recommended to consider the 95% percentile of the passing height distribution (UNI, 2012; ONR, 2013). In addition, the Austrian standard considers the Eurocode principles and considers the block passing height multiplied by a safety coefficient varying from 1.05 to 1.3 depending on a consequence class, i.e. related to both the effect on the RPE and the elements at risks nature (Mölk and Hofmann, 2013).

The freeboard aims at avoiding impacts close to the crest, which can be highly detrimental to the structure efficiency. Indeed, an impact close to the crest leads to higher structure deformation, favouring the structure over topping or rolling over (Mölk and Hofmann, 2011; Breugnot et al., 2015). Also, blocks having a high rotational energy may roll over the RPE in case of an impact close to the crest (Kister, 2015).

Table 2 Recommendations for the minimum freeboard to consider, in different countries.

Country (réf.)	Recommended freeboard (min)	Context
France (Calvino et al., 2001)	Block radius*1	Radius of the largest expected block
Italy (UNI, 2012)	Block radius*1	
Austria[i] (ONR, 2013)	Block radius*2	Unreinforced RPE with rockery at the uphill face and an inclination of at least 50°
	Block radius*3	Reinforced RPE with a uphill face inclination less than 70°
	Block radius*2	Reinforced RPE with a uphill face inclination higher than 70°
	Block radius*4	Other embankments (made of compacted soil only)

i: see the paragraph below for the definition of the freeboard according to this standard

The recommended freeboard is generally expressed as a multiple of the block size. As shown in Table 2 it ranges from 1 to 4 times the block radius depending on the case. The freeboard considered by the Austrian standard is measured along the face of the RPE (in accordance with H'' in Figure 3), and not along the vertical axis. In addition, the Austrian standard considers the distance between the embankment crest and the top point of the block, and not its mass centre. Other references are not explicit on these points.

2.3. Uphill face inclination

In order to reduce the risk of rolling over, the steepness of the uphill face of the RPE should be increased. Rolling over may occur in case of a block rolling before reaching the structure and with a high rotational velocity or as a result of an impact close to the RPE crest, by a block with a high rotational velocity.

In France, a steepness of at least 65° is recommended (Calvino et al., 2001). Steeper inclinations are sometimes mentioned in specific studies (Simmons et al., 2009). The Austrian standard suggests a steep face and recommends freeboard depending on the face steepness.

2.4. Comments on these recommendations

Table 2 reveals that the required structure height is different depending on the text considered, for given block radius and passing height. The freeboard along the vertical axis based on the Austrian standard is at least 2.5 times higher than that when considering other recommendations, with a maximum up to 4 times. This will lead to huge differences in

structure height and volumes, in particular when dealing with large blocks, and will probably make some projects unfeasible for costs, available place and natural slope stability reasons.

These recommendations were proposed based on empirical knowledge, except for the Austrian ones. In this latter case, small scale experiments were conducted in the lab (Hofmann and Mölk, 2012), considering RPE varying in size and construction type. Globally, there are only a few research works addressing the influence of the geometrical characteristics of the RPE and of the block kinematics prior the impact on the functional efficiency of RPE. Existing ones are rather recent (Plassiard and Donzé, 2009; Toe et al., 2013; Kister, 2015) As a consequence, neither the inclination of the block incident trajectory nor its rotational velocity is considered for the functional design (the Austrian standard introduces this parameter for structural design purpose only, without any indication about the statistic estimator to consider).

In terms of incident trajectory, evidences from the field showed that a block with an upward incident trajectory could over top a vertical face RPE after an impact more than one block radius from its crest (Figure 4). In this case, it was favoured by the large deformation of the RPE facing as a result of the impact.

Figure 4 This 3-m-tall gabion embankment was cleared by a block after an impact more than 1 m below its crest, by a block having an upward incident trajectory (Ste Marie de Cuines (73), France).(S. Lambert)

The rotational kinetic energy is often neglected because it is generally less than 10 – 15% of the total block energy (Chau, et al., 2002; Bourrier and Hungr, 2011). Numerical simulations have suggested that both the block rotational velocity and trajectory inclination have a strong influence on the ability of the block to roll over the RPE while considering a freeboard as large as 0.8 times the block diameter (Plassiard and Donzé, 2009). The influence of the rotational energy has been confirmed by small-scale tests (Kister, 2015; Figure 5), even for low rotational energies. This is even more pronounced in case of low uphill steepness face values.

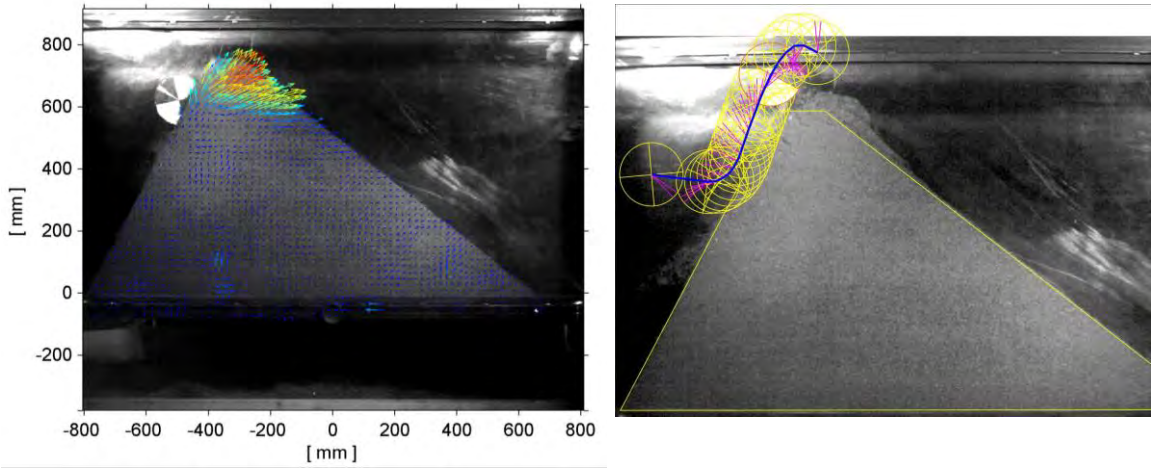

Figure 5 Quasi-2D small scale experiments showing high displacement fields at the crest (left) and over topping of structure by the block resulting from a high rotational energy (right) (Kister et al., 2014).

Thanks to real scale field tests Clerici et al. (2013) showed that the movement of a bloc rolling towards the embankment crest could be significant. The tested embankment was 3 m. in height, with a crest thickness of 1.7 m. The structure was reinforced with geosynthetics and exhibited an uphill face angle of 71°. The embankment was impacted by a sphere (diameter 1.5 m) rolling down the natural slope, with velocities between 10 m/s and 15.75 m/s. The upward movement of the sphere along the embankment face during the impact was up to 1.5 m.

While trajectory simulation results are of paramount importance for the design of RPE, no specific recommendations are proposed for a proper use of these tools.

Some recommendations suggest considering the 95% percentile of the block passing height for defining the structure height. This suggestion leads to the following comments:

- This percentile is less dependent on the simulation number than the 99% percentile or the maximum. Nevertheless, there is no requirement in terms of minimum number of block reaching the RPE required for obtaining a reliable 95% percentile of the passing height, while this value is sensitive to the number if less than 1000, at least.
- A distinction between 2D and 3D tools in terms of passing height statistics, should be made, in particular because, the latter case requires a higher number of simulation and the definition of the way to establish statistics depending on the digital model elevation resolution (Lambert et al., 2013).
- Except for the Austrian recommendations, there is no indication on the block point to consider for determining the block passing height, and consequently the RPE height. This may lead to confusion, as trajectory simulation tools either consider the block lower point, or the block mass centre.

None of the recommendations explicitly requires conducting the simulation in the presence of the embankment, i.e. accounting for the modified slope profile and for the ditch digging in particular. These significant changes strongly influence the block trajectory and should be accounted for.

In a similar mode, none of the recommendations suggest conducting simulations for estimating the effective residual risk on the new profile to assess the projected structure's efficiency in stopping the blocks. The residual risk depends on the occurrence of quite rare to extremely rare events resulting in embankment overtopping. For instance, if the 95% percentile is considered as design criteria, such cases may result from an unexpected reaction of the RPE to impact by a block within the 0-95% range, outliers in the 95-100% range or events related to scenarios not considered for the design (in terms of return period for instance). These critical cases, whose identification globally requires a large number of trajectory simulations, are characterized by large passing heights, high energies or high rotational velocities in the vicinity of the embankment.

Besides, the correct simulation of these critical and rare trajectory cases faces the limitations of the trajectory analysis tools, in particular in the embankment vicinity. In the embankment vicinity, the impact orientation is quasi-normal to the impacted surface, and coupling between the translational velocity and the rotational velocity may dramatically change the reflected block trajectory. This context thus differs from more classical trajectory analysis contexts for which parameters were calibrated (Lambert et al., 2013). The coupling between the translational velocity and the rotational velocity as well as the shape of the block are generally roughly accounted for in these models event though they seem to play an important role in the block's trajectory (Chau et al., 2002; Usiro et al., 2006). Toe et al. (2013) conducted small scale experimental tests with a sphere, a cube and a parallelepiped that were dropped on a slope terminated by an embankment. The block trajectory was modelled using two techniques (probabilistic and discrete element method). It was shown that approximately 40% of the spheres had been able to surmount the embankment, while no cube and no parallelepiped had passed the embankment in the tests (Figure 6).

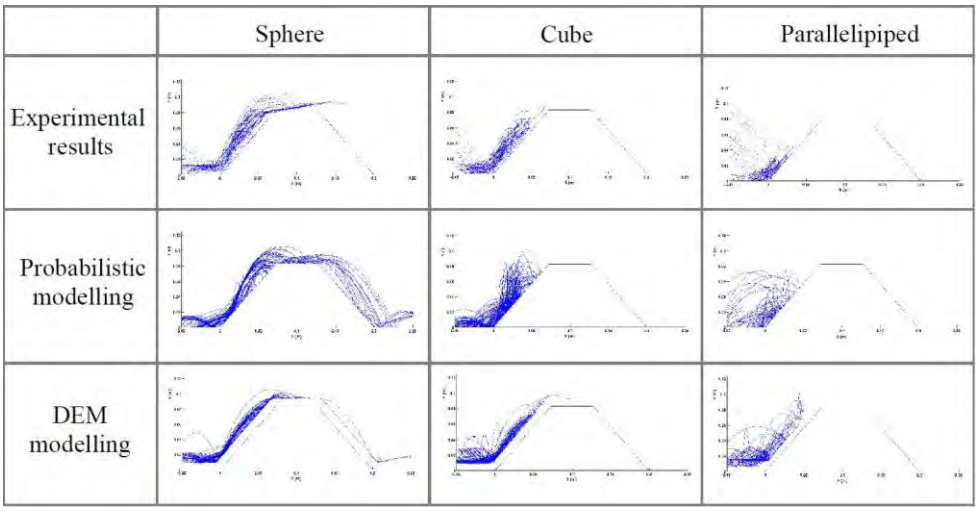

Figure 6 Experimental and simulated trajectories for three different block shapes (Toe et al., 2013).

Also, the spatial resolution of trajectory analysis tools may not be appropriate to satisfactorily account for the slope profile in the vicinity of the embankment, mainly for 3D codes (Lambert et al., 2013). Basically, a raster digital elevation model with a resolution of 2 m cannot reproduce the rapid slopes changes observed in the ditch and at the embankment.
As a consequence, particular care must be taken to satisfactorily model the trajectory of a block in the embankment vicinity with the aim of evaluating its efficiency in reducing the risk

Last, these recommendations concern RPE build to stop single blocks and not rockslides neither than successive and frequent rockfall. In such cases, the volume of solid material to contain in the ditch should be considered for defining the structure height. In the case of successive and regular rockfall, the height of the RPE should be the sum of the maximum permissible thickness of deposited material, the block passing height and freeboard.

3. Structural design

The impact of a block, whose typical velocity ranges from 5 to 30 m/s and whose mass ranges from a few to tens of thousands of kilograms, results in a dynamic localized loading lasting between 0.03 and 0.2 s and generating strain rates in the impact direction higher than 0.1 s^{-1}. The design of earth-structures, such as RPE, exposed to such a specific dynamic loading confronts the engineers with

i. the large and irreversible deformations induced,
ii. the nonlinear soil stress-strain behaviour, and
iii. the interaction between the different components of the structure (reinforcing components and soil).

As a consequence and by contrast with the functional design, the design with respect to impact has been addressed through many research works.

In the following, these works are briefly mentioned to analyse the embankment response. Then the available design methods are described and their limitations are discussed. Specific sections are dedicated to the today's only existing standards (UNI, 2012; ONR, 2013).

3.1. Specific research

The increasing need for efficient protection structures against high-energy block impacts has motivated research for more than 30 years. These are based on experimental, analytical and numerical developments. The main experimental research is presented in the following subsections.

3.1.1. Small-scale experiments

The first experiments were conducted in the 1980s in view of constructing a huge embankment with a 200-MJ capacity based on small-scale structures (Corté et al., 1989; Lepert and Corté, 1988). The 1/100 scale embankments made of sand were exposed to centrifuge impact tests at a 100-g acceleration (Figure 7). The impact force and acceleration within the embankment were recorded. In practice, these experiments confirmed that the planned RPE (7.2 m high and 800m long) would be effective against a 200-m^3 volume block with a velocity of 26 m/s.

The Technical University of Vienna also conducted small-scale experiments with the main objective of investigating the influence of the geotextile (Blovsky, 2002 and 2004; Brandl and Blovsky, 2004). Twenty model tests were carried out on embankments scaled at 1:50. The parameters investigated were the soil compaction, the uphill face steepness and the geotextile layout. Embankments with and without geotextiles were tested (Figure 8). In the former, different geotextile anchoring lengths were considered, also considering geotextile wrapping on both faces. Impacts were repeated several times, measuring the impact force. Comparisons were made based on the sum of impulses after three successive impacts by an instrumented pendulum used as impactor.

In Austria again, Hofmann and Mölk (2012) conducted small scale experiments (1-g) on structures varying in type and size while varying the impact conditions (Figure 9, Figure 10). The impactor was a steel sphere. The embankments were either made of sand only, sand and rip-rap face, or reinforced sand. Based on the results of the numerous experiments conducted, the authors proposed the basic essentials of the Austrian standard-guidelines for the design of RPE (ONR, 2013, see section 3.6).

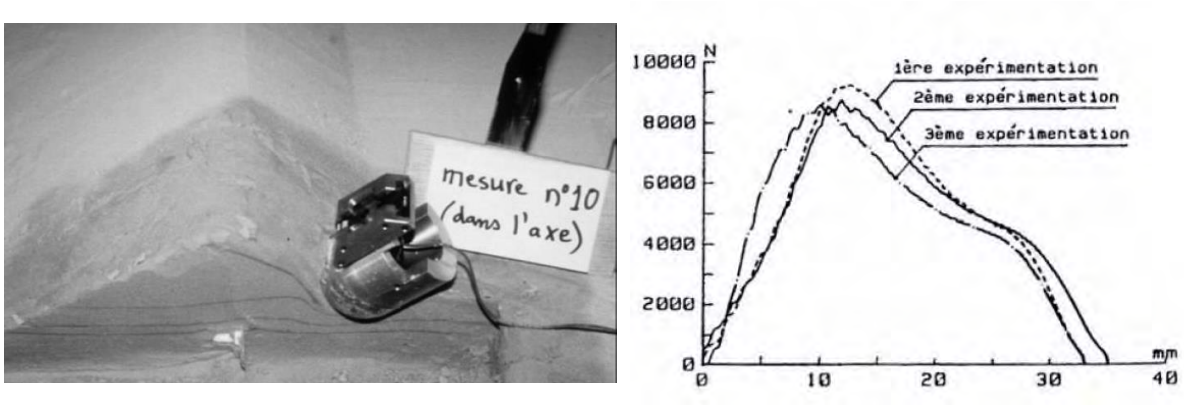

Figure 7 Centrifuge impact tests on an embankment conducted in France in the 1980's: impact embankment and impact force measurements (Lepert and Corté, 1988)

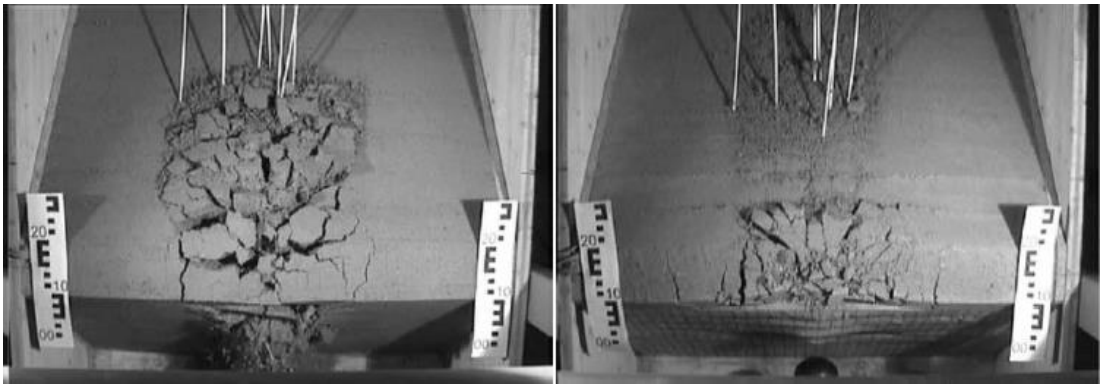

Figure 8 Post-impact top views of small-scale embankments showing the influence of the geotextile on the downhill face deformation: without/with geotextile, left/right (from Brandl and Blovsky, 2004).

Figure 9 Small-scale experiments conducted by Hofmann and Mölk (2013). Left: impact on an unreinforced structure. Right: reinforced structure after two impacts.

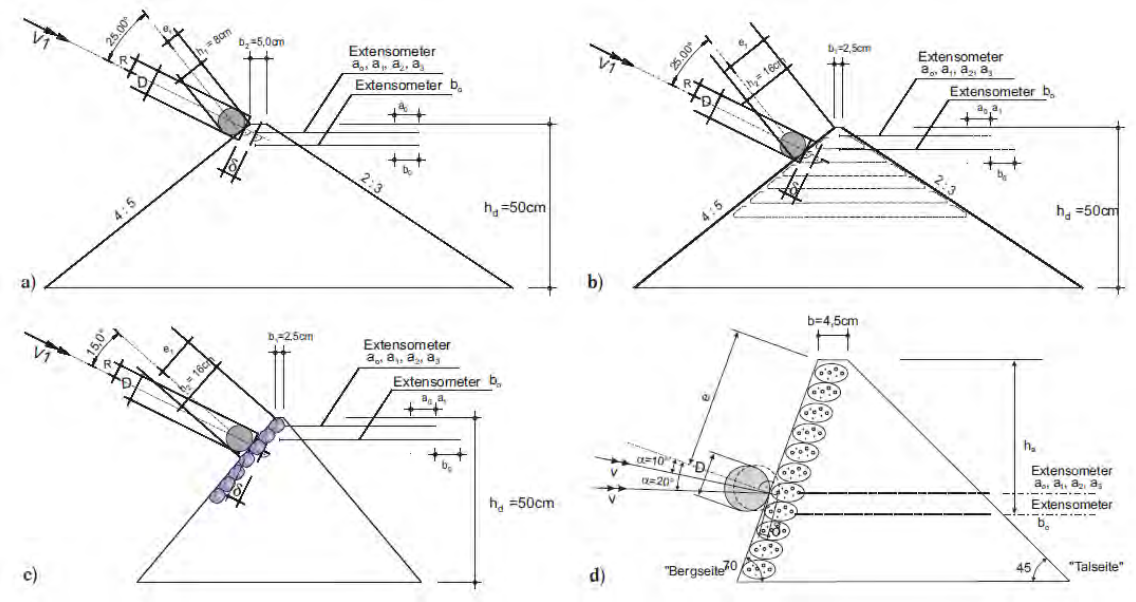

Figure 10 Illustration of the variety of embankment type and geometry and loading conditions in the small-scale experiments conducted by Moelk and Hofmann (2012).

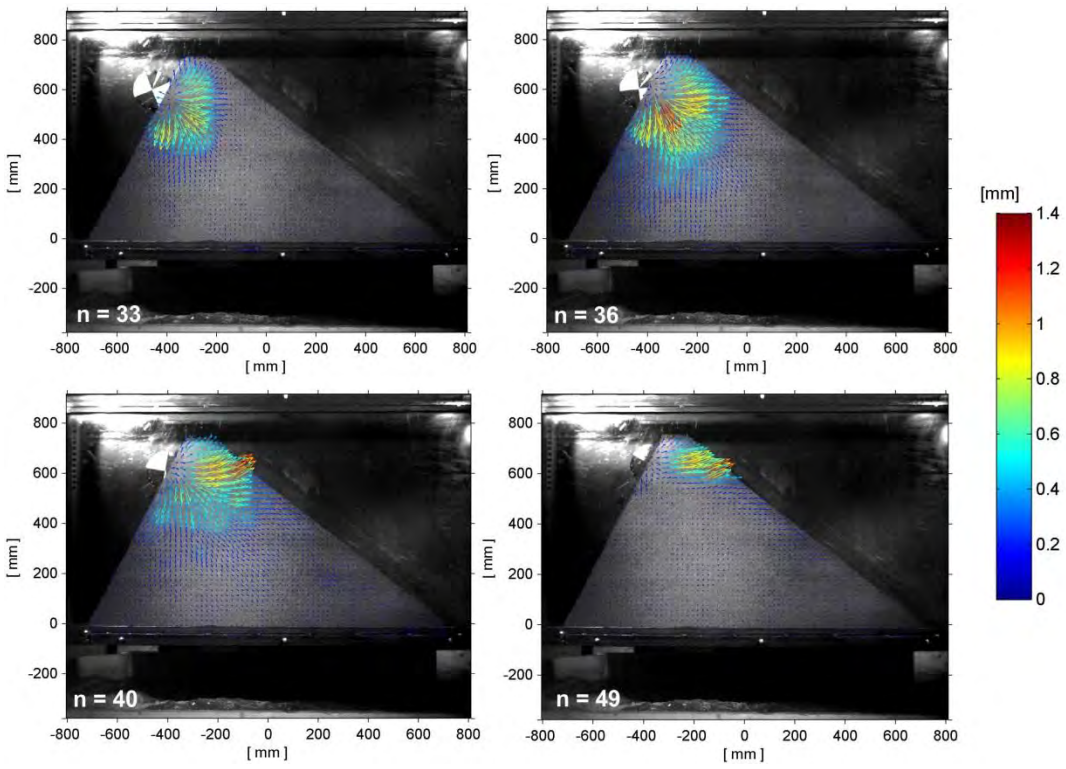

Figure 11 Displacement field at 4 ms, 10 ms, 18 ms and 36 ms observed by Kister (2015).

More recently, small scale and half scale experiments were conducted at Lucerne University of Applied Science and Arts, in quasi-2D respective in 3D conditions (Kister et al., 2014; Kister, 2015). Particle Image Velocimetry (PIV) allowed tracking over time of the displacement field inside the embankment. Additional the impactor's trajectory had been determined in the quasi-2D-tests (Figure 11). Embankments, differing in cross-section geometry (symmetric/asymmetric) and in crest width, were impacted by 6 different projectiles, differing by their shape, volume and unit mass. These experiments in particular showed the influence of the block rotational energy, block shape, block material and impact point location on the embankment deformation and for overtopping.

Small-scale experiments constitute a cost-saving alternative to real scale experiments, in particular with the aim of conducting parametric studies. The obtained results are of great qualitative value. Nevertheless, questions related to scaling issues and the extrapolation of results to the real scale may rise. This is particularly true for small scale tests under gravity, and less for centrifuge tests. On the other hand centrifuge tests are usually based on very small models because of the limited place in the centrifuge and so very often a realistic relationship of grain-size distribution of the RPE material and the RPE dimensions is not given.

3.1.2. Real scale experiments

The first real-scale impact experiments involved a structure type developed by the Colorado Department of Transportation in view of ensuring safety along an important road through a canyon (Burroughs et al., 1993; Hearn et al., 1995, 1996). The tests concerned a structure made of soil reinforced with geosynthetics, 24 m long, 3 m high and either 1.8 or 2.4 m thick, with vertical sides (Figure 12). Eighteen rock blocks of different shapes and masses were rolled down a hill against the barrier. The maximum block energy before the impact was 1400 kJ. The downhill face deformation increased nonlinearly with the boulder's kinetic energy, following a power law (Hearn et al., 1996). It decreased with the structure thickness: for a 1400-kJ impact, this deformation was 0.75 m and 0.35 m for a 1.8-m- and 2.4-m-thick structure, respectively (ref. A1/A3 in Table 3).

In the end of the 1990s, the behaviour of a new type of structure was investigated through real-scale experiments (Yoshida, 1999). This structure consisted of a soil-reinforced earthwork protected by two layers of soil bags, placed uphill (Figure 13). The soil bags were exposed to the impact to act as an energy dissipater to reduce the impact force on the reinforced embankment. Blocks were rolled down the hill, resulting in impact energies ranging from 58 to 2500 kJ (ref. C1/C3 in Table 3). All the blocks were stopped without a collapse of the structure. The deformation on the uphill face was measured. More recent experiments were conducted on similar structures, but no significant data is available (Protec Engineering, 2011).

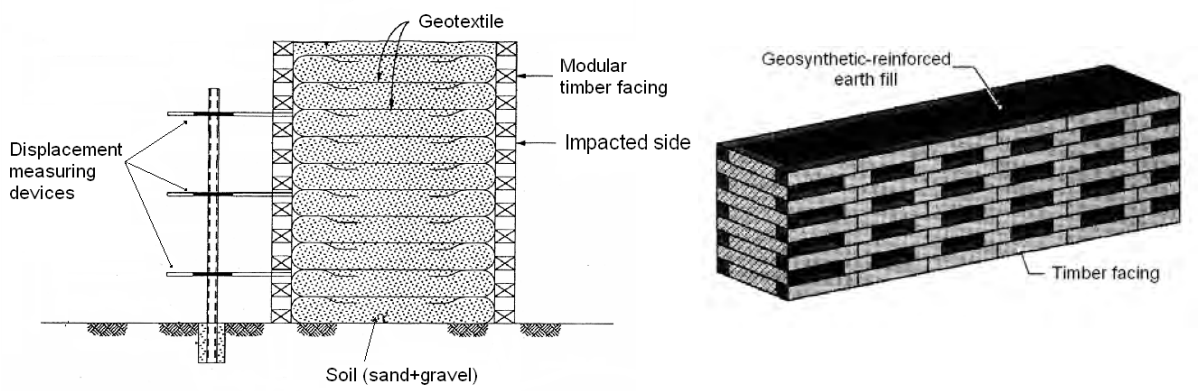

Figure 12 Structure tested by the University of Colorado (adapted from Burroughs et al., 1993; Hearn et al., 1995)

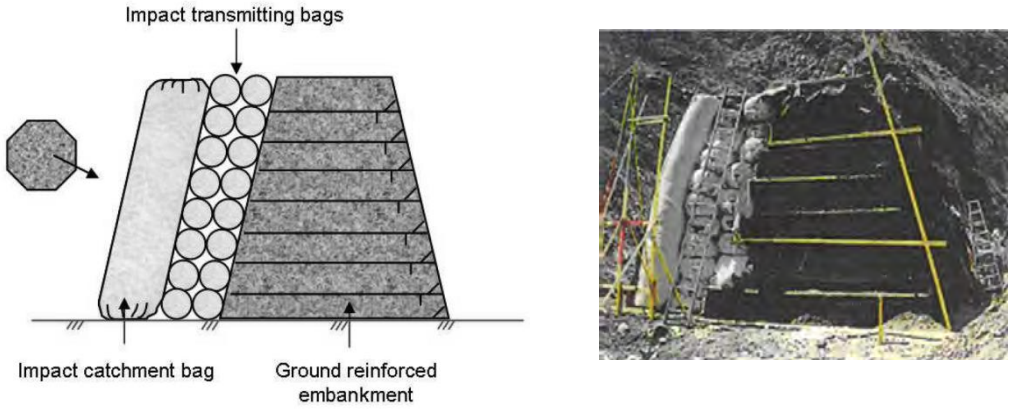

Figure 13 Embankments tested by Yoshida (1999).

Since the end of the 1990s, an important study has been conducted by the University of Torino on geosynthetic reinforced embankments (Peila et al., 2000, 2002, 2007, 2011; Ronco et al., 2009). Real-scale structures were tested on a site dedicated to rockfall protection structure testing (Figure 14). The equipment can convey blocks up to 10 tons at a velocity of 30 m/s. The blocks had almost no rotation when hitting the structure. A total of eight impact tests on five different embankments were performed. The impacted structures were reinforced with geosynthetics, except for one structure that was made of compacted soil (ref. B1 to B3 in Table 3). The parameters investigated were the geosynthetic type, the soil type and the block mass.
These reinforced embankments were demonstrated to be efficient against successive 4500-kJ impacts. This research is the most exhaustive work on the topic to date, including experiments and numerical modelling aiming to develop both design charts and numerical tools to be used for design purposes (Brunet et al., 2009; Ronco et al., 2010, Grimod and Giacchetti, 2013) and allowing back analysis of natural impacts (Peila, 2011).

In Japan, three real-scale structures differing in their construction materials were exposed to impacts (Sung et al., 2008; Aminata et al., 2009). Impact tests were either performed rolling blocks down a 17 m high hill or using a boulder suspended from a crane released from a height of 11 m, reaching a maximum energy of 110 kJ. The impacted structures were a geogrid-reinforced wall, 2 m high, and two walls made of ductile cast iron panels containing boulders (Figure 15). Block penetration, block velocity and impact force were derived from the measurement of block acceleration.

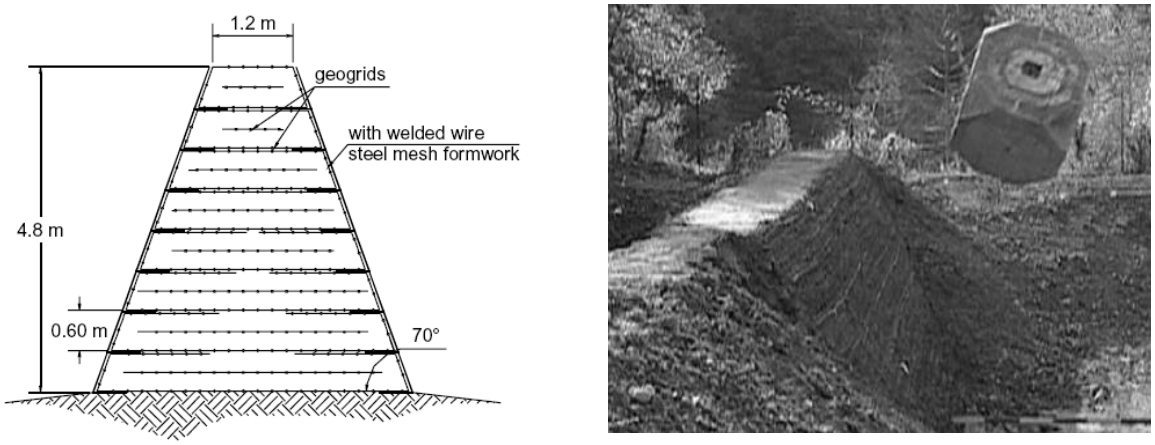

Figure 14 Embankments tested by the University of Torino (Peila et al., 2002).

Table 3 Some experimental data concerning impact experiments with energies higher than 1000 kJ.

Ref.	Structure Type	Height (m)	Thickness (crest/base) (m)	Block Mass (kg)	Translational Veloc. (m/s)	Translational En. (kJ)	Impact Height (m)	Deformation Uphill -side (m)	Deformation Downhill -side (m)
A1	MSE wall	3.05	1.82	5300	19.5	1010	1.5	0.6	0.2
A2	+ wood(1)	3.05	1.82	8300	18.3	1400	1.4	0.9	0.7
A3		3.7	2.4	8400	18.3	1410			0.34
B1	Reinforced(2)	4.2	0.9/5	5000	31.7	2500	3	0.6	0.23
B2		4.2	0.9/5	8780	31.3	4350		1	0.9
B3	Unreinforced(2)	4.2	0.9/6	8780	31.3	4350	3	1.5	collapse
C1		4	3.3/5.3	3300	24	970	2	0.22	0
C2	GeoRockwall(3)	4	3.3/5.3	7700	24	2000	2-3		0.09
C3		4	3.3/5.3	17000	17.7	2700	3-4		0.5
D1	MSE wall +	4.2	2.2/4.3	10100	15.7	1243	2.31	1.56	0.266
D2	Geocell	4.2	3/5.1	17100	13.9	1567	2.85	1.44	0.091
D3	face(4)	4.2	2.2/4.3	17100	14.4	2037	2.55	1.73	0.239
E1	Gabion	3	3/11	6500	18	1040	2.1	0.42	0
E2	face+dam(5)	3	3/11	6500	26	2200	2.1	0.71	0

(1) Hearn et al., 1996; (2) Peila et al., 2002, 2007;(3) Yoshida et al., 1999; (4) Maegawa et al., 2011; (5) Lambert et al. (2014).

Maegawa et al. (2011) investigated the concept of sandwich structures as pioneered by Yoshida (Yoshida, 1999). The impacted structures differ in the structure's face, which is composed of geocells filled with gravel instead of soil bags. Impacts ranging from 786 to 2709 kJ were obtained by rolling a block down a 37-m-high slope onto the structure. Eight tests were performed on two types of structure. Deformation on the uphill face and the block acceleration were measured (ref. D1 to D3 in Table 3). All blocks were stopped.

Cellular rockfall protection structures have recently been investigated by Heymann et al. (2010) and Lambert et al. (2014). These structures are made of gabion cages filled with different materials depending on their location in the structure. The aim was to reduce the stresses transmitted within the structure by increasing the diffusion of stress as well as dissipation of the impact energy. In this purpose, shredded tires were used after demonstrating their limited environmental impact (Hennebert et al., 2014). Both half-scale and real-scale structures were impacted (Figure 16). Different fill materials were considered, including shredded tire–sand mixtures and ballast. Three different real-scale structures were subjected to an impact by a 6500-kg spherical boulder, with a maximum velocity of 25 m/s (ref. E1 and E2 in Table 3). Measurements in particular concerned accelerations of the boulder and within the structure, the transmitted forces and the structure deformations. Large deformation was observed in the structure. Figure 17 shows that velocities higher than 3 m/s were reached at a 1 m distance from the impacted surface, over a short period of time, and that compaction and loosening were observed after the impact up to 4 m from the impact point.

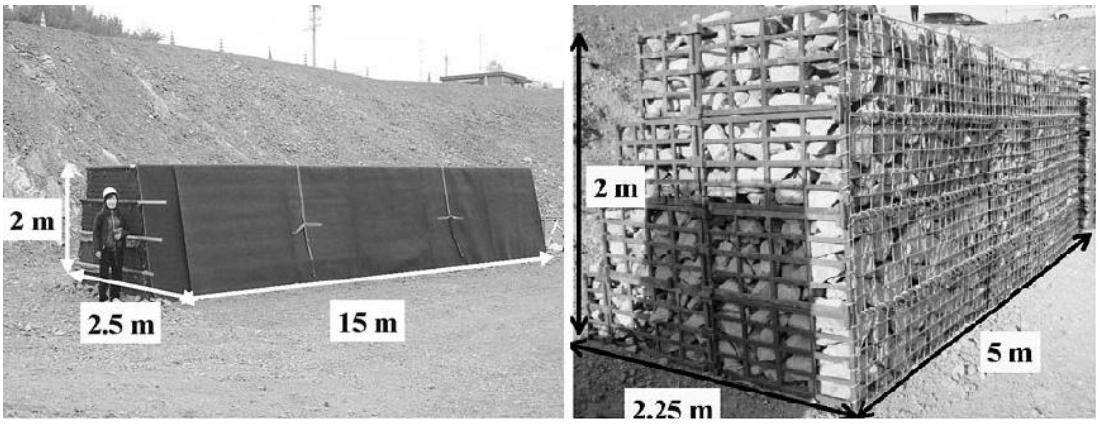

Figure 15 Two of the three structures recently investigated in Japan (Sung et al., 2008; Aminata et al., 2009).

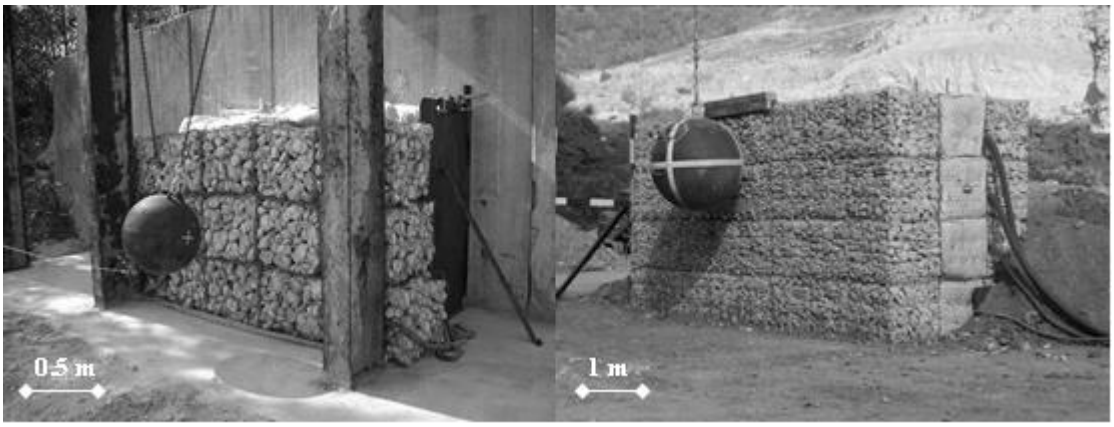

Figure 16 Half-scale and full-scale structures tested by Heymann et al. (2010) and Lambert et al. (2014).

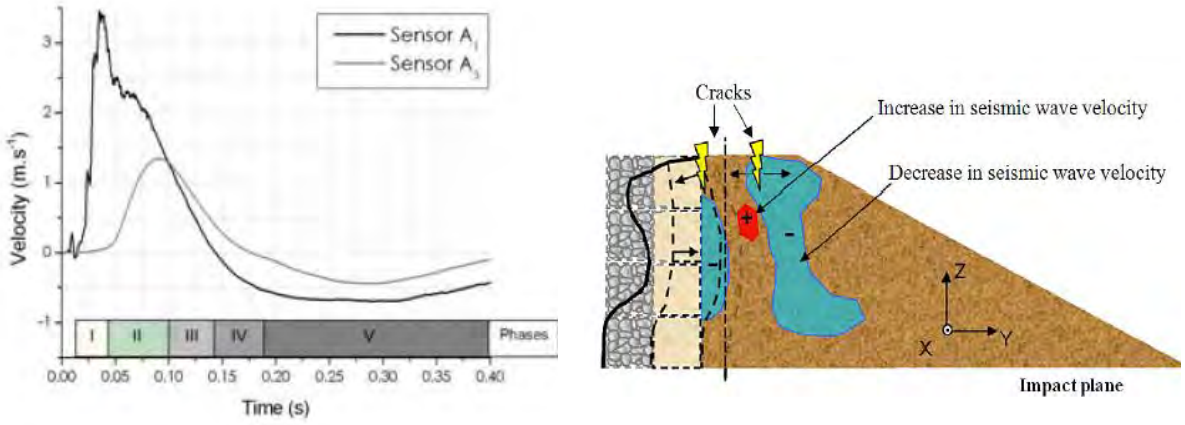

Figure 17 Velocities measured within the RPE at 2 distances from the impact point (left) and post-impact observations (Lambert et al., 2014)

Figure 18 Experiments conducted by Clerici et al. (2013)

Figure 19 6600 kJ impact experiment conducted by Mongiovi et al. (2013)

More recently, real-scale impact experiments were conducted in Italy, by the University of Brescia (Clerici et al. 2013) and by the University of Trento (Mongiovi et al., 2014). The former was conducted impacting a reinforced RPE by spheres rolling down a slope and developing energies up to 0.8 MJ (Figure 18). The latter also concerned a reinforced RPE, 4.8 m high, but with impact energies of almost 7 MJ, the highest ever reached in real scale experiments (Figure 19). In both cases, the block velocity was measured and the post-impact structure deformation was monitored by laser scan. In addition, experiments conducted by the University of Trento involved acceleration measurements within the RPE. Nevertheless, only limited data are available on these two experimental works.

3.1.3. Numerical approaches

As a complement to experimental investigations, various numerical models have been developed. Some were developed in parallel to the real-scale experiments, and rather fair agreements were obtained. The aim with some of these tools was to extend the study of the RPE response to higher impact energies than in the experiments (Ronco et al. 2009) or for addressing the influence of the block kinematics (Plassiard, 20007, Plassiard and Donzé, 2009; Murashev et al., 2013, Breugnot et al., 2015). The Finite Element Method (FEM) had been used by Burroughs et al. (1993), Peila et al. (2002, 2007), Sung et al. (2007) and Murashev et al. (2013). FEM-based approaches require an explicit method and a re-meshing algorithm taking rockfall dynamics into account and modeling large deformations (Peila et al., 2007). The Finite Difference Method (FDM) has been used by Jarrin and Meignan (2010). On the contrary, the Discrete Element Method (DEM) is based on Newton's equation of motion and naturally allow modelling large deformations. DEM-based approaches have been used by many authors (Hearn et al., 1995, 1996; Carotti et al., 2004; Nicot et al., 2007; Plassiard and Donzé, 2009, 2010; Bertrand et al., 2010; Bourrier et al., 2011; Lorentz et al., 2010). Breugnot et al. (2015) have proposed the use of a combined discrete-continuum approach in order to derive advantages of the discrete approach in the impact area and of the finite element approach in the far field. They investigated the influence of the block shape, impact location and the ratio of mass to velocity for a same kinetic energy.

Even if allowing conducting parametric studies, the numerical models are mainly research oriented, because they are complex, require specific skills and the calculations are time consuming. To some extent, these models are out of reach for most of the design companies. As an illustration, the literature is extremely poor in terms of application of such models to specific study cases (Lorentz et al., 2010; Murashev et al., 2013). Last, these models are mainly used by their developers and are not accessible for their reliability to be evaluated.
Consequently, these numerical works won't be addressed in details but reference to some of these will be made in the following sections, when relevant.

Despite the great variability of testing conditions and structure types, real-scale experiments globally provide a valuable database for investigating the response of RPE to block impact. Table 3 reports some experimental results obtained on real-scale structures with impact energies higher than 1000 kJ. The capacity of the embankment, in terms of the impact energy it can withstand without collapsing, is the most important information obtained. The analysis of the response of impacted structures may also be based on the residual deformation on both uphill and downhill faces of the embankment after an impact. In particular, the downhill face deformation can be considered as a simple design criterion, because it governs post-impact structure stability (Ronco et al., 2009).

3.2. What can be learned about the response of an embankment to block impact?

The different published works presented in the previous section, and involving real-scale and small scale experiments as well as numerical modelling, gives elements for describing the response of a RPE to a block impact and helps to understand the main mechanisms involved.

The response of the RPE to impact, until collapse, may be described as a three-phase process, as proposed by Lambert and Bourrier (2013) (Figure 20).

When the block starts penetrating the RPE, a high stress is generated in the vicinity of the impacted area, with peak values higher than 1 MPa (phase 1). The increase in stress leads to the compaction of granular materials with possible particle crushing, depending on the embankment fill material characteristics: the narrower the soil grading, the larger the particle size and the higher the stress, the greater the chance of grain crushing.
The rest of the structure exhibits almost no significant changes. It basically acts as a buttress allowing compaction and particle crushing on the uphill face.
The very high stress gradient, which expands from the uphill face to the downhill face of the RPE induces displacement of the grains locally. A displacement field appears in the stressed zone. This displacement field has a tendency to move upward while going through the structure (Lambert et al., 2013; Kister, 2015).

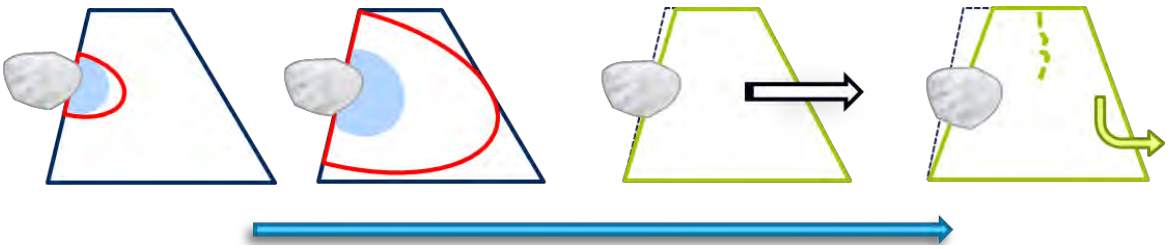

1. *Compression* 0 to 50 ms	2. *Global displacement* 50 to 200 ms	3. *Collapse*
- *Compression wave propagates* - *Plastic zone develops* - *Energy dissipated by compaction, crushing* - *Impact force peak reached* - *Part of the RPE acts as a buttress* - *Buttress effect progressively vanishes*	- *Average structure velocity increases* - *Energy dissipated by friction*	- *Differential displacements induce cracks* - *Collapse results from the downhill face displacement*

Figure 20 A 3-phases schematic description of the RPE response to impact, until collapse (Lambert and Bourrier, 2012).

Progressively, the front of the stressed volume moves within the RPE and, concomitantly, the buttress effect vanishes with time. The amplitude of the stress peak decreases with the travelled distance, due to both geometrical and material attenuations. After a given period of time and especially for slender constructions, the displacement field may involve the whole RPE cross-section (phase 2). Indeed, as the downhill face is a free boundary, the stress increase results in a downhill-oriented movement of this face. The displacement then concerns a volume with lateral extension higher than twice the block diameter (Blovsky, 2002, 2004; Peila et al., 2007; Hofmann and Mölk, 2013; Lambert et al., 2013; Kister, 2015). Besides, the displacement is more pronounced closed to the crest than at the RPE base, where no displacement is observed. This displacement of part of the RPE leads to dissipation by friction, along shear planes developing through the structure.

Finally, if the stress increase close to the downhill face is high enough, soil loosening and bulking may occur on the downhill face as well as on the crest (phase 3) (Blovsky, 2002, 2004; Hofmann and Mölk, 2013; Lambert et al., 2014; Kister, 2015). Cracks parallel to the face may develop within the structure as a result of these displacements (Peila et al., 2002; Lambert et al., 2014, Kister, 2015). The structure finally may collapse, as a result of the downhill face large displacement.

The occurrence and magnitude of the different mechanisms mentioned depend on the impact energy in proportion to the embankment's capacity to absorb energy.
For low impact energies, both the penetration required to stop the block and the stress generated within the embankment are small (ref A1, B1, C1 in Table 3). The residual downhill

face deformation is small compared to the block penetration. The impact energy is dissipated by compaction and grain crushing in the vicinity of the impact area while only a small part propagates by elastic waves. In such as situation, there is neither phase 2 nor a phase 3.

With a higher impact energy, both the block penetration and stress within the embankment increase. The volume of material undergoing plastic strains increases, similar to what is observed for ground compaction (Mayne and Jones, 1983). The downhill face displacement increases and for slender structures, the displacement may progressively tend toward the value of the uphill face displacement (e.g., ref. A1 and A2 in Table 3). Nevertheless, the thicker the embankment, the lower is the downhill face displacement (e.g., ref. D1, D2, E1 and E2 in Table 3).

Dissipative mechanisms depend on the time considered and on the position in the structure. Compaction is predominant close to the impact, at the impact beginning. At far distance from the impact, compaction is much less because of the spatial energy attenuation of a “point load”, which is in inverse proportion to the distance. On the contrary, energy at larger distance from the impact and for larger times may be dissipated along shear planes developing as a result of the structure displacement. Overall energy dissipation through soil compaction remains predominant during the impact process, with an estimated proportion of about 75 to 80% of the block’s kinetic energy (Ronco et al., 2009, Kister and Fontana, 2011).

The structure’s response versus time thus reveals the influence of the different parameters related to the material characteristics: the parameters associated with their compressive response, friction angle and unit mass. The influence of these parameters on the whole structure’s behaviour depends on the impact energy, the structure’s dimensions and the structure’s boundary conditions. For example, the friction angle has limited importance as long as there is no large differential displacement. This influence increases with the block kinetic energy.

Reinforcement layers significantly improve the ability of an embankment to withstand the impact (ref. B2/B3 in Table 2). Such reinforcement layers, made of geogrid or geotextile, spread the impact load along the embankment axis (Peila et al., 2007). Nevertheless, such a beneficial effect implies a mechanical continuity of the geotextile layers, along the longitudinal axis of the RPE, requiring bonds or overlapping between two layers, while it’s rarely the case.

The localized deformation of the embankment may result in burn-up of the reinforcement layer as well as in a tension along the longitudinal axis of the embankment. This differs from the static case accounting for gravity loads, where the reinforcement layer is loaded along the transverse axis of the embankment direction (Peila et al., 2002; Brandl and Blovsky, 2004). The impact load is thus distributed to soil masses at a distance on both sides of the impacted area. In the impact vicinity, the resulting confining effect by the layer increases the penetration resistance of the embankment. Moreover, if reinforcement also concerns downhill face of the RPE, the layer restrains the displacement of this face and thus increases the ability to withstand

the impact (Blovsky, 2002, 2004) (Figure 8). The negative counterpart is that horizontal planar reinforcement layers may offer a preferential plane for shear rupture (Figure 21).

Last, but not least, the impact response of the embankment strongly depends on the impact height: the closer the impact to the crest, the higher the penetration, with detrimental effects on the structure stability (Breugnot et al., 2015). Even if not addressed in detail, the impact inclination is thought to have a significant influence: the penetration is higher in case of a downward inclination according to Murashev et al. (2013) and higher for impact trajectories more or less perpendicular to the face (Kister, 2015).

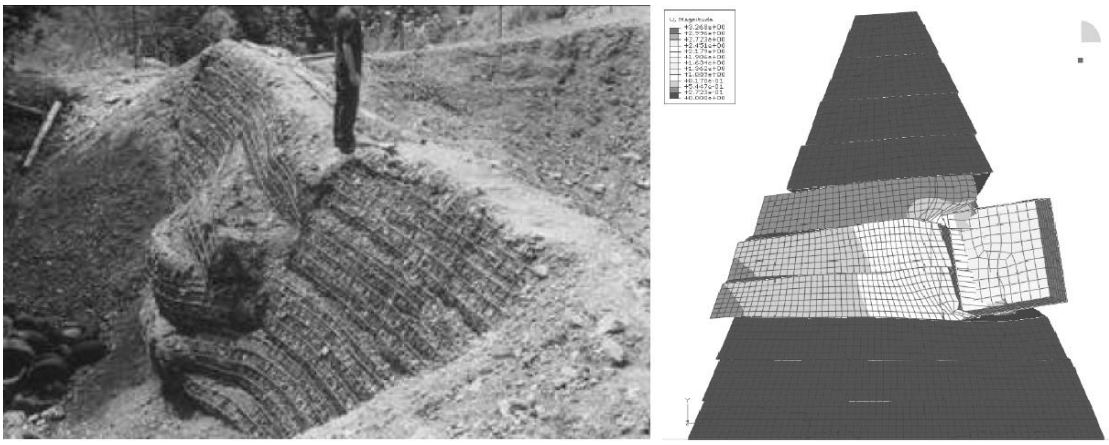

Figure 21 Reinforcement layers offer a preferential plane for shear rupture (Ronco et al., 2009).

3.3. Current design methods

In spite of their important protective role, the design of embankments is generally based on simplistic approaches. Also, contrary to rockfall protection galleries (or rock-sheds), there are neither recommendations nor guidelines concerning their design in any of the countries concerned, except the recent Austrian standard (ONR, 2013). Even if in some cases, specific and rather complex studies have been conducted (Lepert and Corté, 1988; Brandl and Blovsky, 2004; Lorentz et al., 2010), the vast majority of existing structures have been designed with basic approaches, considering dynamics only to a minor extent.

3.3.1. Typology of existing methods

The approaches in use today differ in their level of complexity and their ability to account for the dynamics. Existing structures have been designed considering different approaches (adapted from Lambert and Bourrier, 2013):

- Type 1: based on its mass, the embankment is assumed to be able to stop the block and withstand the impact. The structure is just designed with respect to gravity loads.

- Type 2: penetration criteria-based approaches estimate the penetration of the block in the embankment, which is multiplied by a factor of 2 to 3 to obtain the minimum embankment

thickness (Brunet et al., 2009). This is based on a criterion of post-impact stability of the deformed structure (Ronco et al., 2009).

- Type 3: pseudo-static approaches consider a load that is statically equivalent to the dynamic impact load for designing the embankment (Jaecklin, 2006; Kister and Fontana, 2011). A safety factor may be considered, expressing the uncertainties associated with the hypothesis of a statically equivalent loading (Brandl and Adam, 2000). The structure's static stability is checked based on classical methods devoted to embankment stability while considering this load in combination with gravity loads.

- Type 4: energy approaches assess the ability of the embankment in withstanding the impact based on analytical estimations of the energy dissipated within the embankment. In this purpose, the impact can either be described in terms of block incident kinetic energy or impact force. Energy dissipation is computed considering an Impact Disturbed Zone (IDZ). The IDZ is the volume of the RPE exposed to severe loading resulting in large displacements, strains, and changes in the mechanical characteristics. The first dissipative mechanism accounted for is friction along shear planes assuming that the IDZ moves as a rigid body (Tissières, 1999; Brandl and Adam, 2000; Kister and Fontana, 2011; Kister, 2015). In reinforced structures, the IDZ is often delimited by the reinforcement layers offering a preferential shear rupture plane (Ronco et al., 2009; Carotti et al., 2000). Energy dissipation through soil compaction can also be considered either by analytical approaches (Jarrin, 2001) or by considering of ratio of compaction energy dissipation (Ronco et al., 2009; Kister, 2015). The design consists in assessing that the structure deformation required to dissipate the block's kinetic energy is consistent with the embankment dimensions. For this purpose, the uphill deformation due to the block penetration may be deduced from the impact force (Ronco et al., 2009).

- Type 5: numerical modelling approaches, based on specific numerical tools for modelling the impact and evaluate the deformation of the embankment, using either finite difference or finite elements methods (FDM, FEM) or discrete element methods (DEM) (e.g. Peila et al., 2007; Lorentz et al., 2010; Jarrin and Meignan, 2010; Murashev, 2013; Breugnot et al., 2015).

Types 2–4 generally involve determining the block penetration or the impact force. Different equations have been proposed for determining either the one or the other with respect to rockfall related applications (Table 4). Details concerning these equations are provided in the next sections.

Types 5 approaches being less accessible to design engineers in general, as requiring specific skills and backgrounds, these will not be detailed in the following. Priority is given to analytical methods more commonly used, which are much more accessible and rapid to use.

The proposed classification is similar to that proposed by Kister (2015), considering design approaches 2 to 4.

3.3.2. Block penetration estimation

The penetration of a block into the embankment has been estimated using different equations, depending on the author as illustrated in Table 4. These are detailed in the following, together with equations that are relevant in the field of rockfall. The original expressions have been modified considering a same system of symbols and using SI units as defined in Table 5.

These methods and their limitations will be discussed in section 3.3.4.

Table 4 Methods for estimating the block penetration and impact force, explicitly used for RPE design purpose

	Method proposed by	Referred to in
Penetration	Kar (1978)	Paronuzzi (1989), Carotti et al. (2004), Maccaferri (2009), and Frenez et al. (2014). Specifically accounting for reinforcement layers in Cargnel and Nössing (2004);
	Calvetti and di Prisco (2007)	Brunet et al. (2009)
	Grimod and Giacchetti (2013)	Willye (2014)
Force	Mayne and Jones (1983)	Peila et al. (2007)
	Montani (1998)	Jaecklin (2006)
	Labiouse et al. (1996)	Peila et al. (2007), Ronco et al. (2009), Frenez et al. (2014)
	FEDRO (2008)	Kister and Fontana (2011)

Table 5 Symbols used in sections 3.3.2 and 3.3.3

Symbol	Unit	Definition
E	kPa	Young's modulus of the impacted material
Es	kPa	Young's modulus of the projectile
F_i	N (unless specified)	Impact force
F_i^*	N (unless specified)	Characteristic value of the impact force (generally the maximum impact force, unless specified)
g	m/s²	Gravity
G_{dyn*}	kPa	Shear modulus of the impacted material
H_c	m	Projectile free falling height
m	kg	Mass of the projectile
M_E	kPa	Impacted material static elastic modulus (Swiss standard)
N	-	coefficient depending on the shape of the projectile (nose factor)
N_γ	-	Soil bearing capacity factor
p	m	Block penetration
r	m	Radius of the projectile (sphere or equivalent sphere)

t	m	Soil layer thickness
v	m/s	Projectile velocity before impact
ϕ	Rad	Friction angle of the impacted material
γ	kN/m^3	Soil unit weight
σ_d	kPa	unconfined compressive strength of the impacted material
ν	-	Poisson coefficient of the impacted material

Kar (1978) evaluated the penetration depth of bombs and missiles on soil protection shelter structures, based on real scale experiments. Kar (1978) proposed determining the penetration from:

$$p = \frac{4.06 \cdot 10^5}{\sqrt{\sigma_d}} \cdot N \cdot \left(v \cdot \frac{E}{Es} \right)^{1.25} \cdot \frac{m}{r^{2.31}} \qquad (1)$$

Calvetti and di Prisco (2007) proposed the chart in Figure 22 for estimating the penetration depending on the block falling height and radius. This chart was obtained from numerical simulations using the BIMPAM model, calibrated using results of impacts of a 850-kg boulder on granular layers with 1 to 2 m in thickness.
It is here proposed that this chart is conveniently captured by:

$$p = 0.027 \cdot r \cdot v + 0.24 \qquad (2)$$

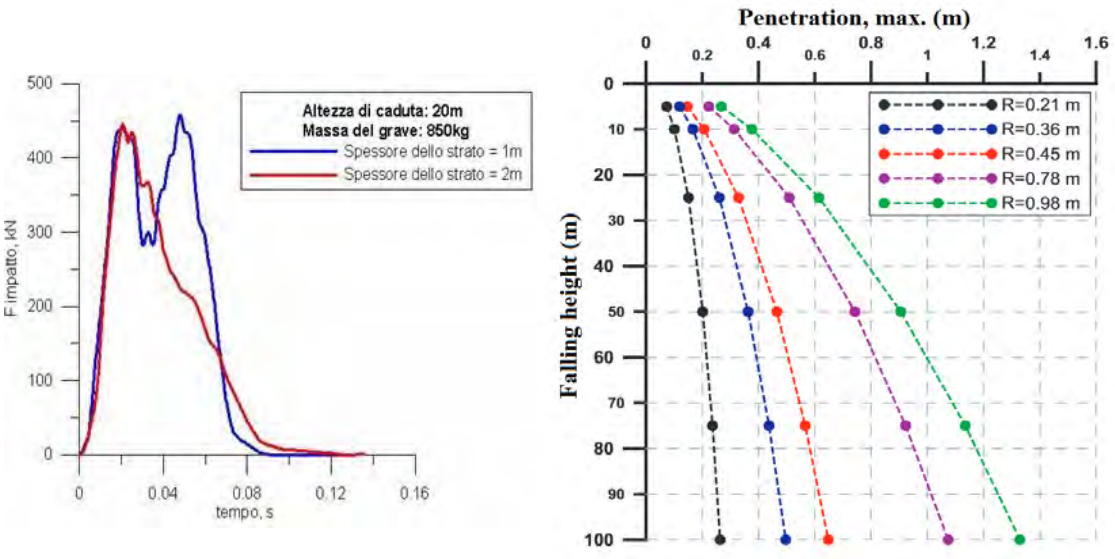

Figure 22 Based on impact experiments with an accelerometer-equipped sphere (left) Calvetti and di Prisco (2007) proposed a chart fort estimating the block penetration

Pichler et al. (2005) considered formulae developed for non-deformable ogive-nose impactors penetrating concrete and soil targets, and proposed by Li and Chen (2003):

$$p = 2 \cdot r \cdot \sqrt{\frac{1 + k\pi/4N'}{(1 + I/N')} \cdot \frac{4k}{\pi} \cdot I}, \qquad when \;\; p \leq 2 \cdot r \cdot k \tag{3}$$

$$p = \frac{4 \cdot r}{\pi} \cdot N' \cdot \ln\left[\frac{1 + I/N'}{(1 + k\pi/4N')}\right] + k, \qquad when \;\; p \succ 2 \cdot r \cdot k \tag{4}$$

In these expressions, I is related to the impact intensity, N' depends on the mass, shape and radius of the projectile, and type and mass density of the impacted material, and k is the dimensionless depth of a surface crater.
I is given by:

$$I = \frac{m \cdot v^2}{8 \cdot R \cdot r^3}$$

Where R is a strength-like indentation resistance of the impacted materials.

In the experiments conducted by Pichler et al. (2005) with cubic boulders dropped on coarse gravel, R was found to vary between 8.13 and 10.98 MPa and N' equal to 2.385. More detailed information concerning the calculation of I and N' can be found in Pichler et al. (2005).

The parameter k strongly depends on the projectile tip shape, according to Figure 23. If the tip is flat, k should be set to 0.707*(2r), according to the theory of Prandl. If the tip of the projectile is curved or cone-shaped, then it will penetrate the target, which is assumed as half-space. In these cases, k may be defined as k = 0.707+H/(2r) where H is the height of the tip. Consequently, for a projectile with a hemispherical tip k = 1.207.

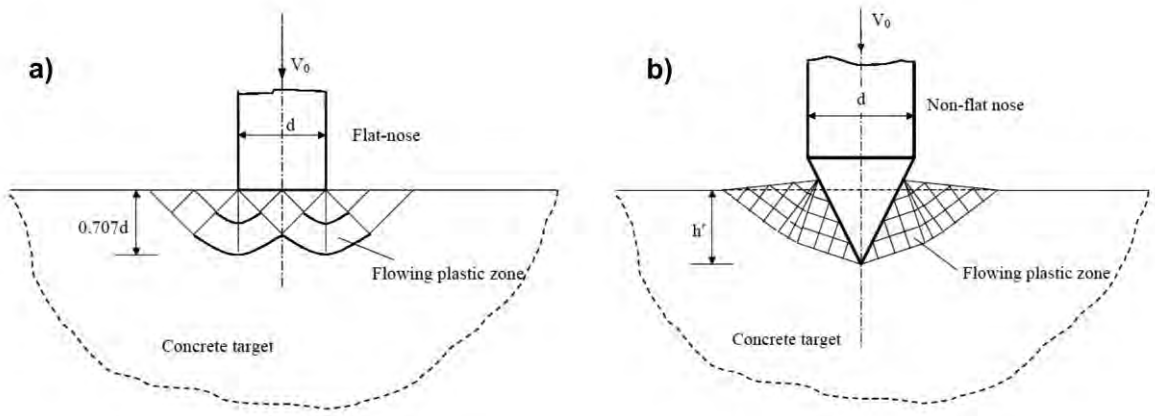

Figure 23 Slip line field of concrete crater created by a) a flat-nose projectile, b) by a projectile with arbitrary nose (Li and Chen, 2003).

Based on the work conducted at the University of Torino, Grimod and Giacchetti (2013) proposed to determine the penetration with:

$$p = p_c \cdot \frac{1}{2} \cdot m \cdot v^2 \cdot \frac{k}{\pi \cdot r^2} \tag{5}$$

Where p_c is the ratio of the block kinetic energy that is dissipated by plastification in the embankment (typically 0.85, see Ronco et al. 2009), k is a coefficient depending on the reinforcement material and the type and compaction level of the soil. This estimate is considered by Willye (2014) while also accounting for a factor depending on the block shape.

Based on a similar approach as that used for shallow foundations design, Wang and Cavers (2008) proposed:

$$p = \left(\frac{m \cdot v^2}{1.067 \cdot \gamma \cdot N_\gamma} \right)^{0.33} \tag{6}$$

Finally, if the impact force is known, based for example on the estimation methods presented in the next section, the block penetration, can also be computed as:

$$p = \frac{m \cdot v^2}{F_i} \tag{7}$$

This relation is obtained from the work done by the force acting on the embankment over the whole impact duration, considering that the block velocity is then 0. This work equals the translational kinetic energy of the block before impact, given by:

$$KE_{trans} = \frac{1}{2} \cdot m \cdot v^2 \qquad \mathrm{W} = \int \mathrm{F_i} \cdot \mathrm{dx} = \mathrm{F_{medium}} \cdot \mathrm{p}$$

If the maximum is considered as the characteristic impact force value, F_i^*, and assuming that the maximum impact force is twice the medium force, this yield to:

$$\frac{1}{2} \cdot m \cdot v^2 = \frac{1}{2} \cdot F_i^* \cdot p$$

and finally to equation (7).

Equation 7 has been used by Carotti et al. (2004), Peila et al. (2007), FEDRO (2008) and Ronco et al. (2009) among others.

Other existing formulas developed with the aim of estimating the penetration of rigid bodies (projectile…) in soil are not detailed here as these are not referred to in rockfall engineering related documents (see for example a list in Montani, 1998).

3.3.3. Impact force estimation

As a preliminary comment, it must be pointed out, that the definition of a static force that is equivalent to a dynamic loading, F_i*, is not straightforward. Most often, the maximum impact force is considered as the characteristic value to be used for this purpose, but this may be an asymptotic value, due to the shape of the impact force curve with time revealing that the maximum correspond to a very short duration peak by comparison with the whole impact duration (Lambert et al., 2014).

Different expressions have been proposed for determining the impact force of a rigid body onto soil, either issued from ground compacting technique developments or from research in the field of rockfall. The expressions presented in the following have been explicitly used for RPE design purpose (Table 4). Again, the original expressions have been modified considering a same system of symbols and using SI units, as defined in Table 5. These methods and their limitations will be discussed in section 3.3.4.

Based on ground compaction tests, Mayne and Jones (1983) proposed:

$$F_i^*[\mathrm{kN}] = \sqrt{\frac{32 \cdot H_c \cdot G_{dyn}^* \cdot r \cdot m \cdot g}{\pi^2 \cdot (1-\nu)}} \tag{8}$$

Labiouse et al. (1996), proposed to use an expression derived from the elastic collision theory (Hertz):

$$F_i^*[\mathrm{kN}] = 1.765 \cdot r^{0.2} \cdot M_E^{0.4} \cdot \left(m \cdot H_c \cdot \frac{g}{10^3} \right)^{0.6} \tag{9}$$

Even though this expression is directly derived from the Hertz theory, a rather good agreement was obtained with the impact results (Labiouse et al., 1996; Montani, S., 1998). These tests concerned a granular layer 0.35 to 0.5m in thickness, resting on a concrete structure and impacted by boulders with energies up to 100 kJ, without rotation.

Based on the same set of experiments, Montani (1998) proposed the following equation for computing the impact force:

$$F_i^*[\mathrm{kN}] = 1.35 \cdot \exp\left(\frac{r}{3 \cdot t} \right) \cdot r^{0.2} \cdot M_E^{0.4} \cdot (\tan\phi)^{0.2} \cdot \left(m \cdot H_c \cdot \frac{g}{10^3} \right)^{0.6} \tag{10}$$

This relation was derived from the Hertz theory and was checked to be consistent with results of the impact experiments in the case of a granular layer resting on a slab.

The Swiss guideline concerning rockfall protection galleries (FEDRO, 2008) considered the previously mentioned work for proposing that the impact force on the cushion layer covering the galleries is obtained by:

$$F_i^*[kN] = 2.8 \cdot t^{-0.5} \cdot r^{0.7} \cdot M_E^{0.4} \cdot \tan\phi \cdot \left(\frac{m \cdot v^2}{2} \cdot \frac{1}{10^3} \right)^{0.6} \quad (11)$$

The Japanese Rockfall Protection Handbook (JRA, 2000; see also Yoshida et al., 2007), considering the classical model of the elastic collision of two spheres, proposed a formula for an impact of a block onto a cushion layer covering a shed:

$$\mathrm{F_i^*[kN]} = 2.108 \cdot \left(\frac{\mathrm{m \cdot g}}{10^3} \right)^{0.66} \cdot \lambda^{0.4} \cdot \mathrm{H_c}^{0.6} \cdot \left(\frac{\mathrm{t}}{2 \cdot \mathrm{r}} \right)^{-0.58} \quad (12)$$

According to the authors, the parameter λ typically ranges from 1000 kPa for sand, up to 3000 kPa for compacted fill. Even if introduced by the authors as such, this parameter should not be considered as the Lame's parameter used in the theory of elastic waves.

Plassiard and Donzé (2009) presented a formula for the equivalent static force deduced from numerical simulations using the Distinct Element Method (DEM). The model parameters were calibrated using the results of the experiments conducted by Pichler et al. (2005). For the impact of a sphere on an embankment with a symmetric cross section they found that the equivalent static force is only a function of the kinetic energy of the block:

$$F_i^* = 225 \cdot \left(\frac{m \cdot v^2}{2} \right)^{0.66} \quad (13)$$

Ploner et al. (2005) considered Newton's second law, which can be expressed as:

$$\mathrm{m \cdot \Delta v} = \int_{\Delta t} \mathrm{F_i dt}$$

From the impact experiments presented in Montani et al. (1998), Ploner et al. (2005) considered an impact duration Δt of 50 ms. During this period, the block is stopped and, consequently, $\Delta \mathrm{v} = \mathrm{v}$. Finally, Ploner et al. (2005) considered that the impact force was constant during the impact, leading to:

$$\mathrm{F_i^*} = \frac{\mathrm{m \cdot v}}{\Delta \mathrm{t}} \quad (14)$$

Ploner et al. (2005) used this force value for embankment design purpose. It is worth highlighting that the average is considered, and not the maximum impact force value.

On the contrary, Hofmann and Mölk (2012) considered the maximum value of the impact force, leading to the equivalent static force given by:

$$F_i^* = \frac{2 \cdot m \cdot v}{\Delta t} \quad (15)$$

But equation (15) is referred to be used just for checking the results received by:

$$F_i^* = \frac{v^2 \cdot m}{p} \quad (16)$$

The penetration depth p in equation (16) to estimate the equivalent static force will be taken out of the diagrams in Figure 32.

3.3.4. Limitations in Types 2 - 4 approaches

The analytical methods mentioned in the previous sections and corresponding to the design approaches of types 2 to 4, provide design engineers with easy-to-use tools. Nevertheless, their relevancy is limited due to the uncertainty associated with each method, resulting from over-simplifications or shortcuts.

Estimation of the impact force and block penetration

For instance, the penetration is overestimated by up to a factor of 2 using the expression proposed by Kar (1978) whereas it is underestimated down to about 50% using the models proposed by Labiouse et al. (1996) and by Mayne and Jones (1983) (Oggeri et al., 2004; Carotti et al., 2004; Peila et al., 2007). Symmetrically, the opposite trends are observed when estimating the impact force. For a specific case, a ratio of 1:5 between the highest and the lowest impact force values may be obtained depending on the method considered (Kister and Fontana, 2011).

Figure 24 shows the equivalent static forces estimated from different methods in the case of a block with a diameter of 2.5 m and a velocity of 20 m/s impacting an unreinforced embankment with a crest width of 2 m (named b in this figure). The smallest value for the equivalent static force is given by the formula of Plassiard and Donzé (2009) for embankments with a symmetric cross section. On the opposite, the FEDRO formula results in the highest value when considering a layer 0.5 m in thickness (named t in this figure). In the end, the force varies in a ratio of 1 to 4 depending on the method.

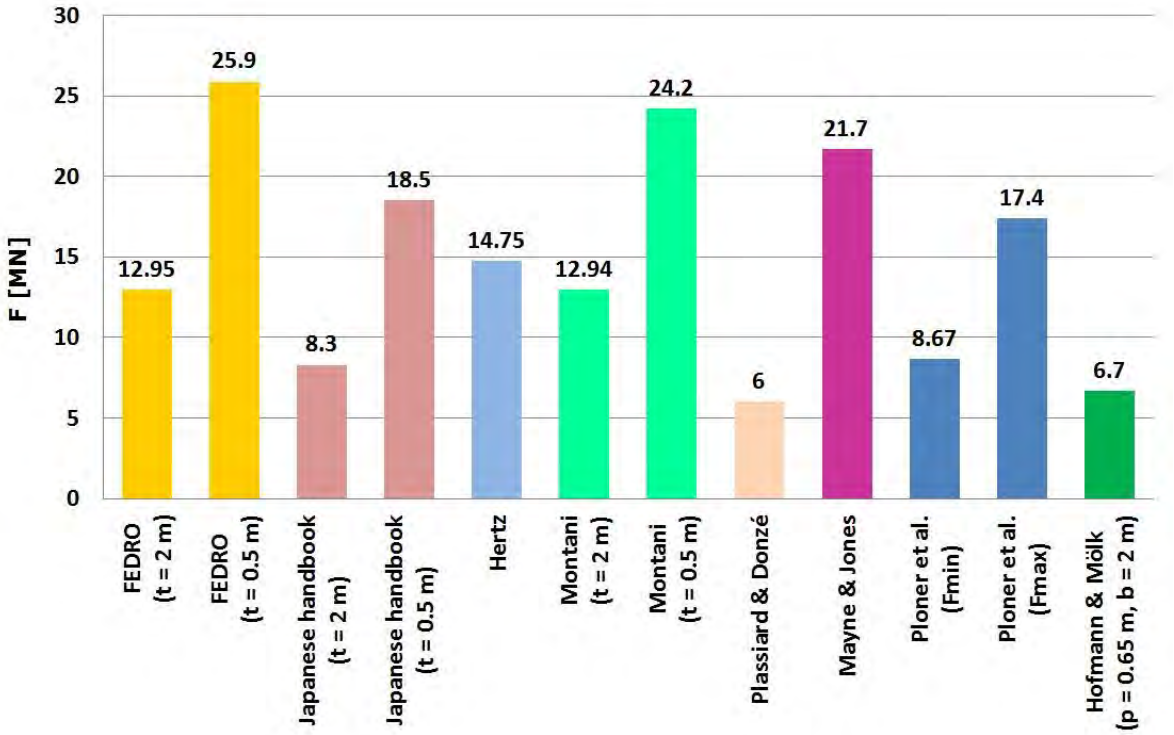

Figure 24 Equivalent static force estimated from different models (2.5 m block diameter and 20m/s initial block velocity) (Kister and Fontana, 2011, supplemented)

The main reason for these differences is that many of these methods were derived from experiments conducted in specific contexts that differ from the impact of a block on a RPE. Kar's model was developed for cohesive non-frictional soils impacted by ogive-nose projectiles at a minimum velocity of 300 m/s. Mayne and Jones's model was developed for heavy soil tamping, with a hammer having a flat tip. Labiouse's model was developed for granular strata, a 1-m maximum thickness, lying on a rigid support and exposed to impact by a spherical object amounting less than 100 kJ in energy.

Compared to the impact of a block on an embankment, these contexts differ in the projectile velocity and shape as well as the impacted structure's mechanical characteristics, dimensions and boundary conditions. An embankment is a free-standing finite volume structure, typically 3 to 7 meters in thickness in the impact direction. It is most often made of frictional non cohesive materials. It is exposed to the impact by blocks, more or less cubic or spherical in shape, with velocities in the range of 5-30 m/s, and energies from 1000 kJ to tens of MJ.

The difference in boundary conditions concerns equations 9 - 12, proposed by Labiouse et al. (1996), Montani (1998), FEDRO (2008) and JRA (2002), respectively. To a lesser extent, equations 3, 4 and 6, proposed by Pichler et al. (2005) and Wang and Cavers (2008), may also be concerned as based on experiments on a semi-infinite domain. Because some of these equations account for the impacted soil layer thickness (equations 10 - 12) their use for RPE

design purpose is tricky due to the difficulty in defining the thickness to consider (Kister, 2015).

The difference in loading conditions mainly concerns equations 1, 3 - 4 and 7. Some equations were derived from experiments conducted with ogive-nose projectiles with velocities up to 10 times that of rockfall, and without rotation. In Addition, most of these involved materials differing very much in their properties from soil, like for example concrete.

Equations 14 and 15 require assumptions concerning the impact duration (Δt). This impact duration depends on the construction material, in particular of the face (rip-rap vs. compacted soil for example). It also depends on the embankment width, as the impact by large blocks may induce a global RPE displacement conversely proportional to its width, resulting in longer impact duration for impacts close to the crest (Breugnot et al. 2015). Also, the shape of the block has a significant influence on the impact duration (Breugnot et al. 2015). This parameter may be rather variable with strong consequences on the force computed according to equations 14 or 15. For instance, according to Hofmann and Mölk (2012) Δt may vary in the interval 0.05 to 0.15 s for unreinforced embankments. For embankments reinforced with geogrids, Δt may vary in the interval 0.10 to 0.20 s (Figure 25).

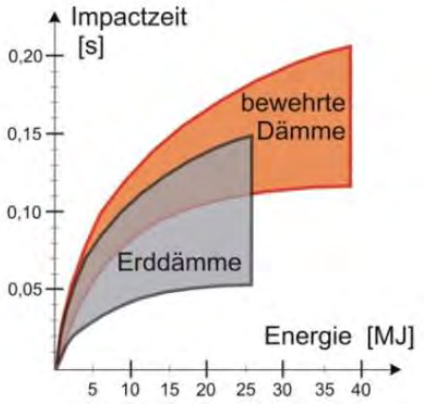

Figure 25 Impact duration estimated by Hofmann and Mölk (2012) and considered in ONORM (2013).

On the contrary, equations 5 and 13, proposed by Grimod and Giacchetti (2013) and Plassiard and Donzé (2009), are relative to embankments impacted by blocks. Nevertheless, in the former case the question of the extrapolation to other type and shape of structures rise. In the later, the proposed equation is based on numerical simulations and the same authors have shown it depends on other parameters too (Plassiard and Donzé, 2010).

It should be noted that the soil parameters considered in some of these equations are derived from static tests and concern the elastic response of soils: M_E, E and ν. The question of the validity of models intended to mimic high strain response of granular systems based on such parameters rise. Additional the parameter λ, which is used in the Japanese Rockfall Protection Handbook, does not agree with the definition of the Lamé parameter, which is used in the theory of elasticity and propagation of acoustic waves. A discussion on this is given in Kister

(2015). Mölk and Hofmann (2013) suggest that in general soil parameters are more favourable at dynamic loading than at static loading. On the other hand, for example, the shear modulus G decreases with increasing shear strain (**Erreur ! Source du renvoi introuvable.**).
Even if for specific contexts, the various authors found an agreement between experimental results and predicted ones, there is no real guarantee concerning the validity of the models, based on these parameters, when considering other materials or loading conditions (i.e. block size and velocity).

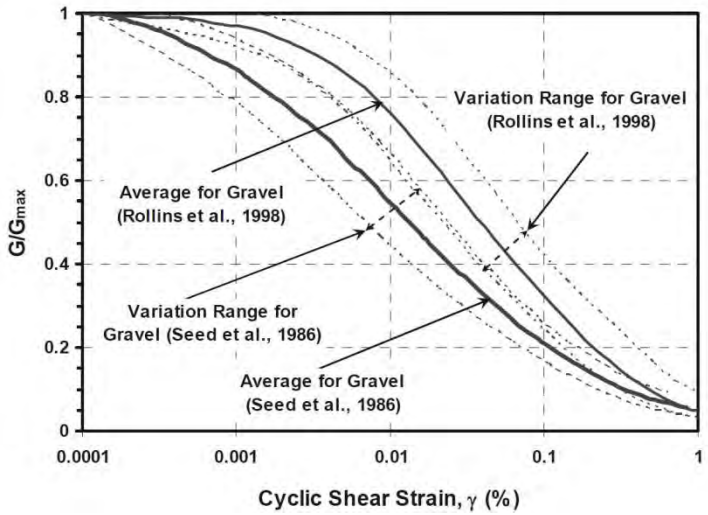

Figure 26 Typical G/Gmax ~ γ relationships for gravels (Liao et al., 2013).

In the same vein, the interaction between the soil and reinforcing geosynthetic, in terms of both interface friction and confining effect, has never been addressed to localized impact loading. The friction between these materials is modelled using friction angles and cohesion values derived from pull-out and shear tests with comparatively low deformation rates, whereas this interface has been clearly shown to govern embankment collapse (Peila et al., 2007; Ronco, 2009). Complementary investigations on the impact response of the different materials are therefore necessary. This will improve numerically based extrapolations to high-impact-energy events. The dynamic interaction between the geosynthetic and the soil should be investigated as a priority, focusing first on the friction and then on the confinement effect by the geosynthetic material in cases of localized impact.

The only equation introducing a parameter related to dynamics is equation 8, provided by Mayne and Jones (1983). They used a dynamic shear modulus G_{dyn}* instead of a static modulus of elasticity. But because the dynamic shear modulus is a function of the shear strain γ, they defined the value of G_{dyn}* as one-tenth of the dynamic shear modulus G_{max}, measured for small strains in seismic tests (**Erreur ! Source du renvoi introuvable.**). This relationship was primarily found by Hansbo (1977, 1978) for dynamic consolidation of soil and rockfill by falling weight.

Relevancy of the static equivalent load

Apart from the previous comments made on the analytical methods, the approach consisting in considering a statically equivalent load for modelling the impact force (Type 3) may not be fully appropriate.

The main reason is that this approach neglects some of the mechanisms at work during the impact, which governs the actual response of the whole structure, as depicted in section 3.2. In particular, this response depends on the stress transmitted with time within the structure, which in turn depends not only on the impact force, but also on other geometrical and mechanical parameters related to the embankment. It has been shown that for a given impact force the granular material characteristics may strongly affect the maximum value of the transmitted stress as well as its spatial distribution (Laue et al., 2008; Lambert et al., 2009; Heymann et al., 2010; Calvetti and di Prisco, 2011). The shape of the block has also been shown to have an influence on the impact force and on the transmitted stress (see the state of the art as described in Montani, 1998; Degago, 2007). And, this transmitted stress is a key factor in the RPE collapse, as suggested in section 3.2. The impact force is thus not only difficult to estimate, but is also partly inappropriate to account for what occurs within the embankment.

Relevancy of energy approaches

The analytical energy approaches (Type 4) are attractive in the sense they are based on phenomenological considerations. Nevertheless, their reliability depends on the quantification of the different energy dissipation terms: soil compaction first and then friction along shear planes. This implies defining a priori the IDZ volume and surfaces concerned by compaction and friction, respectively whereas these strongly depend on the loading conditions (impact energy and impact point location) and embankment material characteristics, which constitute the limitations of energy analytical approaches.

The first assumption concerning these methods is the definition of the IDZ. Tissières (1999) proposed a very simple model of the IDZ (Figure 27), defined by two vertical planes distant of the block diameter, and by a horizontal plane parallel to the foundation of the RPE. Hofmann and Mölk (2012) considered that the position with respect to the vertical axis of the horizontal plane delimiting the IDZ was defined by the block lower point (Figure 27). Based on an ultimate strength kinematic approach, Subrin et al. (2006) proposed to consider a basal plane with an inverse inclination (Figure 28).

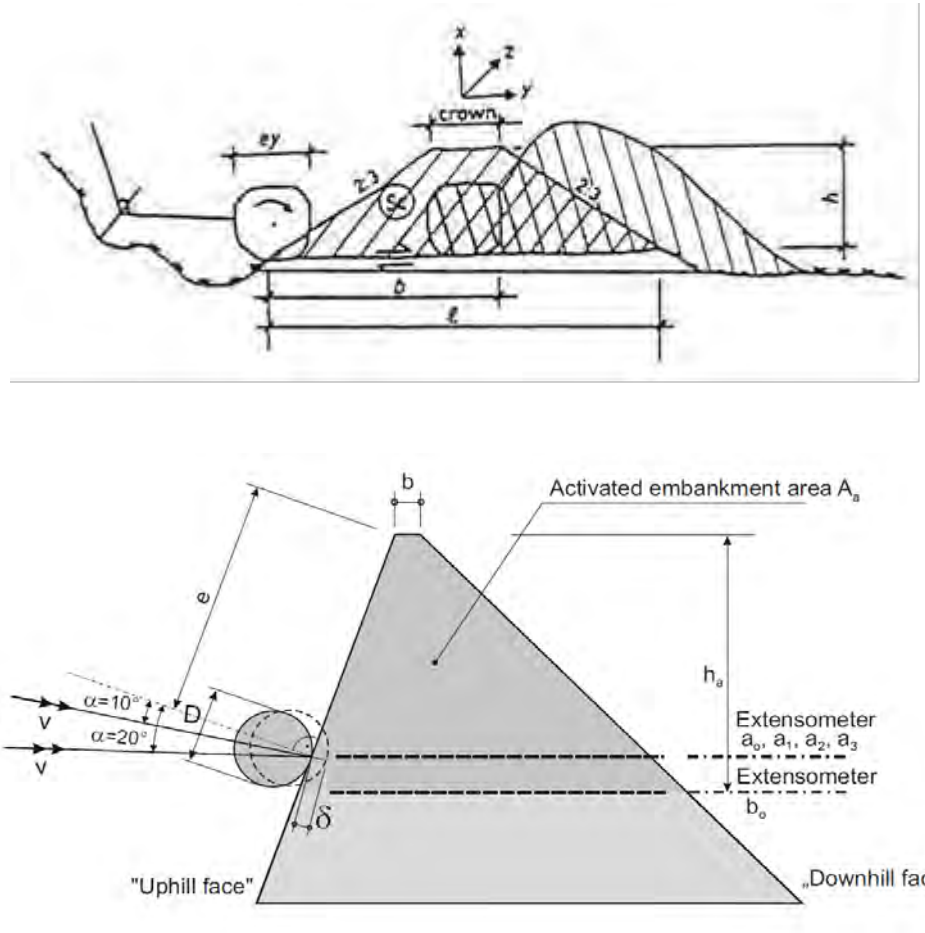

Figure 27 Model of the impact disturbed zone (IDZ) considered by Tissières (1999) (top) and by Hofmann and Mölk (2012) (bottom).

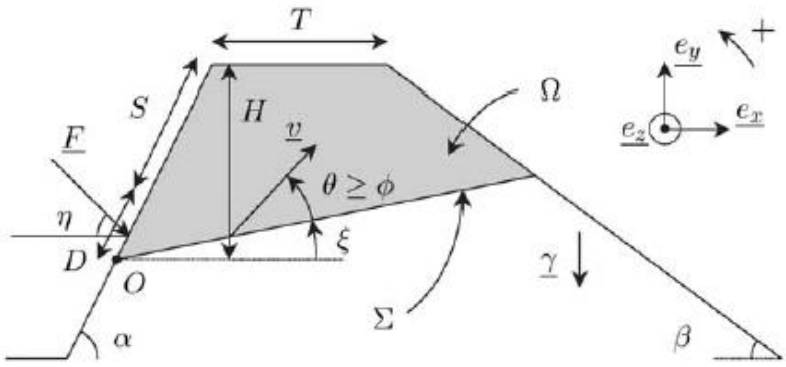

Figure 28 IDZ considered by Subrin et al. (2006).

In order to account for the block incident inclination, some authors have proposed to tilt the basal face of the IDZ (Kälin, 2006; Frenez et al., 2014; Kister and Fontana, 2011) (Figure 29). Kälin (2006) justified this choice based on the experiments conducted by the University of Torino on an unreinforced RPE (ref. B3 in Table 3) before using this IDZ for the design of the embankments of Wilerwald.

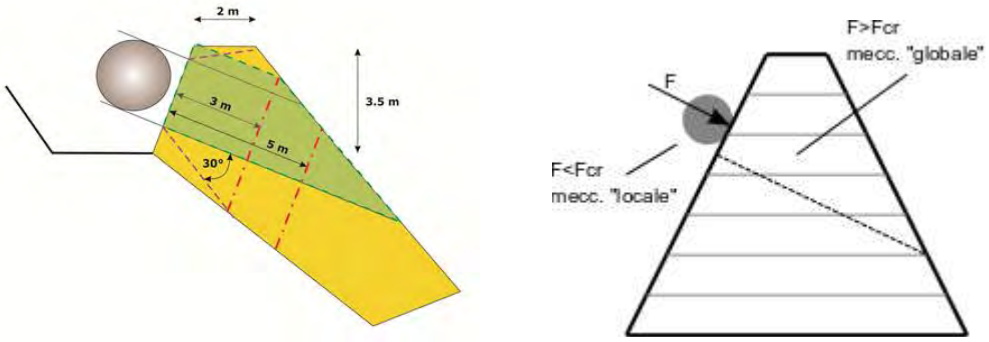

Figure 29 IDZ considered by Kister and Fontana (2011) (left) and Frenez et al. (2014) (right).

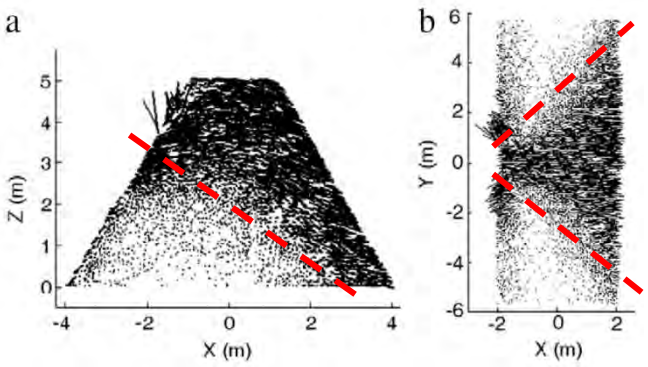

Figure 30 Displacement within the RPE during the impact. Results of DEM simulations a) by cross section, b) horizontal slice. (Plassiard and Donzé, 2009).

The idea of a tilted basal face of the IDZ seems to be underpinned by results of numerical simulations by Plassiard and Donzé (2009, 2010). Their results show relatively large displacements inside the embankment body above an inclined plane (Figure 30 a).

The IDZ is also delimited by two lateral planes. The simplest approach consists in considering two vertical and parallel planes, distant of the block diameter (Tissières et al., 1999, Kälin, 2006; Frenez et al. 2014). It is in contradiction with results presented in Figure 30 b showing that the IDZ forms a cone. This was observed in small scale experiments (Hofmann and Mölk, 2012; Blovsky, 2002, 2004) as well as in real scale experiments (Peila et al., 2002). Moreover, the dimension of the IDZ in the longitudinal axis has been shown to be higher than 5 times the block diameter for different small scale structure types (Mölk and Hofmann, 2013).

Last, the quasi-2D and 3-D experiments conducted by Kister (2015) suggested that the IDZ shape is much more complex than that proposed by the different models.

In the end, the definition of the IDZ appears highly questionable, in terms of geometry, while it is of paramount importance for computing the dissipated energy with these methods.

3.3.5. Limitations in Types 5 approaches

Existing numerical models have mainly been developed in research contexts. Some were used for developing design charts, designing specific structures, or to back analyse natural impacts (e.g. Ronco et al., 2010, Lorentz et al., 2010; Jarrin and Meignan, 2010; Peila, 2011; Murashev et al., 2013).

Even if, at first glance, models developed based on commercially available software seems easy to use, satisfactorily modelling the impact response of RPE requires highly specific skills. This in particular concerns not only the constitutive laws and mechanical characteristics to consider but also a comprehensive knowledge of the different numerical methods and theirs limits. For this reason, numerical tools are out of reach of most of the companies concerned by the design of RPEs. Also, the computation time is very long for some of the existing numerical models (Breugnot et al., 2015).

Besides, as for any numerical model an experimental data based calibration is required for guarantying the validity of the simulation results. Most often, the model parameters are calibrated based on static tests, such as triaxial tests. Some models have been validated by comparison with impact tests, on soil layers or RPEs. But due to the limited number of real scale experiments, and consequently the limited variety in structure type concerned, this validation cannot be conducted for any type of RPE, in terms of geometrical and mechanical characteristics, as well as impact conditions. Simulations out of the cases considered in the experiments should be considered as extrapolation, with possible consequence on the results relevancy. This holds for any type of modelling approach (FEM, FDM or DEM).

Other limitations more specific to the considered modelling approach may raise. For example, the DEM seems to be an ideal tool for modelling the RPE response to impact as it represents it as a collection of discrete elements and it is based on Newton's law of motion. But, in order to keep the computation time reasonable, each element is chosen much larger than the grain constituting the debris used for a real embankment's construction material (Figure 31). The difficulty is then to define the "micro-parameters" governing the interaction between these large particles so that the macro-response of the RPE represents an approximation of sufficient accuracy (see for example Breugnot et al., 2015 for a detailed description). This calibration may be based on triaxial tests results, complemented with free falling tests results, as for example in Plassiard (2007). In those back analysis the "micro-parameters" had to be varied in such a way that measured and calculated data fit together. But the question of the comparability of, for example, a slow-motion triaxial test and a high-dynamic impact scenario remains.

Figure 31 DEM model of embankment and block, both made of "glued" spheres (Plassiard and Donzé, 2010)

3.4. Applications of the Eurocodes

From a practical standpoint, the design of rockfall protection embankments challenges geotechnical engineers with the principles of currently used methods such as the Eurocodes.

Passive rockfall protection structures are not within the scope of specific Eurocodes and should be considered special structures. Moreover, the impact load should not be calculated as an accidental action according to EN 1991-1-7 (CEN, 2007), as the expressions given were developed for very different impacts and may lead to asymptotic values. Application of the Eurocodes principles requires accounting for the particular purpose of this type of structure. For example, Durville et al. (2010) have proposed a two-step procedure evaluating first the ability of the structure to intercept a block and second its post-impact residual characteristics. An ultimate limit state (ULS) verification is conducted considering the impact as an accidental situation and a block of a given mass, corresponding to a given scenario, and of maximum energy. The aim is to ensure that this block is stopped, even if the RPE collapses. Then a serviceability limit state verification is conducted to assess the post-impact embankment characteristics and considering an impact by the same block with a medium energy. This application of the Eurocodes is subjective and others could be considered.
Even if the principles of the Eurocodes may be adapted to the case of RPE, questions concerning the parameters defining the loadings may rise. The embankment response depends on both the energy of the block before impact and on the impact location. A low-energy event on the top of the structure may be more detrimental than a high-energy impact at its toe (Bertrand et al., 2010). Therefore, various combinations of these two variables should be considered, using their respective detailed statistical distributions. Moreover, the impact loading may be considered either accidental or variable, which influences the safety coefficients used for the design.

A straightforward application of the Eurocodes for the load case impact therefore does not appear meaningful. The engineer must manage the wide range of interpretation of these standards. The means to adopt the Eurocode principles, the definition of situations as well as the determination of the safety factors clearly remain the responsibility of the design engineer.

This has been briefly addressed in Grimod and Giachetti (2013), Grimod and Segor (2014) for designing existing structures. Ronco et al. (2009) also made reference to the Eurocodes for defining safety factors to be applied for the design block energy and passing height.

3.5. Italian recommendations

The Italian standard on the definitive and executive design of rockfall protection measures gives some recommendations for the input data for designing an RPE (Uni, 2012). No recommendation is given for the design properly speaking (i.e. how to use the input data for verifying the structure response). It is nevertheless indicated that the block penetration should be compared with the RPE width.

The design correspond to the case of a given single block volume in a given release area. The design of the RPE relies on the passing height and kinetic energy distributions of this block at the RPE location as obtained form trajectory simulations.

The impact point on the RPE is determined as the 95-% percentile of the design block passing heights distribution.

For this impact point, the design block velocity is the 95-% percentile of the velocity distribution, multiplied by a safety coefficient related to the trajectory simulation results quality. This coefficient varies between 1.04 and 1.21, depending on both the resolution of the digital elevation model and the way the restitution coefficients were determined.

The design block mass is the mass of the block estimated by geological survey multiplied by a safety coefficient depending on the method used to determine the volume (1.02 to 1.1).

The design kinetic energy is obtained from the design block velocity and design block mass. In case of human threat, this energy can be multiplied by a safety coefficient in the 1-1.2 range depending on the consequences in case of structure failure.

The Italian standard recommends that all the blocks from a given release scenario are stopped, accounting for the variety of block trajectories and rotational velocities in the RPE vicinity.

This standard is mentioned by Grimod and Segor (2014) for the design of the RPE built in Cogne (Italy). For this project, the structure was designed at the serviceability limit state in order to keep the deformation minimum after successive impacts, and thus reducing maintenance costs.

This standard provides a pragmatic framework for designing the RPE, mainly concerning the use of trajectory simulation results. It is worth highlighting that coefficients when cumulated range between 1.06 and 1.6, approximately, with huge consequences on the RPE cost and feasibility. Nevertheless, the maximum value may be reduced down to 1.3 if more precise data

are used for block mass estimation and propagation simulations. The main limitation in this standard is that no indication is given for the RPE design with respect to the block impact.

3.6. Austrian recommendations

The aim of this section is to briefly introduce the Austrian RPE structural design recommendations (ONR, 2013). This standard is based on the experiments conducted by Hofmann and Mölk (2012).

It explicitly refers to the Eurocodes (CEN, 2004). The impact by the rockfall is considered as an exceptional design situation, and the design addresses the ultimate limit state only.

The design block volume is established based on the block volume distribution and depends on the event frequency: percentile values of 95 to 98% of the volume distribution are considered from seldom to very high frequency events.

The design follows a type-3 approach. The static equivalent force is calculated from the impact energy, by estimating the block penetration in the structure and the impact duration.

The design considers a so-called dimensionless impact energy E^*:

$$E^* = \frac{m \cdot v^2}{2 \cdot (\rho \cdot g \cdot A_a \cdot D \cdot h_a)} \qquad (17)$$

Where m [kg] and v [m/s] are the mass and velocity of the block, ρ represents the soil density [kg/m³], g the gravity acceleration [m/s²], A_a the activated area [m²], D the block diameter [m] and h_a the activated height of the IDZ [m] (see Figure 27).

The velocity considered corresponds to the 99-% percentile of the velocity distribution obtained conducting trajectory simulations with the design block.

The activated area is defined according to the principle defined in Figure 27, bottom. The activated height depends on the block passing height as defined in section 2.2 and on the block radius. The activated area is calculated as:

$$A_a = \frac{(b + c)}{2} \cdot h_a \qquad (18)$$

Where b and c are the crest width [m] and the width of the structure at the lower block point height [m], respectively. Replacing A_a in Equation (17) by Equation (18) shows very clearly that the height h_a has been taken into account twice, but the third dimension was not taken into account in this formulation of a dimensionless impact energy E^*.

With the calculated value of E*, the penetration depth δ is determined according to the chart presented in Figure 32.

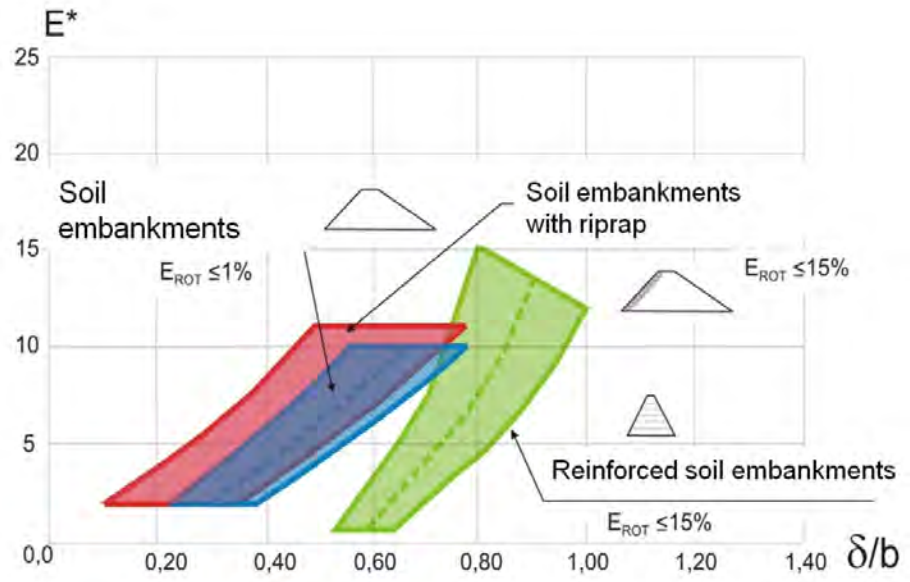

Figure 32 For a given embankment geometry and type, this chart may be used to estimate the block penetration δ for a given crest width b, and the dimensionless impact energy E according to Hofmann and Mölk (2013)*

The design equivalent static force is estimated using the formula:

$$F_d = \frac{v^2 \cdot m}{\delta} \cdot \gamma_{E,kin} \qquad (19)$$

Where:

- $\gamma_{E,kin}$ is a safety coefficient (1.0 to 1.15) depending on the consequence class,
- δ is the penetration depth determined according to Figure 25.

The static equivalent force estimated using equation (19) is applied to the IDZ, in addition to gravity loads, for assessing the ultimate limit service state (ULS). In this purpose, the force is applied in the direction of the incident trajectory inclination.
The standard does not provide any indication on the width of the IDZ to consider. Mölk and Hofmann (2013) suggest considering width of 5 - 6 and 8 - 9 times the block diameter for unreinforced and reinforced embankments, respectively.
Apart from the comments made in section 3.3.4 and in previous paragraph, this design approach is debatable in the sense many discrepancies appears in the method (Kister, 2015). These concerns:

- Experiments were conducted with a steel sphere, with a higher unit mass than a rock, resulting in a higher penetration (so-called “bullet effect”);

- E* doesn't accounts for the IDZ width (see Eq. 17 and Eq. 18);
- The force-time and velocity-time diagrams considered are not consistent one with each other. The former is based on an elastic model, with symmetric behaviour with time, while the latter is based on a plastic model.

This standard makes reference to the block rotational energy. It appears in the chart presented in Figure 32 with complements given in an annex and recommending that the maximum part of rotational energy to total kinetic energy should be less than:

- 1% for pure soil RPEs;
- 15% for RPEs with a rockery facing as well as for reinforced RPEs.

Nevertheless, there are no data supporting these limits and the value given for pure soil RPEs seems unrealistically low in practical.

It also has to be taken into account that the application of the ONR 24810:2013 may lead to large constructions as shown for an example in Figure 33.

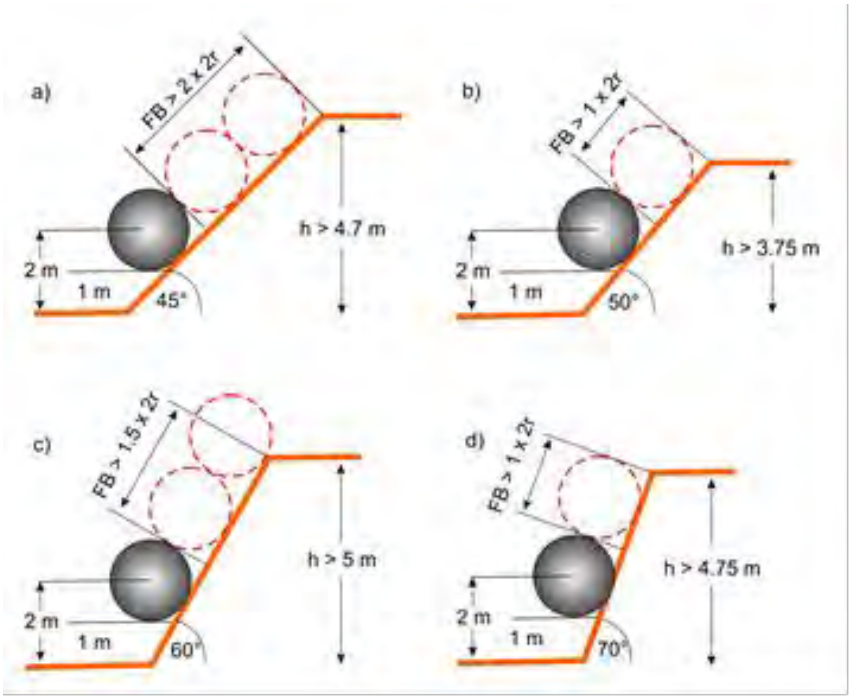

Figure 33 Visualization of the recommendations given in ONR 24810:2013 for the freeboard (see Table 2) for a block with diameter 2 m and passing height 2 m (measured to the mass centre)

4. Conclusion

RPE have been used for more than 50 years. Many research works have been conducted since the end of the 80's with the aim of improving their design, in particular with respect to the structure ability in withstanding the impact. Some of these research results have percolated down to engineering practices, either through national recommendations or design methods. In

particular, some recommendations have been published for defining the structure geometry (structure height and face inclination). Different engineering-oriented methods have been developed over the last two decades to predict the ability of RPE to withstand impacts.
Although embankment design with respect to both trajectory control and impact stability has been significantly improved, a number of limitations have been identified and should be kept in mind by design engineers.

The main limitations concerning the functional design of embankments stem from the rockfall simulation codes. In the design process, these codes are used to determine the rock passing heights and velocities respectively energies even though they are not calibrated for this purpose. Rockfall simulation codes are generally calibrated and/or validated by back analysis of previous rockfall events or rockfall experiments that are compared solely on the rocks' stopping distance. Trajectory analysis tools therefore provide relevant results for rock stopping distances: however their accuracy in estimating the rock kinematics is generally more limited. Most of the programs use simple physical models as the lumped mass model to calculate the trajectory and simple block geometry like a sphere or a cylinder for the description of the impact process with the topography. Additional, the coefficients of restitution defined only as a function of the block velocity before and after the impact, may not be able to describe the impact process with a sufficient accuracy (Kister et al, 2005, Bourrier et al., 2012). Modelling the mechanical interaction between the block and the embankment also has limitations. In particular, models for the interaction between the block and the embankment as well as with the surfaces in its vicinity lack of realism mainly due to limited knowledge on the actual impact response of the materials concerned. In addition, 3D rockfall simulation codes are currently used and calibrated with a spatial resolution that does not satisfactorily model the embankment shape (Lambert et al., 2013). Consequently, the spatial resolution of the models does not allow one to obtain a good estimate of the residual risk.

In terms of guidelines with respect to the functional design of RPE, recommendations defining a global methodology for, in particular, the definition of the design scenarios and protection goals as well as the use of rockfall trajectory simulations tools and their results are needed. These recommendations should account for the variety and limitations of the currently used tools as well as for the uncertainties. It should provide indications on the way to characterize the residual risk, based on the design scenario considered. A first draft of such a recommendation was given by Rovina et al. (2011) and could be updated and complemented.

As for embankment design with respect to impact, satisfactorily accounting for the dynamics, requires taking into account the complexity of the mechanisms at work during the impact and estimating their amplitude with time, which depends on the impact energy, embankment material characteristics and dimensions. As a consequence, analytical models are not yet satisfactory for this purpose. They fail to give good estimates of impact forces, block penetration, and energy dissipation terms. Numerical models are costly but may be identified as relevant tools for the design of embankments, providing a validation based on real-scale experiments involving impact energies of similar amplitude. In a research process, these

methods could be used jointly with experiments to improve current analytical models for different loading cases.

It has to keep in mind that RPEs generally are designed for a special scenario. So such a protection structure will only be able to offer a protection up to a certain decided level. But for this level a protection goal has to be defined. As protection goal the FEDRO defines the frequency of fatalities per year to be less than 10^{-5}. The protection goal defined by FOEN is a frequency of fatalities per year to be less than 10^{-4} - 10^{-5} (BAFU, 2016). Events corresponding to scenarios no considered or outside of the protection goal must be accepted as possible residual risk.

The analysis of existing experiments as well as existing recommendations given in this part A of the research report showed that there is still a lack of information concerning the design of RPE. Nevertheless the construction of RPEs is still going on and as it will be shown in part B of the report the basics used for the design of a RPE differ significantly from place to place in Switzerland. So there is a need for recommendations corresponding to the best practice. These recommendations should include references to the following topics:

- definition of scenarios and protection goals,
- simulation,
- design of the RPE,
- consideration of uncertainties and
- how to manage residual risks.

But also cross references to existing recommendations and standards as for example BAFU (2016) have to be included.

References

- Agliardi, F., Crosta, G.B., 2003. High resolution three-dimensional numerical modelling of rockfalls. International Journal of Rock Mechanics and Mining Sciences 40, 455-471.
- Agliardi, F., Crosta, G.B., Frattini, P., 2009 Integrating rockfall risk assessment and countermeasure design by 3D modelling techniques. NHESS 9, 1059-1073/
- Aminata, D., Yashima, A., Sawada, K., Sung, E., 2009. New protection wall against rockfall using a ductile cast iron panel. Journal of natural disaster science 30 (1), 25-33.
- BAFU, 2016. Schutz vor Massenbewegungsgefahren - Vollzugshilfe für das Gefahrenmanagement von Rutschungen, Steinschlag und Hangmuren
- Bertrand, D., Lambert, S., Gotteland, P., Nicot, F., 2010. Les merlons à technologie cellulaire. In: Lambert S., Nicot F. (Eds), Géo-mécanique des instabilités rocheuses: du déclenchement à l'ouvrage. Hermès, Paris, 369-402. (in French).
- Blovsky, S., 2002. Bewehrungsmöglichkeiten mit Geokunststoffen, PhD thesis, TU Wien.
- Blovsky, S., 2004. Model tests on protective barriers against rockfall. 15th European Young Geotechnical Engineers Conference, Dublin, Ireland.
- Bourrier, F., Lambert, S., Heymann, A., Gotteland, P., Nicot, F., 2011. How multi-scale approaches can benefit cellular structure design. Canadian geotechnical journal 48, 1803-1816.
- Bourrier, F., Hungr, O., 2011. Rockfall dynamics: a critical review of collision and rebound models. In: Lambert, S., Nicot, F. (Eds), Rockfall engineering. John Wiley and Sons, New York, ISTE ltd, London, 175-210.
- Bourier, F., Berger, F., Tardif, P., Dorren, L., Hungr, O., 2012. Rockfall rebound: comparison of detailed field experiments and alternative modelling approaches. Earth Surface Processes and Landforms, vol. 37, n° 6, 656-665.
- Brandl, H., Adam, D., 2000. Special applications of geosynthetics in geotechnical engineering. Proceedings of the 2nd European Geosynthetics Conference and Exhibition- Eurogéo II, Bologna, Italy, 305-310.
- Brandl, H., Blovsky, S., 2004. Protective barriers against rockfall. Proceedings of the 3rd European geosynthetics conference-Eurogéo III, Munich, Germany, 95-100.
- Breugnot, A., Lambert, S., Villard, P., Gotteland, P., 2015. A discrete/continuous coupled approach for modeling impacts on cellular geostructures. Rock Mechanics and Rock Engineering, Doi: 10.1007/s00603-015-0886-8.
- Broccolato, M. and Segor, V. and Recalcati, P. and Salis, S., 2010. Two major geogrid reinforced rockfall barriers in northern Italy; Proc of 9th International Conference on Geosynthetics, 1765-1768.
- Brunet, G., Giacchetti, G., Bertolo, P., Peila, D., 2009. Protection from High Energy Rockfall Impacts Using Terramesh Embankment: design and Experiences. Proceedings of the 60th Highway Geology Symposium, Buffalo, New York, 107-124.
- Burroughs, D.K., Henson, H.H., Jiang, S.S., 1993. Full scale geotextile rock barrier wall testing, analysis and prediction. Proceedings of Geosynthetics '93, Vancouver, Canada, 959-970.
- Calvetti, F., di Prisco C., 2007. Linee guida per la progettazione di gallerie paramassi. Starrylink, Italy (in Italian), 184 pp.
- Calvetti, F., di Prisco C., 2011. A new design method for rockfall shelters covered by granular layers. In: Lambert, S., Nicot, F. (Eds), Rockfall engineering. John Wiley and Sons, New York, ISTE ltd, London, 343-373.
- Calvino, A., Dumont, P., Durville, J.-L., Dussauge, C., Effendiantz, L., Evrard, H., 2001. Parades contre les instabilités rocheuses. Guide technique, Collection environnement, Les risques naturels, LCPC, Paris, 143 pp. (in French).

- Cargnel, O., Nössing, L., 2004. Comportamento di opere passive interessate da scoscendimenti massivi. Proceedings of Convegno Bonifica di versanti rocciosi per la protezione del territorio, Trento, Italy, 419-434.
- Carotti, A., Peila, D., Castiglia, C., Rimoldi, P., 2000. Mathematical modelling of geogrid reinforced embankments subject to high energy rock impact. Proceedings of the 2nd European Geosynthetics Conference and Exhibition- Eurogeo II, Bologna, Italy, 305-310.
- Carotti, A., di Prisco, C., Vecchiotti, M., Recalcati, P., Rimoldi, P., 2004. Modeling of geogrid reinforced embankments for rockfall protection. Proceedings of the 3rd European Geosynthetics Conference, Munich, Germany, 675-680.
- CCC, 2013. Technical Guideline for Rockfall Protection Structures. Christchurch City Council ○ 1. Version 2 Final March 2013, 26 p.
- CEN, 2004. EN 1997-1, Eurocode 7: Geotechnical design - Part 1: General rules. European committee for standardisation, Brussels, 168 pp.
- CEN, 2007. EN 1991-1-7, Eurocode 1 - Actions on structures- Part 1-7: General actions - Accidental actions. European committee for standardisation, Brussels, 62 pp.
- Chau, K.T., Wong, R.H.C., Wu, J.J., 2002. Coefficient of restitution and rotational motions of rockfall impacts. Rock mechanics and mining science 39, 69-77.
- Clerici, A., Giuriani, E., Cambiaghi, D., Isceri, A., Vassena, G., Marchina, E. and Cominoli, L. 2013. Rockfall Full Scale Field Tests. Landslide Science and Practice, Springer Berlin Heidelberg. Eds Margottini, Canuti, Paolo and Sassa, 461-467.
- Corté, J., Lepert, P., Rochet, L., 1989. Design of a protective system against rock falls; example of RN 90 highway. Revue générale des routes et aérodromes 669, 114-117.
- Coulon, E., Bruhier, J., 2006. Les merlons renforcés de protection. Proceedings of Rencontres géosynthétiques 2006, Montpellier, France, 367-372 (in French).
- Degago, S.A., 2007. Impact tests on sand with numerical modeling, emphasizing on the shape of the falling object. Masters Thesis, NTNU, Trondheim, Norway, 140 pp.
- Descoeudres, F., 1997. Aspects géomécaniques des instabilités de falaises rocheuses et des chutes de blocks. Publications de la société suisse de mécanique des sols et des roches 135, 3-11.
- Durville, J.-L., Guillemin, P., Berthet-Rambaud, P., Subrin, D., 2010. Etat de l'art sur le dimensionnement des dispositifs de protection contre les chutes de blocks. Collection Études et recherches des LCPC - série Géotechnique et risques naturels, Paris, 84 pp.
- FEDRO, 2008. Directive 12006: Actions de chutes de pierres sur les galeries de protection. OFROU, Bern, Switzerland, 22 pp.
- Frenez, T., Vecchiotti M., Danzi A., 2014. Un nuovo approcio per la progettazione di rilevati paramassi in terra rinforzata – il progetto di Chizzola (Ala, Trento). XXV Convegno nazionale di geotecnica. 4-6 giugno, Baveno.
- Gerbert, S., Hespel, F., 1999. Geotextile's reinforced wall for natural risk protection works. Proceedings of Rencontres géosynthétiques, Bordeaux, France, 147-150.
- Grimod, A. and Giacchetti, G., 2013. Protection from High Energy Impacts Using Reinforced Soil Embankments: Design and Experiences. Landslide Science and Practice, Springer Berlin Heidelberg. Eds Margottini, Canuti, Paolo and Sassa, 189-196
- Grimod, A. and Segor, 2014. V. Reinforced soil rockfall embankment to absorb high energy impacts along the regional road SR 507 Aymavilles-Cogne, Aosta (Italy); Proc. of GeoRegina 2014 september 28-october 1
- Hansbo, S., 1977; Dynamic consolidation of rockfill, Proc. 9th International Conference on Soil Mechanics and Ground Engineering, Vol. 2, pp. 241 - 246, Tokyo.
- Hansbo, S., 1978. Dynamic consolidation of soil by a falling weight, Ground Engineering, Vol. 11, pp. 27 - 36
- Hara, T., Tsuji, A., Yashima, A., Sawada, K., Tatta, N., 2009. Dynamic interaction between pile and reinforced soil structure - Piled Geo-wall. Proceedings of the International

Symposium on Prediction and Simulation Methods for Geohazard Mitigation, Kyoto, Japan, 457-463.
- Hearn, G., Barrett, R.K., Henson, H.H., 1995. Development of effective rockfall barriers. Journal of transportation engineering 121 (7), 507-516.
- Hearn, G., Barrett, R.K., Henson, H.H., 1996. Testing and modelling of two rockfall barriers. Transportation research record 1504, 1-11
- Hennebert, P., Lambert, S., Fouillen, F., Charrasse, B., 2014. Assessing the environmental impact of shredded tires as embankment fill material. Canadian Geotechnical Journal. Vol. 51 (5), p. 469–478, Doi: 10.1139/cgj-2013-0194.
- Heymann, A., Lambert, S., Haza-Rozier, E., Vinceslas, G., Gotteland, P., 2010. An experimental comparison of real–scale rockfall protection sandwich structures. Proceedings of the 11th International Conference on Structures Under Shock and Impact, Tallinn, Estonia, 15-26.
- Hoek, E., 2007. Practical rock engineering. Available online: http://www.rocscience.com/.
- Hofmann, R., Mölk, M., 2012, Bemessungsvorschlag für Steinschlagschutzdämme. Geotechnik, Vol. 35, pp. 22-33.
- Hofmann, R., Vollmert, L., Mölk, M. 2013. Rockfall-protection embankments - design concept and construction details. 18th International conference on soil mechanics and geotechnical engineering, Paris, 2-6 September 2013,
- Jaecklin, F., 2006. Innovative design for repairing Gondo mudslide by 20m high geogrid wall. Proceedings of the 8th international conference on geosynthetics, Ozaka, Japan, 1223-1228.
- Jarrin, P. 2001. Trajectographie des blocks rocheux. Master thesis, ENSMP, Paris.
- Jarrin, J.P., Meignan, L., 2010. Geomechanical modelling of rockfall protection bunds submitted to a dynamic impact. Proceedings of Journées Nationales de Géotechnique et de Géologie de l'Ingénieur JNGG2010 - Grenoble 7-9 juillet 2010
- JRA, 2000. Japan Road Association: Japanese Rockfall Protection Handbook (in Japanese)
- Kälin, A., 2006. Steinschlagverbauung Wilerwald, Gurtnellen, Projektbasis, Bauprojekt, 07.09.2006.
- Kar, A.K., 1978. Projectile penetration into buried structures. Journal of Structural Division, ASCE 104 (1), 125-139.
- Kister, B., Heldner, C., Ettlin, A., 2005. Der Einsatz numerischer Berechnungsverfahren zur Simulation der Steinschlagproblematik, Luzerner Baukolloquium Geotechnik, 4. März 2
- Kister, B., Fontana, O., 2011. On the evaluation of rockfall parameters and the design of protection embankments – a case study. Proceedings of Interdisciplinary workshop on rockfall protection - Rocexs 2011, Innsbruck, Austria, 31-32.
- Kister, B., Horat, P., Berger, T., 2014. Quasi-2D-experiments visualization of impacts on embankments. Proceedings of Interdisciplinary workshop on rockfall protection - Rocexs 2014, Lecco, Italy,
- Kister, B., 2015. Development of basics for dimensioning rock fall protection embankments in experiment and theory (in German), research project FEDRO 2012/003, FEDRO report 1524.
- Labiouse, V., Descoeudres, F., Montani, S., 1996. Experimental study of rock sheds impacted by rock blocks. Structural Engineering International 3, 171-175.
- Labiouse, V., Heidenreich, B., Desvarreux, P., Viktorovicth, M., Guillemin, P., 2001. Etudes trajectographiques, Prévention des mouvements de versants et des instabilités de falaises. In Programme Interreg II C, 155-205 (in French and in Italian).Lambert, S., Gotteland, P., Nicot, F., 2009. Experimental study of the impact response of geocells as components of rockfall protection embankments. Natural Hazards and Earth Systems Sciences 9, 459-467.
- Lambert, S. and Bourrier, F., 2012. What we learned from rockfall impacts. Workshop Dynamic Rockfall Impacts, Bern, 28 November 2012.

- Lambert, S., Bourrier, F., Toe, D., 2013. Improving three-dimensional rockfall trajectory simulation codes for assessing the efficiency of protective embankments. International Journal of Rock Mechanics and Mining Sciences, Vol. 60, p. 26-36. Doi:10.1016/j.irmms.2012.12.09.
- Lambert, S. and Bourrier, F., 2013 Design of rockfall protection embankments: A review, Engineering Geology, 154, pp 77 – 88, 2013
- Lambert, S., Heymann, A., Gotteland, P., Nicot, F. 2014. Real-scale investigation of the kinematic response of a rockfall protection embankment. Natural Hazards and Earth Systems Science. Vol. 14, p. 1269–1281, Doi: 10.5194/nhess-14-1269-2014.
- Laue, J., Chikatamarla, R., Springman, S., 2008. Do we need coded load assumptions for rockfall protection measures? Proceedings of Interdisciplinary workshop on rockfall protection, Morschach, Switzerland, 55-57.
- Lepert, P., Corté, J., 1988. Centrifuge modeling of the impact of large blocks of rock on a protection structure. Centrifuge 88, Paris, France, 457-465.
- Li, Q., Chen, X., 2003. Dimensionless formulae for penetration depth of concrete target impacted by a non-deformable projectile, Int. J. Impact Eng. 28 (1): pp 93–116.
- Lorentz, J., Plassiard, J-P., Muquet, L., 2010. An innovative design process for rockfall embankments: application in the protection of a building at Val d'Isère. Proceedings of the 3rd Euro Mediterranean Symposium on Advances in Geomaterials and Structures - AGS 2010, Djerba, Tunisia, 277-282.
- Maccaferri, 2009. Rockfall embankments – in Cretaz (Cogne – Aosta), Reinforced soil with the Green Terramesh system, case history, Rev: 01, January 2009.
- Maegawa, K., Tajima, T., Yokota, T., Tohda, M., 2011. Slope-rockfall tests on wall embankments reinforced with geosynthetics. Proceedings of the 6th international structural engineering and construction conference, Zürich, Switzerland, 641-646.
- Mannsbart, G., 2002. Geosynthetic reinforced protection structures in mountainous regions-examples of safe and cost-effective alternatives to conventional structures. Proceedings of the 7th International conference on geosynthetics, Nice, France, 299-301.
- Masuya, H., Amanuma, K., Nishikawa, Y., Tsuji, T., 2009. Basic rockfall simulation with consideration of vegetation and application to protection measure. Natural Hazards and Earth System Sciences 9, 1835-1843.
- Mathieu, Y., Marchal, J., 1989. Déviation de la route nationale 90 à Aigueblanche – Réalisation d'un massif renforcé par géotextile et parement Pneusol: le Pneutex. Bulletin des Laboratoires des Ponts et Chaussées 162, 77-80 (in French)
- Mayne, P.W., Jones, S.J., 1983. Impact stresses during dynamic compaction. Journal of Geotechnical Engineering 109, 1342-1346.
- Mölk, M., Hofmann, R., 2011. The Austrian standard ONR 24810: design of rock-fall protection measures. Partial factor of safety-approach and best practice for the design of rock-fall embankments. Proceedings of Interdisciplinary workshop on rockfall protection – Rocexs 2011, Innsbruck, Austria, 45-46.
- Mölk, M. and Hofmann, R. 2013 Design of rockfall embamkments according to the Austrian ÖNORM rule ONR 24810:2013. 6th Colloquium "Rock Mechanics - Theory and Practice. Vienna.
- Mongiovi, L., Bighignoli, M., Danzi, A. and Recalcati, P. 2014. An impact test on a reinforced earth embankment. Proceedings of Interdisciplinary workshop on rockfall protection - Rocexs 2014, Lecco, Italy,
- Montani, S., 1998. Sollicitation dynamique de la couverture des galeries de protection lors de chutes de blocks. PhD thesis, EPFL Lausanne, Switzerland (in French).
- Morino, A., Grassi, P., 1990. Design and construction of a reinforced earth embankment for protection against rock falls. Proceedings of the 4th International Congress on Geotextiles, Geomembranes and Related Products, The Hague, The Netherlands, 124.

- Murashev, A., Easton, M. and Kathirgamanathan, P., 2013. Advanced numerical modelling of geogrid-reinforced rockfall protection embankments Proc. 19th NZGS Geotechnical Symposium. Ed. CY Chin, Queenstown.
- Nicot, F., Gotteland, P., Bertrand, D., Lambert, S., 2007. Multi-scale approach to geo-composite cellular structures subjected to impact. International Journal for Numerical and Analytical Methods in Geomechanics 31, 1477-1515.
- Oggeri, C., Peila, D., Recalcati, P., 2004. Rilevati paramassi. Proceedings of Convegno Bonifica di versanti rocciosi per la protezione del territorio, Trento, Italy, 191-232 (in Italian)
- ONR, 2013. ONR 24810: Technischer Steinschlagschutz – Begriffe, Einwirkungen, Bemessung und konstruktive Durchbildung, Überwachung und Instandhaltung, ASI Austrian Standards Institute (Österreichisches Normungsinstitut), Ausgabe 15.01.2013.
- Paronuzzi, P., 1989. Criteri di progettazione di rilevati paramassi. Geologia tecnica 1, 23-41 (in Italian).
- Peckover, F.L., Kerr, W.G., 1977. Treatment and maintenance of rock slopes on transportation routes. Canadian Geotechnical Journal 14 (4), 487-507.
- Peila, D., Castiglia, C., Oggeri, C., Guasti, G., Recalcati, P., Sassudelli, F., 2000. Full scale tests on geogrid reinforced embankments for rock fall protection. Proceedings of the 2nd European Geosynthetics Conference and Exhibition, Bologna, Italy, 317-322.
- Peila, D., Oggeri, C., Castiglia, C., Recalcati, P., Rimoldi, P., 2002. Testing and modelling geogrid reinforced soil embankments to high energy rock impacts. Proceedings of the 7th International conference on geosynthetics, Nice, France, 133-136.
- Peila, D., Oggeri, C., Castiglia, C., 2007. Ground reinforced embankments for rockfall protection: design and evaluation of full scale tests. Landslides 4 (3), 255-265.
- Peila, D., 2011. Ground reinforced embankments for rockfall protection: From real scale tests to numerical modelling. In: Lambert, S., Nicot, F. (Eds), Rockfall engineering. John Wiley and Sons, New York, ISTE ltd, London, 393-426.
- Pichler, B., Hellmich, Ch., Mang, H. A., 2005. Impact of rocks onto gravel - Design and evaluation of experiments, International Journal of Impact Engineering 31 pp 559–578.
- Plassiard, J.-P. Modélisation par la méthode des éléments discrets d'impacts de blocs rocheux sur structures de protection type merlons, Phd-Thesis, Sciences de l'ingénieur, Université Joseph-Fourier, Grenoble, 2007
- Plassiard, J.-P., Donzé, F.-V., 2009. Rockfall impact parameters on embankments: a discrete element method analysis. Structural engineering international 19 (3), 333-341.
- Plassiard, J.-P., Donzé, F.-V., 2010. Optimizing the design of rockfall embankments with a discrete element method. Engineering Structures 32 (12), 3817-3826.
- Ploner, A., Sönser, Th., Tropper, W., 2000. Planung von optimierten Steinschlag- und Felssturzschutzmassnahmen, Felsbau, 18, Heft 1.
- Protec Engineering, 2011. www.proteng.co.jp/english/dike_testing.html.
- Rimoldi, P., Lorizzo, R., Pettinau, D., Rocallo, C., Secci, R., 2008. Impressive Reinforced Soil Structures in Italy. Proceedings of the 1st Pan American Geosynthetics Conference, Cancun, Mexico, 789-798.
- Ronco, C., Oggeri, C., Peila, D., 2009. Design of reinforced ground embankments used for rockfall protection. Natural hazards and earth system sciences 9, 1189-1199
- Ronco, C., Oggeri, C., Peila, D., Bertolo, P., Ferraiolo, F., Giacchetti, G., 2010. Numerical modeling of ground reinforced embankments used for rockfall protection. Proceedings of the 3rd Euro Mediterranean Symposium on Advances in Geomaterials and Structures-AGS 2010, Djerba, Tunisia, vol. 2, 269-276.
- Rovina, H., Liniger, M., Jordan, P., Gruner, U., Bollinger, D., 2011. Empfehlungen für den Umgang mit Sturzmodellierungen, Swiss Bull. angew. Geol., Vol. 16/1.

- Simmons, M., Pollak, S., Peirone, B., 2009. High energy rock fall embankment constructed using a freestanding woven wire mesh reinforced soil structure. Proceedings of the 60th Highway Geology Symposium, Buffalo, New York, 290-301.
- Subrin, D., 2006. Modélisation analytique et numérique pseudo-statique des merlons de protection contre les chutes de blocks rocheux. Proceedings of Journées Nationales de Géotechnique et de Géologie, Lyon, France, 145-152 (in French)
- Sung, E., Yashima, A., Aminata, D., Sugimori, K., Sawada, K., Inoue, S., Nishida, Y., 2008. Numerical assessment of the performance of protecting wall against rockfall. Proceedings of the 5th International Symposium on Earth Reinforcement, Kyushu, Japan, 861-867.
- Tissières, P., 1999. Ditches and reinforced ditches against falling rocks. Proceedings of the Joint Japan-Swiss Scientific Seminar on Impact load by rock fall and design of protection structures, Kanazawa, Japan, 65-68.
- Toe, D., Lambert, S., Bourrier, F., Berger, F., 2013. Improving rebound models in 3D rockfall simulation codes used for the design of protection embankments. 8-th International Symposium on Impact Engineering (ISIE2013), Osaka, Japon, 2-4 sept.
- UNI, 2012. UNI 11211-4:2012: Opere di difesa dalla caduta massi - Parte 4: Progetto definitivo ed esecutivo (in Italian).
- Usiro, T.; Kusumoto, M.; Onishi, K.; Kinoshita, K., 2006. An experimental study related to rockfall movement mechanism, Doboku Gakkai Ronbunshu FVOL. 62, No. 2, pp 377-386.
- Wang, B. and Cavers, D.S., 2008. A simplified approach for rockfall ground penetration and impact stress calculations. Landslides, January 2008.
- Willye, D.C., 2014. Rock Fall Engineering. CRC Press. 270 p.
- Whitside, P.G.D., 1986. Discussion on rockfall protection measures. Conference on rock and excavation engineering in an urban environment, Hong Kong, pp 490-492.
- Yoshida, H., 1999. Recent experimental studies on rockfall control in Japan. Proceedings of the Joint Japan-Swiss Scientific Seminar on Impact load by rock fall and design of protection structures, Kanazawa, Japan, 69-78.
- Yoshida, H.; Nomura, T.; Wyllie, D. C.; Morris, A. J., 2007. Rockfall sheds - application of Japanese designs in North America, 1st North American Landslide Conference, June 5th 2007, #98205 ASCE.

Lucerne University of
Applied Sciences and Arts

HOCHSCHULE
LUZERN

Technik & Architektur

Analysis of Existing Rockfall Embankments of Switzerland (AERES)

Part B: Analysis of the collected data and comparison with up-to-date knowledge

Stéphane LAMBERT[1] and Bernd KISTER[2]

[1] Irstea, 2 rue de la papeterie, 38402 Saint Martin d'Hères cedex, France, + 33 4 76 76 27 94, stephane.lambert@irtsea.fr

[2] Lucerne University of Applied Sciences and Arts, Technikumstrasse 21, CH – 6048 Horw, Switzerland. Current position: kister - geotechnical engineering & research, Neckarsteinacher Str. 4 B, D – Neckargemünd, +49 6223 71363, kister-ger@t-online.de

Commissioned by the Federal Office for the Environment (FOEN)

July 2017

Imprint

Commissioned by
Federal Office for the Environment (FOEN), Hazard Prevention Division, CH-3003 Bern.
The FOEN is an agency of the Federal Department of the Environment, Transport, Energy and Communications (DETEC).

Contractors
Lucerne University of Applied Sciences and Arts, CH-6048 Horw
Irstea, F-38402 Saint Martin d'Hères

Authors
Bernd Kister
Stéphane Lambert

FOEN support
Bernard Loup, Hazard Prevention Division
Arthur Sandri, Hazard Prevention Division

Notes
The AERES report consists of three parts:
- Part A: State of knowledge
- Part B: Analysis of the collected data and comparison with up-to-date knowledge
- Part C: Small-scale experiments

This study/report was prepared under contract to the Federal Office for the Environment (FOEN). The contractor bears sole responsibility for the content.

Suggested form of citation for Part B
Lambert S., Kister B. 2017: Analysis of Existing Rockfall Embankments of Switzerland (AERES); Part B: Analysis of the collected data and comparison with up-to-date knowledge. Federal Office for the Environment, Bern, 21 p.

Foreword

This document reports on the collection of data concerning RPE built in Switzerland and their analysis. It follows and makes implicit reference to the report entitled "Part A: state of knowledge".

This collection was conducted during interviews with cantons and design companies concerned by this type of protective structure, with the aim of giving a global image of this structure park, in terms of dimensions and design, as well as providing pieces of information on the design methods in use in Switzerland nowadays.

The RPE inventory is not intended to be exhaustive but to be representative of the Swiss park. The study gathers exhaustive data concerning a large number of RPE and their design. The interviews revealed that the total number of RPEs in Switzerland by far exceeds 250 units. The data collection mainly focuses on more recent structures as older structures suffer from limited available documentation and very simple design. Consequently, restricting the study to newest ones is not detrimental to the aim of this study.

This report first describes the RPEs concerned by the data collection, before giving a brief overview of design approaches in use. Then, RPEs are analysed, in order to evaluate the current design practices with respect to impact strength. In this purpose, structures are compared one to each other. Basically, the aim of this comparison is to see to which extent the lack of well-established design rules leads to variability in the design of RPEs. The lack of well-established design rules should result in an inconsistency in the structure dimensions and possibly in apparently under-sized structures. Then, a simple and expedient assessment criterion, based on up-to-date knowledge, is proposed in order to evaluate the RPEs. Furthermore, the collected data are compared to criteria proposed by Kister (2015) based on small and half scale experiments. Last, the freeboard, if defined for the RPEs, had been compared to the target values given by the Austrian standard ONR 24810 (2013).

Content

1. Park description

1.1. Park considered

On total, the analysis is based on 68 embankments designed less than 20 years ago, except one built in the beginning of the 80's. 10% are still projects, but are considered in this study as it provides indications on the currently used design methods.

This sample is considered representative of existing embankments and provides a clear illustration of the design methods in use nowadays in the different cantons of Switzerland. More precisely, 13 cantons are concerned, with variable number of RPEs each (1 in BL, GL, OW and TI, 2 in JU and LU, 3 in VD, 4 in UR, 5 in NE and SZ, 10 in GR, 11 in BE and 22 in VS).

Some Swiss RPEs were also intended to intercept snow avalanches. The design of most of these structures was governed by snow avalanche containment criteria: these structures were not considered in the study.

The data were collected considering RPEs as continuous units. When two or more structures are located on the same site and result from the same design, these structures had been considered as different. In case the dimensions vary along its length, the tallest profile and corresponding design parameters are considered.

1.2. Dimension and shape

The RPEs are described based on data related to their shape and dimensions along their length (L) and cross sectional shape, as illustrated in Figure 1.

The dimensions of the RPEs considered in the analysis range between 15 and 700 m in length and 1.5 and 13 m in height. Approximately 64% of the embankments have a height of 4 m or less, but only approximately 6% have a height larger than 7 m (Figure 2). The average values are 155 m in length and 4.3 m in height respectively (Table 1). It is worth highlighting that the cumulative length of the 68 embankments exceeds 10 km.

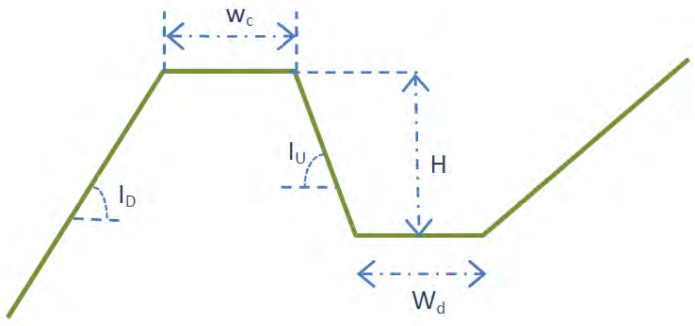

Figure 1 Definition of main data used for describing the cross section of the RPEs

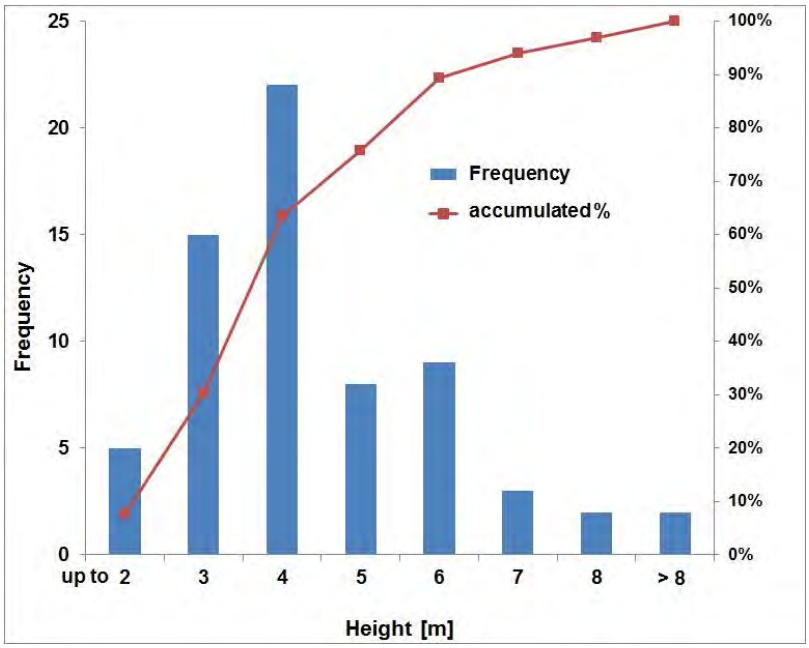

Figure 2 Bar chart of embankment height

Table 1 Minimum, maximum and average values for parameters describing the 68 RPEs

	W_c (m)	H (m)	L (m)	I_U (°)	I_D (°)	W_d (m)
Min.	1	1,5	15	33	33	0,5
Max.	8,6	13,2	700	87	80	14
Average	2,1	4,3	155	65	43	4

The vast majority of the RPEs is made of compacted soil, with a rockery facing at the uphill slope. About 30% of the RPEs exhibit a bi-linear uphill face with two different inclinations. The higher inclination corresponds to the lower part made of rockery. In such cases, an average inclination value was considered for I_U (Table 1). The motivations for such a design choice are:

(i) high inclination is required for stopping rolling blocks and thus mainly concerns the lower part of the uphill face and

(ii) soil close to the crest favour the energy dissipation and thus stopping blocks with high passing height, while avoiding downhill ejection of block or rockery fragments resulting from the impact on the rockery facing.

About 15% have their uphill face made of compacted soil (or debris) and consequently have lower uphill inclination values (down to 33°). Less than 10% of the RPEs include reinforcing elements (geogrid mainly, in the core or face only). About 20% of the RPEs have a downhill face with an inclination higher than 45°, obtained either with rockery or reinforced earth.

1.3. Intended structure capacity

The design with respect to the protection function of the 68 RPEs was conducted by 13 different companies.

In many cases, trajectory simulation results used for designing the structure were provided by another company than the design company. One or two of the following codes were used for this purpose: RockyFor3D, RofMod, RockFall (Dr Spang), CRSP, Ramms, RocPro, RocFall (rocscience). In some rare cases, no simulations were conducted. Half of the simulations include the RPE in the profile. More than 60% of the simulations were conducted using 2D models. When provided, the number of runs is most often less than 1000.

Table 2 Minimum, maximum and average values defining the impact loading by the block

	Weight (kN)	Velocity (m/s)	Kinetic energy (kJ)	Passing height (m)
Min	15	10	159	0
Max	1600	33,4	50000	6
Average	262	21,8	7478	2,2

These structures were designed considering reference blocks with a weight and a kinetic energy in very wide ranges: 15 to 1600 kN and 160 kJ to 50 MJ, respectively (Table 2). About 40% and 64% of the embankments have been designed for stopping blocks with a kinetic energy less than or equal to 2000 and 4000 kJ respectively (Figure 3). 18% of the RPEs were designed for kinetic energies higher than 10 MJ.

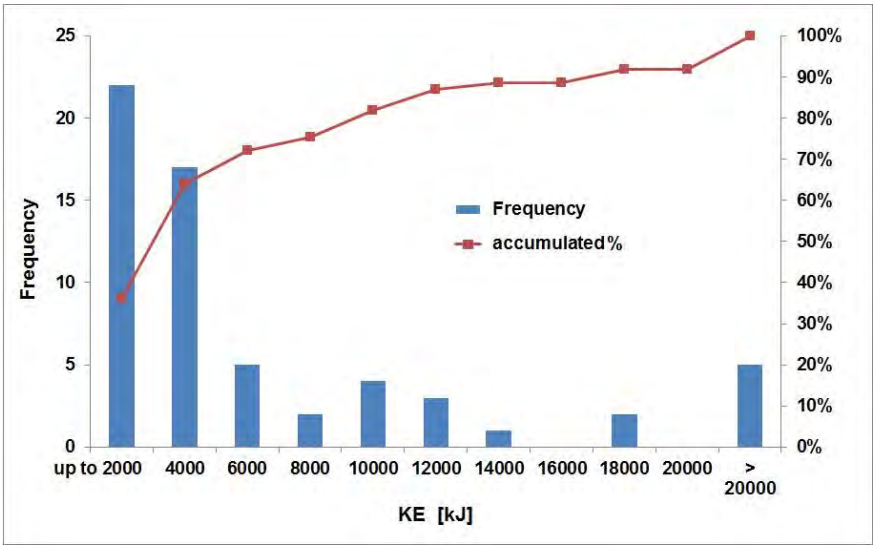

Figure 3 Bar chart of kinetic energy used for the design, total 61 embankments

2. Design methods overview

2.1. Design with respect to block trajectory control

The percentile used for defining the design values vary from 90 to 100%. Some cantons impose 95%. Besides, the accepted residual hazards (i.e. after RPE erection) vary according to the element at risk and return period of the event (30, 100 or 300 year return period). Significant percentages of

blocks overpassing the RPE are sometimes accepted in case of a 300-year return period event. Last, construction cost is also a strong constraint, sometimes leading to the acceptance of a higher risk level (use of EconoMe).

The design with respect to block trajectory control mainly refers to the block passing height. Nevertheless, the analysis of the available reports concerning the 68 RPEs revealed that there was no unique definition of the block passing height from one company to the other. It sometimes concerns the block lower point, higher point or gravity centre, depending in particular on the trajectory simulation tool used. In addition, in many cases the considered definition is not explicitly indicated. Besides, in some cases, the passing height is obtained from simulations in the absence of RPE while in others its projected topography is considered. As a consequence, the collected data are biased and no conclusion may be derived.

The authors of this study recommend using the distance along the vertical axis from the toe of the uphill face of the RPE and the block gravity centre position as resulting from rockfall propagation simulations integrating the projected topography. This definition is consistent with the definition of the RPE height given in Figure 1.

While both the trajectory inclination and the block rotational velocity before the impact on the RPE face have been shown to affect the efficiency of the RPE in stopping the block, the corresponding values are very seldom provided.

There is also no consensus in terms of freeboard to consider, when indicated. The ratio of the freeboard to the block radius is extremely variable (0 to 1.2). The construction cost is often an argument for reducing the freeboard.

2.2. Structural design

Globally, the structural design of RPEs is empirical, based on the experience and habits of the design company. For instance, no information concerning the structural design is given for more than 60% of the 68 RPEs. On the other hand, some design companies have developed their own approach for designing embankments.

The impact loading was considered for the design of ten RPEs, four considering the recommendations provided by the Austrian standard (ONR 24810) and one considering the method proposed by Tissières (1999). Five were designed following the recommendations by FEDRO (2008), “Exposure of rock sheds due to rockfall”, for estimating the static equivalent force.

3. Analysis

In the absence of reliable, well established or recognized design method, the park is analysed based on three different approaches:

1. RPEs are compared one to each other, for tracking anomalous cases, based on the basic assumption that for a given energy the RPEs should have very similar dimensions.
2. Then a simple but pragmatic assessment criterion is used. The proposed criterion accounts for the main mechanisms occurring during the impact of the embankment by a block. It has been developed considering the existing real scale experiments data available in the literature.
3. Last, the structure park is evaluated based on criteria proposed by Kister (2015) after conducting small and half scale experiments.

The number of RPEs concerned by the different approaches depends on the availability of the necessary data. 54 and 47 RPEs out of the 68 were concerned by approaches (1, 2) and 3 respectively.

3.1. Cross-comparison

This comparison is conducted based on the idea that for similar impact cases the RPEs should exhibit similar dimensions. This assumption is acceptable for this structures park, as it is rather homogeneous in terms of structure type and constitutive materials.

Figure 4 gives the mid-height width of RPEs, sorted according to their height, together with the block kinetic energy these RPEs are supposed to resist. For a given class of structure dimensions, certain variability in block kinetic energy is observed. For example, the block kinetic energy for structure no.°28 is much higher than that for structure no.°1, of similar height and mid-height. This also holds for RPEs no.°14 and no.°29 compared to RPEs no.°57 and no.°58 respectively. As for RPEs with a height higher than 6 m, the block kinetic energy is very high for 4 RPEs compared to others while the difference in dimensions is not that pronounced (ID-Nos. 42, 43, 62 and 63).

Nevertheless, it is not possible at this stage to conclude on the proper design of these structures. The main conclusion is that there exists a discrepancy from one structure to the other. This may results from the lack of well established design rule.

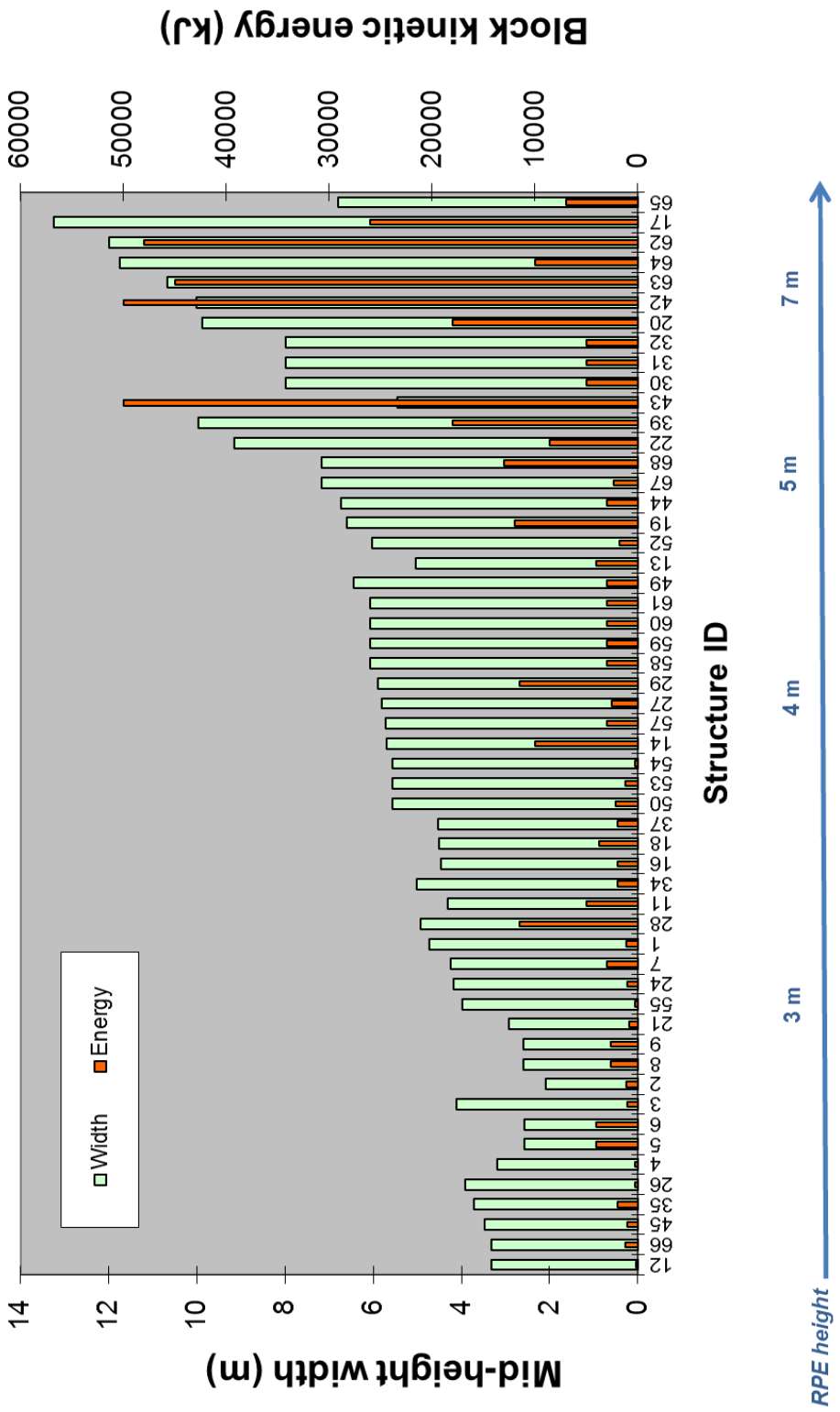

Figure 4 Comparison of RPEs based on their height and mid-height width

3.2. Real scale experiments based efficiency criterion

3.2.1. Criterion definition

A criterion considering real scale experiments data available in the literature is proposed in order to expediently assess the efficiency of a RPE in withstanding the impact by a block.

The ability of an embankment in resisting the block impact may be assessed based on its post-impact deformation and in particular on the displacement of the downhill face, opposite the impact. Indeed, the post-impact structure stability is strongly related to the displacement of this face. In case the impact energy exceeds the structure capacity the structure will be destroyed and the downhill face displacement will be very large.

Figure 5 plots the post-impact displacement values measured by different authors after conducting real-scale impact experiments involving block with energies in the 1000-5000 kJ range. The impacted structures were 3 to 4.2 m in height, 3 to 4.3 m in mid-height width with an uphill face inclination of 60 to 90°. Impacts were mainly located in the structure mid—height vicinity and the blocks had downward incident trajectories. Even if the global trend shows an increase in displacement with the block kinetic energy, a high scattering is observed.

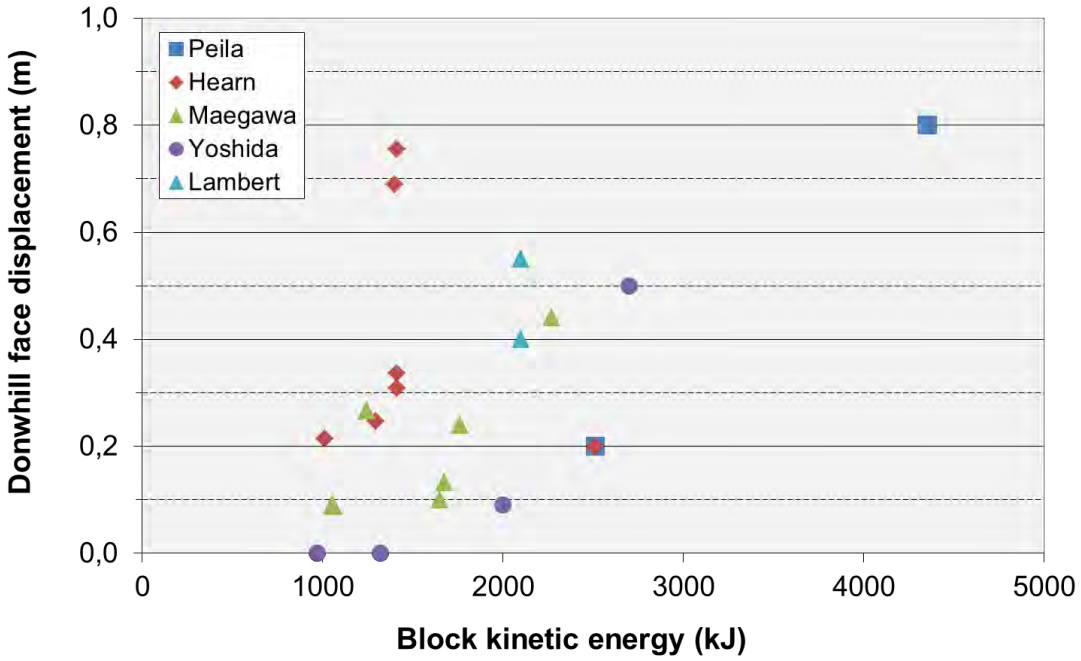

Figure 5 Post-impact downhill displacement measured after real scale experiments (for detailed information, see Table 3 of report “Part A: state of knowledge”)

The scattering is due to differences from one impacted structure to the other in terms of vertical cross sectional shape and dimensions, design and construction materials. The height ranged from 3 to 4.2 m and the mid-height width ranged from 3 to 4.3 m. Structures tested by Hearn were rectangular in cross section, with facings and core reinforced with timber and geotextile respectively. Peila tested reinforced structures with a trapezoidal cross sectional shape. Both faces were reinforced, allowing increasing the structure impact strength (Peila et al., 2002), in a ratio that can be estimated up to 2 from the small scale experiments conducted by Blovsky (2004). This

explains why displacements are much smaller than for structures for which only the uphill face is reinforced. Data provided by Lambert et al. (to be published) concern rectangular in cross section sandwich structures made of gabion cages.

In spite of these differences, this data set provides a reliable and valuable basis for developing a simple and expedient RPE assessment criterion.

The criterion was developed with the aim of finding a simple relation between the downhill face displacement and the block kinetic energy. Due to the differences in structure dimensions and impact energy, the experimental results should be normalised. As for the block kinetic energy, it is proposed to normalize this parameter by the structure dimensions. Indeed, the block kinetic energy is transferred to the structure where it is dissipated mainly by compaction, but also by friction. The amplitude of both these dissipative mechanisms depends in particular on the structure dimensions: the smaller the structure, the smaller the dissipation. In an initial approach, the cross sectional area of the structure along the vertical axis may be considered as representative of the structure dimensions in the impact direction. As for the downhill displacement, it is proposed to normalize this parameter by the mid-height structure width, which is representative of the structure dimension in the impact direction, irrespective of the cross sectional structure shape.

Figure 6 shows the results presented in Figure 5 normalised by the structure cross sectional area and by the structure mid-height width. It can be seen that the displacement is higher than 25% of the structure width when the ratio of kinetic energy to cross section area exceeds 250 kJ/m². The 25% limit displacement value is in accordance with some methods proposed in the literature suggesting that above this limit, the structure is no longer stable after the impact.

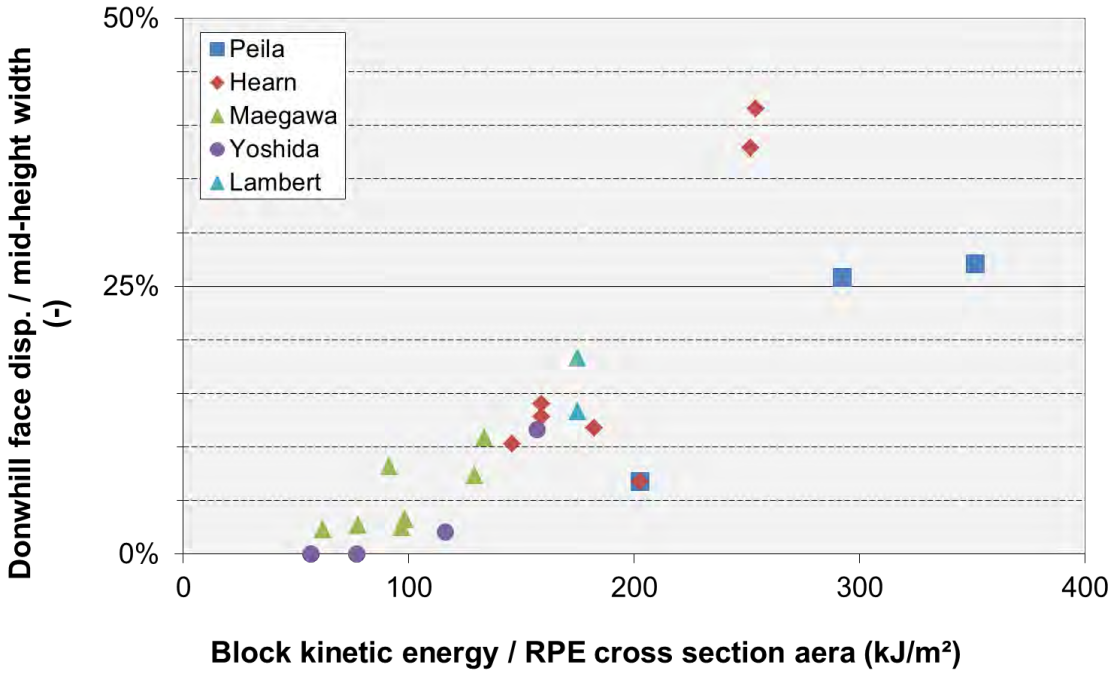

Figure 6 Relative downhill face displacement as a function of the ratio of the block kinetic energy to the RPE cross section area after real scale impact tests. (for detailed information, see Table 3 of report "Part A: state of knowledge")

Considering this finding, the nominal structure capacity assessment criterion is defined as:

$$C_{25} = \frac{KE/A}{250}$$

where KE is the block kinetic energy (kJ), A is the structure cross section area along the vertical axis calculated from the ditch elevation (m²). A C_{25} value less than 1 indicates that the structure is able to withstand the block kinetic energy, considering that the maximum allowable downhill displacement is less than 25% the mid-height width.

Basically, this criterion means that above a value of 1, the kinetic energy of the boulder is in excess with respect to the embankment capacity in stopping the block while limiting the deformation to a given value.

The validity of this criterion, and in particular of the 250 threshold value, is related to the experimental conditions (structure design, block kinetic energy…). These conditions are:

- Reinforced structure;
- RPE with an height in the 3 - 4.2 m range, and a mid-height width in the 3 - 4.3 m range;
- Block with a 30° approx. downward incident trajectory;
- Impact point located at a significant distance from the crest (at least ¼ of the structure height).

The relevancy of this criterion may be questionable out of this validity domain. For example, an impact closer to the RPE crest or with an incident trajectory less than 30° would be more detrimental to the structure.

It can be observed that the 25% relative displacement value is a safe value. Indeed, results from Peila have shown that collapse occur for relative displacement higher than 40% in case of a structure reinforced on both faces.

Before applying this criterion to Swiss RPEs it has been applied to structures presented in the literature. In particular, some recent publications detail the design of existing structures, based on various methods, and with specific focus on the structural design with respect to block impact strength. Table 3 gives the C_{25} for RPEs described in 5 different publications. All the concerned structures are reinforced, with a height ranging from 5.4 to 10 m. None of the C_{25} values for these structures exceeds the threshold value of 1, suggesting this criterion is consistent with the different methods used for these specific structures.

Table 4 Application of the C_{25} criterion to RPEs detailed in the literature

Authors		Frenez et al., 2014	Lorentz et al., 2010	Grimod and Giachetti, 2013	Simmons et al., 2009	Rimoldi et al., 2008
Block kinetic energy	*MJ*	4	10	3	10	15
Structure height	*m*	5,4	6,5	10	8	10
Structure cross section	*m²*	22	44	88	50	76
C_{25}	-	**0,7**	**0,9**	**0,2**	**0,8**	**0,8**

Considering the data collected in the frame of this study, the main limitation with this criterion is the structure type. The vast majority of RPEs built in Switzerland are unreinforced ground compacted structures with a rockery facing. In such cases, larger downhill face displacements are expected, with relative values exceeding by far the 25% limit for the same kinetic energy. This means that a C_{25} much smaller than 1 should be adopted for unreinforced structures. As a consequence the limit value considered in the following is fixed to 0.5.
The criterion thus becomes: $KE < 125 * A$

Besides, the application of this criterion to this structure park faces the problem of data availability and reliability. For instance, the block incident angle is very seldom provided and the definition of the block passing height is extremely variable from one case to the other. As a consequence, two of the criteria defining the validity domain could not be checked.

3.2.2. Results

Figure 7 gives the C_{25} value of the 54 RPEs for which the required data are available. The analysis reveals that more than 42% of the RPEs have a C_{25} value less than 0.5 (23 RPEs) and thus may be considered able to withstand the impact by the block (Figure 7).

On the other hand, the C_{25} exceeds the value of 1 in 17 cases, among which 7 cases exceed the value of 2. It is worth highlighting that 2 out of these 7 critical cases could not be clearly identified after the cross comparison (ID-Nos. 5 and 6). On the contrary, the 4 tallest ones were identified (ID-Nos. 42, 43, 62 and 63). For these later cases, the C_{25} is used out of its validity domain in terms of RPE height, and impact point. For instance, in 2 cases the height is higher than 7 m and the free board is less than half the design block diameter (ID-Nos. 62 and 63). The damage potential to elements at risk of these high kinetic energy blocks justify conducting complementary analysis on these highly critical structures.

To a lesser extent, the proper design of RPEs having a C_{25} value between 0.5 and 2 should also be assessed.

Prior to any assessment of apparently critical structure, the relevance of using the C_{25} should be checked depending on the impact case vs. the experimental conditions. Second, the acceptability of the destruction of the RPE should be checked versus the return period of the event considered: destruction may be tolerated in case of a 300-year return period event but not for a 30-year one.

3.3. Small scale experiments based efficiency criterion

As a result of small and half scale tests with rotating blocks, Kister (2015) suggested criteria related to the efficiency of pure soil embankments in stopping a block, considering the risk of both structure punching through and over topping. Kister (2015) concluded from the experiments that in order to prevent from these risks, the structure should be such that the three following criterion should be fulfilled:

(i) The batter at the uphill slope should be at least 60°.
(ii) The thickness of the crest, w_c in Figure 8, should be 1.2 times the design block diameter.
(iii) At the impact point the thickness of the embankment should be 3 times the block diameter.

Following these three statements a cross section for an embankment can be constructed graphically. This cross section is shown in Figure 8.

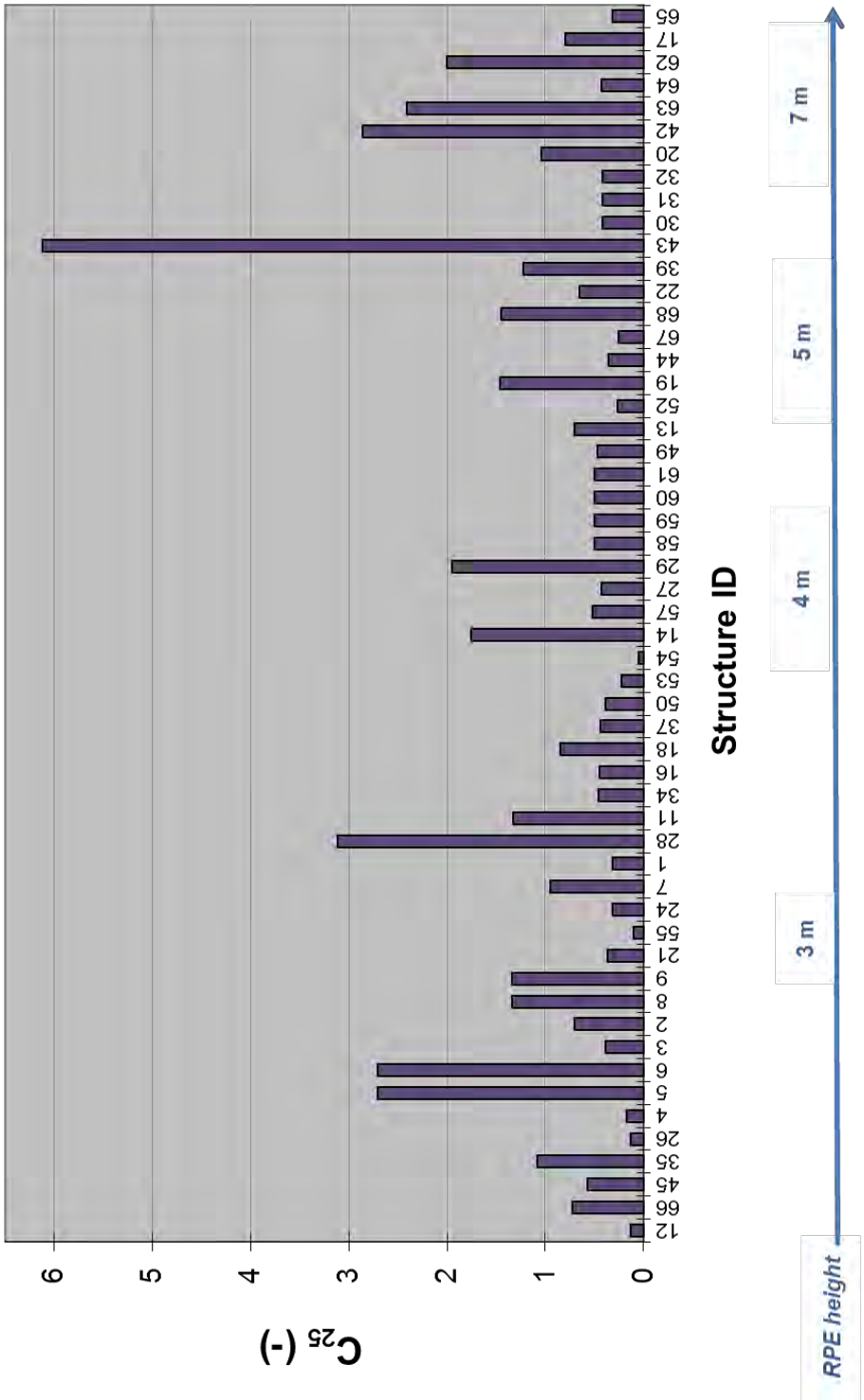

Figure 7 Application of the C_{25} efficiency criterion to RPEs

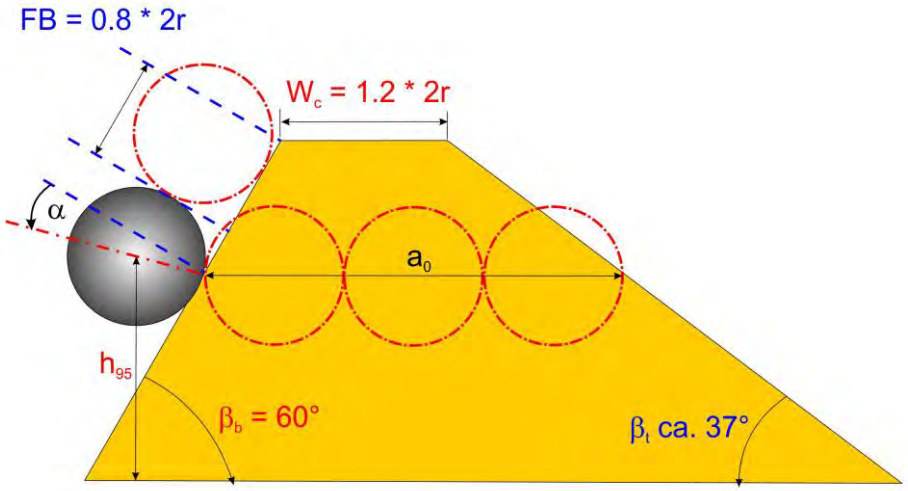

Figure 8 Cross section graphically constructed taking into account the three conditions given by Kister (2015)

For embankments with rockery criterion (i) is generally fulfilled. The criterion (ii) could be checked for 51 embankments where data of crest thickness as well as data of block volume or mass was available. The block diameter was calculated assuming that the block shape was a sphere. In the end, this criterion is fulfilled for 14 RPEs (Figure 9).

9 RPEs have a crest width-to-block diameter value less than 0.5. These are the most critical as most of the experiments with this ratio led to structure punching, in particular for a rotating block with an impact close to the crest. These 9 most critical RPEs have in common a relatively small crest width value (1 to 1.5 m). The concerned cases may be classified in two configurations:

- RPE height less than 3 m, exposed to a more or less rolling block with a diameter close to the structure height (typically 2.6 m) (ID-Nos. 1, 2 and 3)
- RPE taller than 3 m and exposed to a block with a high passing height with respect to the structure height so that the freeboard is less than 1 block radius (ID-Nos. 11, 62, 63, 64 and 68).

In both configurations, the structure width at the impact height is less than three times the block diameter. The block is thus faced by a relatively small volume of the RPE as opposition, favoring punching of the RPE.

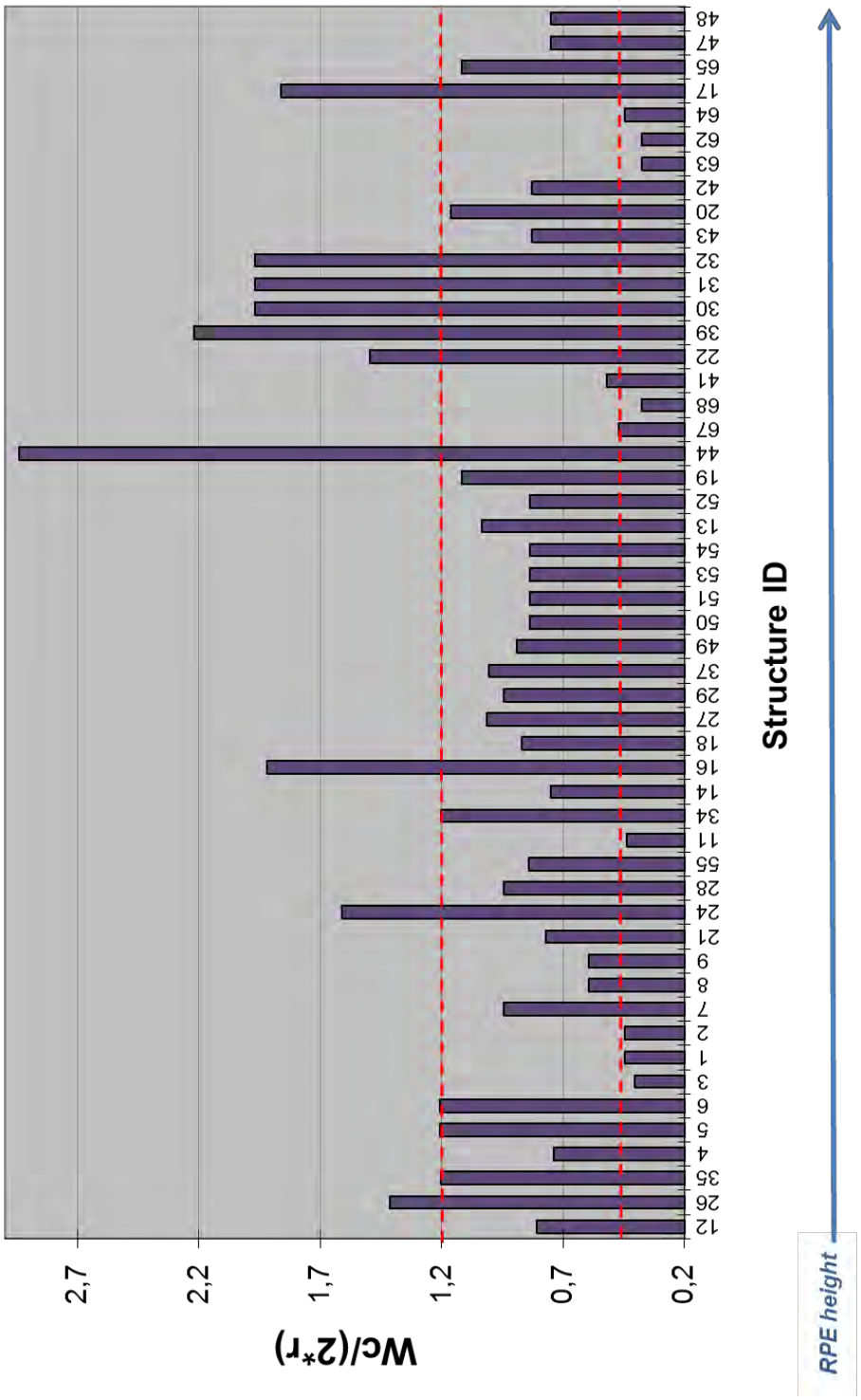

Figure 9 *Ratio of crest width to block size with limit values according to the approach proposed by Kister (2015)*

3.4. Discussion

The previous sections aimed at addressing the structural efficiency in resisting the impact by the block. Two approaches have been proposed to provide an expedient tool for roughly assessing the efficiency of the RPE from data related to the block and to the structure dimensions. These two approaches were developed based on different experimental data sets, and consequently have their own limitations and validity domains, in particular in terms of structure type. These two approaches may be considered complementary and, as a consequence, it is proposed to use these two approaches in parallel.

Among the 47 RPEs for which available data allow conducting these two approaches in parallel, 23 meet the C_{25} criterion (50%) and 14 meet the crest width-to-block ratio (30%), but only 6 meet both criteria (13%). Conversely, for 16 RPEs the two criteria are not met (34%). More notably, 12 RPEs are highly critical (C25 > 2 and crest width-to-block ratio < 0.5) for one of the two criterion (26%) and 2 are highly critical for both (4%). Considering that these criteria are based on different approaches with their own limitations, particular focus should be placed on this set of critical structures. For theses cases, further investigations may be conducted.

The functional efficiency of the RPEs is only addressed by the last approach. Basically, the functional efficiency is related to the uphill face inclination and to the freeboard.

3.5. Freeboard criterion according to ONR 24810

As already mentioned above, the functional efficiency of a RPE in case of an impact load is not only a question of the stability of the construction itself. The second scenario which has to be taken into account is the surmounting of a RPE by a block while the embankment will not be punched through and the damage is of minor extent. This part of functional efficiency is called fitness for purpose of a structure and has also to be taken into account for the design of a RPE. The Austrian standard ONR 24810 (2013) tries to solve this problem by defining different values for the freeboard depending on the construction type, the embankment's uphill slope inclination and the type of the facing (see part A of the report). As the minimum value defined in ONR 24810 the freeboard should be larger than one block diameter.

A freeboard had been listed in the available documents for 20 of the 68 embankments, this is about 30%. The freeboard dimension varies between 0.3 and 2.7 m and is shown in Figure 10.

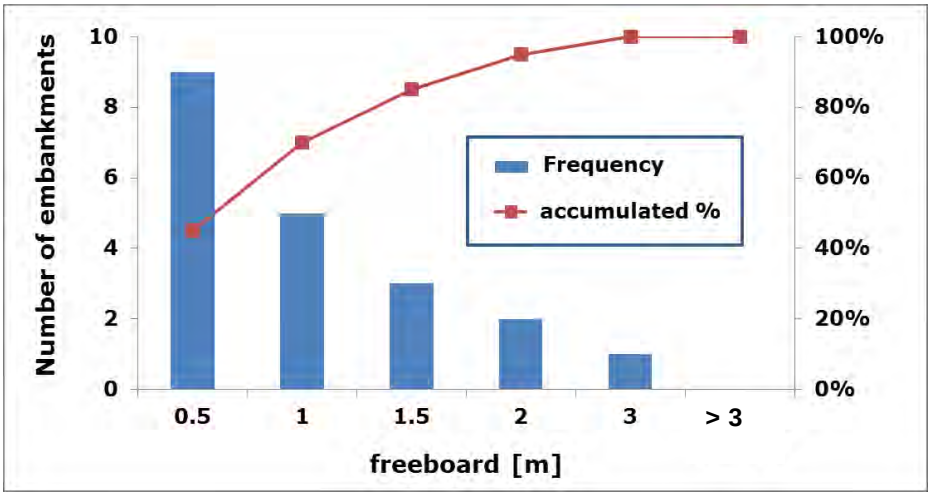

Figure 10 *Bar chart of freeboard used in the design of the RPEs*

Only for 11 of these 20 RPEs also the block diameter was given respectively could be calculated from the available data. Not one of these 11 RPEs fulfills the minimum value defined in ONR 24810. For 7 of the RPEs (8, 9, 10, 50, 51, 52, 53 and 54) the ratio of freeboard to block diameter was less than 0.25. For the design of RPE no. 3 and no. 22 the freeboard was chosen to be approximately the half block diameter. Only the part of RPE no. 2 with a batter of 70° and reinforcement comes up with a ratio freeboard to block diameter of 0.89 and therefore reaches approximately the minimum value of ONR 24810.

3.6. Post-construction events

Up to now only a few post-construction events had been recorded for the 68 embankments. Moreover the quality of the collected data differs widely. In most cases the block size is recorded and for a few examples a survey of the impact marks on the slope had been done. But an estimation concerning block energy or block velocity is missing.

In none of the recorded examples an embankment was punched through by a block. And in most cases the damage was relatively low and could be repaired with minor effort. On the other hand there exist examples, where a pure soil embankment had been surmounted by a block. This occurred for a trajectory perpendicular to the RPE axis as well as for a trajectory with an acute angle to the RPE axis.

No surmounting of an embankment with rockery at the uphill slope has been reported up to now. Only in one event a rock chip was released during the impact onto the rockery and it was able to surmount the RPE.

Figure 11 *Damage of a RPE with rockery at the uphill side after block impact (Tiefbauamt Graubünden)*

4. Conclusion

The analysis of the collected data allows drawing some conclusions regarding both the design methods in use and the Swiss structure park.

As for the design methods, the first remark concerns the difference in the definitions of the input parameter required for the design of RPEs. It has been shown that there was no consensus on the way to interpret and use the trajectory simulations results. In particular, the statistical estimator is extremely variable from one case to the other for both the block passing height and the kinetic energy (percentile). It is stressed that high percentile values requires high number of trajectory simulations to give relevant values, and more precisely high number of blocks passing the point where the passing height or kinetic energy is computed.
The second remarks concern basic geometrical definitions of the structure height and block passing height in particular. The different definitions observed introduce ambiguity that is detrimental to the structure design.
As an additional remark concerning the input parameters, the authors would recommend to promote conducting trajectory simulations accounting for the structure in the slope profile (2D or 3D) in order to provide relevant passing heights and kinetic energies of the block just before reaching the RPE. Nevertheless, it is reminded that most of the trajectory tools are not appropriate for simulating the rebound on the RPE face.

The consultation of the design reports revealed that a vast majority of RPEs in Switzerland are soil compacted structures with rockery uphill facing. The design of the structure height, including a freeboard, is extremely variable from one case to the other. Also, a limited number of RPEs were designed accounting for the dynamic loading, mainly considering the Austrian standard (ONR 24810). As a result of the absence of unique design method with respect to impact strength, a significant scattering is observed in the structure park in terms of structure dimensions for a given block kinetic energy.

In this context, the structure park was assessed with respect to the impact strength of the RPEs considering two approaches specifically developed for this purpose.
This expedient assessment method was applied to the structure park drawing the attention on 1/3 of the park that may not resist the impact by the design block. Based on this, further and detailed structure evaluations are suggested.

References

- Blovsky, S., 2004. Model tests on protective barriers against rockfall. 15th European Young Geotechnical Engineers Conference, Dublin, Ireland.
- FEDRO, 2008. Directive 12006: Actions de chutes de pierres sur les galeries de protection. OFROU, Bern, Switzerland, 22 pp.
- Frenez, T., Vecchiotti M., Danzi A. 2014. Un nuovo approcio per la progettazione di rilevati paramassi in terra rinforzata – il progetto di Chizzola (Ala, Trento). XXV Convegno nazionale di geotecnica. 4-6 giugno, Baveno.
- Kister, B., 2015. Development of basics for dimensioning rock fall protection embankments in experiment and theory (in German), research project FEDRO 2012/003, FEDRO report 1524.
- Lorentz, J., Plassiard, J-P., Muquet, L., 2010. An innovative design process for rockfall embankments: application in the protection of a building at Val d'Isère. Proceedings of the 3rd Euro Mediterranean Symposium on Advances in Geomaterials and Structures - AGS 2010, Djerba, Tunisia, 277-282.
- ONR, 2013. ONR 24810: Technischer Steinschlagschutz – Begriffe, Einwirkungen, Bemessung und konstruktive Durchbildung, Überwachung und Instandhaltung, ASI Austrian Standards Institute (Österreichisches Normungsinstitut), Ausgabe 15.01.2013.
- Peila, D., Oggeri, C., Castiglia, C., Recalcati, P., Rimoldi, P., 2002. Testing and modelling geogrid reinforced soil embankments to high energy rock impacts. Proceedings of the 7th International conference on geosynthetics, Nice, France, 133-136.
- Rimoldi, P., Lorizzo, R., Pettinau, D., Rocallo, C., Secci, R., 2008. Impressive Reinforced Soil Structures in Italy. Proceedings of the 1st Pan American Geosynthetics Conference, Cancun, Mexico, 789-798.
- Simmons, M., Pollak, S., Peirone, B., 2009. High energy rock fall embankment constructed using a freestanding woven wire mesh reinforced soil structure. Proceedings of the 60th Highway Geology Symposium, Buffalo, New York, 290-301.
- Tissières, P., 1999. Ditches and reinforced ditches against falling rocks. Proceedings of the Joint Japan-Swiss Scientific Seminar on Impact load by rock fall and design of protection structures, Kanazawa, Japan, 65-68.

Lucerne University of
Applied Sciences and Arts

HOCHSCHULE
LUZERN

Technik & Architektur

Analysis of Existing Rockfall Embankments of Switzerland (AERES)

Part C: Small-scale experiments

Bernd KISTER[1] and Stéphane LAMBERT[2]

[1] Lucerne University of Applied Sciences and Arts, Technikumstrasse 21, CH – 6048 Horw, Switzerland.
Current position: kister - geotechnical engineering & research, Neckarsteinacher Str. 4 B,
D – Neckargemünd, +49 6223 71363, kister-ger@t-online.de

[2] Irstea, 2 rue de la papeterie, 38402 Saint Martin d'Hères cedex, France, + 33 4 76 76 27 94,
stephane.lambert@irtsea.fr

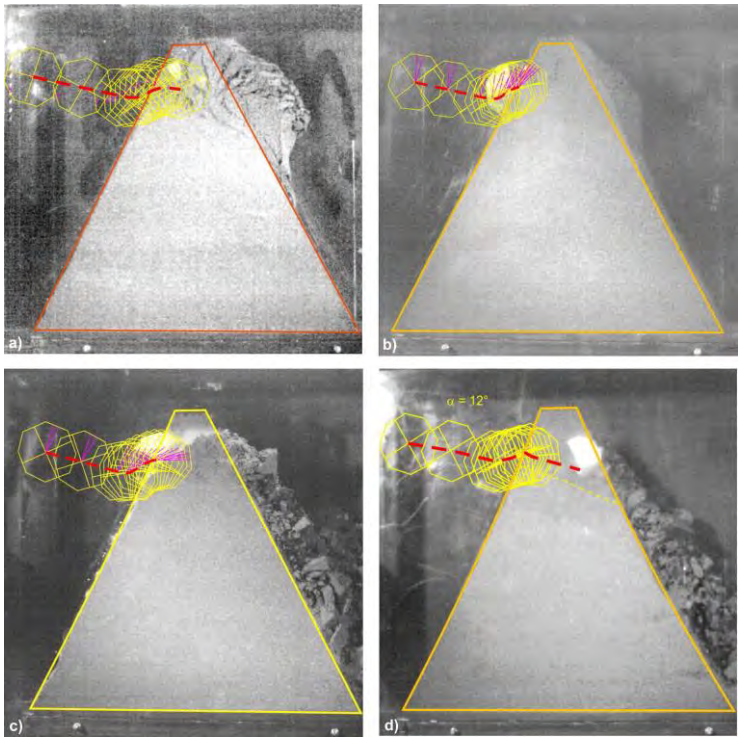

Commissioned by the Federal Office for the Environment (FOEN)

July 2017

Imprint

Commissioned by
Federal Office for the Environment (FOEN), Hazard Prevention Division, CH-3003 Bern.
The FOEN is an agency of the Federal Department of the Environment, Transport, Energy and Communications (DETEC).

Contractors
Lucerne University of Applied Sciences and Arts, CH-6048 Horw
Irstea, F-38402 Saint Martin d'Hères

Authors
Bernd Kister
Stéphane Lambert

FOEN support
Bernard Loup, Hazard Prevention Division
Arthur Sandri, Hazard Prevention Division

Notes
The AERES report consists of three parts:
- Part A: State of knowledge
- Part B: Analysis of the collected data and comparison with up-to-date knowledge
- Part C: Small-scale experiments

Suggested form of citation for Part C
Kister B., Lambert S. 2017: Analysis of Existing Rockfall Embankments of Switzerland (AERES); Part C: Small-scale experiments. Federal Office for the Environment, Bern, 90 p.

Content

1 Introduction

Hofmann & Mölk (2012) have done small scale tests on embankments with and without riprap at the uphill slope (Fig. 1.1a). They stated that the impacting sphere will not move upward in case of riprap on the slope while the impacting sphere was rolling or jumping towards the embankment's crest in the case of pure-earth embankments as well as in the case of reinforced embankments with geogrids. Fig. 1.1 shows the riprap used by Hofmann & Mölk in their experiments in comparison to a real embankment in Switzerland with rockery at the uphill slope. It seems to be that the relative surface roughness of the riprap used by Hofmann & Mölk (2012) shows a larger unevenness than that one of the real embankment, especially in the context of the corresponding block diameter.

Fig. 1.1: a) riprap used in the tests of Hofmann & Mölk (2012), b) rockery surface of embankment Gretla, Canton Grisons (Photo: Tiefbauamt Graubünden).

The statements of Hofmann & Mölk concerning the freeboard have been transferred to the Austrian technical guideline ONR 24810:2013 and it is said that the freeboard for an embankment with riprap and a slope angle of 50° or more should be at least one block diameter while for an embankment without riprap or geogrid reinforcement the freeboard should be at least two block diameters. For an embankment with geogrid reinforcement and a slope angle of 60° or more the freeboard should be at least 1.5 block diameter, for an embankment with geogrid reinforcement and a slope angle of 70° or more the freeboard should be at least one block diameter. Fig.1.2 shows a comparison for the embankment height for an example of a block with a 2 m diameter and an impact height of 2 m. The impact height is measured from the block center to the ditch level.

According to Fig. 1.2 the embankment height in this example may vary between 3.8 m and more than 5 m depending on what kind of construction will be selected. The smallest embankment height is achieved using rockery at the uphill slope and a slope angle of 50°. But Kister (2015) has shown by small-scale and half-scale experiments that the uphill slope of a rockfall protection embankment should be constructed at least with an angle of 60°. However no riprap had been used in those tests, the embankment models had been constructed by pure soil. Moreover in practice an embankment slope made of rockery will not be constructed with a slope angle of about 50°, but with a slope angle in the range of 60° to 80° (see part B of the report).

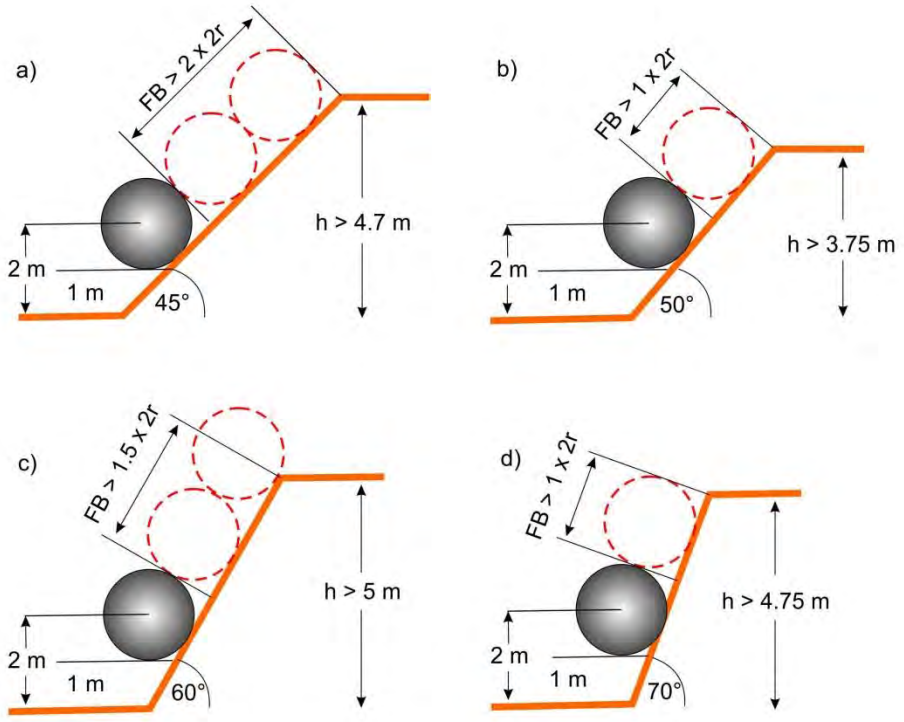

Fig. 1.2: Minimum height of a rockfall protection embankment according to ONR 24810:2013 for a block with diameter 2 m and an impact height of 2 m (based on the block center), a) pure earth embankment without riprap / rockery and slope angle approx. equal to debris friction angle of about 45°, b) embankment with riprap / rockery and a minimum slope angle of at least 50°, c) embankment reinforced with geogrids and slope angle 60°, d) embankment reinforced with geogrids and slope angle 70°.

In Switzerland rockfall protection embankments with rockery at the uphill slope is a very common construction type (see part B of the report). There are examples with rockery up to the crest while other designers preferred a construction where the upper part of the embankment had been made only of soil. Whereas at the first construction type the slope follows a straight line, at the second construction type the slope has a bi-linear profile. Both types of slopes have been investigated by small-scale quasi-2D-impact experiments (Fig. 1.3).

To investigate the influence of roughness of the rockery in the small-scale quasi-2D-impact tests two types of stone arrangement had been used:

- Stones had been placed parallel to the slope angel. This resulted in a relatively smooth slope surface (Fig. 1.3a).
- Stones had been placed with its largest dimension horizontally. This resulted in a stepped surface for the slope, i.e. in a rough slope surface (Fig. 1.3b).

Due to limit available place some embankments had been constructed with rockery at both slopes. The behavior of such a construction under impact load was also investigated.

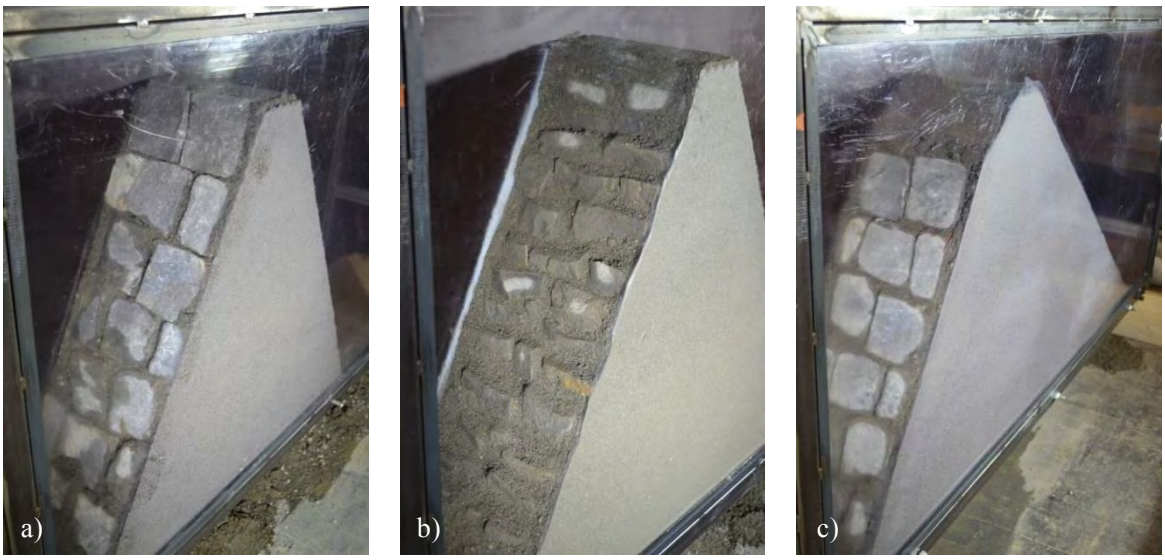

Fig. 1.3: Orientation of stones at the "uphill" slope: a) upright, b) horizontal, c) upright, upper part of the slope without stones, but with a reduced slope angle.

Fig. 1.4: Example of a rockfall protection embankment in Canton Valais with rockery placed in the lower part and soil at the upper part of the uphill slope. The surface roughness of the rockery may be described as smooth and is comparable with the surface roughness in Fig. 1.3a) and c) (Photo: S. Lambert).

2 Quasi-2D-Experiments

2.1 Experimental set-up

Quasi-2D-embankment models made of sand and with a thickness of 20 cm have been constructed in a box with one side made of acrylic glass to observe the impact by a high-speed camera (Fig. 2.1, on the left). The impact process was recorded with a frame rate of 500 Hz that is 1 picture every 2 x 10^{-3} s. To analyze the displacement field inside the embankment the Particle Image Velocimetry (PIV) has been used. The procedure the PIV was used is described in Kister (2015).

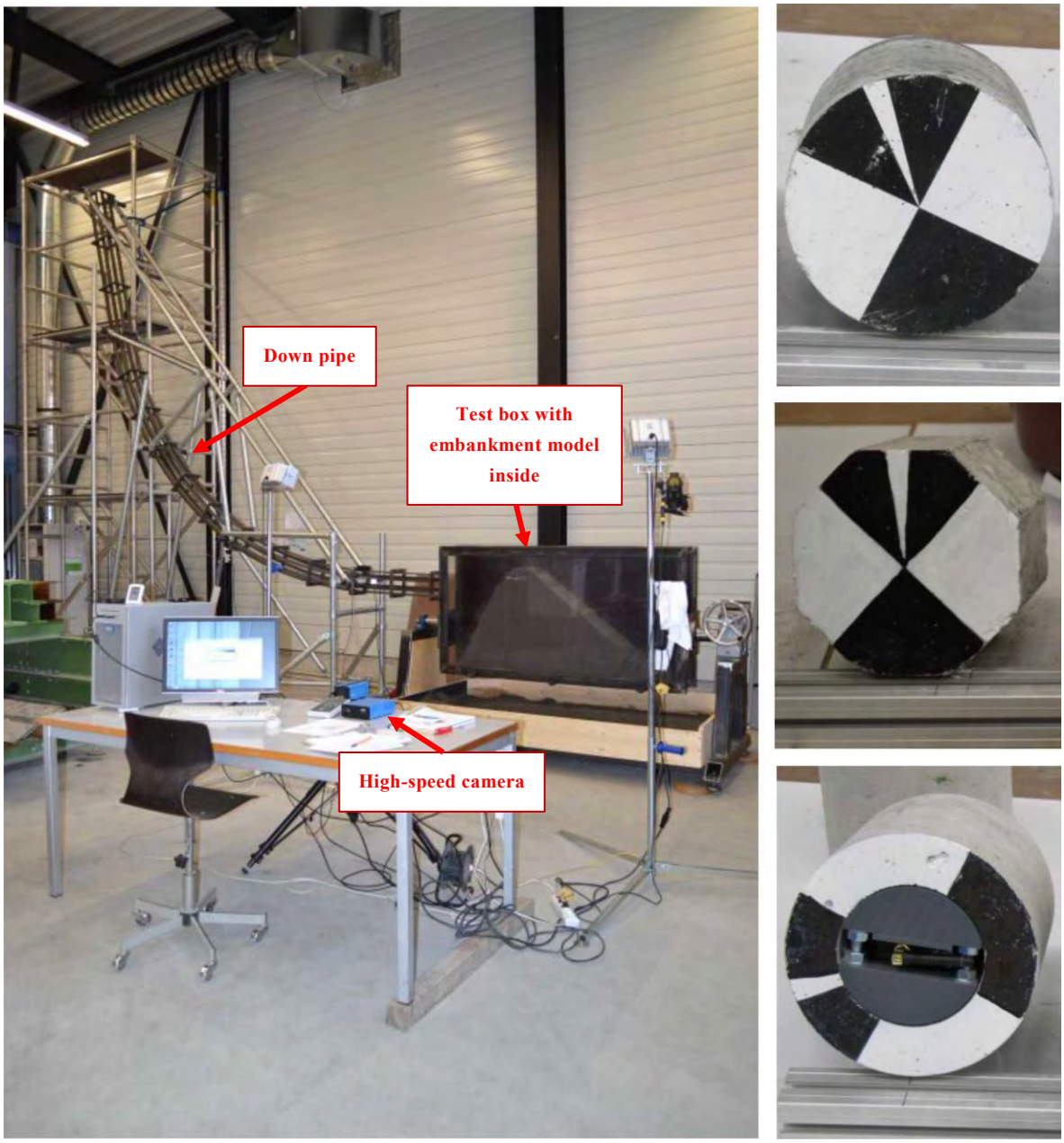

Fig. 2.1: Experimental set-up for the small scale quasi-2D-impact tests, left: test facility, right: impactors G (at the top), OKT (central) and GS with triaxial acceleration sensor (bottom).

Small scale experiments had been executed with a cylinder G, a hollow cylinder with an acceleration sensor inside GS and an impacting body with octagonal cross-section OKT (Fig. 2.1, on the right). The impactors G and OKT are made totally of concrete. In a first test the impactor GS was also made of pure concrete, but was destroyed in the test on the stony slope. So a new impactor GS with higher capability of resistance had to be built. The new impactor GS has a steel lining as exterior facing and an aluminum lining as inner facing. The annulus space was filled with concrete.

Body	Material	caliber	weight
Cylinder G	Concrete	Diameter: 16 cm	7.44 kg
Hollow cylinder GS	Jacket: Steel Body: concrete Core retainer: Aluminum	External diameter: 16 cm Inner diameter: 9.4 cm	6.76 kg
Body OKT	Concrete	Distance between 2 sides: 14.8 cm	6.77 kg

Table 2.1: Material, dimensions and weights of the impactors used in the tests. Height of all impactors: 16 cm.

The sensor used inside the impactor GS was a triaxial acceleration sensor with measurement range ± 200 g. The sensor was placed together with a mini data logger inside the hollow cylinder (Fig. 2.2).

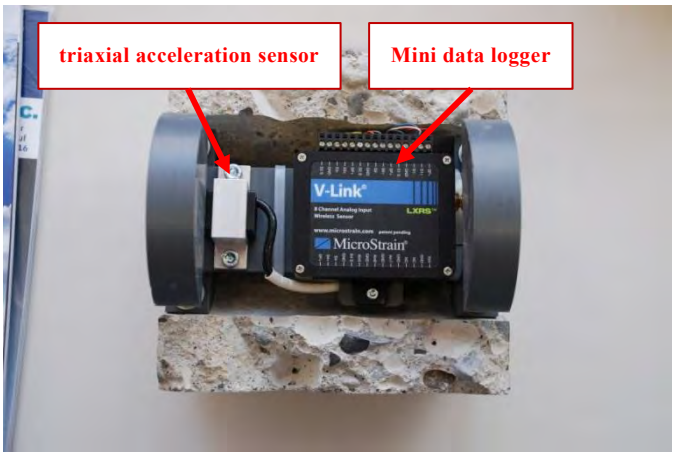

Fig. 2.2: Triaxial acceleration sensor and mini data logger inside impactor GS.

The impacting bodies have been accelerated by gravitational acceleration and with the help of a kind of down pipe with a rectangular cross section (Fig. 2.1). Because of friction between the impacting bodies and the down pipe the impacting bodies start to rotate when moving down the down pipe.

The down pipe was mounted at a framework in such a manner that the complete down pipe could be rotated to a certain extent. This rotation results in a modification of the angle of impact. Tests have been done with two different adjustments of the down pipe. In most tests of this test series an inclination at the exit of 9.3° was used. Additional a few tests have been done with an inclination at the exit of approx. 1.3° (Fig. 2.3).

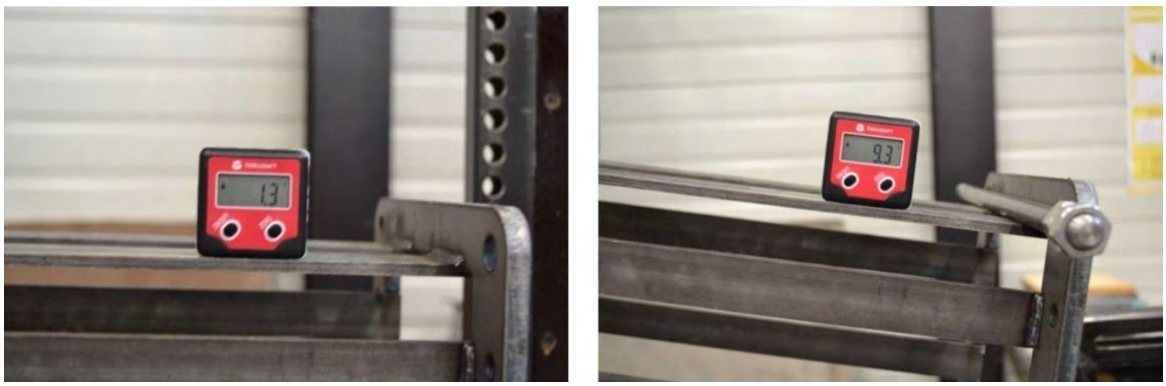

Fig. 2.3: Inclinations of the down pipe exit used in the tests.

2.2 Embankment material

The construction material for the embankments was made by mixing 2 different sands and fine gravel. The mix was done in such a way, that the resulting soil was very similar in its grain-size distribution to that one used by Blovsky (2002). Fig. 2.4 shows the grain-size distribution of both soils for comparison and also the grain-size distribution of the construction material of a prototype embankment specified by Blovsky (2002).

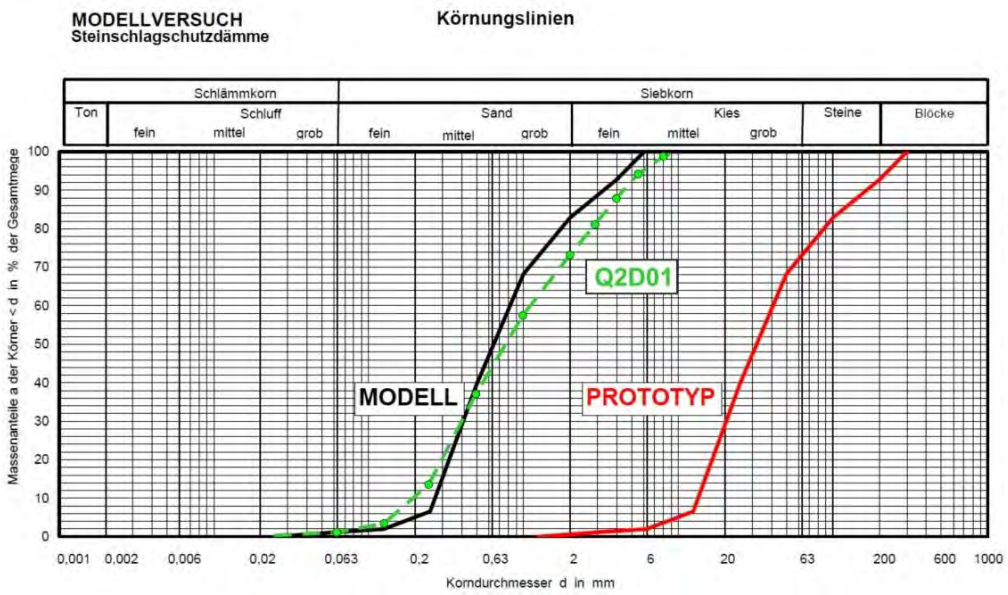

Fig. 2.4: Comparison of the grain-size distribution of the material Q2D01 used in the tests with the grain-size distribution of the model sand used by Blovsky (2002) and the grain-size distribution of the construction material specified by Blovsky for a prototype embankment.

While constructing the embankment models the mass of soil, which was used for the construction, was measured to determine the soil density. If no stones are used in the model to represent the rockery, the embankment volume could be easily calculated. But if stones had been used it was necessary to subtract the volume of the stones from the total embankment volume to get a proper estimation of the soil volume for density calculation. To simplify matters also the weight of the stones had been determined and the stone volume was calculated using the stone density. This stone volume was subtracted from the total embankment volume and with the remaining volume the soil density was determined. Fig. 2.5 shows the frequency distribution of the determined densities, the average density of the soil had been determined to 1840 kg/m^3.

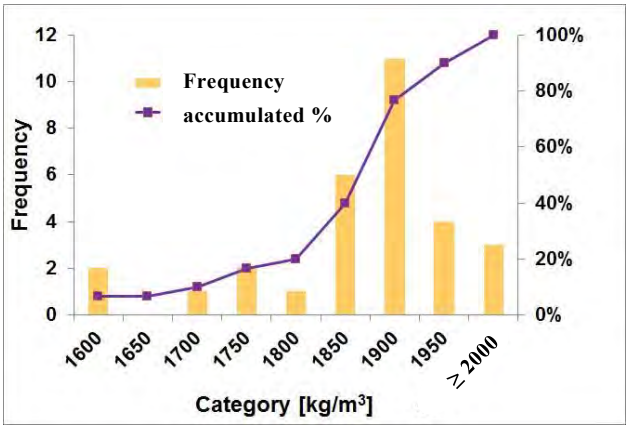

Fig. 2.5: Frequency distribution of the measured density.

At the end of a test, 3 soil samples had been extracted to determine the water content. The minimum value of the water content in the test series was determined to 4.3%, the maximum value of the water content in the test series was determined to 9.1%. As average value over all tests a water content of 6.3% has been determined. The frequency distribution of the water content of all measurements is shown in Fig. 2.6.

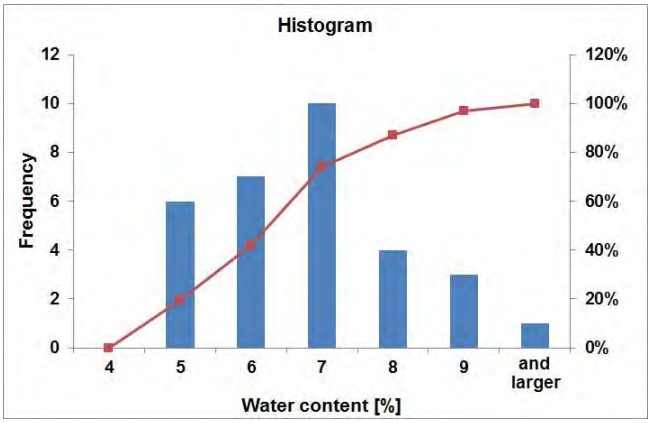

Fig. 2.6: Frequency distribution of the water content of all measurements.

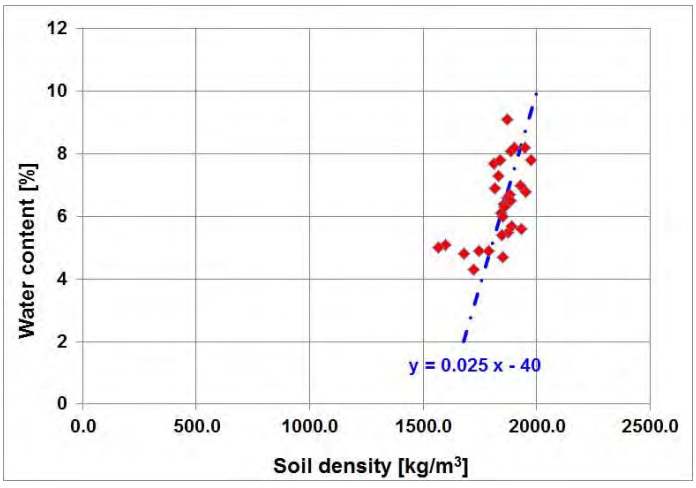

Fig. 2.7: Water content versus soil density of soil Q2D01 in the test series.

Fig. 2.7 shows the water content versus soil density for soil Q2D01. The graph shows that the relationship between soil density and water content may be described approximately by the linear function y = 0.025 x – 40 for the test conditions.

Additional to the tests shown before, the soil Q2D01 was filled in layers into a barrel and compacted. The same procedure was used as for the construction of the embankments. Then a dynamic cone penetrometer test was carried out and CBR values as well as resilient modulus M_R were determined (Fig. 2.8). The resilient modulus M_R was determined according to the formula given by George & Uddin (see TRB, 2008):

$$M_R = 235.3 \cdot DCPI^{-0.48}$$

The resilient modulus is a stiffness parameter, which describes the soil's ability to store and to release elastic energy during a dynamic load and unload process. But it is not a parameter to describe failure. With the formula of George & Uddin the resilient modulus for soil Q2D01 was determined to be in the range of 50 to 70 MPa (Fig. 2.8, left hand). The first 3 measurement points in the diagram had been neglected because of insufficient overburden at the beginning of the test.

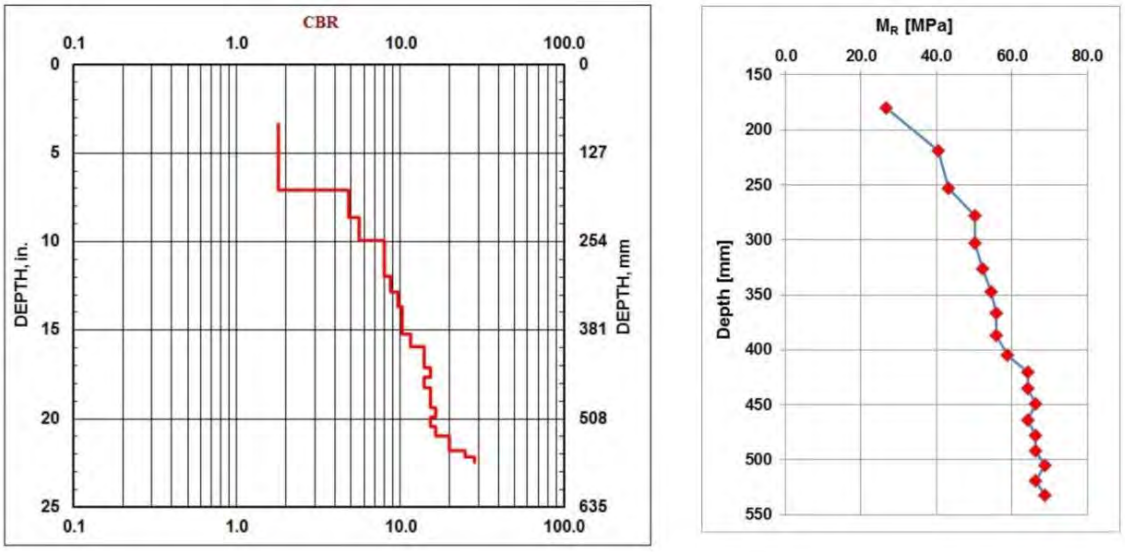

Fig. 2.8: Results of dynamic cone penetrometer test on soil Q2D01

The friction angle of soil Q2D01 was estimated by applying Dhawan's method on the grain-size distribution shown in Fig. 2.4. A friction angle of 39° was estimated for a middle degree of compactness and 45° for a high degree of compactness.

The "rockery" used in the models have been constructed with a local siliceous sandstone called Guber-Quarzsandstein. This material is mined at the stone quarry Guber near Alpnach and shows a real high toughness. To determine the rock density, the static elastic parameters and the uniaxial compressive strength two specimens had been drilled out of a larger block (Fig. 2.9, left). The mean value of the rock density was determined to be ρ_{St} = 2617 kg/m^3. The results of the laboratory tests on the 2 specimens are shown in table 2.2.

Specimen	Uniaxial compressive strength σ_{ucs} [MN/m^2]	Young's modulus E_{stat} [GPa]	Poisson's ratio ν_{stat} [-]
P1	190	47 (40 – 100 MPa)	0.28 (40 – 100 MPa)
P2	172	63 (40 – 100 MPa)	0.34 (40 – 100 MPa)

Table 2.2: Uniaxial compressive strength, Young's modulus and Poisson's ratio of Guber-Quarzsandstein, load range 40 – 100 MPa.

Fig. 2.9: Left: Block of Guber-Quarzsandstein and specimens P1 and P2, which had been used for uniaxial compression test, right: Selected pieces of Guber-Quarzsandstein before placed in the model embankment.

2.3 Preparation of embankment models

The geometry of the model embankments was constructed by using two panel sheets, which had been placed inside the box (Fig. 2.10, on the left). To construct the embankment the box was turned upside down (Fig. 2.10, on the right) and the soil and stones had been placed in the box by layers. Every soil layer has been carefully compacted. Joints between the masonry stones have been filled with soil.

Fig. 2.10: Left hand: Test box in horizontal position with already installed panel sheets. Right hand: Test box in upside down position ready for filling with soil material. Insulating wall panels (in yellow) had been used for varying the crest's dimension without changing the slope inclination.

After completion of the embankment construction the bottom plate was mounted and then the box was turned in upright position (Fig. 2.11, on the right). Now the cover plate and both panel sheets were removed and the embankment was ready for a test.

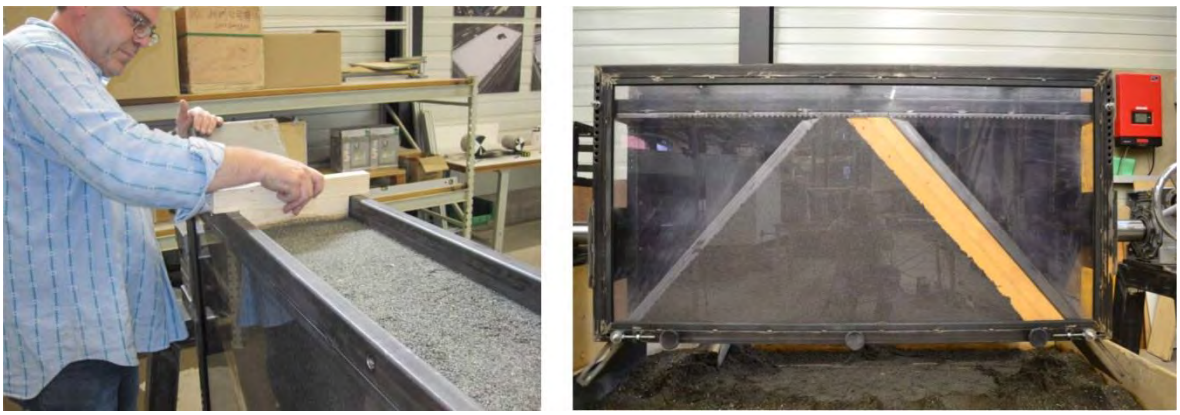

Fig. 2.11: Left hand: Planing of the embankment's base before the bottom plate is mounted. Right hand: Test box in upright position. Cover plate and both panel sheets are still in place.

2.4 Geometry of embankment models

The main scope of work was to study the impact onto an embankment slope with rockery. Due to this the slope angle at the "uphill side" of the embankment was chosen to be rather steep. Most tests have been done with a batter of 2:1 (approx. 63°). A few tests have been done with a steeper slope, i.e. a batter of 5:2 (approx. 69°) resp. 5:1 (approx. 80°).

At the "downhill slope" most tests have been done with a batter of 2:1. But for comparison with the tests described by Kister (2015) also embankments with a batter of 4:5 have been used in the tests. Fig. 2.12 gives an impression of the used cross sections of the model embankments.

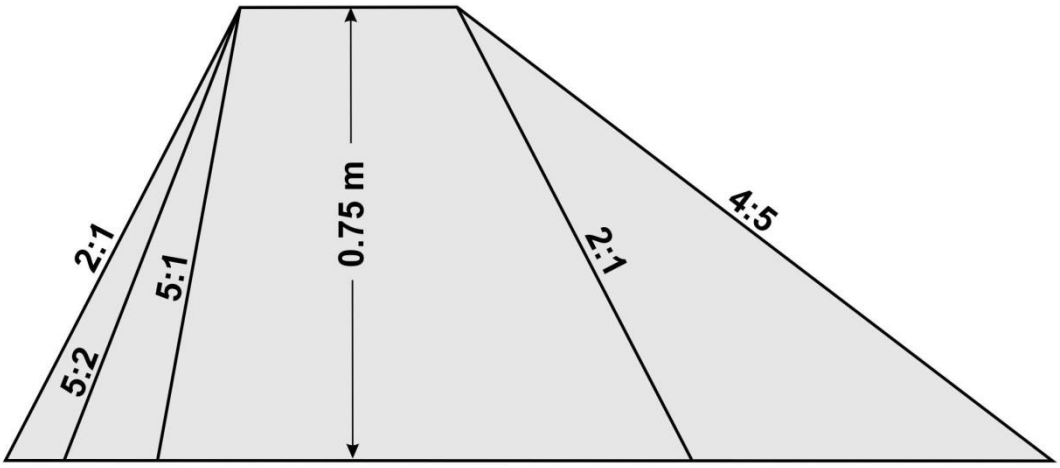

Fig. 2.12: Different slope angles used in the tests.

The visible height of the model embankments in the test box was in all tests 0.75 m. For the total height of the embankments 2 cm have to be added at the basement. This part is hidden by the framework of the test box.

As already shown by Kister (2015) the relationship between the size of the impacting block and the embankment's crest is very significant. The impact tests on pure soil model embankments showed that the embankment crest should be at least 1.2 times the diameter of the dimensioning bloc. Hereby it is assumed that the freeboard is at least 0.8 times the block diameter.

Because of the significance of the relationship between the size of the impacting block and the width of the embankment's crest on one hand and the assumption that the "rockery" will increase the capability of resistance of the embankments on the other hand, two classes of tests on embankments with "rockery" have been executed. In class 1 the crest width was chosen to be smaller than the block diameter. The mean value of the ratio crest width a_c to block diameter 2r is approximately 0.5. In class 2 the crest width a_c was chosen to be larger than the block diameter 2r. In this case the mean value of the ratio a_c/2r is approximately 1.1.

Additional to the embankment geometry described in Fig. 2.12, an embankment cross-section had been used in the tests, which was constructed with a bi-linear slope at the "uphill side". At the slope's lower part stones had been placed, while the upper part of the "uphill side" was made of soil (Figures 2.13 and 1.3c). The use of this type of geometry in the test series was a result of the interviews done with representatives of the cantons and consulting engineers.

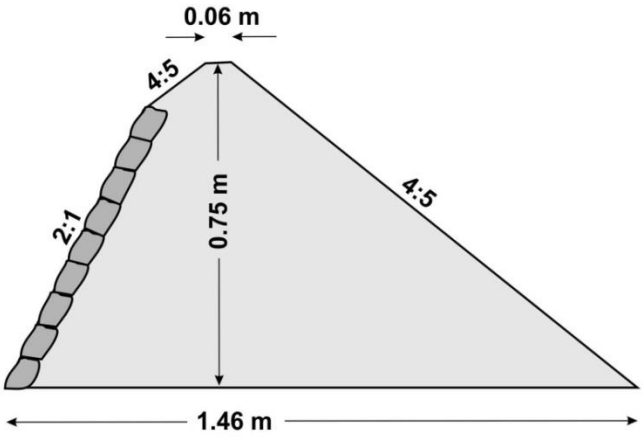

Fig. 2.13: Embankment cross-section with a bi-linear slope at the "uphill side".

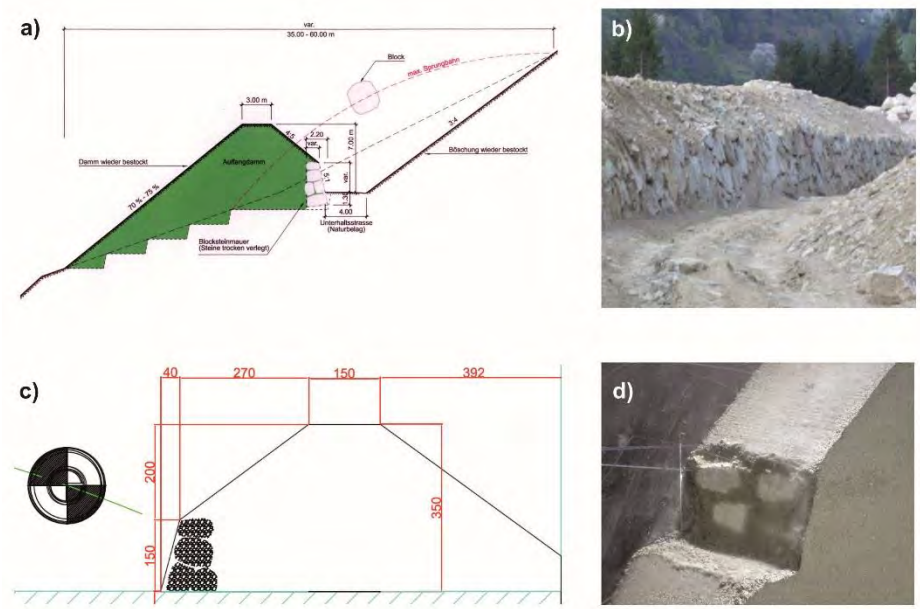

Fig. 2.14: Embankment Gurtnellen: a) design of embankment Gurtnellen North (Kälin, 2006), b) rockery at embankment Gurtnellen South (Photo: B. Kister), c) cross section of the model embankment on a scale of 1:20, dimensions are in mm, d) rockery of the model embankment.

In addition to the geometry with a bi-linear slope shown in Fig. 2.13 an embankment model was used which represents the cross section of the rockfall protection embankment Gurtnellen North on a scale of 1:20 (Fig.2.14).

2.5 Scaling factor

Blovsky (2002) as well as Hofmann & Mölk (2012) used model embankments with a height of 0.5 m. But the prototype which was taken as a basis in the two investigations is not the same. While Blovsky used a prototype with a height of 25 m as basis for defining the geometrical scaling factor λ ($\lambda = 25/0.5 = 50$), the prototype of Hofmann & Mölk has only a height of 16.5 m, which results in a geometrical scaling factor $\lambda = 33$. Taking into account the prototype height used by Hofmann & Mölk and the model height shown in Fig. 2.12 this will result for the tests of this report in a scaling factor λ of approx. 22.

But in Switzerland most rockfall protection embankments do not reach a height like the prototypes defined by Blovksy or Hofmann & Mölk. The survey of existing rockfall protection embankments in Switzerland showed that an embankment height of 8 m or more is rather rare (part B of the report, Fig. 2.15).

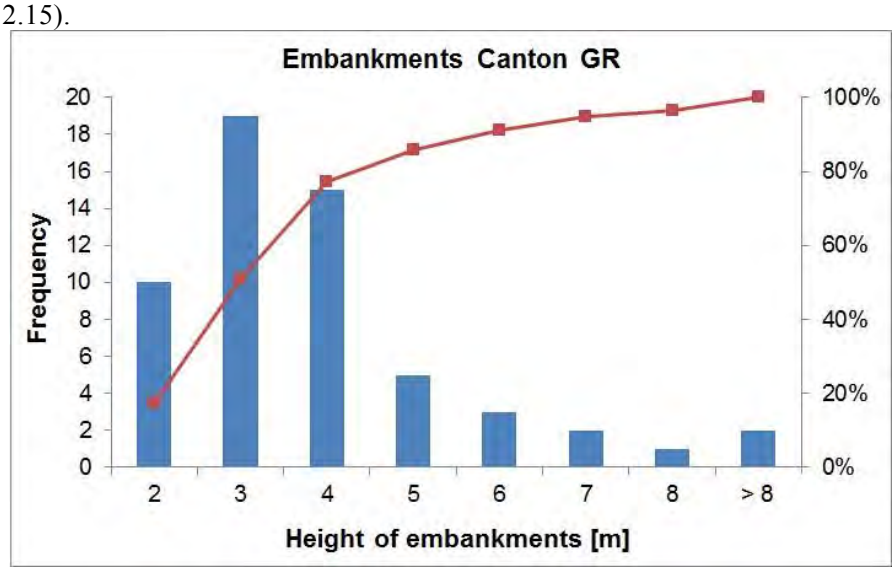

Fig. 2.15: Bar chart of the height of 57 embankments in Canton Grisons

So as a prototype an embankment with a height of 7 m was defined for the models presented in Figures 2.12 and 2.13. This will result in a scaling factor λ of about 9 for the geometry. In case of the Gurtnellen model the scaling factor for the geometry is $\lambda = 20$. The scaling factors for geometry, block velocity and energy are summarized in Table 2.3.

physical quantity	model Gurtnellen	all others
geometrical data	$\lambda = 20$	$\lambda = 9$
block velocity	$\lambda^{1/2} = 4.47$	$\lambda^{1/2} = 3$
energy	$\lambda^4 = 160'000$	$\lambda^4 = 6'561$

Table 2.3: Scaling factors for geometrical data, block velocity and energy.

2.6 Executed tests

Within the framework of this project totally 34 experiments with quasi-2D-embankment models have been done. But not all of these tests could be analyzed in full. So, during two tests a blackout of the high-speed camera occurred. As a consequence of this the first impact in one test and the second impact in another test were not recorded. The test, where the first impact was not recorded, was repeated. Because of the minor significance of the second impact, the other test was not repeated. When doing the first test with impactor GS, made completely of concrete, this impactor was fragmented, when it hits the "rockery" and so no analysis of this test could be done.

The 34 executed tests may be subdivided as follows:

According to the used impactor:

- 9 tests had been done using block G.
- 12 tests had been done using block OKT.
- 13 tests had been done using block GS with the sensor inside.

According to the differences in slope construction:

- 8 tests had been done with the geometries shown in Fig. 2.12 with masonry stones placed parallel to the slope as shown in Fig. 1.3 a).
- 2 tests had been done with the geometry shown in Fig. 2.13 with masonry stones placed parallel to the slope as shown in Fig. 1.3 c) and no stones at the upper part of the slope.
- 12 tests had been done with the geometries shown in Fig. 2.12, but with masonry stones placed horizontally as shown in Fig. 1.3 b).
- 5 tests had been done with the geometries shown in Fig. 2.12, but with the masonry stones on both embankment slopes. The masonry stones have been placed horizontally, as shown in Fig. 1.3 b) resp. Fig. 2.16.
- 5 tests had been done with the geometries shown in Fig. 2.12, no masonry stones had been used in the tests. These tests complement the test series shown by Kister (2015).
- 2 tests had been done with the Gurtnellen model.

Fig. 2.16: Proportion of stone and soil layer in horizontal sections: a) at the upper third of the embankment, b) at the bottom of the embankment.

Based on the relationship between the size of the impacting block and the embankment's crest width 16 tests may be assigned to class 1, $a_c/2r \approx 0.5$ and 14 tests to class 2, $a_c/2r \approx 1.1$.

Fig. 2.17: Roughness of the "rockery" with masonry stones placed horizontally for slopes with batter 2:1, 5:2 and 5:1. The roughness is reduced with increase of slope steepness.

One test had been done on an embankment with 3 layers of fly-screen in a vertical distance of 15 cm as a kind of "geogrid reinforcement" in the upper part of the embankment to stabilize the downhill slope. The fly-screen has been used because no geogrid in model scale was available. Because a lateral fixation of the reinforcement is missing in the quasi-2D-experiments the results of this test have been rather poor. Therefore no further experiment with that kind of test arrangement was executed.

To identify a test easily by its name generally a labeling consisting of 4 parts is used:

- The first part of the name denotes the impactor which was used in the test. In this test series this is G, GS or OKT.
- The second part contains information concerning the embankment's slopes. The first two numbers refer to the batter of the uphill slope. The second two numbers refer to the batter of the downhill slope. There is one exceptional case. Three numbers, 251, had been used for batter 5:2.
  If those numbers are followed by a letter, masonry stones had been used in the test. An H indicates that the stones had been placed parallel to the uphill slope. The letter F indicates the masonry stones had been placed horizontally. If two letters F are used, masonry stones have been placed on both slopes of the embankment.
  If the letter F or H is followed by a letter G the test has been done while the complete test box was raised to achieve a larger value for the freeboard without doing changes at the down pipe.
- The third part of the name specifies the crest dimension in centimeters.
- The fourth part of the name is an indication of the inclination of the down pipe. For an inclination of 9.3° at the exit the identifier 11 is used. For the lower inclination of approx.1.3° at the exit the identifier 01 is used (Fig. 2.3). Most tests had been done with an inclination of 9.3° at the exit.

For example, a test named OKT_2121FF_18_11 was done with impactor OKT, the embankment cross section was symmetric with a batter of 2:1 on both sides and masonry stones placed horizontally at both slopes. The crest size was approx. 18 cm and the inclination of the down pipe at the exit was 9.3° as shown in Fig. 2.3 on the left.

For the one experiment, which was done with "geogrid reinforcement" at the downhill slope, a G was added as a fifth part of the name.

Fig. 2.18: Model with the "geogrid reinforcement" at the downhill slope.

Fig. 2.19: Bagginess of the "geogrid reinforcement" after the impact.

Sometimes an additional number is used at the end of the test label. If this number is set to 1, this denotes it was the first impact of the test. Number 2 or higher denotes additional impacts on the same model. To shorten the test name the number 1 has been omitted, if only the first impact was of interest or no further impact was done.

3 Test results

3.1 Impact angle, block velocity and energy before impact

The impact angle α is a significant parameter for the impact process as shown by Kister (2015). The impact angle is the angle between the perpendicular to the embankment slope and the block's trajectory. By definition, the angle is positive, if the trajectory is below the perpendicular (Fig. 3.1a) and negative, if the trajectory is above the perpendicular.

A positive impact angle leads to an upward directed velocity component during the impact process (Fig. 3.1b). The larger the positive impact angle, the larger is the upward directed velocity component and with it a force which pushes the block towards the embankment's crest. On the other hand, if the impact angle is negative, the velocity component parallel to the slope will be directed downward and is therefore opposite to the rolling direction of the block.

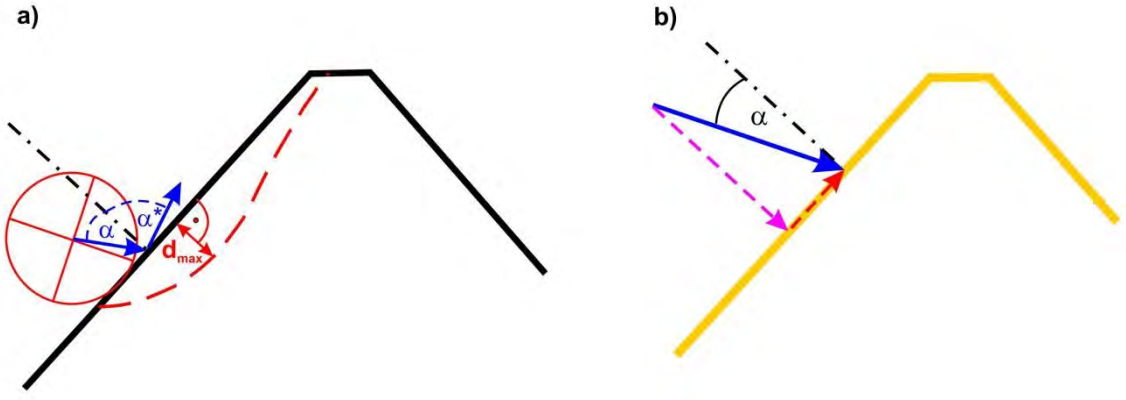

Fig. 3.1: a) Definition of impact angle α, exit angle α and maximum penetration depth d_{max}. b) A positive impact angle leads to an upward directed velocity component during the impact process.*

Impact angle as well as translational and rotational block velocities had been determined by using 3 pictures just before the impact with different positions of the impactor (Fig. 3.2). The distance and angle of rotation of the block had been measured, the time difference of the pictures was given by the frame rate of 500 Hz of the high speed camera recording.

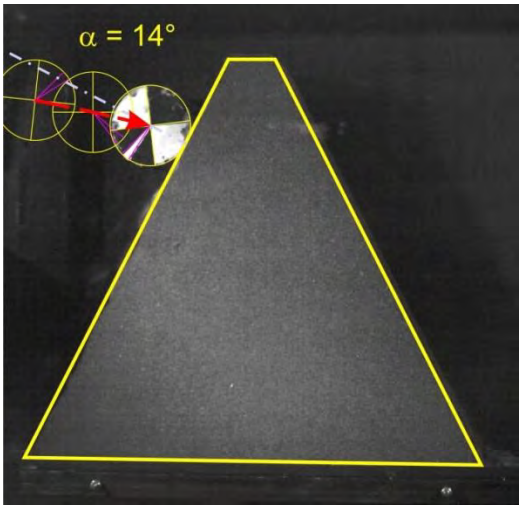

Fig. 3.2: Impact angle α as well as the translational and rotational block velocities have been determined by measurement of three positions of the impacting block.

For a batter of 2:1 on the "uphill" slope 27 tests have been done in total with all three types of impactors. The minimum impact angle was determined to be 8°, the maximum impact angle was determined to be 15°. Both values were received in tests with impactor GS. The mean value of the impact angle of all 27 tests in round figures is 12°. Fig. 3.3 shows the frequency distribution vertical-bar graph of the impact angle.

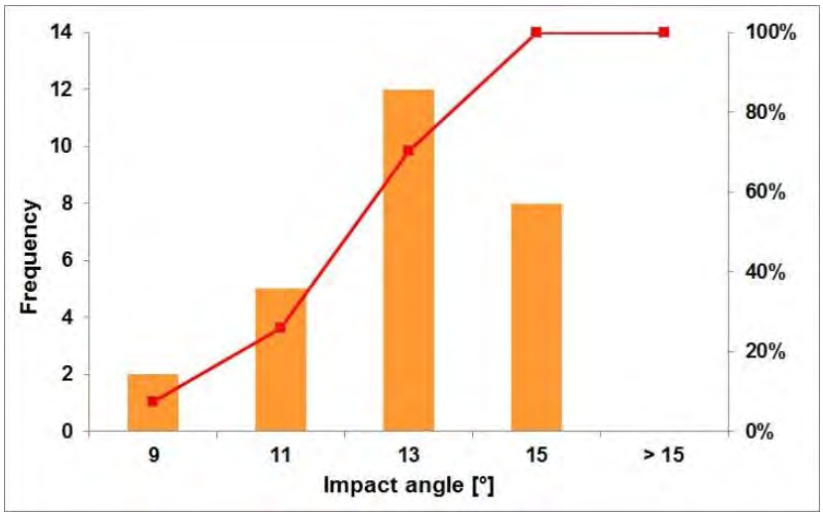

Fig. 3.3: Bar chart of the frequency of impact angle obtained during 27 tests on a slope with batter 2:1.

Two tests had been done on a slope with a batter 5:2, one with impactor G and the other with impactor OKT. In both tests the impact angle has been determined to be 8°. Increasing the batter of the slope to a value of 5:1 resulted in a negative value for the impact angle of -4° (G) respective -5° (OKT). In that case the trajectory is above the perpendicular and this result in a downward directed velocity component, which is contrary to the rolling movement of the block.

The translational block velocity v was determined according to Fig. 3.2 for 31 tests. The mean value of the translational velocity just before the impact had been determined to 6.5 m/s. Taking into account the scaling factor $\lambda^{1/2} = 3$ of Table 2.3 this result in a block velocity in the "prototype world" of 19.5 m/s, which is a quite realistic value for block velocities in rockfall events.

The minimum value of the velocity v = 5.6 m/s was received with that block GS, which was made solely of concrete and which was broken during the first test (test GS_2145H_9_11). The highest velocity v = 7.1 m/s was reached with a block GS too, but now with the new block with a steel lining as exterior facing (GS_2121FF_18_11). Having regard to the 3 different block types, one may see a slight difference in the translational velocities. With a mean value for the velocity v = 6.3 m/s the block G was the most slowly impactor. The block OKT was a little bit faster with v = 6.5 m/s. The highest mean value for the velocity v = 6.7 m/s was achieved for block GS with the steel lining as exterior facing. But the differences in these values for the translational velocities are all within the error of measurement, which has been determined to be about 0.5 m/s.

In the tests with the Gurtnellen model translational velocities of 6.1 m/s and 6.9 m/s had been determined with impactor GS. This is in the same range as determined in the other tests with impactor GS.

Much more significant are the differences concerning the rotational velocity of the 3 kinds of impactors. The block OKT was sliding on its edges in the down pipe at least during the last third of this way. Therefore the rotational velocity at the impact was very slow and in the range of 0 to 13 Hz. The concrete block G got the highest values for the rotational velocities. The mean value here was ω = 79 Hz. In test GS_2145H_9_11 with the pure concrete block the rotational velocity was ω = 74 Hz, which is in the range of the values received with block G. With a mean value for the rotational velocity of ω = 39 Hz the block GS with the steel lining as exterior facing achieves just half the value of the rotational velocity of the concrete block G. The tests done on the Gurtnellen model achieved similar results for the rotational velocity. The lower rotational velocity of impactor GS with a steel facing is a result of the lower friction between steel facing of the block and steel of the down pipe. Fig. 3.4 shows rotational versus translational block velocity of the three impactors. In the graph the differences in rotation is obvious.

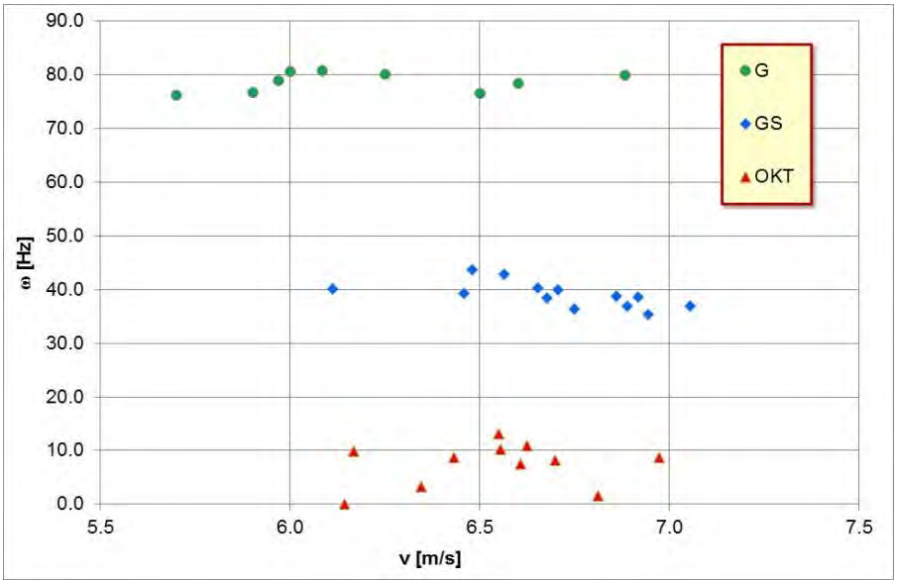

Fig. 3.4: Rotational versus translational block velocity

Fig. 3.5 shows rotational and translational energy determined in the different tests. All data points received with the impactor GS are located between the lines E_{rot}/E_{trans} = 0.1 and E_{rot}/E_{trans} = 0.2. Due to the very low rotation of impactor OKT all data points of these tests are below the line E_{rot}/E_{trans} = 0.025. All tests results received with impactor G show high values for the ratio of rotational and translational energy in the range of 0.5.

A graph concerning the ratio of rotational to translational energy of blocks can be found in the Japanese Rockfall Protection Handbook (JRA, 2000) as well as in the paper of Yoshida (1998). In this graph the most data pairs of rotational and translational energy are located between the upper boundary line with the value 0.2 and the lower boundary line with the value 0.02. Usiro et al. (2006) had done real scale tests on a 41 m high slope to determine the ratio of rotational to translational energy in rockfall events. They had done tests with concrete bodies (sphere: 200 kg, cube: 520 kg) as well as tests with 10 natural rock blocks (120 kg up to 2060 kg). According to these tests a lower and an upper boundary value for the ratio of rotational to translational energy of natural blocks during rockfall can be given. The lower boundary value is 0.025, while the upper boundary value is 0.2. But larger values than 0.4 had been achieved for the ratio of rotational to translational energy for the concrete sphere.

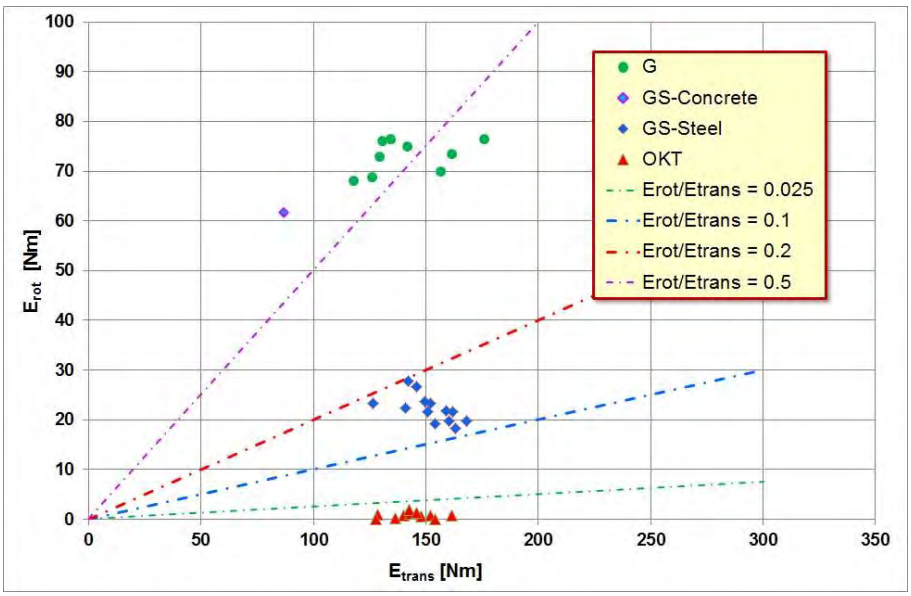

Fig. 3.5: Comparison of rotational and translational energy data of the impacting blocks G, GS and OKT.

The test results concerning the ratio of rotational to translational energy received with impactor GS with the steel lining as exterior facing fits very well with data of the ratio of rotational to translational energy found in real scale tests for natural blocks. On the other hand the ratio of rotational to translational energy, received in tests with impactor G, seems to be too high in comparison to the real scale tests with natural blocks, but are in the range of the tests done by Usiro et al. (2006) with a concrete sphere (see also Kister, 2015).

Using the scaling factor for the energy $\lambda^4 = 6561$ in Table 2.3 the impact translational energy of the tests may be transformed to the "prototype" size. This leads to a mean value for the impact translational energy of about 0.95 MJ (without consideration of tests on model Gurtnellen). Fig. 3.5 shows the frequency distribution vertical-bar graph of the transformed energy values. The minimum value of 0.57 MJ was achieved for test GS_2145H_9_11 with the hollow concrete cylinder, which was broken in the first test. The test GS_2145H_9_11 differs also significant from other tests because a very high ratio $E_{rot}/E_{trans} = 0.7$ was achieved.

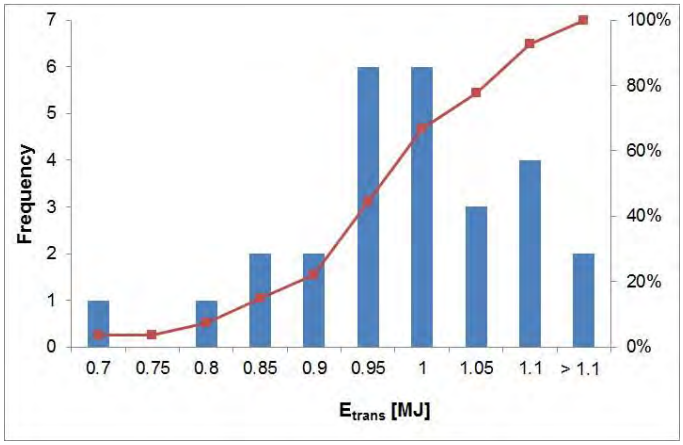

Fig. 3.6: Bar chart of the frequency of transformed translational energy values of the impacting blocks G, GS and OKT. Total number of tests: 31

For the Gurtnellen model the scaling factor for the energy is λ^4 = 160'000 in Table 2.3. So the transformed translational energy in this case is in the range of 20 MJ to 26 MJ. For the Gurtnellen embankments two block sizes, 50 t and 160 t, had been taken into account for the design. The impact velocity for both blocks was assumed to be 25 m/s. This will result to impact energies of 15.6 MJ respective 50 MJ taking into account only the translational energy as was done for the design of the Gurtnellen embankments. So the transformed translational energies are within the two values used for the design of the Gurtnellen embankments and may be interpreted in energy values as a block of about 70 to 85 t with a velocity of 25 m/s.

3.2 Block movement after contact

The tests had been recorded by a high-speed camera with 500 fps i.e. a picture was done every 2 milliseconds. In a first impact analysis step these pictures were used to determine the block's trajectory after the contact with the embankment. The following determining factors had been investigated with that method:

- Block shape and rotational velocity resp. rotational energy
- Shape of the embankment
- Crest width
- Slope facing.

Because of the used experimental set-up the parameters block shape and rotational velocity resp. rotational energy cannot be analyzed independent. If the impactor is a cylinder, this block will have rotation when impacting the embankment due to friction between the cylinder barrel and the down pipe. Otherwise the block with the octagonal cross section is sliding on two edges at the lower part of the down pipe and therefore this block has no or only minor rotation when the block hits the embankment. So a regulation of the rotational velocity respectively the rotational energy of a block is not possible with that kind of experimental set-up.

For the purpose of comparison of embankments with rockery facing and soil facing some of the test results shown in Kister (2015) had been used again in this chapter. Those test results can be identified by their name, because instead using the crest width in cm in these names the letters A or B are used to describe the crest width.

Fig. 3.7 shows the tests results for an embankment with an asymmetric cross section with a slope inclination 2:1 (62.6°) at the "uphill" side and a slope inclination 4:5 (37.3°) at the "downhill" side. On three pictures on the left the trajectories of cylinder G are shown, while on three pictures on the right the trajectories of block OKT are shown. In the tests of the two upper pictures a) and b) the crest width was 8.5 cm resp. 9.5 cm (identification mark B for the crest width). This equates to the crest width used in the new tests shown in the pictures e) and f) with stones placed parallel to the embankments slope (see Fig. 1.3a). In the middle the pictures c) and d) show the trajectories of tests with crest width 18.5 cm resp. 19 cm (identification mark A for the crest width) but no stones on the slopes.

In all three tests with rotating cylinder G the embankment was surmounted during the first impact, but there are differences in the curve progression of the trajectories. In picture a) the relationship of crest width to block diameter is approximately 0.53 and the block punched through the embankment's crest because of low resistance. The trajectory of the block center runs partly inside the contour of the embankment (Fig. 3.7 a).

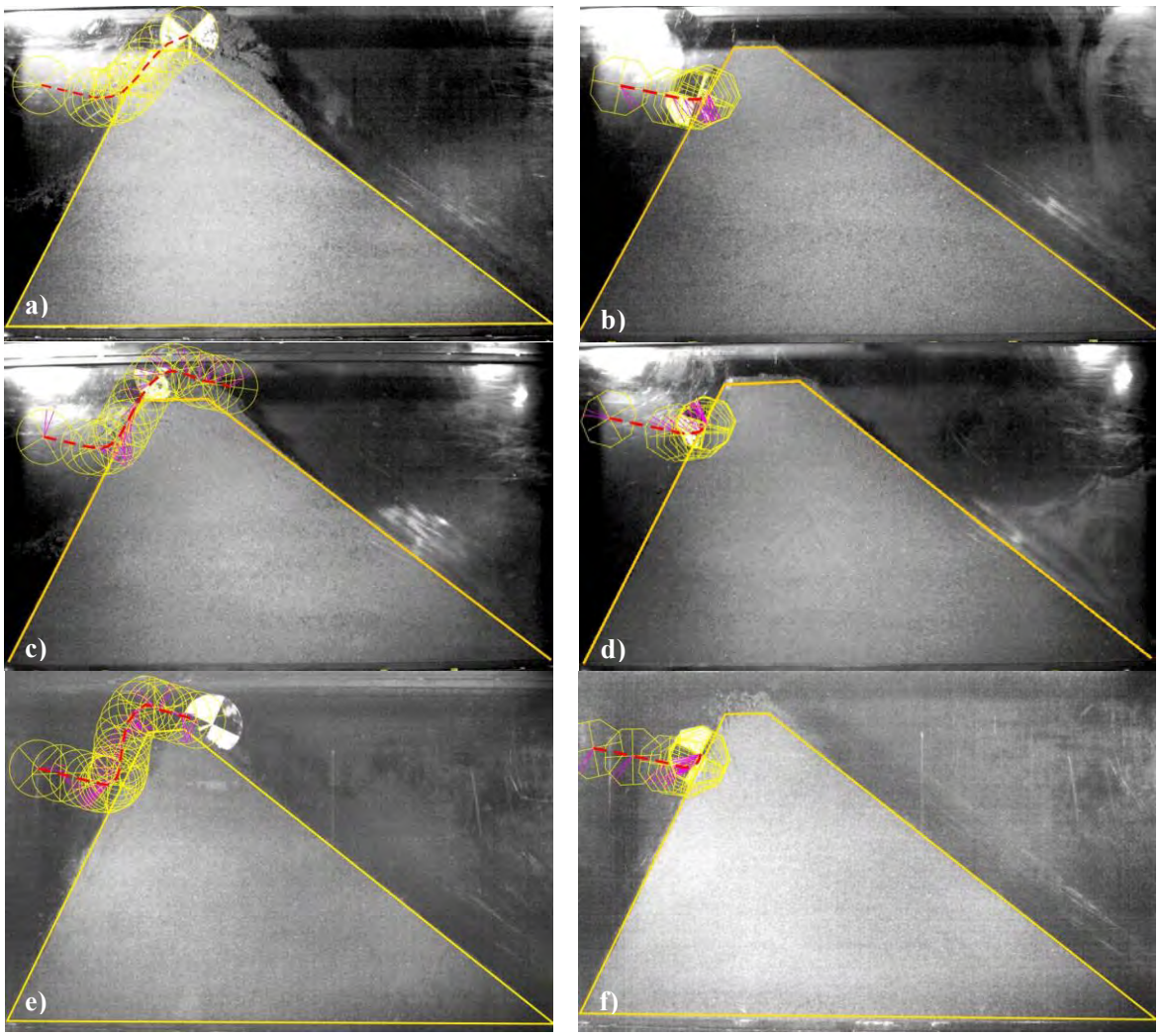

Fig. 3.7: Comparison of the block trajectories after the contact with an embankment with asymmetric cross section: a) G_2145_B_11-1, b) OKT_2145_B_11-1, c) G_2145_A_11-1, d) OKT_2145_A_11-1, e) G_2145H_9_11-1, f) OKT_2145H_9_11-1.

In picture Fig. 3.7 c) the relationship of crest width to block diameter is approximately 1.15 and therefore the impacting block is faced by a larger activated volume of the embankment resp. a larger activated mass. This results in an increase of the resistance of the embankment against the impacting block and so the trajectory of the block center runs along the contour of the embankment but not inside the contour of the embankment.

Fig. 3.7 e) shows the trajectory of a test with an embankment where stones had been placed parallel to the embankment's slope. Even though the relationship of crest width to block diameter in this test is only approximately 0.53, the block G in this case is not able to punch through the embankment's crest. The stones increase the resistance of the embankment and the trajectory of the block center runs outside of the contour of the embankment. But nevertheless the embankment was surmounted by the block G also in this test.

The tests done with the same embankment cross section but now impacted by the block OKT with no or only very low rotation show a very different behavior. The embankment was not surmounted by block OKT due to the first and second impact and the block was neither able to punch through the embankment in those tests. Only with a third impact in test OKT_2145_B_11 the block OKT was able to surmount the embankment. During this third impact the crest was completely destroyed. Furthermore the trajectories of the three tests with block OKT look very similar as shown in Fig. 3.7 b), d) and f).

Table 3.1 summarizes data and results of the tests shown in Fig. 3.7.

Description	Cylinder G	Body OKT
β_{us}: 62.6° β_{ds}: 37.3° a_c: 9 cm OS: no rockery	***G_2145_B_11*** FB approx. 0.6 * 2r 1st impact: block jumped over embankment crest with violent damage	***OKT_2145_B_11*** FB approx. 0.6 * 2r embankment not surmounted 1st impact: crest heavily damaged. 2nd impact: crest with violent damage 3rd impact: crest completely destroyed embankment surmounted
β_{us}: 62.6° β_{ds}: 37.3° a_c: 18.5 cm OS: no rockery	***G_2145_A_11*** FB approx. 0.6 * 2r 1st impact: block jumped over embankment crest with violent damage 2nd and 3rd impact: block jumped over embankment	***OKT_2145_A_11*** FB approx. 0.6 * 2r embankment not surmounted 1st impact: crest slightly damaged. 2nd impact: crest heavily damaged 3rd impact: crest with violent damage embankment not surmounted
β_{us}: 62.6° β_{ds}: 37.3° a_c: 8.5 cm OS: upright	***G_2145H_9_11*** FB approx. 0.7 * 2r block jumped over embankment crest with violent damage stones are completely separated and fell down	***OKT_2145H_9_11*** FB approx. 0.6 * 2r embankment not surmounted 1st impact: crest slightly damaged. 2nd impact: crest damaged, but not completely destroyed
Explanation:	β_{us}: slope angle uphill side β_{ds}: slope angle downhill side a_c: crest width	OS: orientation of stones 2r: block diameter FB: Freeboard

Table 3.1: Summary of the results of the tests shown in Fig. 3.7.

The embankment with an asymmetric cross section with a slope inclination 2:1 (62.6°) at the "uphill" side and a slope inclination 4:5 (37.3°) at the "downhill" side has also been used for impact tests with impactor GS with the steel lining and a triaxial acceleration sensor inside. One test with stones placed parallel to the embankment's slope (Fig. 1.3a) had been done as well as one test with stones placed horizontally to get a rough slope surface (Fig. 1.3 b). The relationship of crest width to block diameter was approximately 0.5. The difference of the translational energies in both tests was approx. 2.6%. The difference of the rotational energies in both tests was less than 4%. The relationship of rotational to translational energy was 0.18 resp. 0.19, which is below the upper boundary of 0.2 found by Usiro et al. (2006) for natural blocks. In both tests the block GS was not able to surmount the embankment, even though the freebord in the tests does not fulfills the requirements of ONR 24810:2013 and was smaller than one block diameter (Table 3.2).

The main difference in the two tests is the impact angle α. In the test GS_2145F_7_11 an impact angle of about 8° was determined while in the test GS_2145H_9_11 the impact angle was larger and reached a value of 13°.

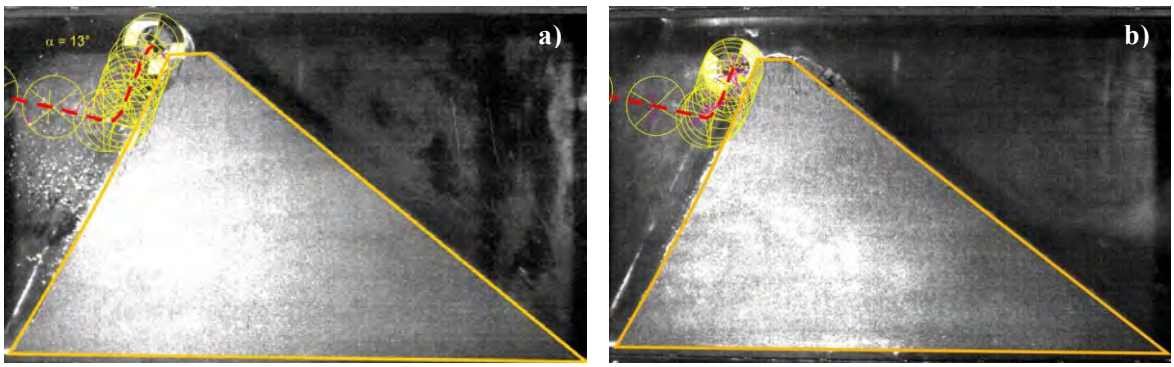

Fig. 3.8: Comparison of the block trajectories after the contact with the embankment with asymmetric cross section and "rockery": a) GS_2145H_9_11-1, b) GS_2145F_7_11-1

The larger value of the impact angle as well as the smoother surface of the "rockery" in test GS_2145H_9_11-1 may explain why block GS reached a higher level in test GS_2145H_9_11-1 than in test GS_2145F_7_11-1 (Fig. 3.8). The larger deformation at the top of the downhill slope with intensive formation of cracks during test GS_2145F_7_11-1 is a result of the horizontally placed stones, which are not able to reduce energy by compaction but transfer the energy to the smaller soil body behind the stones. A summary of the test data and results is given in Table 3.2.

Description	***GS_2145H_9_11***	***GS_2145F_7_11***
β_{us}: 62.6° β_{ds}: 37.3° a_c: 8.5 cm resp. 7 cm	FB approx. 0.85 * 2r embankment was not surmounted, but center of block above crest level 1st impact: crest slightly damaged. 2nd impact: crest damaged, large joints during impact process	FB approx. 0.75 * 2r embankment was not surmounted, but center of block at crest level 1st impact: crest damaged and intensive formation of cracks 2nd impact: crest material was pushed to the "downhill" slope

Table 3.2: Summary of the results of the tests shown in Fig. 3.8.

Two tests had been done with an embankment with a bi-linear slope at the "uphill side". At the lower part with a batter of 2:1 stones had been placed parallel to the embankment's slope. The upper part was solely made of soil and had an inclination of approx. 37° (4:5). One test had been done with cylinder G and the other test with block OKT. In both tests the block hit the embankment immediate under the break of the bi-linear slope at the "rockery" (Fig. 3.9). The impact angle was 13° resp. 14° and therefore more or less the same.

The block mass of block OKT is 7% lower than the mass of block G and block G got a translational velocity at the impact point which is approx. 7.25% higher than the velocity of block OKT at this point. This results in a difference of the translational energy of about 26%. But the comparison of the rotational energy of both blocks showed approximately a factor 100 (block G: 76.3 Nm, block OKT: 0.79 Nm). This led to a completely different behavior of the blocks during the impact process. While block G jumped high over the embankment, block OKT was not able to surmount the embankment and fell back on the "uphill" side. Fig. 3.9 shows the trajectory of both blocks during the tests.

Three additional impact tests had been done with block OKT on the already damaged embankment. This resulted in an increasing penetration depth for block OKT, but the embankment was neither punched through nor was the block able to surmount the embankment. A second impact with block G on the embankment damaged the crest and the stones had been separated and fell down.

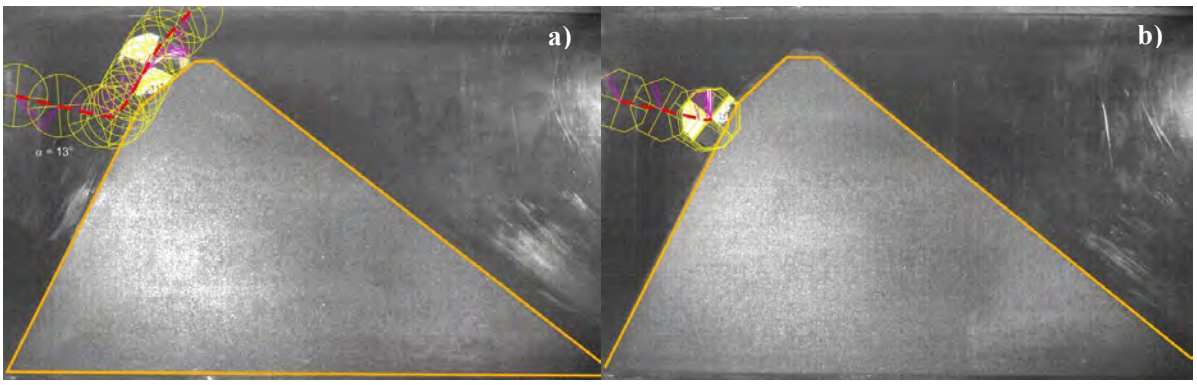

Fig. 3.9: Comparison of the block trajectories after the contact with a bi-linear slope at the "uphill side" of an embankment, "rockery" at the lower part, soil at the upper part: a) G_2145H_4K_11, b) OKT_2145H_6K_11, first impacts.

A summary of the test data and results of the tests G_2145H_4K_11 and OKT_2145H_6K_11 is given in Table 3.3.

Description	***Cylinder G***	***Body OKT***
β_{us}: 62.6° β_{ds}: 37.3° a_c: 4.5 cm resp. 6 cm OS: upright	***G_2145H_4K_11*** FB approx. 1 * 2r block jumped over embankment 1st impact: crest slightly damaged. 2nd impact: crest damaged, stones are completely separated and fell down	***OKT_2145H_6K_11*** FB approx. 1 * 2r embankment not surmounted, crest damaged, but withstands additional three impacts

Table 3.3: Summary of the results of the tests shown in Fig. 3.9.

Impact tests on embankment models with batter 2:1 at both sides had been done for the following surface conditions of the embankment slopes:

a) without stones, embankment made solely out of soil
b) stones placed parallel to the slope at the impact side
c) stones placed horizontal at the impact side
d) stones placed horizontal at both slopes.

The tests had been done with block G as well as with block OKT. The crest to block diameter ratio for these tests was chosen to be approx. 0.56.

Fig. 3.10 shows the trajectory of block G for the test conditions a) to d). In all 4 tests the embankment was not able to stop the block, but the trajectories show significant differences.

For the embankment made solely out of soil a part of the crest was chipped and a large amount of material was sliding down at the "downhill" slope. Block G received a maximum jump height above the crest level and this maximum is located at the "downhill side".

The stones placed parallel to the slope at the impact side in case b) increased the resistance of the embankment and therefore the penetration depth is less than in case a). On the other hand the jump height now is higher, but the maximum height is located above the crest, i.e. the length of the jump is shorter than in case a).

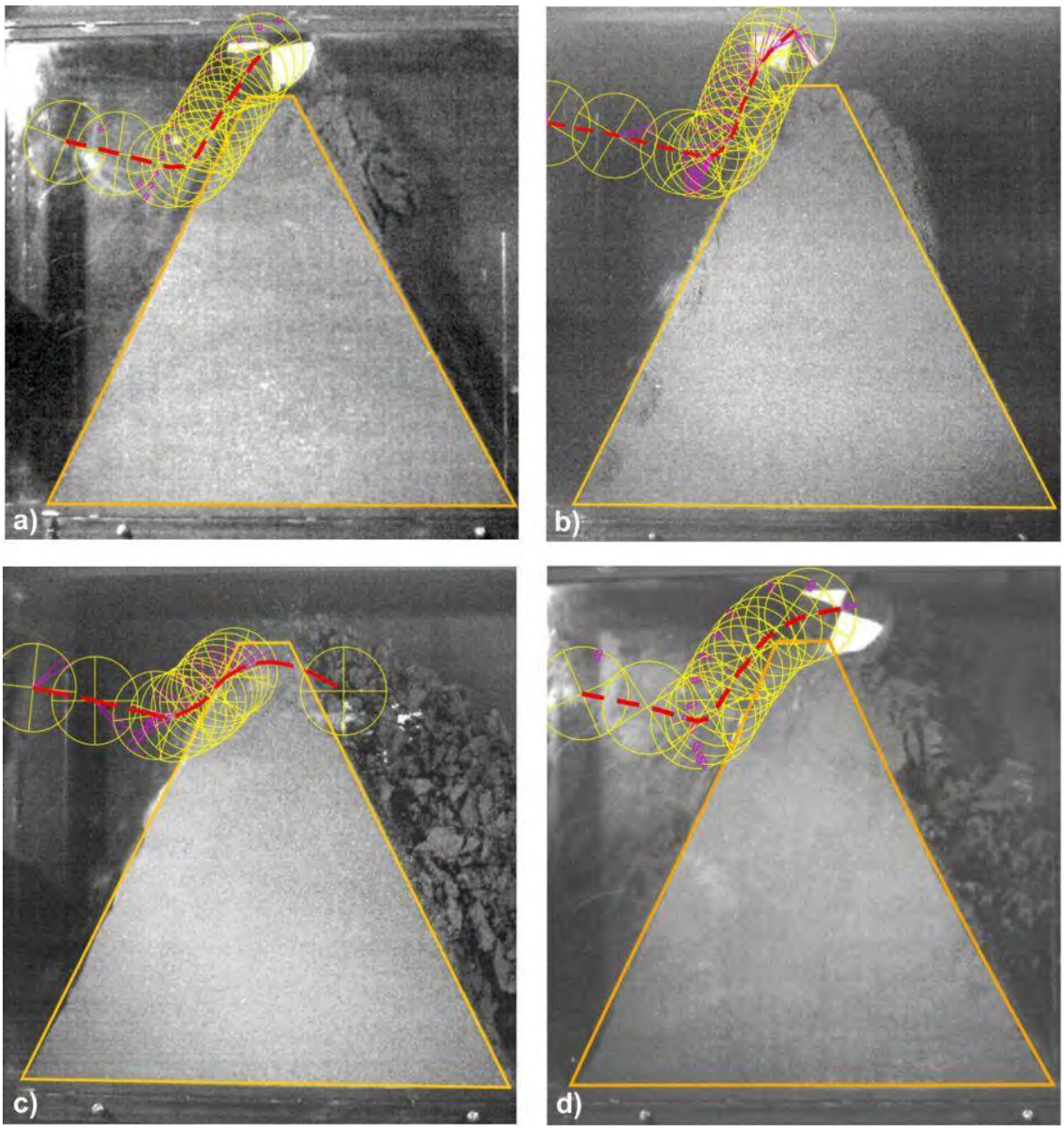

Fig. 3.10: Impact with impactor G on embankment models with batter 2:1 at both sides and crest to block diameter ratio 0.56: a) without rockery (G_2121_9_11-1), b) stones placed parallel to the slope at the impact side (G_2121H_9_11-1), c) stones placed horizontal at the impact side (G_2121F_8_11-1), d) stones placed horizontal at both slopes (G_2121FF_9_11-1).

When the stones had been placed horizontally (see Fig. 2.16), the block punched through the embankment's crest (Fig. 3.10 c). An upward movement of the block can also be seen in case c), but the difference between impact point and maximum trajectory level is less in this test compared with the cases a), b) and d). In addition the trajectory of the block center is running within the contour of the embankment (Fig. 3.10 c). As already mentioned the stones are not able to reduce energy by compaction but transfer the energy to the soil body behind the stones. The soil body behind the stones in this case is smaller than in cases a) and b), that means the resistance of the soil is less than in case a) or b), which ends up in the destruction of the crest.

Additional stones placed horizontal at the "downhill" slope as done in case d) increase the weight and therefore the resistance of the embankment's crest. This resulted in a larger upward movement of the block G and the block cuts the crest and surmounts the embankment.

The same four embankments, but now impacted by block OKT with no or minor rotation, show a very different behavior in comparison to the tests with block G. In all four tests the block OKT was not able to surmount the embankment. But already the first impact destroyed the embankment's crest totally (Fig. 3.11).

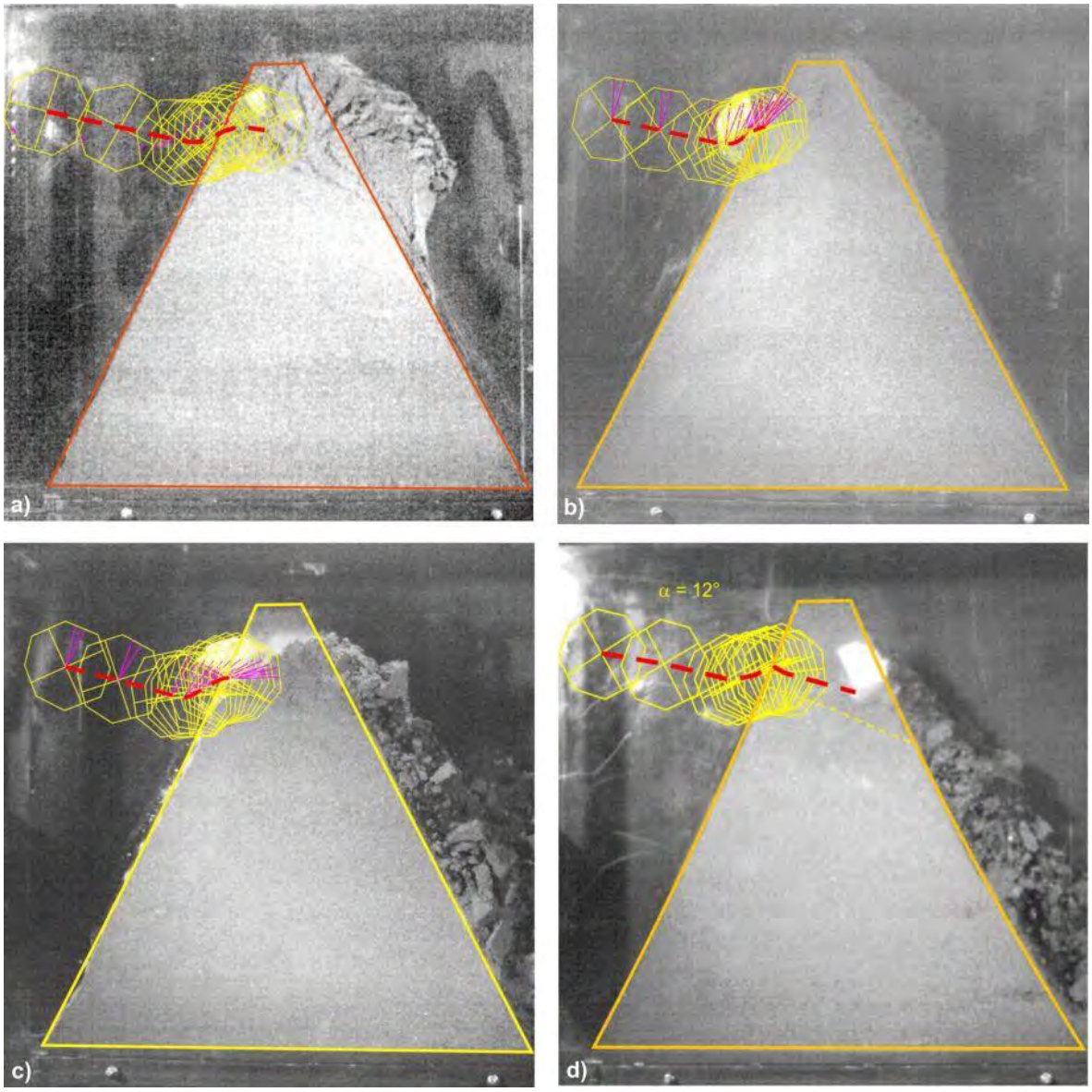

Fig. 3.11: Impact with impactor OKT on embankment models with batter 2:1 at both sides and crest to block diameter ratio 0.56: a) without rockery (OKT_2121_9_11-1), b) stones placed parallel to the slope at the impact side (OKT_2121H_7_11-1), c) stones placed horizontal at the impact side (OKT_2121F_8_11-1), d) stones placed horizontal at both slopes (OKT_2121FF_9_11-1).

There are significant differences between the four tests. In the tests OKT_2121_9_11-1 (Fig. 3.11a) and OKT_2121FF_9_11-1 (Fig. 3.11d) block OKT produced a shear plane during the test, which is approximately parallel to the perpendicular line to the slope and its extension takes course to the center of block OKT at impact position. The impact angle in the two tests is 13° respective 12°. So the shear plane is not parallel to the impact direction. During the tests OKT_2121H_7_11-1 and OKT_2121F_8_11-1 no such shear plane is visible.

The penetration depth of block OKT in the tests OKT_2121H_7_11-1 and OKT_2121F_8_11-1 is less than in the two other tests and reached an amount which is only a little bit larger than the outside radius of block OKT. This resulted in a rollback of the block on the "uphill" slope. The penetration depth in the tests OKT_2121_9_11-1 and OKT_2121FF_9_11-1 is much deeper. The block reaches the "downhill" slope with its contour, i.e. the block punched through the embankment's crest. Additional in both cases the block OKT remains at the top of the destroyed embankment crest.

So it can be stated that for block OKT the stones increase the resistance of the embankment in the tests OKT_2121H_7_11-1 and OKT_2121F_8_11-1 while an additional stone layer, which was used in test OKT_2121FF_9_11-1 at the "downhill" slope for that slender construction, is counterproductively and may led to secondary rockfall produced by stones, which will be pushed out of the rockery. A summary of the test data and results of the tests is given in Table 3.4.

Description	Cylinder G	Body OKT
β_{us}: 62.6° β_{ds}: 62.6° a_c: 8.5 cm resp. 7 cm OS: no rockery	***G_2121_9_11*** FB approx. 0.6 * 2r block jumped over embankment crest with violent damage	***OKT_2121_9_11*** FB approx. 0.7 * 2r embankment not surmounted, but crest totally destroyed
β_{us}: 62.6° β_{ds}: 62.6° a_c: 8 cm OS: upright	***G_2121H_9_11*** FB approx. 0.6 * 2r block jumped over embankment crest with violent damage	***OKT_2121H_7_11*** FB approx. 0.7 * 2r embankment not surmounted, but crest totally destroyed
β_{us}: 62.6° β_{ds}: 62.6° a_c: 8 cm OS: horizontal	***G_2121F_8_11*** FB approx. 0.6 * 2r embankment was punched through, crest totally destroyed	***OKT_2121F_8_11*** FB approx. 0.7 * 2r embankment not surmounted, but crest totally destroyed
β_{us}: 62.6° β_{ds}: 62.6° a_c: 8 cm OS: horizontal	***G_2121FF_9_11*** FB approx. 0.6 * 2r block jumped over embankment crest with violent damage	***OKT_2121FF_9_11*** FB approx. 0.6 * 2r embankment not surmounted, but crest totally destroyed

Table 3.4: Results of tests with an embankment model with batter 2:1 at both sides and crest to block diameter ratio of approx. 0.5.

To analyze the influence of crest thickness, another test series had been done with an embankment model with batter 2:1, but now with a crest to block diameter ratio of approx. 1.1. In this test series block GS was used instead of block G. Block GS has a little bit less weight (GS: 6.76 kg, G: 7.28 kg), but the values for the ratio of rotational to translational energy received with impactor GS in these tests correspond very well with the data found by Usiro et al. (2006) for natural blocks. The ratio of rotational to translational energy determined for block GS was in the interval 0.12 to 0.16 (Fig. 3.5).

Tests had been done for the following surface conditions of the embankment slopes:

a) without stones, embankment made solely out of soil
b) stones placed horizontal at the impact side
c) stones placed horizontal at both slopes.

But even though the ratio of rotational to translational energy of block GS agrees very well with the data of Usiro et al. (2006), the embankment was surmounted by block GS. There was just one exceptional case: In test GS_2121FF_18_11-1 the block GS changed its rotational axis when climbing up to the crest level (Fig. 3.12c). Due to this change of the rotational axis and the corresponding loss of energy, the block was not able to surmount the embankment. Therefore this test was repeated. The repeated test was named GS_2121FF_18_11_B and in this test the embankment was surmounted again. Fig. 3.12 shows the trajectories of block GS for the test conditions a) to c) presented above.

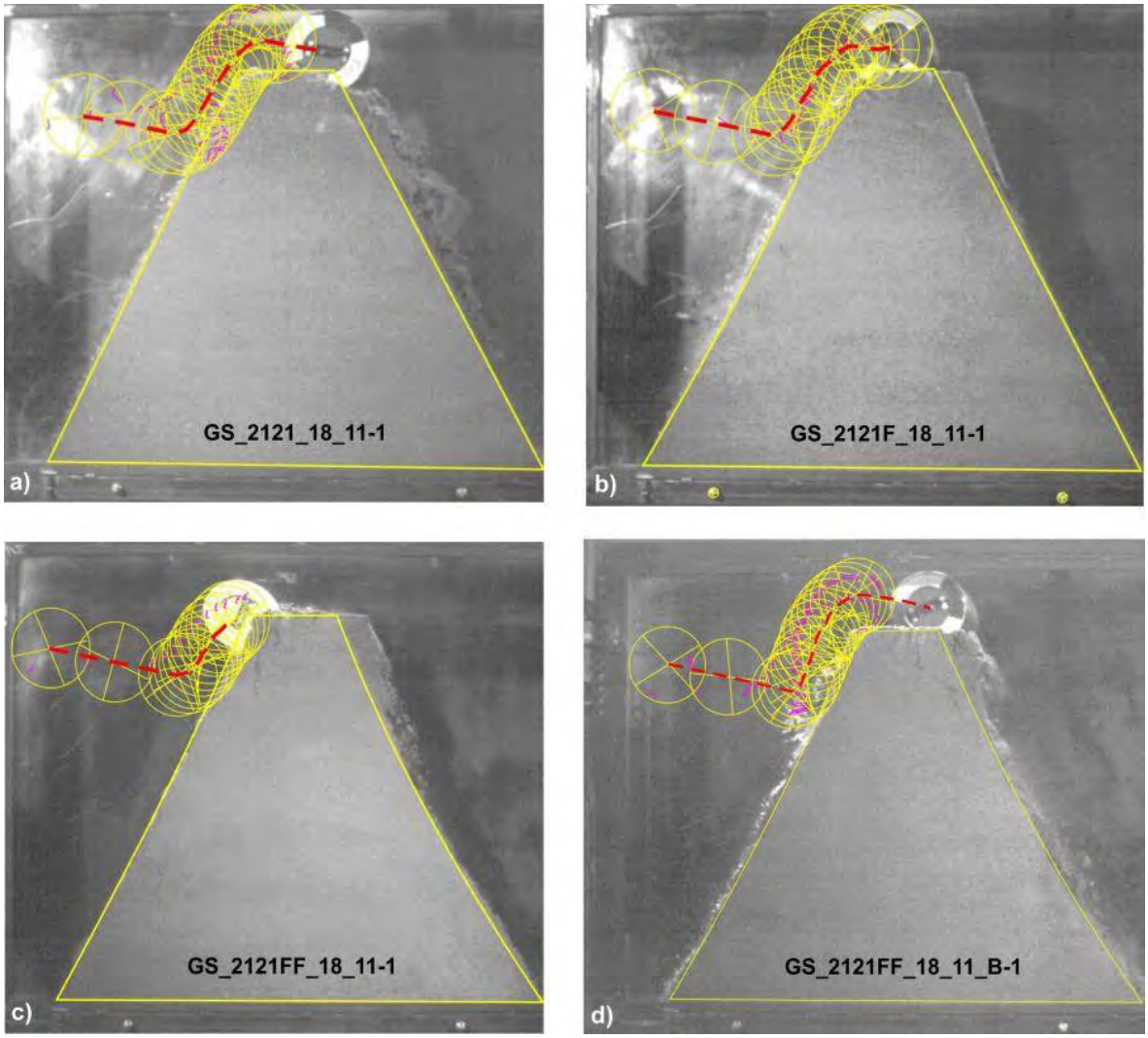

*Fig. 3.12: Impact with impactor GS on embankment models with batter 2:1 at both sides and crest to block diameter ratio approx. 1.1: a) without rockery, b) stones placed horizontal at the impact side, c) and d) stones placed horizontal at both slopes, FB approx. 0.5*2r. Only in test GS_2121FF_18_11-1, shown in picture c), the embankment was not surmounted.*

Embankment models with batter 2:1 at both sides and crest to block diameter ratio approx. 1.1 had also been used for impact tests with body OKT. During the test OKT_2121_18_11-1 a malfunction of the high speed camera occurred and no pictures had been recorded for the first impact. Therefore the test was repeated and the repeated test is named as OKT_2121_18_11-B1 for the first impact and OKT_2121_18_11-B2 for the second impact (Fig. 3.13 a, b).

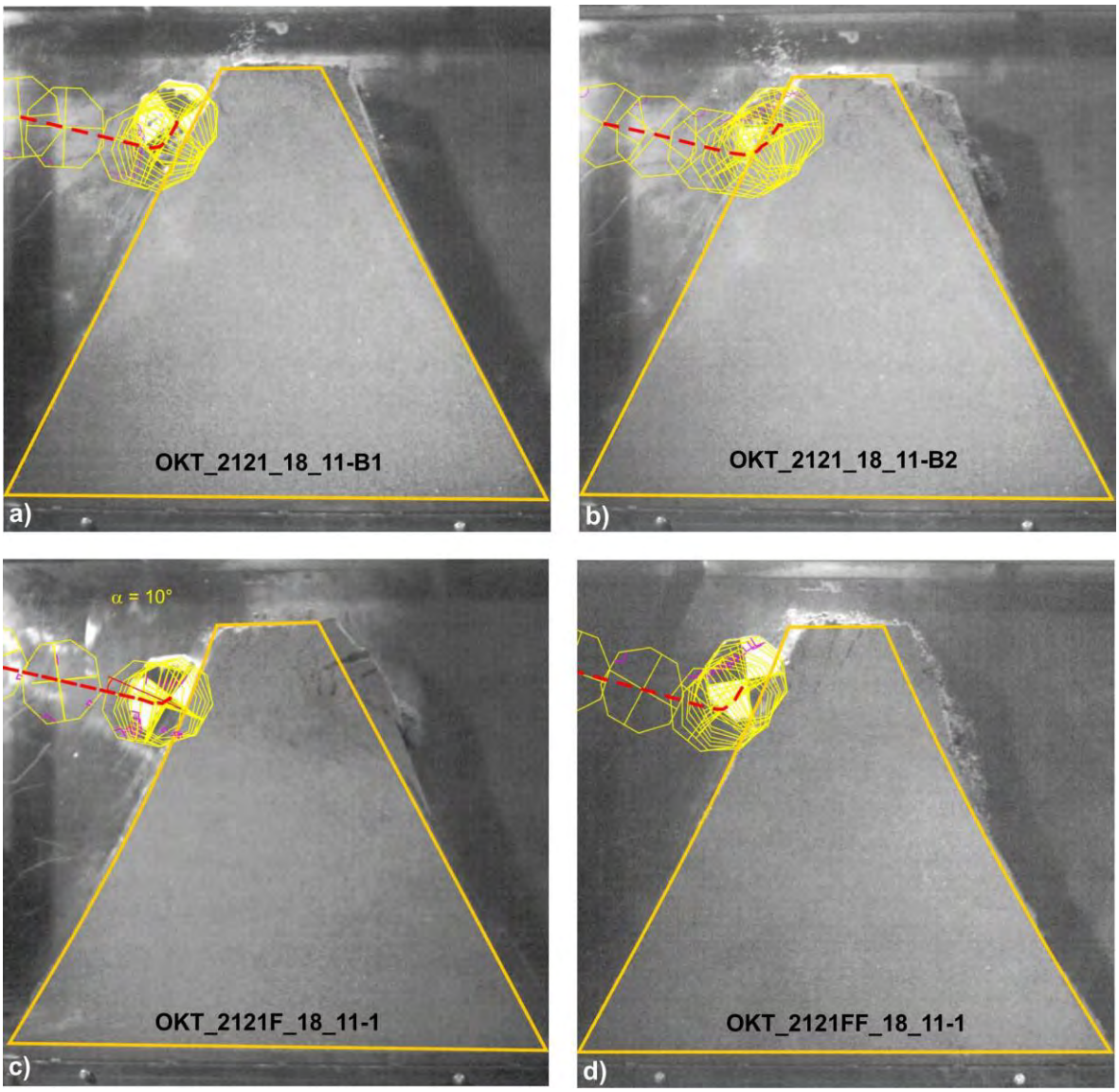

*Fig. 3.13: Impact with impactor OKT on embankment models with batter 2:1 at both sides and crest to block diameter ratio approx. 1.1: a) and b) without rockery, first and second impact, c) stones placed horizontal at the impact side, d) stones placed horizontal at both slopes, FB: 0.7*2r ... 0.8*2r.*

In all tests there is a movement of block OKT upwards to the crest. The penetration depth of block OKT is less than the block radius for all first impacts (Fig. 3.13 a, c, d). As expected the penetration depth reached its largest amount in test OKT_2121_18_11-B1, without any stones. Only for the second impact of test OKT_2121_18_11-B2 the penetration depth is larger, but there was loosening of the embankment material due to the first impact.

The penetration depth in tests OKT_2121F_18_11-1 and OKT_2121FF_18_11-1 is approx. the same (Fig. 3.13c and d). So the "rockery" at the "downhill" slope seems to have no significant influence on the resistivity of the embankment and the penetration depth for a crest to block ratio of approx. 1.1 or larger.

Even though the freeboard in those tests shown in Fig. 3.13 was less than one block diameter, the minimum dimension, which is recommended by the standard ONR 24810:2013, the block OKT was neither be able to punch through the embankment's crest nor to surmount the embankment. But it has to be taken into account that block OKT has no or only very low rotation in the tests.

For all three surface conditions a), b) and c) of the embankment slope, the embankment withstands a second impact too. The penetration depth of the block OKT due to the second impact is deeper (cf. Fig. 3.13, a and b) because the embankment material has been already loosened and displaced by the first impact. The embankment had been heavily damaged or even destroyed due to the second impact, but the task to retain the block was fulfilled in the tests. Test data and results of the tests shown in Fig. 3.13 are summarized in Table 3.5.

Description	***Cylinder GS***	***Body OKT***
β_{us}: 62.6° β_{ds}: 62.6° a_c: 18 cm OS: no rockery	***GS_2121_18_11-1*** FB approx. 0.5 * 2r only one impact embankment surmounted crest with significant damage shear plane visible	***OKT_2121_18_11*** FB approx. 0.8 * 2r embankment not surmounted 1st impact: crest damaged. 2nd impact: significant damage
β_{us}: 62.6° β_{ds}: 62.6° a_c: 17.5 cm / 18 cm OS: horizontal	***GS_2121F_18_11-1*** FB approx. 0.5 * 2r only one impact embankment surmounted crest with significant damage	***OKT_2121F_18_11*** FB approx. 0.7 * 2r embankment not surmounted 1st impact: significant damage. 2nd impact: massive damage, shear plane visible
β_{us}: 68.6° β_{ds}: 62.6° a_c: 18 cm OS: horizontal	***GS_2121FF_18_11-1*** FB approx. 0.55 * 2r only one impact rotational axis changed at crest embankment not surmounted crest with significant damage	***OKT_2121FF_18_11*** FB approx. 0.75 * 2r embankment not surmounted 1st impact: significant damage. 2nd impact: crest totally destroyed, block rolled back
β_{us}: 68.6° β_{ds}: 62.6° a_c: 18 cm OS: horizontal	***GS_2121FF_18_11_B*** FB approx. 0.55 * 2r embankment surmounted 1st impact: crest with large cracks 2nd impact: shear planes visible, crest destroyed	
Explanation:	β_{us}: slope angle uphill side β_{ds}: slope angle downhill side a_c: crest width	OS: orientation of stones 2r: block diameter FB: Freeboard

Table 3.5: Results of tests with an embankment model with batter 2:1 at both sides and crest to block diameter ratio of approx. 1.1.

As shown before, a freeboard less than one block diameter is sufficient to stop the non-rotating or slow-rotating block OKT with edges at an embankment with batter 2:1, even though the impact angle is as large as 10° to 14°. On the other hand the same embankment was not able to stop the rotating block GS, even though the ratio of rotational to translational energy agrees very well with the data of Usiro et al. (2006) found for natural blocks.

To determine the maximum climbing height of block GS during an impact and to get information about the influence of the roughness of the "rockery" surface two impact tests on embankment models with a batter 2:1, but with different "rockery roughness", had been done (Figures 3.14 and 3.15):

a) With stones placed parallel to the slope at the impact side (GS_2121HG_18_11) and
b) With stones placed horizontally at the impact side (GS_2121FG_18_11).

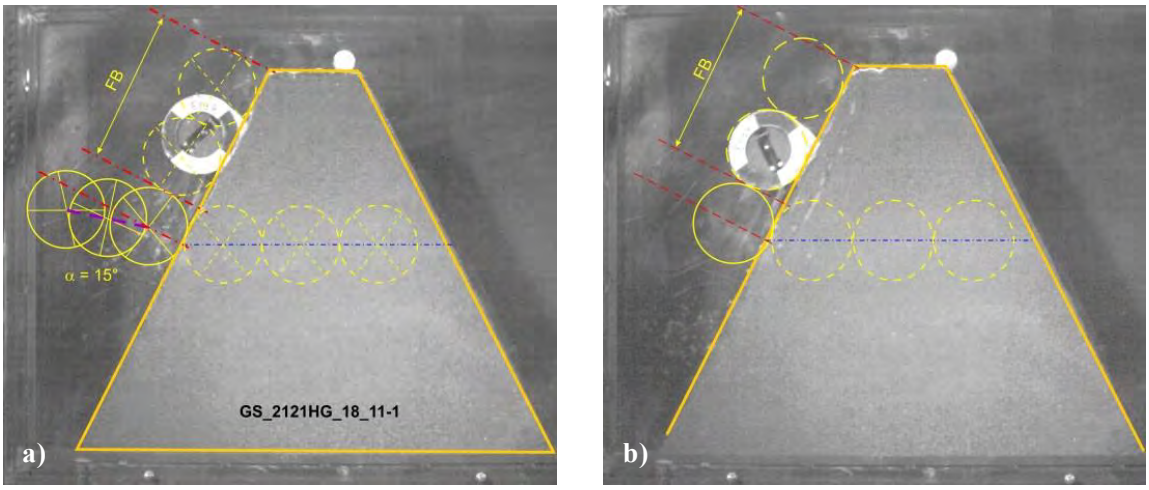

*Fig. 3.14: Test GS_2121HG_18_11: a) first impact, FB = 2*2r, climbing height approx. 1.3*2r, b) second impact, FB = 1.9*2r, climbing height approx. 1*2r.*

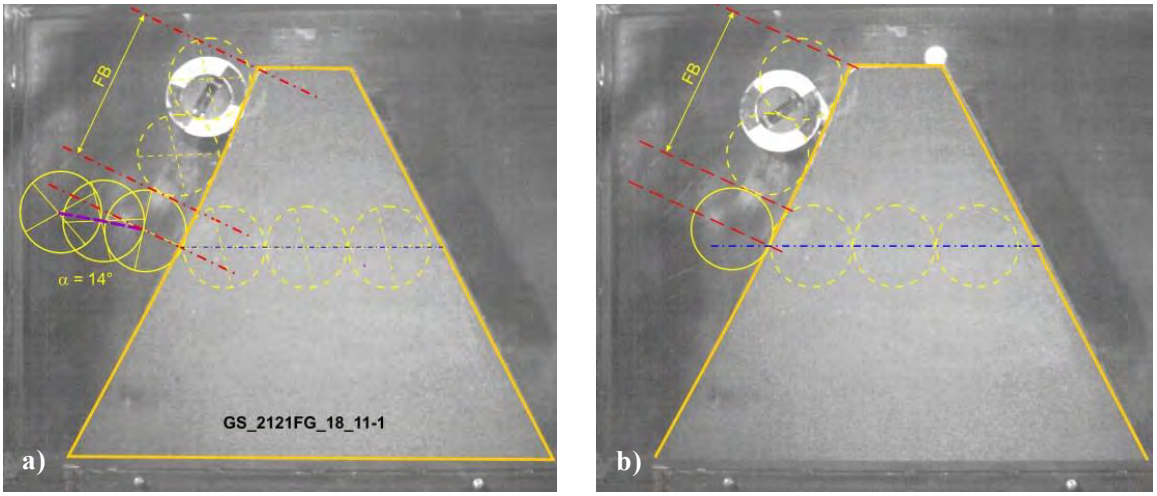

*Fig. 3.15: Test GS_2121FG_18_11: a) first impact, FB = 1.9*2r, climbing height approx. 1.8*2r, b) second impact, FB = 1.9*2r, climbing height approx. 1.55*2r.*

For these tests the freeboard was chosen to be approximately 1.9 block diameter. This value is a little bit less than the value of 2 block diameters specified in standard ONR 24810:2013 as minimum value for the freeboard of pure soil embankments, but significantly larger than the minimum value specified for embankments with rockery. The crest to block diameter ratio was chosen again to be approx. 1.1. The impact point is at a level, where the embankment thickness is larger than three block diameter (Fig. 3.14 and Fig. 3.15) and therefore according to Kister (2015) there was no risk that the embankment will be punched through. On each embankment type a first and a second impact with block GS had been done. In no test the embankment was surmounted by block GS but the experiments showed some remarkable results:

a) The rough surface of the rockery in test GS_2121FG_18_11 led to a larger climbing height for block GS than the "smooth" surface in test GS_2121HG_18_11, although the block velocities had been very similar (see Appendix C1, difference in translational velocity: 1.5%, difference in rotational velocity: 6%). If the climbing height is measured in the same way as the freeboard, i.e. parallel to the slope, the first impact on the rough surface led to a climbing height which is 1.8 the block diameter while the first impact on the smooth surface led to a climbing height of 1.3 block diameter. So the climbing height for the first impact at the rough surface is 28% higher than the climbing height at the smooth surface. For the second impact the climbing height of block GS at the rough surface is approx. 35% higher than the climbing height at the smooth surface. The maximum climbing heights received in the tests are shown in Figure 3.14 respective Fig. 3.15.
b) The first impact of block GS resulted in a larger climbing height than the second impact for both surface roughness types. For the smooth surface the factor for the climbing height between first and second impact is 1.3. For the rough surface this value is a little bit less and approx. 1.2.

These results may be interpreted as follows:

a) In the test with the stepped rough slope surface impactor GS and rockery surface have less contact points than in the test with the "smooth" surface. Additional during the impact process the block GS bounced off the embankment's slope in both tests, but the time without a contact was larger in test GS_2121FG_18_11 than in test GS_2121HG_18_11. Therefore friction losses between impactor and embankment slope are smaller in test GS_2121FG_18_11 than in test GS_2121HG_18_11.
b) Due to the first impact the stones are pushed into the soil and a kind of depression is produced (Fig. 3.16b, Fig. 3.17a and b). When the impactor hits this depression again during the second impact, energy is needed to get out of this depression. This amount of energy is missing, when the impactor is climbing up. Therefore the climbing heights of the second impacts are smaller than the climbing heights of the first impact.

Fig. 3.16a and b show the rockery before and after the first impact. Only little damage is visible to the naked eye and the damage seems to be restricted to the impact area. But at the embankment's crest a crack occurred between rockery and soil (Fig. 3.16 c). This is already an indication for dissolution. In consequence of the second impact a separation between rockery and soil occurred and all stones dropped down. On the other hand, a golf ball, which was placed on the crest of the embankment, showed only a small displacement. But a horizontal crack at the "downhill" slope was detected after the second impact.

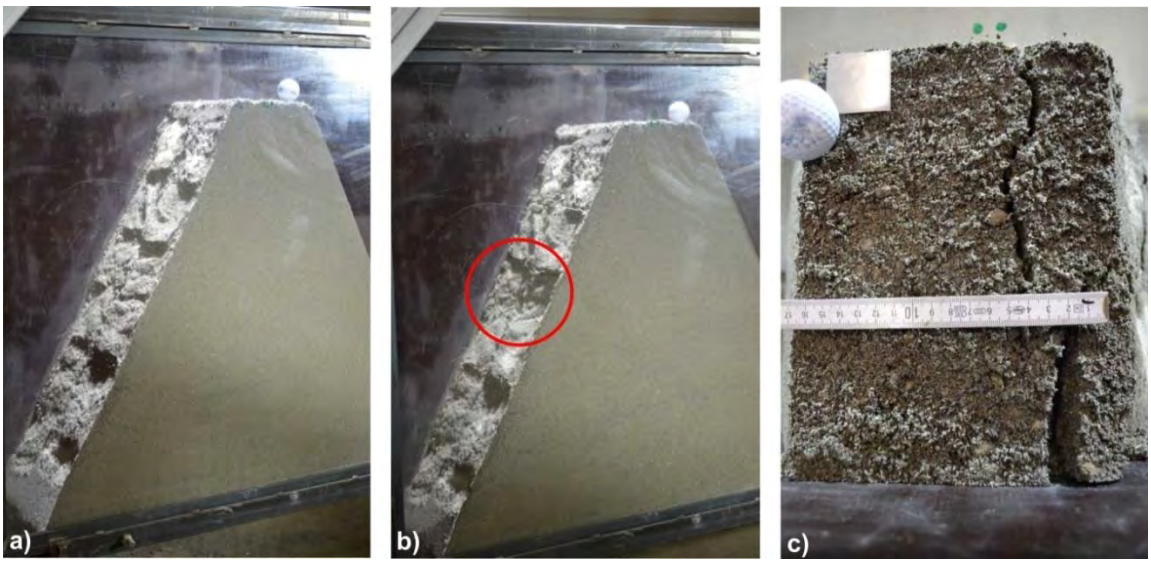

Fig. 3.16: Test GS_2121HG_18_11: a) rockery before first impact, b) rockery after first impact, red circle marks impact position, c) dissolution of stones due to the first impact at the crest, only a small shift of the golf ball at the top occurred due to the impact.

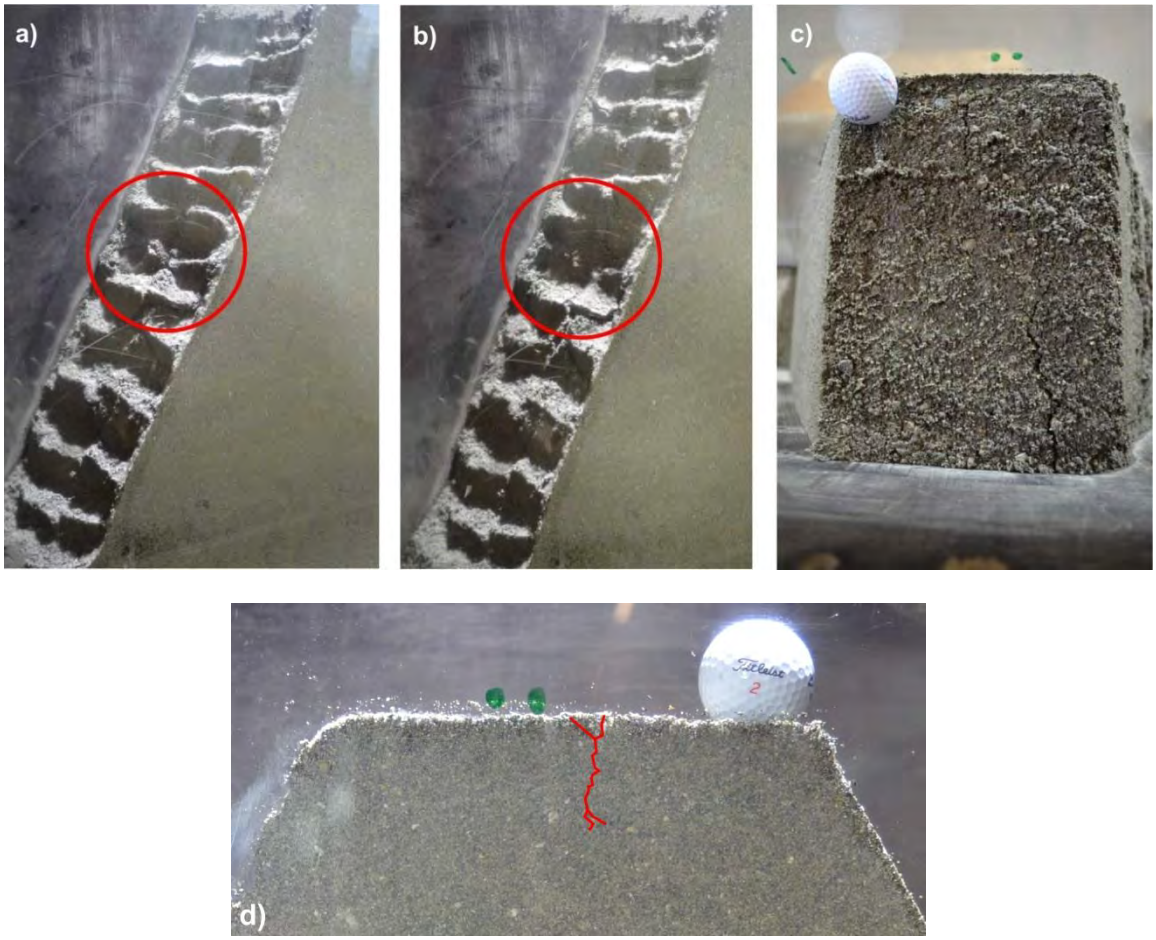

Fig. 3.17: Test GS_2121FG_18_11: a) rockery after first impact, b) rockery after second impact, c) and d) crack formation due to the second impact at the crest; red circle marks impact position.

Fig. 3.17a and b show the rockery made of stones placed horizontally (GS_2121FG_18_11) after the first and second impact. Also in these tests the damage seems to be restricted to the impact area and relatively small. A crack occurred at the crest as a result of the second impact, but was smaller than that one in test GS_2121HG_18_11-1. The crack could be identified visual up to a depth of about 4 cm at the forefront of the test box (Fig. 3.17 d). No crack was visible at the "downhill" slope after the second impact.

To check the influence of the slope angle additional tests had been done with a batter 5:2 and 5:1. For each slope angle a test had been done with block G as well as with block OKT. For a batter of 5:2 in both tests the impact angle has been determined to 8°. For the tests with a batter of 5:1 the impact angle was -4° respective -5°. Taking into account the error of measurement these values can be considered to be identical.

Each test had been done with a crest to block diameter ratio of approx. 1.1. The freeboard in the tests was about 0.5 block diameter (see Table 3.6). But only in test G_25121F_17_11-1 the embankment was surmounted by block G (Fig. 3.18a). The trajectory in this test looks very similar to the trajectory of test G_2121_9_11-1 without rockery (Fig. 3.10a).

The block trajectories of both blocks, G and OKT, determined in the tests with an embankment with a batter of 5:2 are shown in Fig. 3.18. The penetration depth of block G is less than the radius of the block. The block moved upward and removed part of the crest. At the maximum jump height the lower contour line of the block is higher than the crest level (Fig. 3.18a). Cracks occurred during the impact process, but had been closed and destroyed when the block fell back onto the crest.

Block OKT had a translational velocity v, which is close to the translational velocity of block G (G: v = 5.9 m/s, OKT: v = 6.3 m/s, difference: approx. 7%, this is still within the measurement error). Block OKT moved also towards the crest and reached a penetration depth of approx. ½ block diameter (Fig. 3.18b).

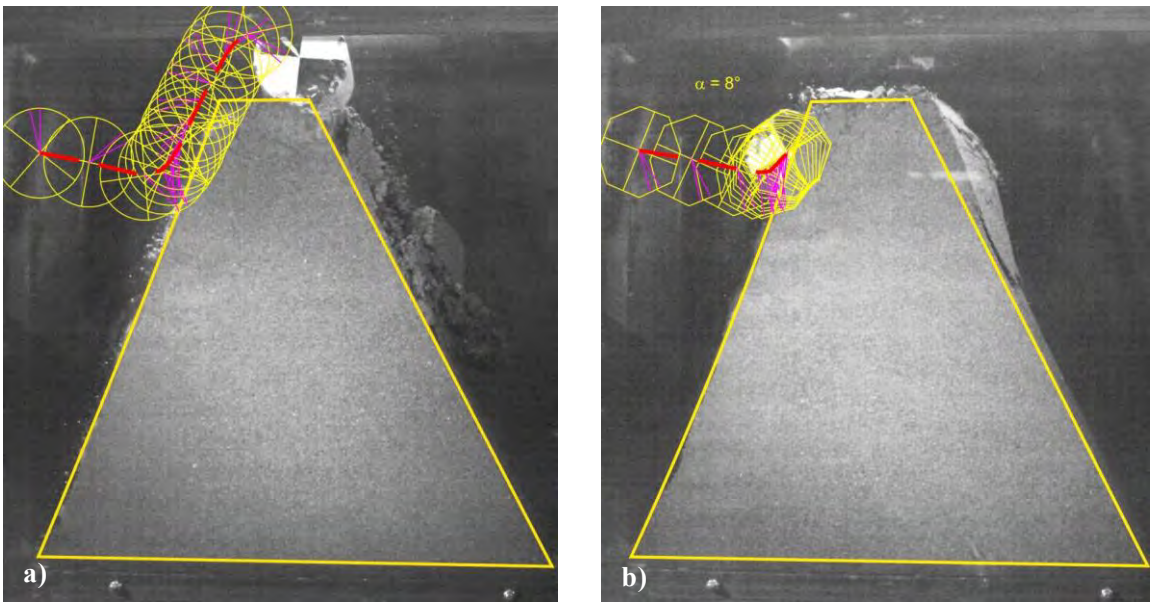

*Fig. 3.18: Influence of block shape and block rotation on the trajectory: Embankment with batter 5:2, i.e. slope angel approx. 69°, a) test G_25121F_17_11-1, FB approx. 0.6*2r b) test OKT_25121F_17_11-1, FB approx. 0.5*2r.*

The embankment's crest was deformed and pushed towards the "downhill" direction by block OKT. Slope instability occurred and a large part of the crest material slid down at the "downhill" slope, but the block was not able to surmount the embankment (Fig. 3.19a). Even a second impact onto the already heavily damaged embankment with block OKT was not able to surmount the embankment. Now the embankment's crest was totally destroyed and block OKT remained on the destroyed embankment (Fig. 3.19b).

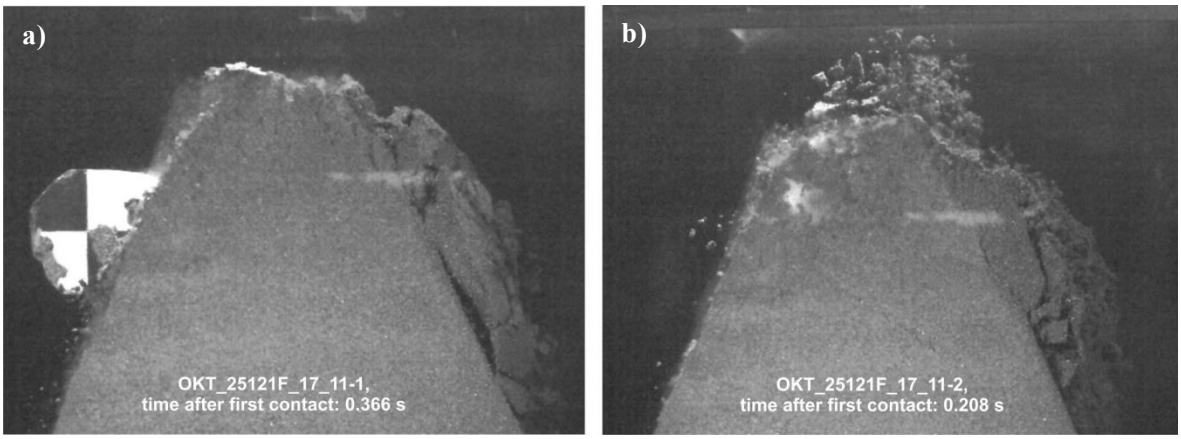

Fig. 3.19: Test OKT_25121F_17_11: a) slope instability due to first impact, block fell back on the "uphill" side, b) slope instability due to second impact, block remain on the destroyed crest.

Beside the difference in the cross section of the two blocks G and OKT there is another parameter which differs significant in the two tests: the rotational velocity. While the rotational velocity of block G is approx. 77 Hz, the rotational velocity of block OKT is only 3.4 Hz just before the impact. From this follows that the rotational energy of block OKT is less than 0.2% of the rotational energy of block G when the block is impacting the embankment.

For the tests G_5121F_17_11 and OKT_5121F_17_11 with a batter 5:1 the block trajectory is above the vertical to the embankment's slope. By definition the impact angle now is negative and the translational velocity component parallel to the slope (see Fig. 3.1b) acts in opposition to the direction of block movement. Neither block OKT nor block G is able to surmount the embankment (Fig. 3.20). In both tests the block fell back to the "uphill" side, but the embankment was totally damaged.

The comparison of Figures 3.20a and 3.18a shows an upward movement of block G, which is significantly less in test G_5121F_17_11-1 than in test G_25121F_17_11-1. But the translational velocities just before the impact are nearly identical (5.9 m/s resp. 6.0 m/s) and the rotational velocities are very similar (77 Hz, 79 Hz). So because in both tests the same block G was used, this difference is traced back to the increased batter 5:1.

Block OKT shows also a lower upward movement in Fig. 3.20b of test OKT_5121F_17_11-1 than in Fig. 3.18b of test OKT_25121F_17_11-1, even though the rotational velocity ω in test OKT_5121F_17_11-1 is more than twice the rotational velocity in test OKT_25121F_17_11-1 (8.1 Hz resp. 3.4 Hz). However it has to be taken into account that the rotational velocity in both tests is very low. A summary of the test data and results of the tests shown in Figures 3.18 and 3.20 is given in Table 3.6.

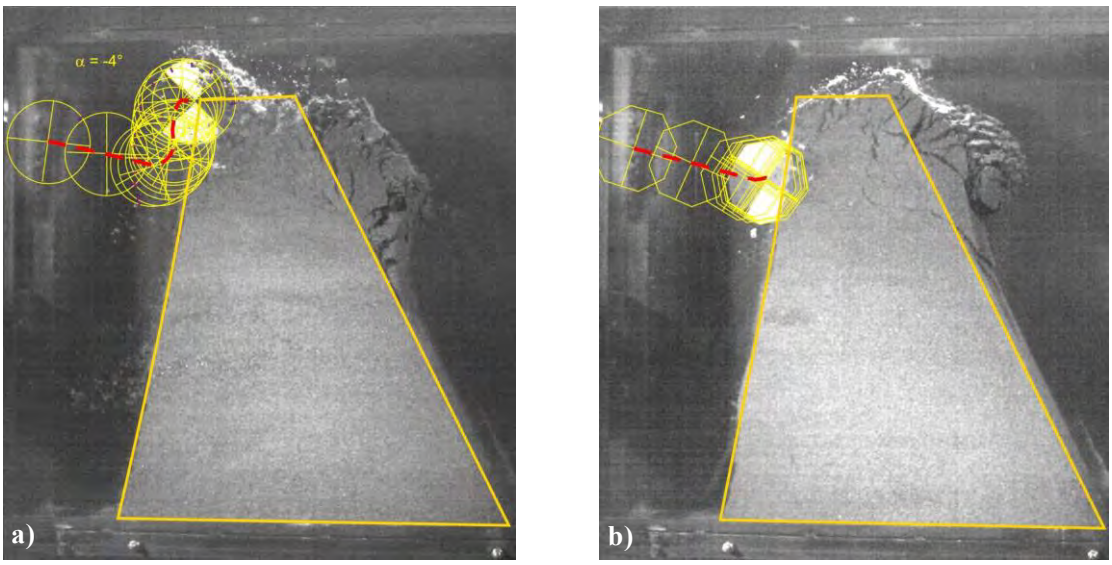

*Fig. 3.20: Influence of block shape and block rotation on the trajectory: Embankment with batter 5:1, i.e. slope angel approx. 79.5°, a) test G_5121F_17_11-1, FB approx. 0.4*2r b) test OKT_5121F_17_11-1, FB approx. 0.5* 2r.*

β_{us}: 68.6° β_{ds}: 62.6° a_c: 16.5 cm OS: horizontal	***G_25121F_17_11*** FB approx. 0.6 * 2r block jumped over embankment crest with significant damage	***OKT_25121F_17_11*** FB approx. 0.5 * 2r embankment not surmounted 1st impact: significant damage. 2nd impact: crest totally destroyed
β_{us}: 79.5° β_{ds}: 62.6° a_c: 17.5 cm OS: horizontal	***G_5121F_17_11*** FB approx. 0.4 * 2r embankment not surmounted, but crest totally destroyed	***OKT_5121F_17_11*** FB approx. 0.5 * 2r embankment not surmounted, but crest totally destroyed.
Explanation:	β_{us}: slope angle uphill side β_{ds}: slope angle downhill side a_c: crest width	OS: orientation of stones 2r: block diameter FB: Freeboard

Table 3.6: Results of tests with an embankment model with batter 5:2 respective 5:1 at the "uphill" slope and crest to block diameter ratio of approx. 1.1.

With the impactor GS three tests, two first impacts and one second impact, had been done on a model on a scale of 1:20 of the Gurtnellen Embankment North (Fig. 2.14). For the first test named as Gurtnellen_1 the embankment model and the down pipe had been arranged in such a way, that the impact point was just below the kink of the bi-linear slope. So the impactor hits the rockery surface of the slope and pushed the topmost stones into the soil body of the embankment. Then the block moves upward the flat-angle soil part of the slope. But the energy loss of the block due to that impact was large enough so that the block was not able to surmount the embankment. Fig. 3.21a shows the block trajectory of this test.

A second impact test had been done on the same model, but now the model was lowered for a few centimeters. This lowering resulted in an impact point, which was now located a little bit above the kink of the bi-linear slope. Now the impactor hits the stones on the top. Because the stone were placed on other stones underneath, neither a large deformation nor a large displacement of the topmost stones was possible. A large amount of energy remained at the block and the embankment was now surmounted with a large jump (Fig. 3.21b).

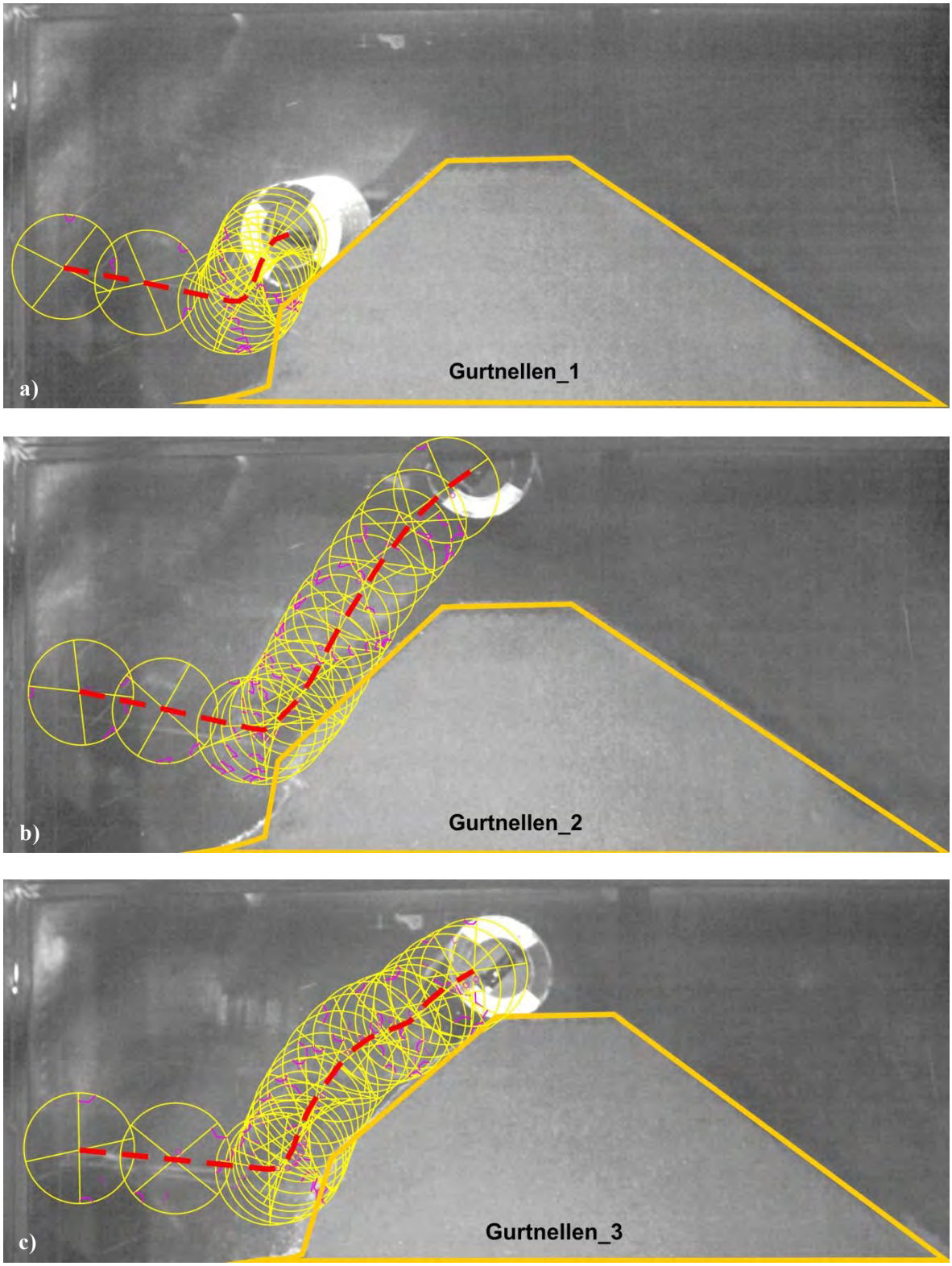

Fig. 3.21: Trajectories received with the embankment model Gurtnellen and impactor GS

The model embankment was constructed a second time and now embankment model and down pipe had been again arranged in such a way, that the impact point was below the kink of the bi-linear slope. In this test the block reached the top of the embankment, but the embankment was not surmounted. Fig. 3.21 c) shows the block trajectory.

3.3 Block deceleration due to impact

The data received with the high speed camera had also been analyzed with the open source program Tracker. The program Tracker is a video analysis tool and was used for center of mass tracks to get information about the translational velocity of a block during the impact process. To do this in the pictures of a test the position of the center of mass has to be visible. For each test a series of about 350 to 450 pictures had to be analyzed.

Additional the block rotation was determined and the rotational block velocity had been evaluated. This was done by hand and on the basis of the trajectory pictures shown in the chapter before. Therefore the number of data points for those analyses are significantly lower.

Impact tests with the same embankment cross section with a batter of 2:1 and stones placed parallel to the embankment's slope at the uphill side had been analyzed for the three impactors G, GS and OKT. The mean value of the translational velocity v of the blocks G and GS before the impact was approx. 6.6 m/s resp. 6.7 m/s. For block OKT the mean value of the velocity was a little bit less, that is to say 6.1 m/s. Within the first 6 ms of the impact process the translational velocity was reduced to a value less than 3 m/s and the graphs for the three impactors look alike (Fig. 3.22). Within the next 16 ms the translational velocity is still reduced, but the amount of deceleration is significantly smaller and differences appear for the 3 impactors G, GS and OKT. 22 ms after the contact the velocity is reduced furthermore, but now the graphs in Fig. 3.22 show only a very small decrease for the mean value of the velocities. The scattering of the data points in Fig. 3.22 gives an idea about the measurement error of that type of analysis with the program Tracker.

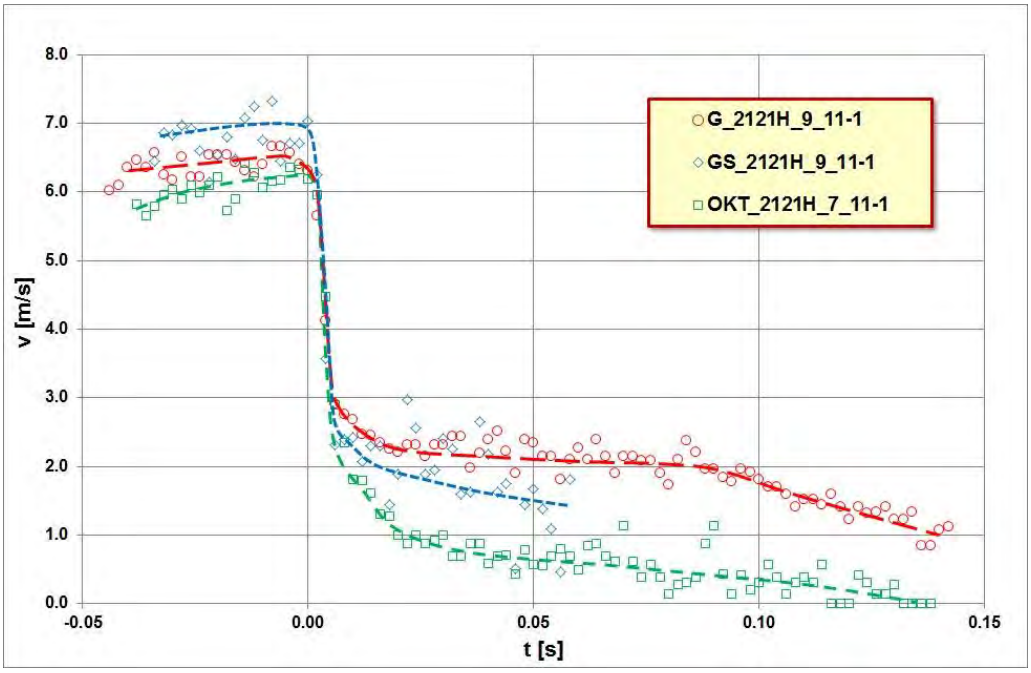

Fig. 3.22: Decrease of translational velocity v of the three used impactors at the same embankment cross section with batter 2:1 and stones placed parallel to the slope surface.

Fig. 3.22 shows the largest amount of deceleration for block OKT with edges and no rotation before it hit the embankment. Within 22 ms the translational block velocity is reduced to 15% of the value before the impact and the translational energy is reduced to 2.3% of the value before the impact (Table 3.7). On the other hand the velocity v of cylinder G made of concrete and with E_{rot}/E_{trans} = 0.45 just before the impact, is only reduced to 35% of the value before the impact in the same period. The translational energy is also reduced, but is still 12% after 22 ms. Block GS with the steel jacket and with E_{rot}/E_{trans} = 0.15 lies in between the values of the two other blocks (Table 3.7).

Impactor	Impact angle	v(t=0) [m/s]	v(t=6 ms) [m/s]	v(t=22 ms) [m/s]	$E_{trans,0}$ [Nm]	$E_{trans,6}$ [Nm]	$E_{trans,22}$ [Nm]
G	13°	6.6 (100%)	2.9 (44%)	2.3 (35%)	162 (100%)	31 (19%)	19 (12%)
GS	12°	6.7 (100%)	2.4 (36%)	1.9 (28%)	152 (100%)	19.5 (13%)	12 (8%)
OKT	14°	6.1 (100%)	2.9 (48%)	0.9 (15%)	128 (100%)	28.5 (22%)	3 (2.3%)

Table 3.7: Mean values of translational velocity and translational energy just before the impact process and 6 ms resp. 22 ms after the contact block – embankment.

Fig. 3.23 shows the decrease of the rotational velocity ω with time for the three impactors. The impactor OKT had no rotation before the impact. Rotation of impactor OKT is produced only by the impact itself and only a very low rotation with a maximum less than 10 Hz occurred. The block OKT had not surmounted the embankment and reached its maximum height 156 ms after the contact. Then the block fell back on the "uphill" slope.

The high rotation of cylinder G is a result of the friction between the concrete surface of the block and the steel down pipe. Because the friction between the steel jacket of block GS and the steel down pipe is less than the friction between concrete and steel, the rotation of block GS is lower than the rotation of block G. After 0.04 s the rotational velocity of both blocks is approximately constant, but on different levels (Fig. 3.23).

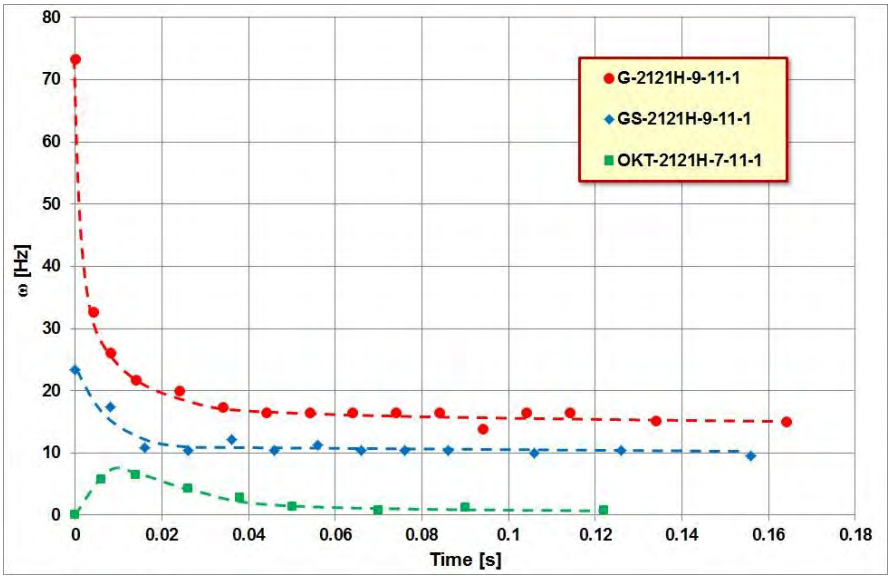

Fig. 3.23: Decrease of rotational velocity ω of the three used impactors at the same embankment cross section with batter 2:1 and stones placed parallel to the slope surface.

Comparing the graphs in Figures 3.22 and 3.23 it seems to be that the higher the block rotation, the lower is the decrease of the translational velocity v. So the statement "The initial rotational kinetic energy favors an increase of the translational kinetic energy during the impact" given by Plassiard & Donzé (2009) may be converted into: A high rotational block energy leads to less reduction in the translational energy than a low rotational energy.

In Figures 3.24, 3.25 and 3.26 the decrease of translational velocity v of the three used impactors is opposed to the destruction occurred at the embankment due to the impact. It is noteworthy that in all three tests the heaviest damage at the embankment occurred at a time, when the block translational energy has already dropped to a significant low level, i.e. less than 15% for the cylinders and less than 5% for block OKT with edges (Table 3.7). On the other hand the embankment was surmounted by block G as well as by block GS despite of such a low translational and rotational velocity. Only in the test with block OKT, where no rotation occurred before the impact, the embankment was able to retain the block.

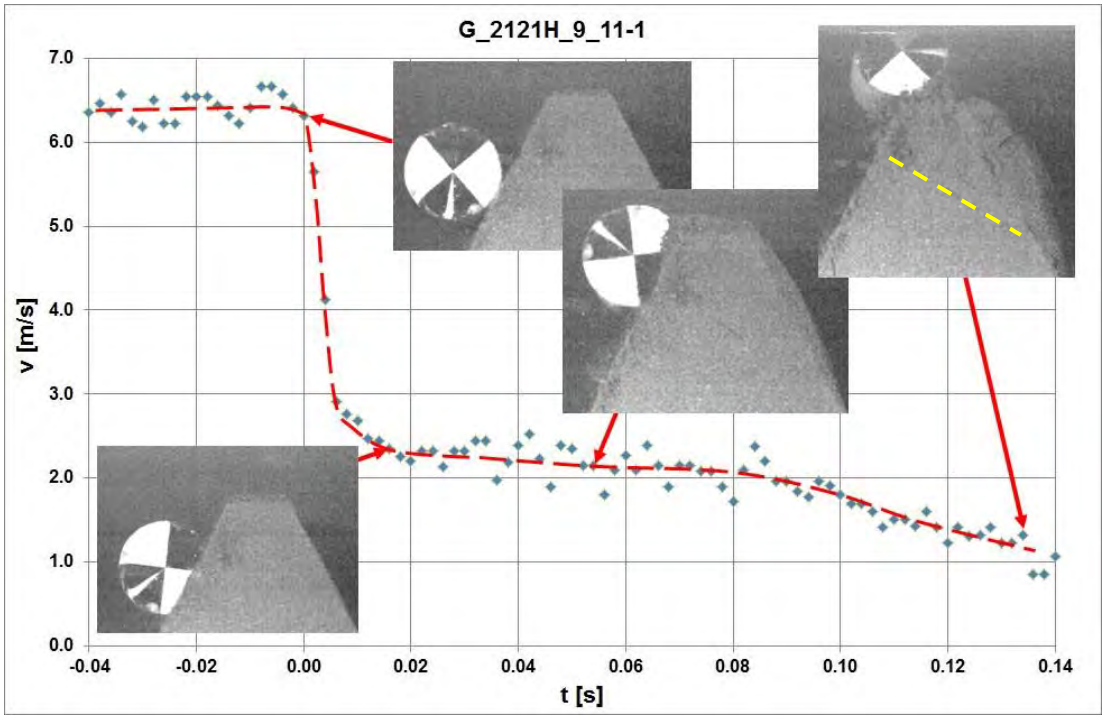

Fig. 3.24: Block deceleration in test G_2121H_9_11-1, red line: assumed mean translational velocity, yellow line marks a failure plane with a dip of approx. 30°.

In test G_2121H_9_11-1 as well as in test GS_2121H_9_11-1 a failure plane occurred during the tests. The failure plane showed a downward dip to the "downhill side" but with a different inclination in the two tests (Fig. 3.24 and Fig. 3.25). In the test with impactor G the inclination of the failure plane is approx. 30° while in the test with impactor GS the inclination is just one half. Such a failure plane was not observed in tests for embankment cross sections of type 1111 or type 2145 which had been studied by Kister (2015). Also in test OKT_2121H_7_11-1 with the non-rotating block (Fig. 3.26) such a failure plane was not detected.

Because the embankment material was the same in all tests and also the impact angle was more or less the same in the three tests (Table 3.7), the reason for such a failure plane may be traced back to the combination of block rotation and the slender structure.

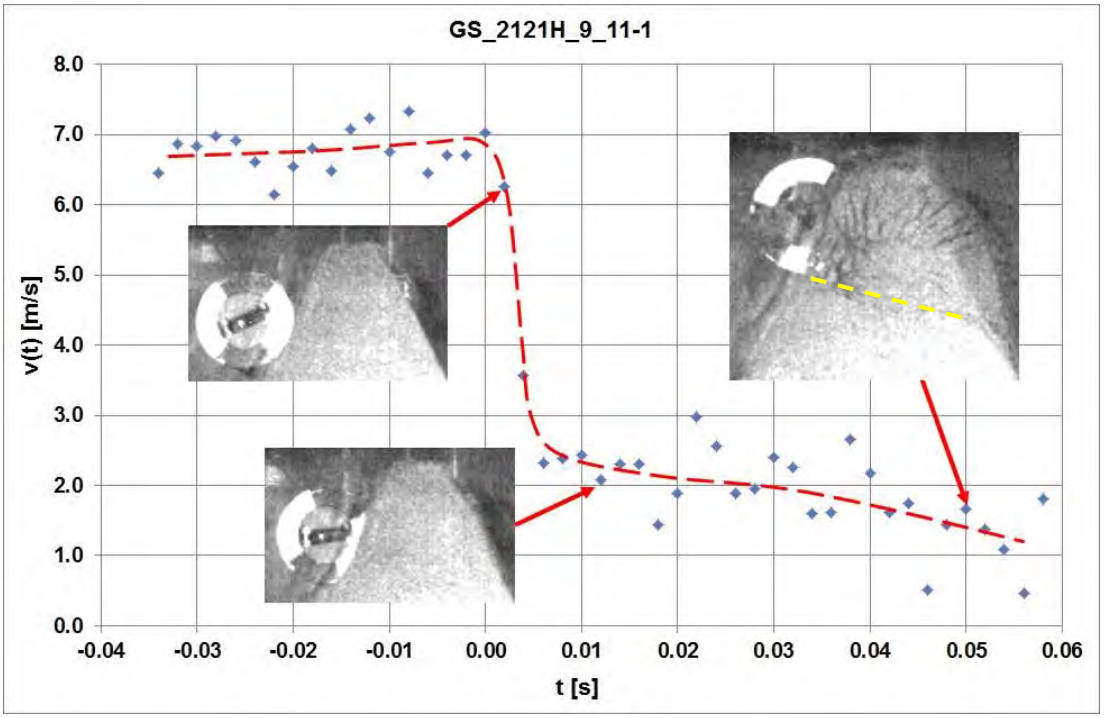

Fig. 3.25: Block deceleration in test GS_2121H_9_11-1, red line: assumed mean translational velocity, yellow line marks a failure plane with a dip of approx. 15°.

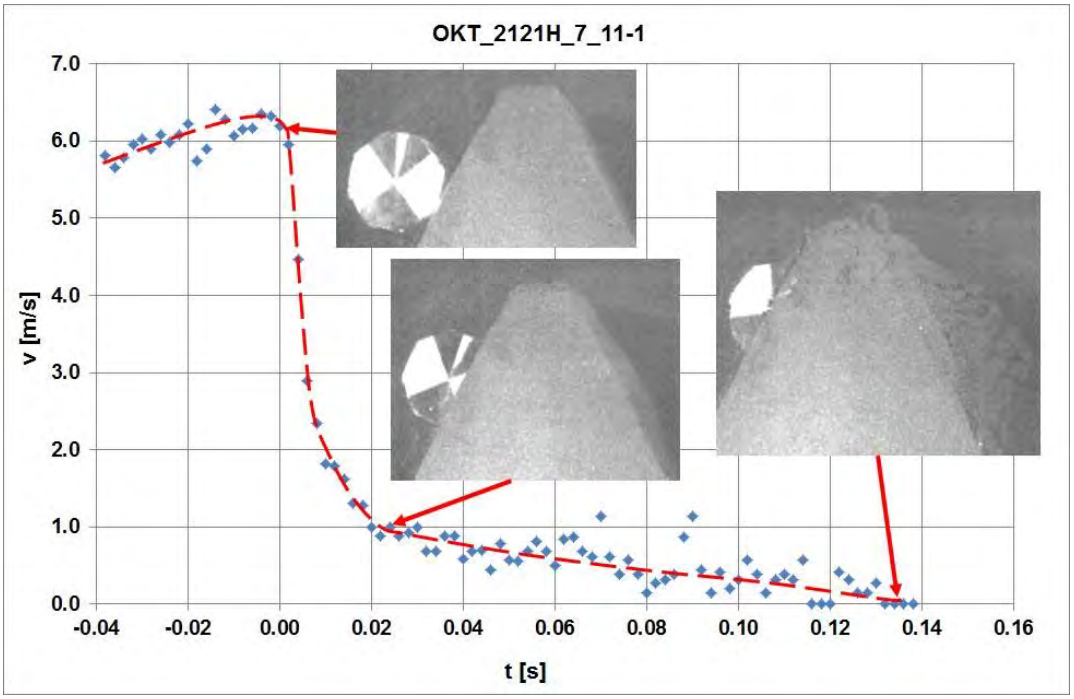

Fig. 3.26: Block deceleration in test OKT_2121H_7_11-1, red line: assumed mean translational velocity

Fig. 3.27 shows the decrease of translational velocity v of impactor G during the impact process at the embankment with cross section with batter 2:1 on both slopes but different surface conditions at the "uphill" slope. For all four tests – without rockery (G_2121_9_11-1), with stones placed parallel to the slope (G_2121H_9_11-1), with stones placed horizontally at the "uphill" slope (G_2121F_9_11-1) and with stones placed horizontally at both slopes (G_2121FF_9_11-1) – the main loss of translational energy occurs within the first 6 to 8 ms after the first contact. The translational velocity v drops from a level of about 6 to 6.5 m/s to a level of 3 m/s or less. This is a translational energy decline of about 75% at least for block G.

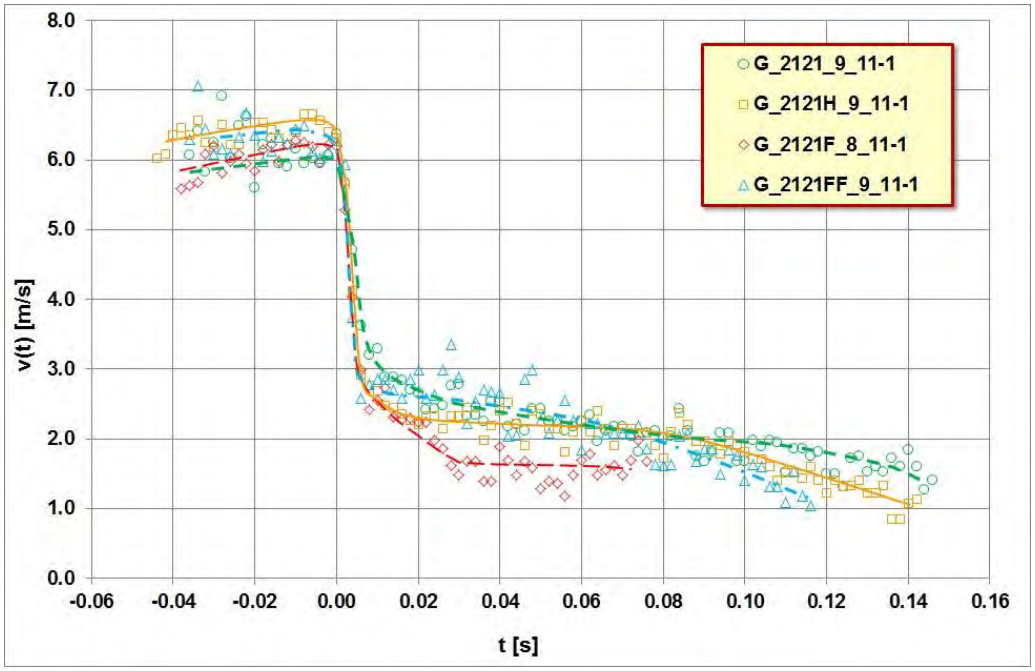

Fig. 3.27: Comparison of translational velocity v versus time t of impactor G for cross section 2121 with different surface conditions at the slope.

Taking into account the measurement accuracy, the data received in the four tests are very close together, especially during the first 6 ms of the impact process. But the curve progression for the period larger than 6 ms shows however some differences (Fig. 3.27). The largest reduction in velocity v is shown for test G_2121F_8_11-1 with the rough slope surface. In the interval 0.03 s to 0.07 s the data points of this test show the lowest values for the velocity v. At the last measurement point in this graph block G had penetrated the embankment by its half diameter. No additional analysis could be done because the block center then vanished in an embankment material cloud. In test G_2121_9_11-1, without rockery, the penetration depth of block G was less and at the last measurement point shown in the graph, the block was already flying directly above the crest with a velocity v larger than 1 m/s. Looking at the graphs in the interval 0.08 s – 0.14 s in Fig. 3.27 it seems to be, that the decline of the block velocity v increases with slope roughness.

Fig. 3.28 shows the reduction of the rotational velocity during the impact process. The rotational velocity ω before the impact varies only between 78 and 81 Hz in the four tests. This results in a difference of less than 4% between maximum and minimum value of the rotational energy of impactor G. But for a time $t > 0.04$ s the rotational velocity of block G in test G_2121F_8_11-1 is twice the rotational velocity of block G in test G_2121_9_11-1 without a stony slope surface.

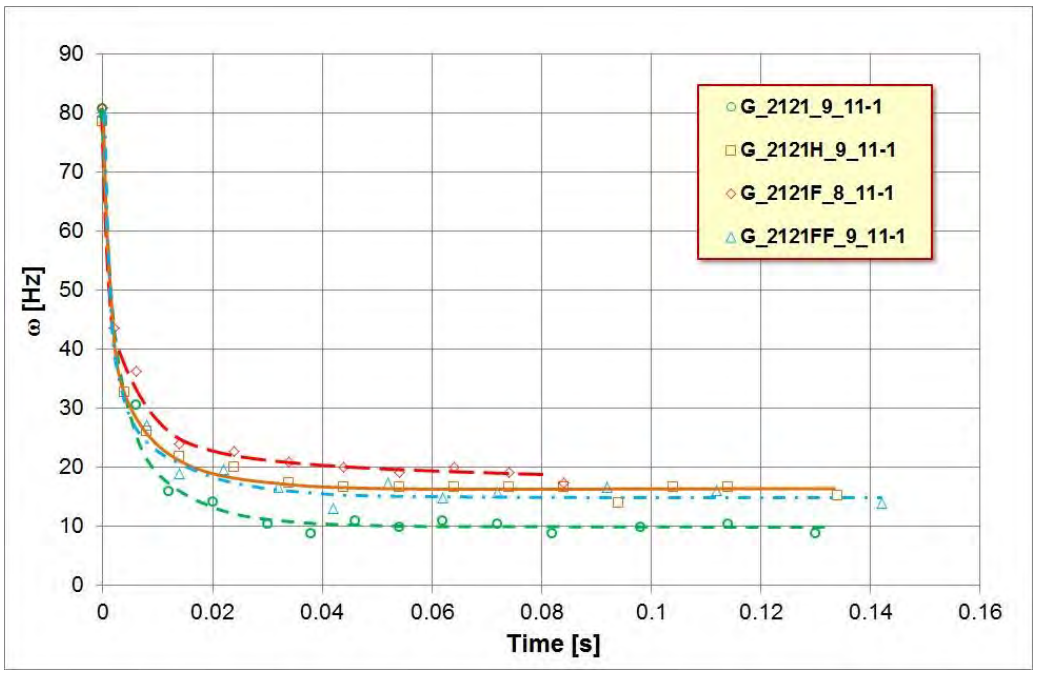

Fig. 3.28: Comparison of rotational velocity ω versus time t of impactor G for cross section 2121 with different surface conditions at the slope.

As shown in Fig. 3.28 the data points of the rotational velocity during the impact process in the tests G_2121FF_9_11-1 with stones placed horizontally and G_2121H_9_11-1 with the stones placed parallel to the slope are close together. The highest rotational velocities had been observed in test G_2121F_8_11-1, even though in this test the slope roughness was the same as in test G_2121FF_8_11-1. The difference in both tests is the placing of stones on the "downhill" slope in test G_2121FF_8_11-1, which reduced the compressible embankment volume. All four tests have in common that the rotational velocity is approx. constant for $t > 0.04$ s (Fig. 3.28).

In Figure 3.29 the decrease of translational velocity v of impactor G in test G_2121F_8_11-1 is opposed to the destruction occurred at the embankment due to the impact. Approximately 8 ms after the contact of block and embankment the growth of a bulge at the opposite slope can be recognized. At that moment the block translational velocity was already reduced to less than 42% of the velocity value before the contact and the translational energy was less than 18% of the translational impact energy. The rotational velocity is less than 50% of the rotational velocity before the contact. The penetration depth is about one quarter of the block diameter.

Approximately 60 ms after the contact, a downward failure plane became apparent with a dip of approx. 30°. If the failure plane is elongated by a line, this line goes more or less directly through the center of the block at that time. The penetration depth of the block is now a half diameter (Fig. 3.29, large picture at the right).

Approximately 80 ms after the contact, the bulge had been transformed into a slide. Block G moved through the loosened embankment material respective pushed a part of this material forward and finally the embankment was surmounted by the block (Fig. 3.30).

It is noteworthy that also in this test the heaviest damage at the embankment occurred at a time, where the block translational energy is already very low (8 Nm). The translational energy at this time is less than 7% of the translational energy just before the contact (131 Nm).

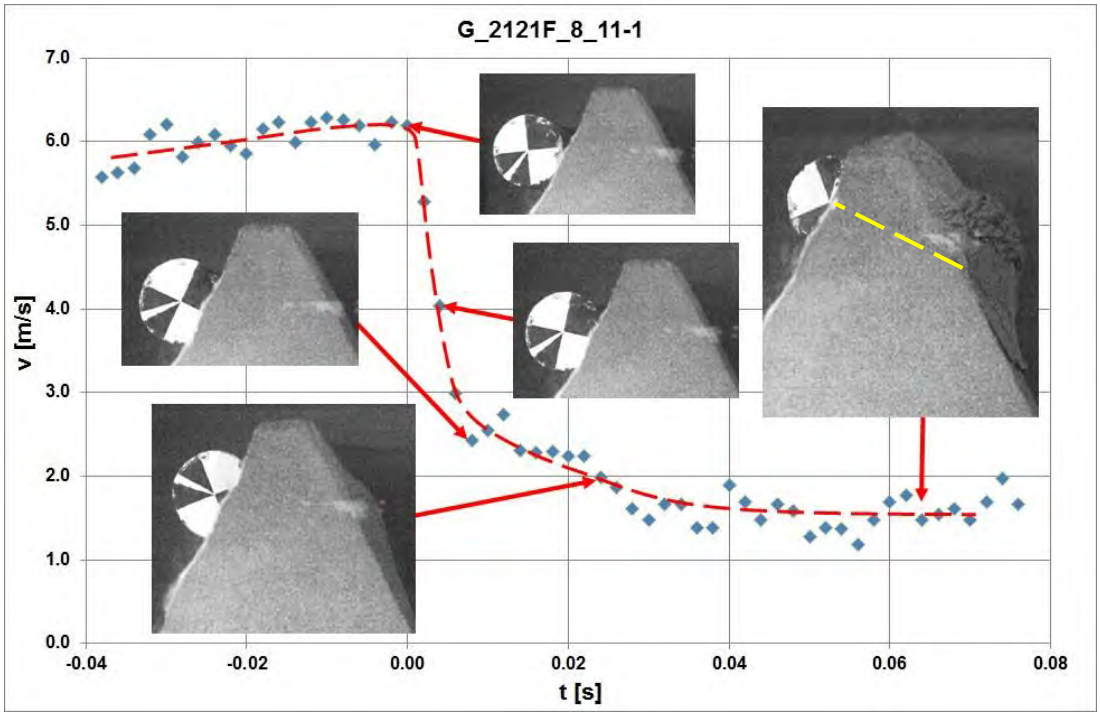

Fig. 3.29: Block deceleration in test G_2121F_8_11-1, red line: assumed mean translational velocity, yellow line marks a failure plane.

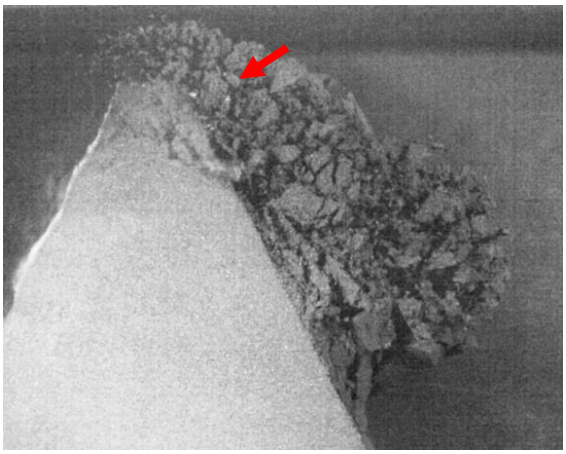

Fig. 3.30: Test G_2121F_8_11-1: Destruction of the embankment's crest by block G (t = 0.224 s after contact). The block is hidden to a very large extent by a cloud of embankment material. Block position marked by the arrow.

The block deceleration determined in tests with block G, but embankment's batter 5:2 resp. 5:1 are shown in Figure 3.31 in comparison to data obtained in the tests with batter 2:1. It is obvious that the translational block velocity v is reduced faster by the steep slope with a batter of 5:1 and to a lower level than in the other three tests. But it has kept in mind that the impact angle for the test with batter 5:1 was -4° (see definition in Figure 3.1). This means there was a velocity component in downward direction of the slope. On the other hand the impact angle in the three other tests was positive (8° for 5:2, 14° for 2:1F and 12° for 2:1 without stones) which results in a velocity component in upward direction.

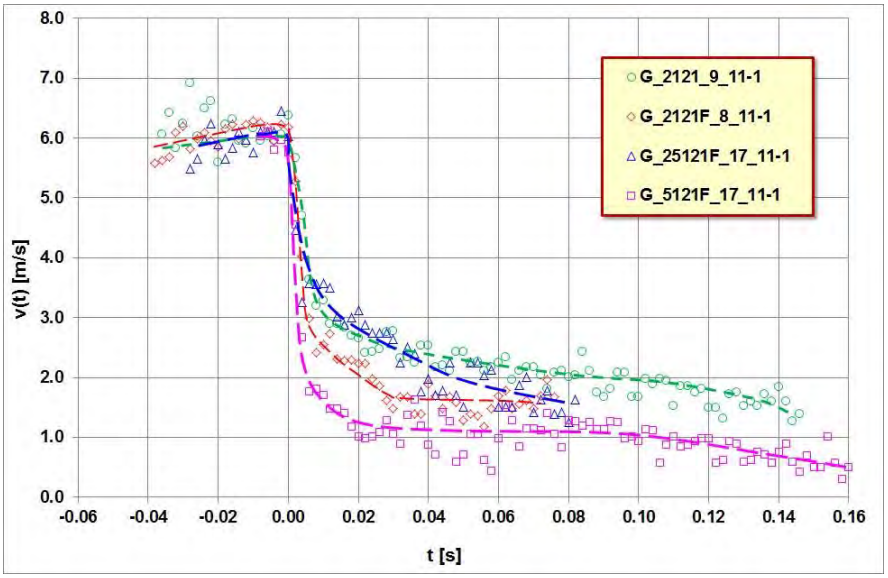

Fig. 3.31: Comparison of translational velocity v versus time t of impactor G for different batter 2:1, 5:2 and 5:1.

For the first 40 ms the graph of test G25121F_17_11-1 with batter 5:2 and rockery is very similar like that one of the test on a slope with batter 2:1 without rockery. But despite the large scattering of the data due to measurement errors it is visible, that the data converges for longer times to the data of the test with batter 2:1 with stones placed horizontally.

20 ms after the first contact in the tests G_2121_9_11-1 and G_25121F_17_11-1 the block velocity is reduced to less than half of the velocity just before the contact. But for the slope with batter 5:1 the velocity is reduced in the same time interval to a value of only 20% of the velocity just before the contact. Assuming the translational energy of block G in test G_2121_9_11-1 is 100% at t = 20 ms, then the block in test G_5121F_17_11-1 has approx. only 19% of that energy determined for the other test. Even 70 ms after the first contact the block G in test G_5121F_17_11-1 has significant lower translational energy than in the other tests. Because the velocity v is nearly identical before the impact for all 4 tests, the steeper embankment slope with batter 5:1 reduces the block energy much better and in a shorter time than the slopes with lower inclination (Table 3.8).

Impactor	Impact angle	v(t=0) [m/s]	v(t=20 ms) [m/s]	v(t=70 ms) [m/s]	$E_{trans,20}$ [Nm]	$E_{trans,70}$ [Nm]
G_2121_9_11-1	12°	6.0 (100%)	2.7 (45%)	2.1 (35%)	27 (100%)	16 (100%)
G_2121F_8_11-1	14°	5.9 (100%)	2.0 (34%)	1.6 (27%)	15 (55%)	9 (56%)
G_25121F_17_11-1	8°	6.1 (100%)	2.7 (44%)	1.6 (26%)	27 (100%)	9 (56%)
G_5121F_17_11-1	-4°	6.0 (100%)	1.2 (20%)	1.1 (18%)	5 (19%)	4 (25%)

Table 3.8: Mean values of translational velocity and translational energy at 20 ms resp. 70 ms after the contact block – embankment for batter 2:1 without and with "rockery", 5:2 and 5:1.

In Figure 3.32 the decline of the rotational velocity ω versus time t is shown. Again all four tests have in common that the rotational velocity is approx. constant for t > 0.04 s (cp. Fig. 3.28). It is interesting to see, that the decline of rotational velocity in the two tests G_2121_9_11-1, with batter 2:1 but no "rockery", and G_5121F_17_11-1, with batter 5:1 and stones placed horizontally, is identical to the greatest possible extent for t > 0.025 s. On the other hand the rotational velocity ω in test G_2121F_8_11-1 is twice the value in the tests G_2121_9_11-1 and G_5121F_17_11-1. The graph of test G_25121F_17_11-1 with batter 5:2 lies in between.

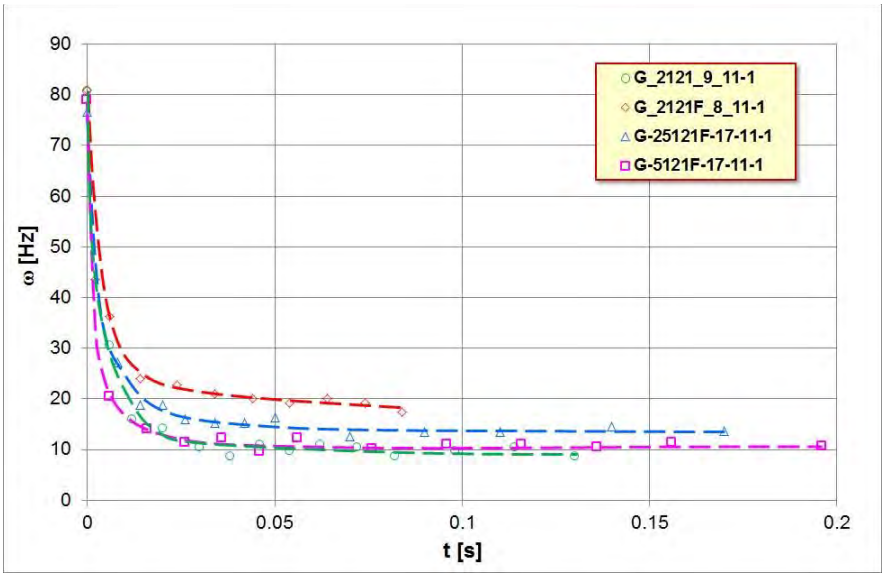

Fig. 3.32: Comparison of rotational velocity ω versus time t of impactor G for different batter 2:1, 5:2 and 5:1.

In Figures 3.33 and 3.34 the decrease of translational velocity v of impactor G is opposed to the destruction occurred at the embankment due to the impact. Again the heaviest destruction of the embankment occurred, when the block already had lost most of its energy. A failure plane with downward dip can clearly be seen again in test G_5121F_17_11-1 (Fig. 3.34).

The Figures 3.35 and 3.36 show the decline of translational and rotational velocity during the impact process in the tests done with impactor GS for the different slope surface conditions. It should be kept in mind, that impactor GS with a steel jacket had a ratio of rotational to translational energy, which is in the same interval as for natural blocks (Usiro et al., 2006, cp. Fig. 3.5).

The measurement error in tests with block GS is larger because of missing cross-lines at the center of the block. As a result a larger scattering of the data points determined with the program Tracker occurred (Fig. 3.35). But also the scattered data shows, that the translational velocity v is less reduced in the test without stones at the embankment's slope than in the tests with stones placed at the embankment's slope.

The differences in the tests with and without stones at the embankment's slope can be seen easier in Fig. 3.36 where the rotational velocity ω versus time is shown for the impact procedure. Here the test without stones on the embankment's slope led to the lowest rotational velocity. The subsidence in the graph of test GS_2121FF_18_11-1 for t > 0.05 s corresponds to a twist of the block GS, when it was on its way in upward direction, and this part of the graph is therefore not comparable with the other data.

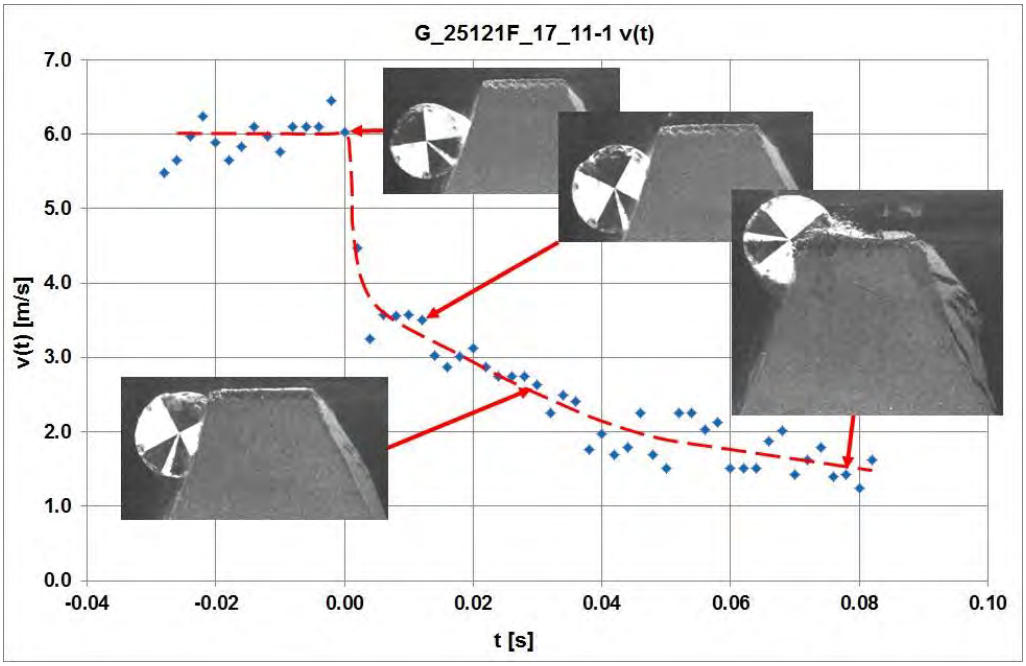

Fig. 3.33: Block deceleration in test G_25121F_17_11-1, red line: assumed mean translational velocity.

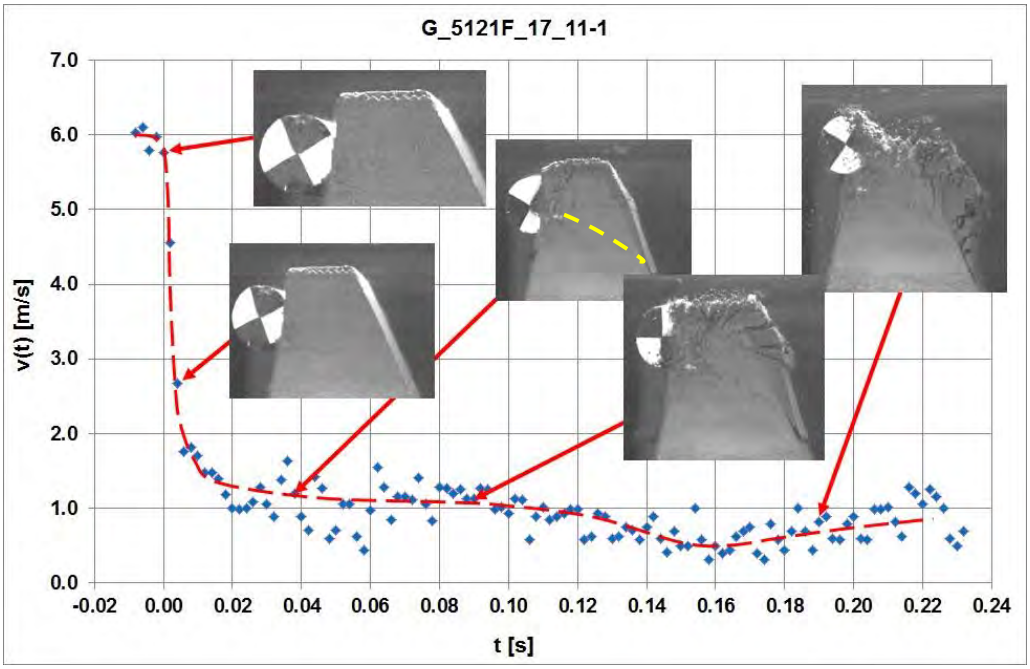

Fig. 3.34: Block deceleration in test G_5121F_17_11-1, red line: assumed mean translational velocity, yellow line marks a failure plane.

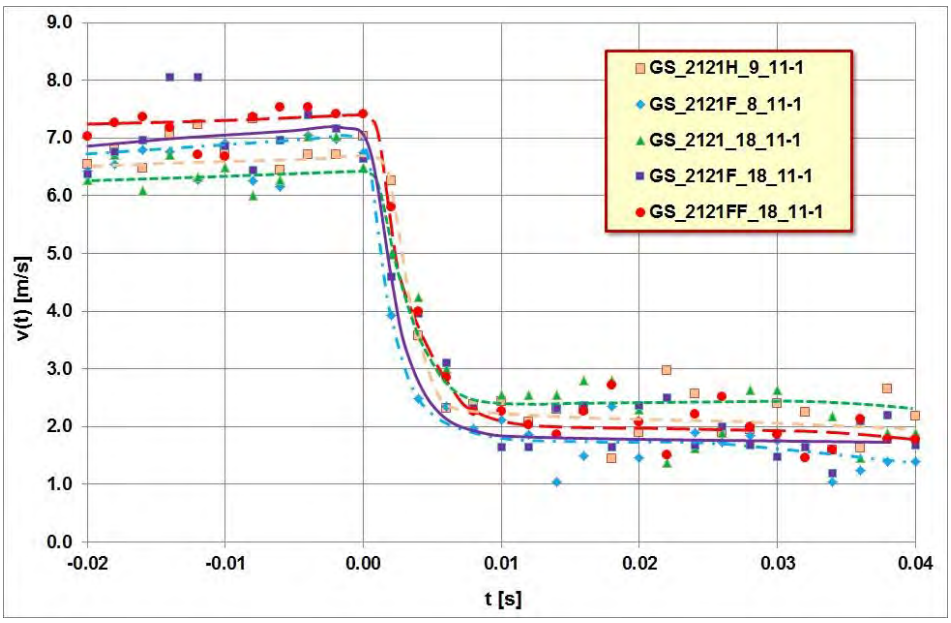

Fig. 3.35: Deceleration of impactor GS at an embankment cross section with batter 2:1, but different surface condition of the slope, lines: assumed mean translational velocity.

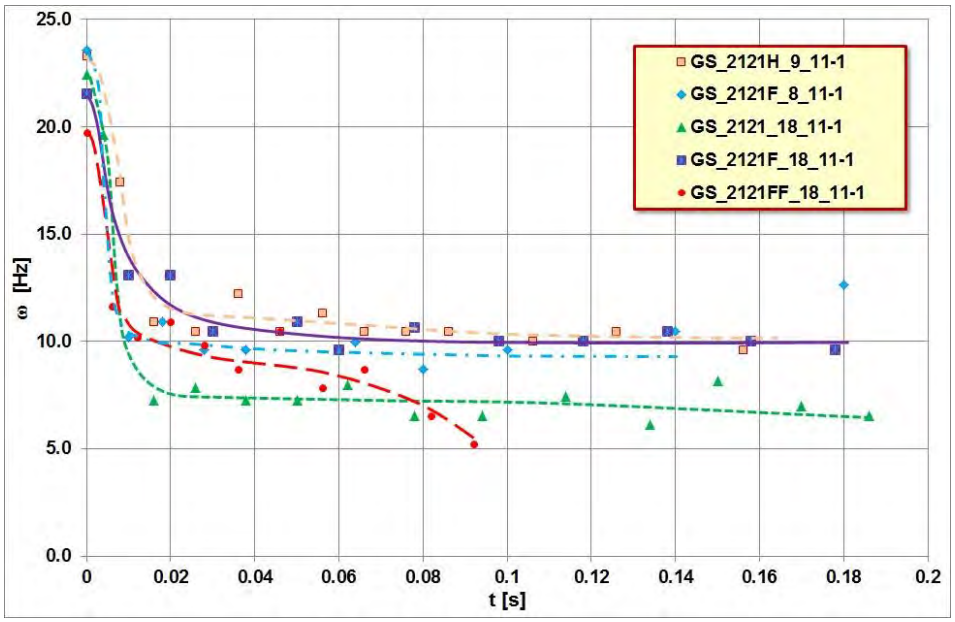

Fig. 3.36: Comparison of rotational velocity ω versus time t of impactor GS for cross section 2121 with different surface conditions at the slope.

In Figure 3.37 the decrease of translational velocity v of impactor GS is opposed to the destruction occurred at the embankment due to the impact. Again the heaviest destruction of the embankment occurred, when the block already had lost most of its energy. A failure plane with downward dip is visible in the right picture of Fig. 3.42 and marked by arrows. The inclination of this failure plane is approx. 25°.

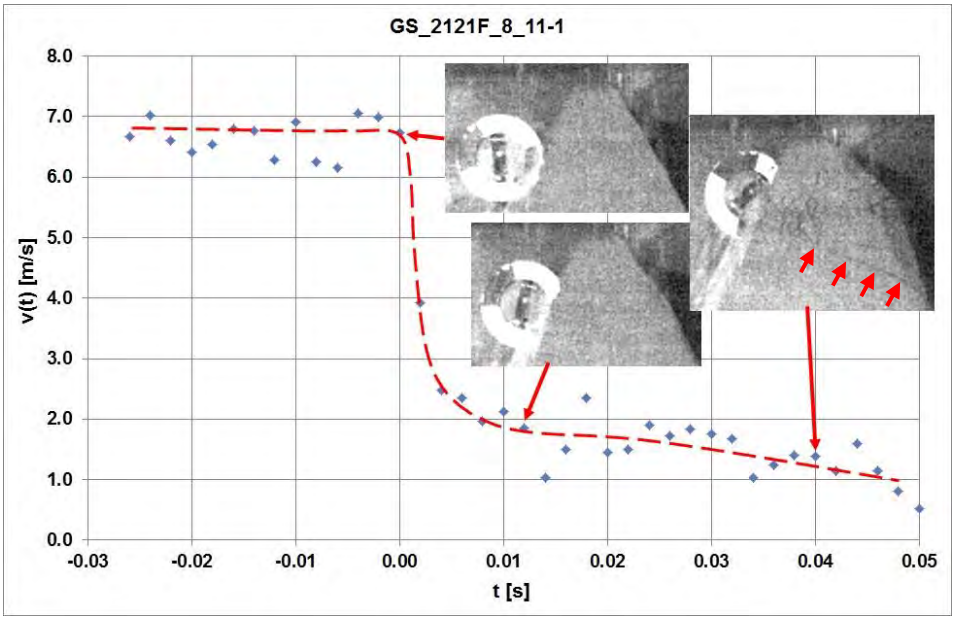

Fig. 3.37: Block deceleration in test GS_2121F_8_11-1, red line: assumed mean translational velocity, arrows mark failure plane.

The tests shown in Figures 3.31 and 3.32 with cylinder G for embankments with different batter had been repeated with the impactor OKT with the octagonal cross section and a low rotational velocity. As mentioned before the block OKT was not able to surmount the embankment in the 4 tests, neither in the three tests with a crest to block ratio of approx. 1.1 nor in test OKT_2121F_8_11-1 with a crest to block ratio of approx. 0.5. But the extent of damage was different and very much larger in test OKT_2121F_8_11-1 with the smaller crest than in the other three tests. Fig. 3.38 shows the decrease of velocity v of impactor OKT at the four embankments with the same surface condition on the slope, but different batter at the "uphill" side.

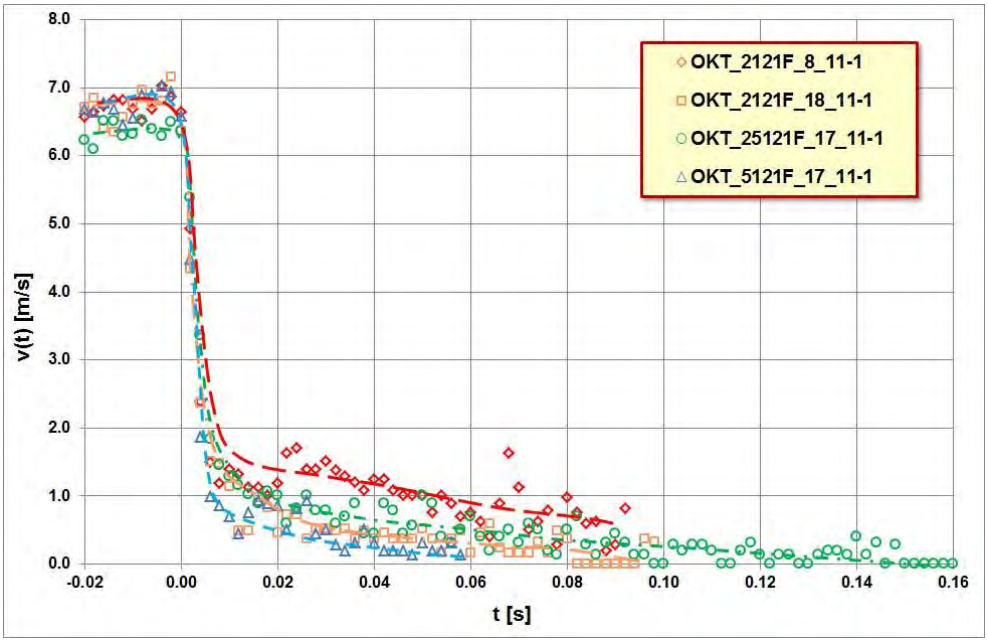

Fig. 3.38: Decrease of velocity v of impactor OKT at embankments with same surface condition on the slope, but different batter at "uphill" side.

The translational velocity in all four tests drops down from a value larger than 6 m/s to a value smaller than 2 m/s within a time period of approx. 6 ms. The block velocity drop in this time period is very similar for all four tests. After this period Fig. 3.38 shows a kind of splitting of the data. The highest block velocity in this time period is determined for the embankment with the small crest to block ratio of approx. 0.5. This may be an indication that the embankment's resistance against impact in this case is less than for the three other tests with crest to block ratio of approx. 1.1.

The embankment with batter 5:1 reduced the block velocity of block OKT much better and in a shorter time than the embankment slopes with lower inclination. Block OKT is stopped and fell back at approx. 0.06 s after the contact of block and embankment. The embankment with batter 5:2 needs more time, approx. 0.14 s, to stop the block OKT. On the other hand the embankment with batter 2:1 and a crest to block ratio of approx. 1.1 needed only about 0.1 s to stop the block OKT and lies in between the other tests. So there is no clear correlation between slope steepness and time interval for the block to stop.

10 ms after the first contact the block velocity v had been reduced in three of the four tests to a value of approx. 20% of the value just before the impact. The exceptional case is the test OKT_5121F_17_11-1 with batter 5:1, where the reduction is larger and the velocity v at 10 ms is only approx. 10% of the velocity before. The translational energy at 10 ms after the first contact in this test is just a quarter of the translational energy in test OKT_2121F_8_11-1 with batter 2:1 (Table 3.9). So also in the case of a block with edges and very low rotation the embankment with batter 5:1 and a negative impact angle is the combination which is able to reduce the kinetic block energy most effectively.

Impactor	Impact angle	v(t=0) [m/s]	v(t=10 ms) [m/s]	$E_{trans,10}$ [Nm]
OKT_2121F_8_11-1	11°	6.6 (100%)	1.4 (21%)	6.6 (100%)
OKT_2121F_18_11-1	10°	6.6 (100%)	1.14 (17%)	4.4 (67%)
OKT_25121F_17_11-1	8°	6.4 (100%)	1.3 (20%)	5.7 (86%)
OKT_5121F_17_11-1	-5°	6.7 (100%)	0.7 (10%)	1.7 (26%)

Table 3.9: Mean values of translational velocity and translational energy at 10 ms after the contact block – embankment for batter 2:1, 5:2 and 5:1.

In Fig. 3.39 the decrease of velocity v versus horizontal displacement x of impactor OKT is shown. The horizontal movement of block OKT stops after 4 cm in case of the embankment with batter 5:1 and this is the shortest distance in the 5 tests shown in Fig. 3.39. On the other hand for the embankment with a crest to block ratio of only approx. 0.5 and a batter 2:1 the horizontal displacement x is more than twice. For the embankment with batter 2:1 and a crest to block ratio of approx. 1.1 the horizontal displacement x is approx. 5 cm. This value is approx. 20% larger than the horizontal displacement x in the test with batter 5:1, but significantly smaller than the value of more than 6.5 cm in the test with a batter of 5:2. So again there is no clear correlation between slope steepness and block stopping. Furthermore it is surprisingly that even in the test OKT_2121_18_11-1_B without stones on the embankment slope and a batter of 2:1 the horizontal displacement x is smaller than in the tests OKT_25121F_17_11-1 and OKT_2121F_8_11-1 with stones on the embankment slope.

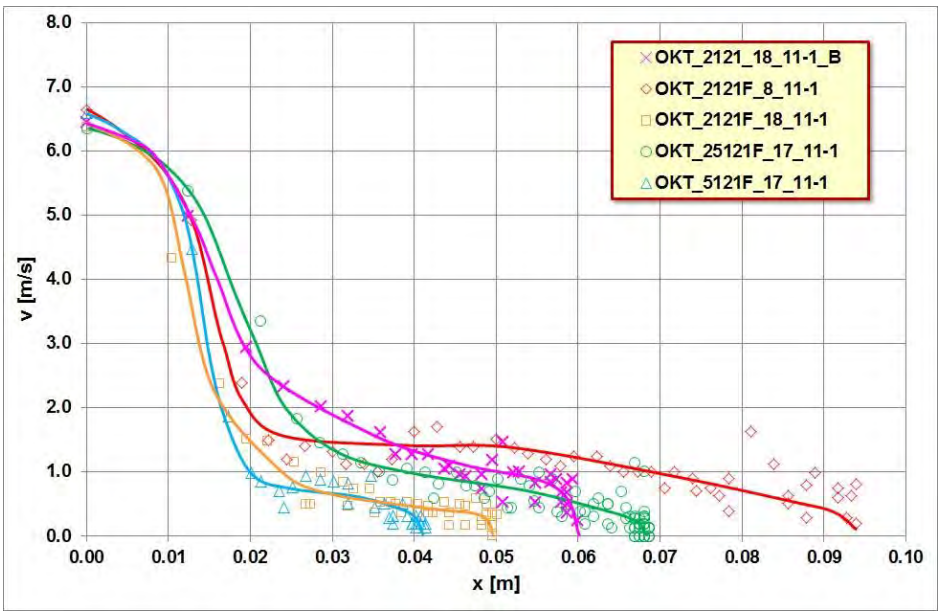

Fig. 3.39: Decrease of velocity v versus horizontal displacement x of impactor OKT at embankments with same surface condition on the slope, but different batter at "uphill" side. For comparison also test OKT_2121_18_11-1_B without stones on the slope is shown.

Fig. 3.40 shows the variation of the rotational velocity ω with time in the four tests with stones placed horizontally at the embankment slope. The rotational velocity of block OKT is low before the impact and in the range of 3 – 13 Hz. Because of the low rotation of block OKT also during the impact process, the measurement of the angle of rotation is difficult. The small changes of the angle of rotation results therefore in a small number of measurement points.

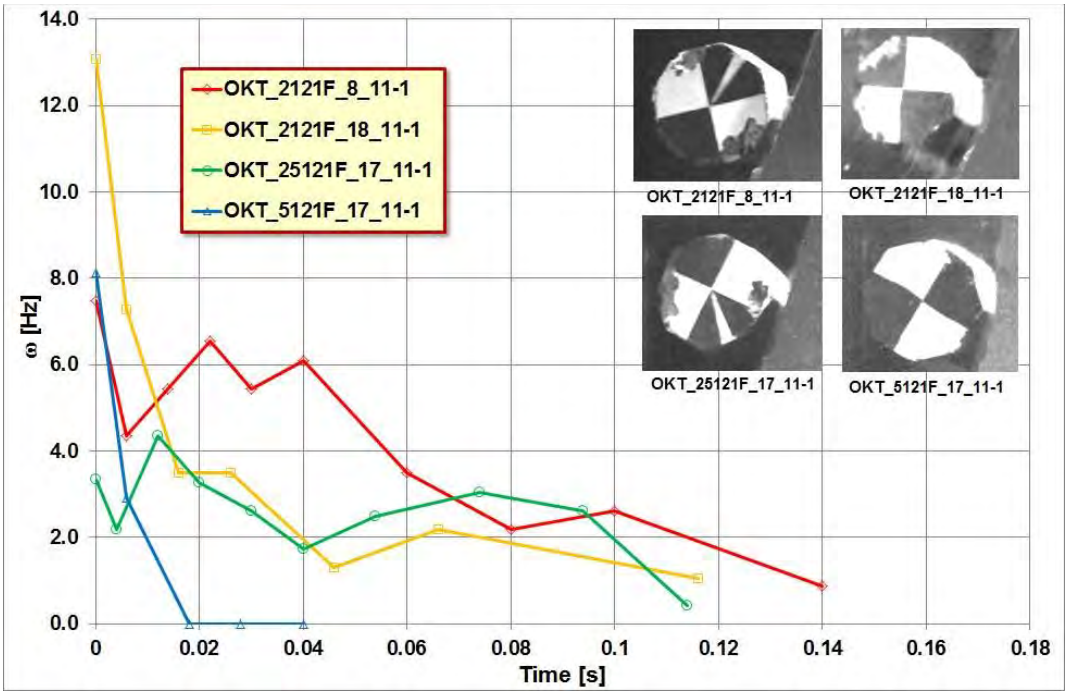

Fig. 3.40: Slowdown of rotational velocity of impactor OKT at embankments with same surface condition of the slope, but different batter at "uphill" side and different crest width.

In all four tests the block OKT hits the embankment with an edge first, but the position of the edge was slightly different when the contact was established (small pictures in Fig. 3.40). This may result in different moments of a torque and may affect the block rotation. So the graphs in Fig. 3.40 did not show a smooth curve but a zigzag line. Nevertheless the fastest stop of block rotation was achieved for the embankment with batter 5:1. For the embankment with a crest to block ratio of only approx. 0.5 and a batter 2:1 the longest time interval was needed for stopping block OKT.

In Figures 3.41 to 3.44 the decrease of translational velocity v of impactor OKT is opposed to the destruction occurred at the embankment due to the impact. Again the heaviest destruction of the embankment occurred, when the block already had lost most of its energy.

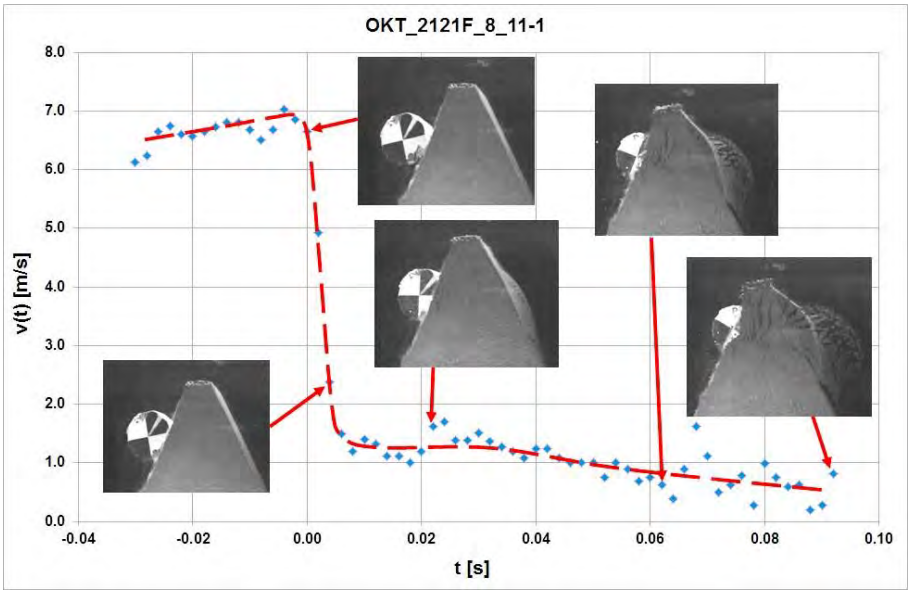

Fig. 3.41: Block deceleration in test OKT_2121F_8_11-1, red line: assumed mean translational velocity.

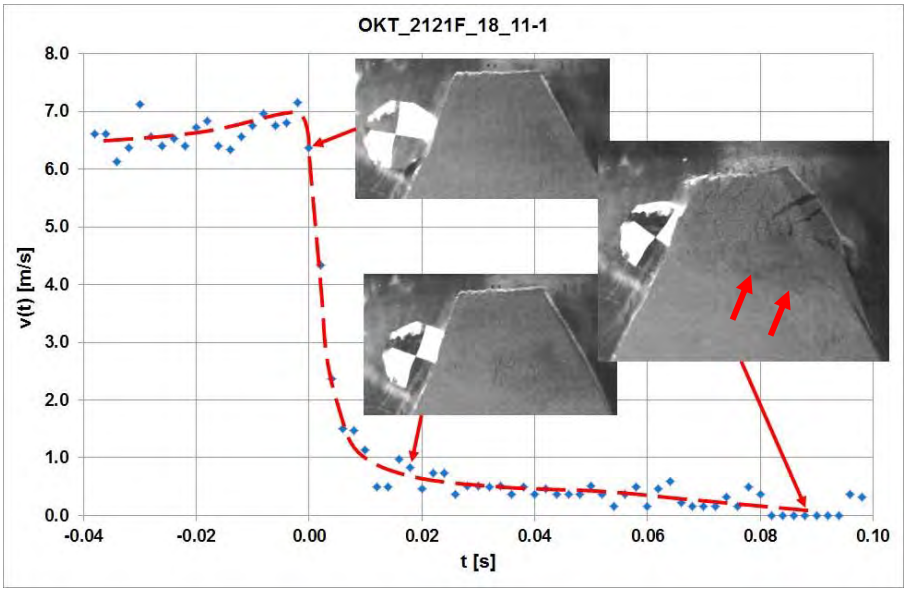

Fig. 3.42: Block deceleration in test OKT_2121F_18_11-1, red line: assumed mean translational velocity, arrows: partly visible shear plane.

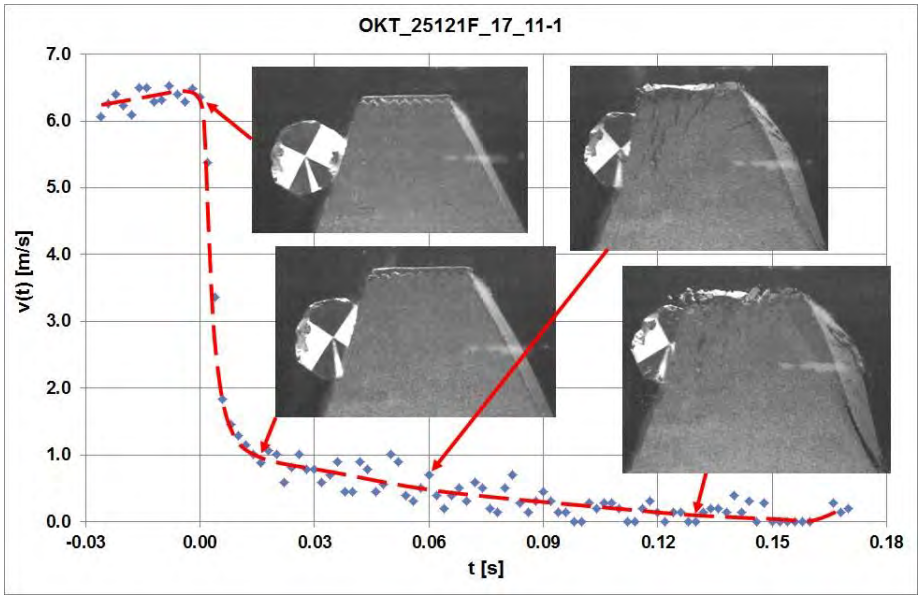

Fig. 3.43: Block deceleration in test OKT_25121F_17_11-1, red line: assumed mean translational velocity.

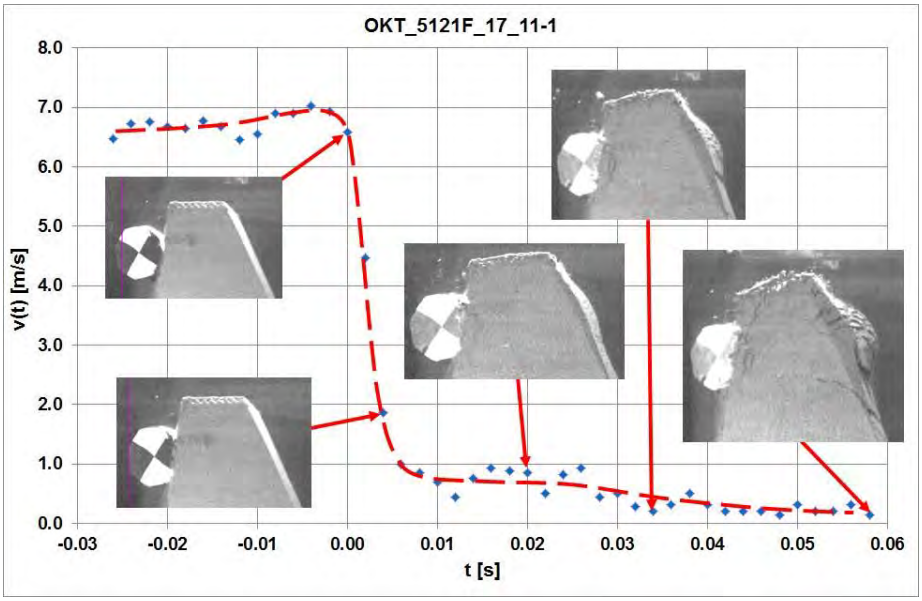

Fig. 3.44: Block deceleration in test OKT_5121F_17_11-1, red line: assumed mean translational velocity.

Due to the impact of block OKT at the opposite slope of the embankment a bulge appears. With increase of the volume of such a bulge tension cracks occur. Those cracks proceed more or less radial to the impact point. A failure plane with downward dip, as it was seen in tests with the rotating cylinders (Figures 3.24, 3.29, 3.37), could not be identified clearly. Only during test OKT_2121F_18_11-1 such a shear plane was visible in parts (Fig. 3.42).

Fig. 3.45 shows the translational velocity versus time for the embankment type 2121 without stones on the slopes, with stones placed horizontally at the "uphill" side and stones placed on both slopes of the embankment. In all three tests the crest width was the same and the crest to block ratio was approx. 1.1.

Just before the impact the velocity of block OKT is very similar in the three tests and is in the interval 6.8 – 7 m/s. During the first 5 ms of the impact process the block velocity graphs show nearly identical curve progression. So the differences in embankment construction seem to be not so important for that part of the impact process. But after the period of 5 ms in test OKT_2121F_18_11-1 the velocity values drop to a lower level than in the two other tests. After 0.02 s the translational block velocity in test OKT_2121F_18_11-1 is reduced to a value of approx. 0.6 m/s while the velocity in the tests OKT_2121_18_11-1 and OKT_2121FF_18_11-1 remains at approx. 1 m/s. During the further test procedure the block velocity is still reduced, but with a significant smaller gradient and the difference between the velocities is approx. constant.

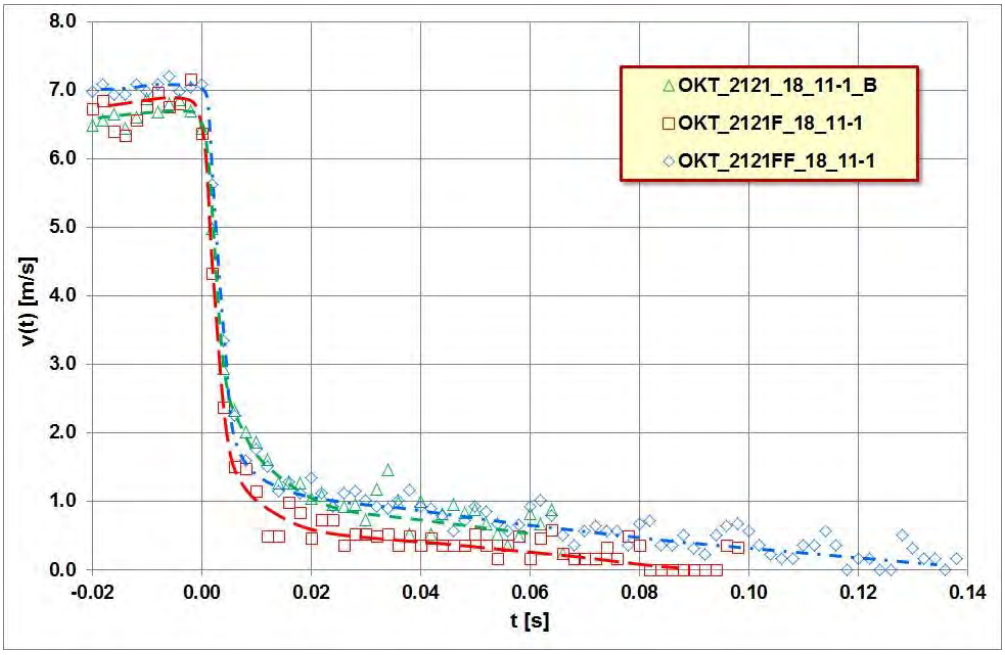

Fig. 3.45: Translational velocity v versus time t determined for the first impact, dashed lines are estimated mean values. The oscillation of the data points in the graphs provides information about the error rate of this kind of measurement.

Assuming the translational velocity at t = 0.02 s may be used completely for a vertical lift of the block, this will result in a calculated height of 2 cm for the velocity v = 0.6 m/s and 5 cm for the velocity v = 1 m/s. The distance impact location to maximum passing height in test OKT_2121FF_18_11-1 is approx. 6.7 cm measured parallel to the slope. Converted to the vertical the value is 5.5 cm. The measured vertical lift in test OKT_2121F_18_11-1 is approx. 1.8 cm. This agrees very well with the values based on the velocities.

Fig. 3.46 shows the decrease of velocity v versus horizontal displacement x of impactor OKT. The largest horizontal movement of block OKT is achieved for the embankment with stones on both sides.

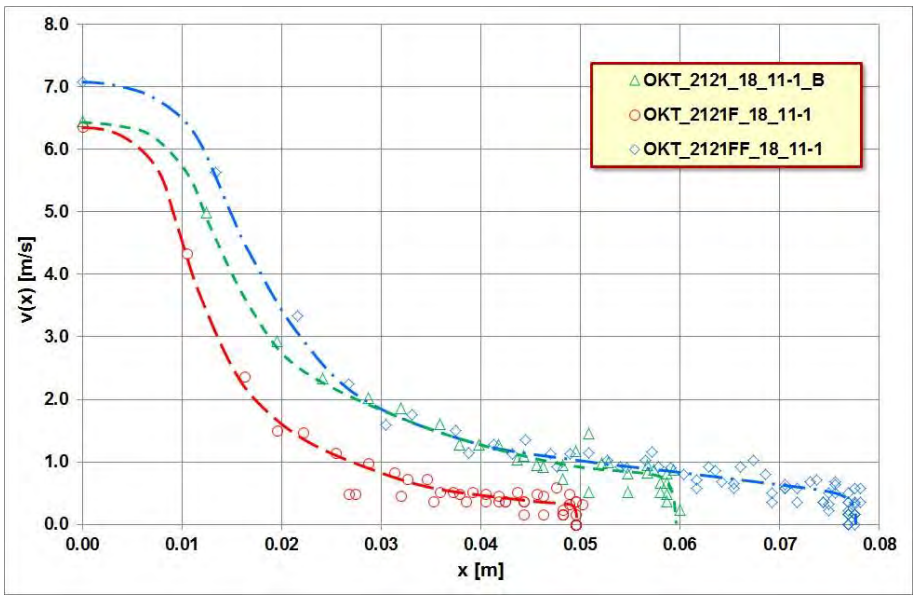

Fig. 3.46: Decrease of velocity v versus horizontal displacement x of impactor OKT at embankments type 2121 without stones on the slopes, with stones placed horizontally at the "uphill" side and stones placed on both slopes of the embankment.

Fig. 3.47 shows the angle of revolution versus time determined during the first impact of the three tests. During the first 0.02 s the curve progression of the three tests are very similar. But then there is a divergence and the block OKT receives a higher angular velocity in test OKT_2121FF_18_11-1 than in the two other tests. So also in the case of a block with edges it seems to be that high rotational block energy leads to less reduction in the translational energy than a lower rotational energy

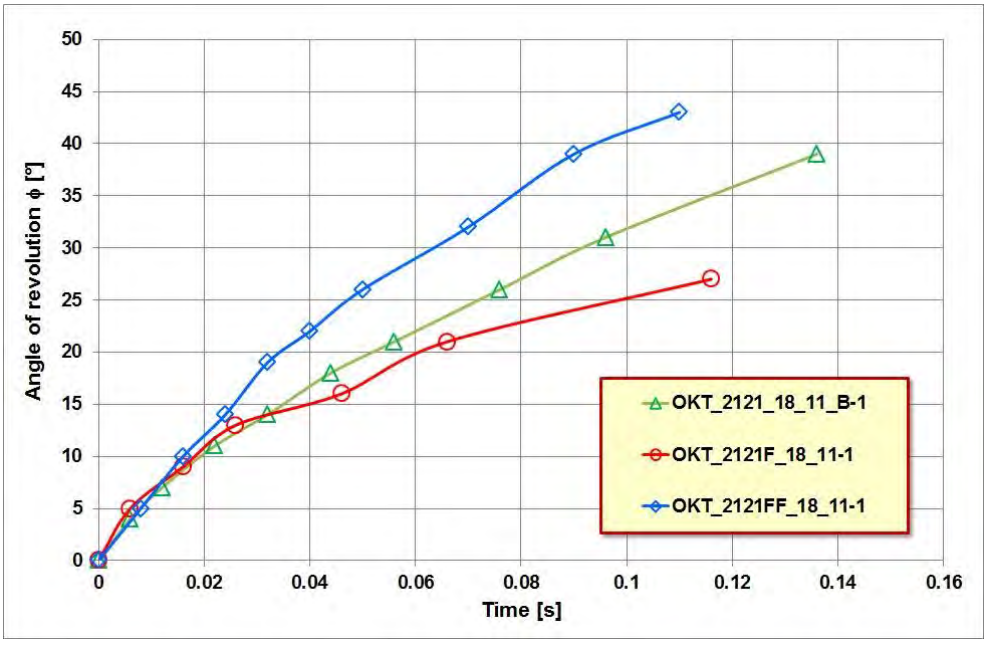

Fig. 3.47: Angle of revolution versus time determined for the first impacts.

The thickness of the stones used to build the "rockery" is very similar and the slope inclination is the same in the above mentioned tests. So the roughness of the slope does not vary very much for slopes with batter 2:1 (q.v. Fig. 2.17), even though the stones had not been placed at the same position in tests OKT_2121F_18_11-1 and OKT_2121FF_18_11-1. Fig. 3.48 shows the difference in the surface structure as well as a difference in the impact mark.

Fig. 3.48: "Uphill" slope before and after the first impact.

The results for the translational velocity v as well as for the rotational velocity ω of the three tests done with the embankment model Gurtnellen are shown in Figures 3.49 and 3.50. The tests had been done with block GS as impactor.

Before the impact the translational velocities of block GS in the tests Gurtnellen 1 (first impact) and Gurtnellen 2 (second impact) are very similar and the mean value is 6.9 m/s (Fig. 3.49). Due to the contact with the embankment the velocity is reduced within a very short period of about 4 ms. Immediately after this period block GS showed a translational velocity v of only approximately 1.5 m/s in test Gurtnellen 1 (impactor hits the uppermost brick course mainly at the front wall and pushed the stones inside the embankment) while v is about 3 m/s in test Gurtnellen 2 (impactor hits the uppermost brick course at the top side). Because the energy goes with the square of velocity v the reduction in translational energy is significantly larger for block GS in test Gurtnellen 1 than in test Gurtnellen 2. Respectively the translational energy of block GS in test Gurtnellen 2 after 4 ms is about 4 times the translational energy of block GS in test Gurtnellen 1 at the same time. This explains why the embankment was surmounted in test Gurtnellen 2, but not in test Gurtnellen 1.

Block GS showed in test Gurtnellen 3 a lower velocity of about 6.1 m/s before the contact, but less energy loss due to the contact than in test Gurtnellen 1 (Fig. 3.49). In both tests the block hit the embankment below the kink of the bi-linear slope. The velocity reduction in test Gurtnellen 1 is approximately 78% while the reduction in test Gurtnellen 3 is only 67%. The higher translational velocity of about 2 m/s allows block GS in test Gurtnellen 3 to reach the crest of the embankment.

Fig. 3.50 shows the decline of the rotational velocity in the tests Gurtnellen 1, 2 and 3. Again the loss of velocity and so also the loss of energy is the largest in test Gurtnellen 1, where block GS hit the embankment just below the kink of the bi-linear slope. The time period to reach a relative constant level for the rotational velocity is approximately 20 ms and therefore significantly larger than for the translational velocity.

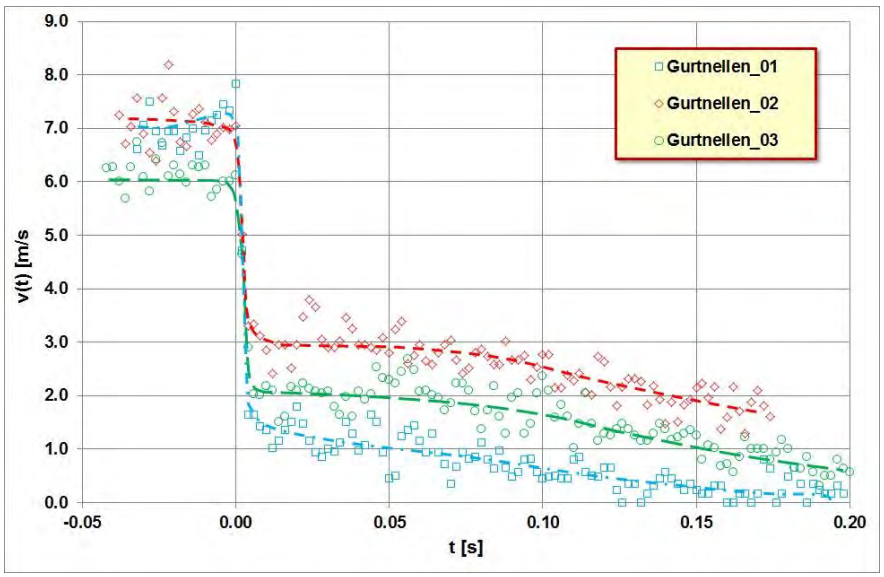

Fig. 3.49: Translational velocity v of impactor GS during the impact process on embankment model Gurtnellen, dashed lines show estimated mean values of velocity v.

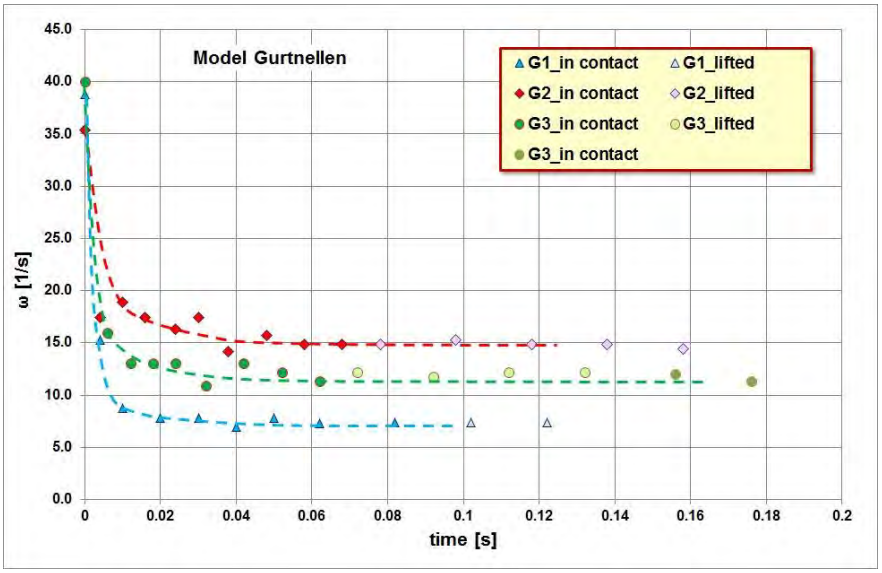

Fig. 3.50: Rotational velocity ω of impactor GS during the impact process on embankment model Gurtnellen

In all three tests the block GS hit the embankment and then it bounced. The period, the block GS was without contact to the slope, is shown in pale colors in the graph in Fig. 3.50.

The three tests done with the model Gurtnellen are insufficient to give a general conclusion, but it can be stated, that the kink of the bi-linear slope plays a significant role for the impact. If the block is rolling or hit the embankment at the lower part of the slope, there is a good chance that the embankment will not be surmounted.

3.4 Drop of energy due to impact

Fig. 3.51 shows the drop of translational energy of block G during the impact onto an embankment with cross section type 2121 for the different types of slope surface conditions in comparison. The data show a tremendous energy drop within the first 10 to 15 ms for all types of slope surface conditions, with and without "rockery". Differences between the four tests are hard to see in Fig. 3.51. After this energy drop the remaining translational energy is reduced with a low gradient.

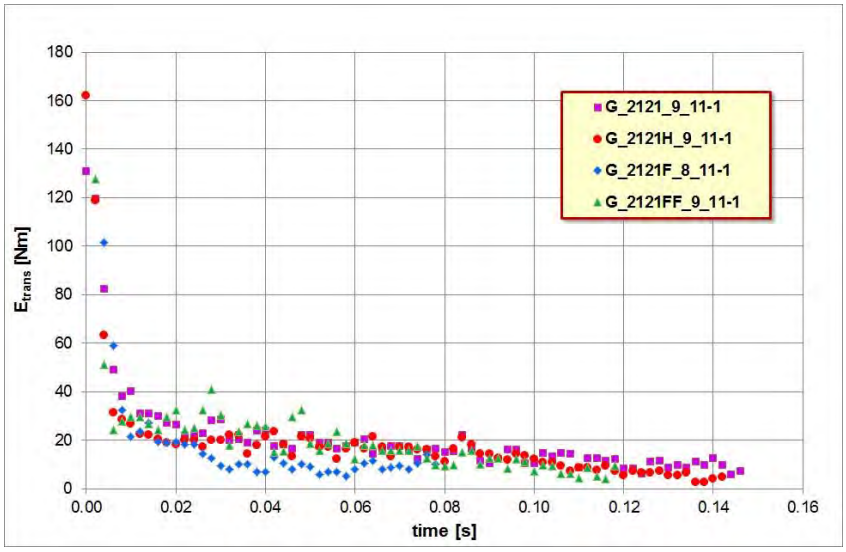

Fig. 3.51: Translational energy versus time of impactor G during the impact process on embankment models with and without rockery at the slopes.

In Fig. 3.52 the energy data is normalized to the respective maximum energy value determined for the test just before the contact (Appendix C1). It is shown that more than 75% of the translational block energy is dissipated within the first 20 ms. A bi-linear upper boundary may be established to describe the energy drop.

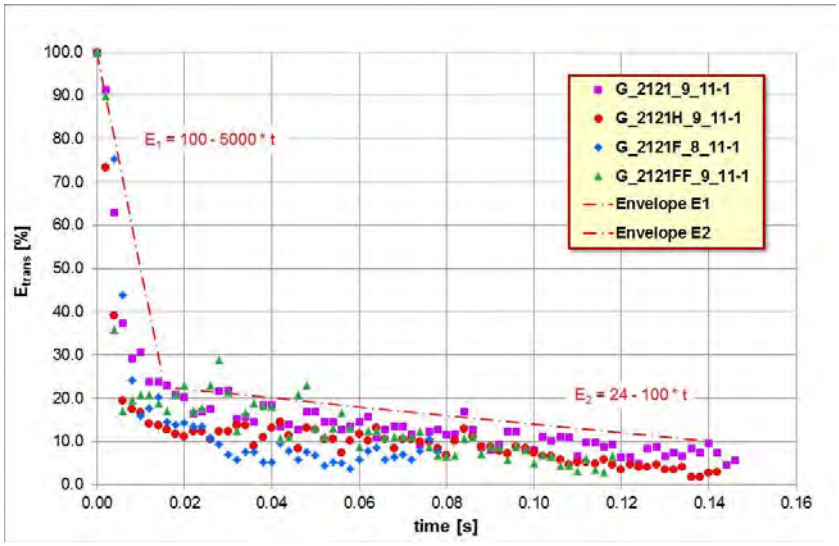

Fig. 3.52: Comparison of the normalized translational energy loss of impactor G, 0.02 s after the first contact between impactor G and the embankment with cross section type 2121 the block has lost at least 75 % of its translational energy.

The influence of the different slope surfaces in the 4 tests is visible in Fig. 3.53, where the normalized translational energy is shown versus the horizontal movement of block G. The highest resistance is given by the embankment with stones placed horizontally at the slope while the minimal resistance is given by the slope without stones. The test results for the embankment with stone placed parallel to the slope surface lies in between. This behavior was expected physically and is based on the different stiffness of soil and rock material respective the combination of these materials at the slopes.

On the other hand the results of the test with "rockery" on both sides of the embankment is surprisingly, because it shows that the roughness of the slope and the orientation of stones are not solely responsible for the curve progression of the energy drop. The smaller volume of soil between the two layers of "incompressible" stones may be the reason for the difference in the energy drop data here in comparison to the test with only "rockery" at the uphill slope.

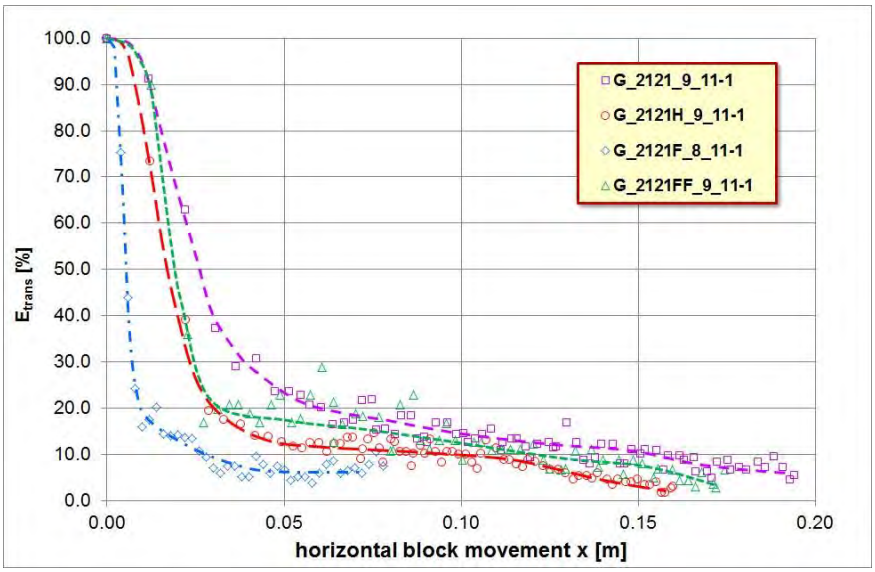

Fig. 3.53: Reduction of the standardized translational energy E_{trans} with horizontal movement x of the block G for the 4 different embankment slope constructions. Dashed lines are estimated mean values.

The reduction of the standardized rotational energy E_{rot} of block G with horizontal block movement x is shown in Fig. 3.54. Again the data show a tremendous energy drop at the start of the impact process for all types of slope surface conditions, with and without "rockery". Differences between the three tests - G_2121_9_11-1 without "rockery", G_2121H_9_11-1 with stones placed parallel to the slope and G_2121FF_9_11-1 with stones placed horizontally at both slopes - are hard to see in Fig. 3.54. Only the data of test G_2121F_8_11-1 shows a significant difference in curve progression and is situated above the three other curves.

Fig. 3.54 shows also that the rotational energy had been reduced to a level of 10% or less within the first 5 cm of horizontal block movement. In the aftermath the block rotation and therefore the rotational energy is approximately constant and the data of the 4 tests showing lines running approximately parallel. This phenomenon, that the rotational energy of rotating cylinders will be more or less constant in the later phase of the impact process, had already been found by Kister (2015) for embankments made of pure soil.

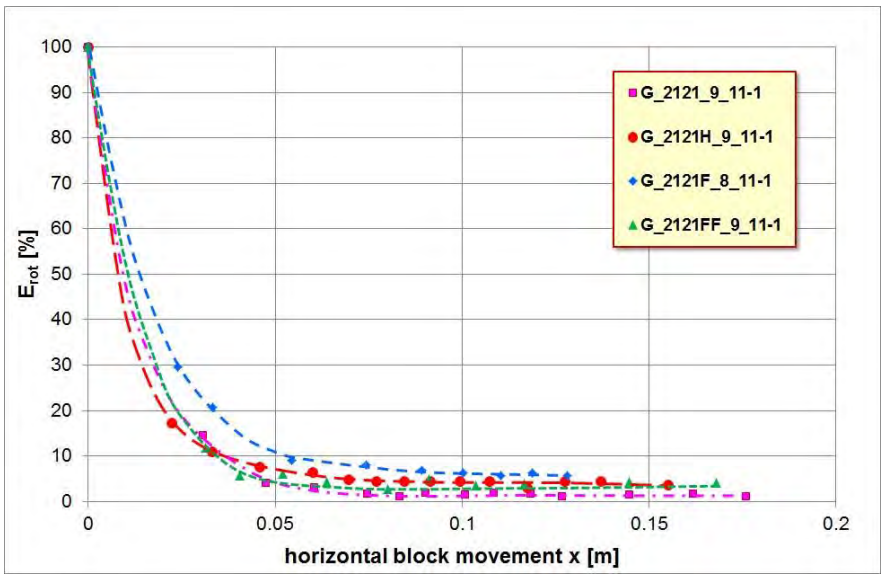

Fig. 3.54: Reduction of the standardized rotational energy E_{rot} with horizontal block movement x of block G for 4 different embankment slope constructions. Dashed lines are estimated mean values.

Figures 3.55, 3.56 and 3.57 are showing the reduction of the standardized translational energy E_{trans} with horizontal movement x of block OKT. All graphs in the three figures have in common that the translational energy had been reduced to a level of 10% or less within the first 3 cm of horizontal block movement during the impact process.

In Fig. 3.55 the results for a crest to block ratio of approx. 0.5 are shown while Fig. 3.56 shows the graphs for the same test arrangement, but for a crest to block ratio of approx. 1.1. Both figures have in common that the embankment only with "rockery" at the uphill slope (2121F) seems to have the largest resistance against the impact of block OKT while the embankment with "rockery" at both slopes (2121FF) seems to have the lowest resistance against the impact of block OKT. The embankment only with "rockery" at the uphill slope (2121F) led also to the smallest values for the maximum horizontal movement of block OKT in the three tests, while the embankment with "rockery" at both slopes (2121FF) led to the largest values for the maximum horizontal movement of block OKT in the three tests (see Figures 3.55 and 3.56). Therefore the "rockery" at the downhill slope may reduce the necessary building ground for an embankment, but does not improve necessarily the resistance against impact.

The influence of the embankment's width is also visible in Figures 3.55 and 3.56. The slender construction led to a larger maximum value of the horizontal block movement. So for example the maximum horizontal movement of about 9.5 cm for embankment type (2121F) for the slender structure with crest width of approx. 8 cm is almost twice the value of 5 cm received for the embankment with crest width of approx. 18 cm. The translational block energy in both tests was identical (142.8 resp. 142.6 Nm, see also Appendix C1).

As already mentioned for Fig. 3.39, velocity v versus horizontal movement x, there is no clear correlation between slope steepness and block stopping (Fig. 3.57).

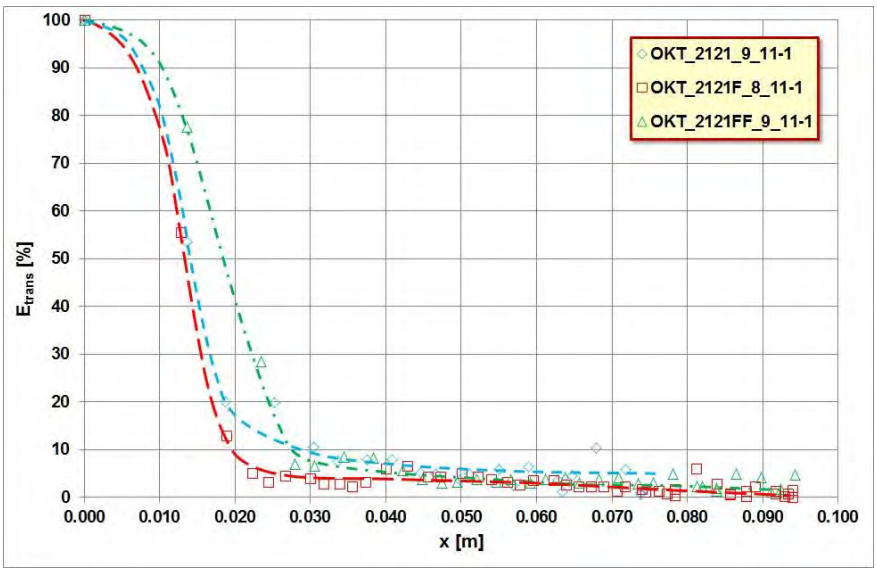

Fig. 3.55: Reduction of the standardized translational energy E_{trans} with horizontal movement x of block OKT for different embankment slope constructions and a crest to block ratio of approx. 0.5. Dashed lines are estimated mean values

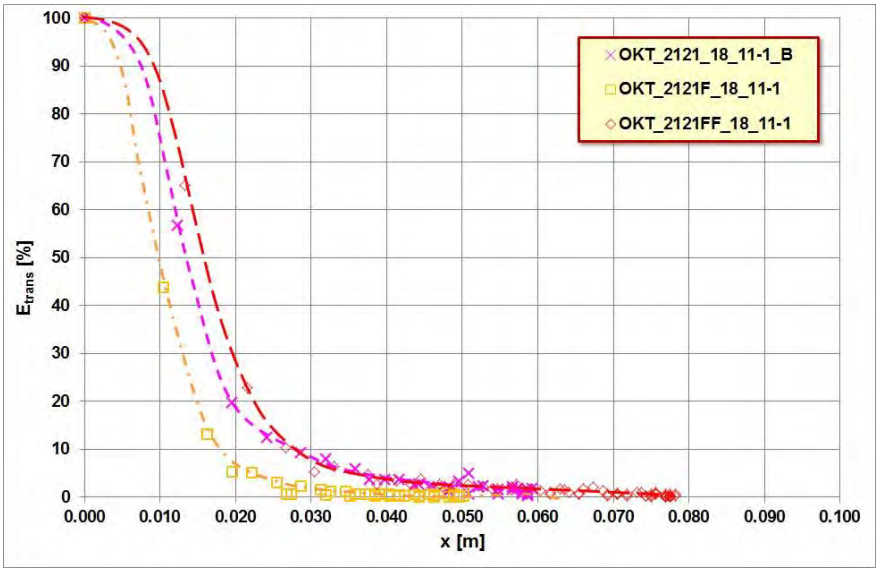

Fig. 3.56: Reduction of the standardized translational energy E_{trans} with horizontal movement x of block OKT for different embankment slope constructions and a crest to block ratio of approx. 1.1. Dashed lines are estimated mean values.

Fig 3.58 shows the standardized translational energy E_{trans} versus time t of the block OKT in the tests. The graph has been limited to a maximum standardized translational energy value of 25% for better visibility. 0.01 s after the first contact the block energy is reduced to a value of 10% or less. So for the time mark 0.02 s after the first contact the block energy of the non-rotating or low-rotating block OKT is much more reduced than for the cylinder G with the higher rotation (Fig. 3.52). The 10%-mark is reached for block G only at 0.14 s after the first contact.

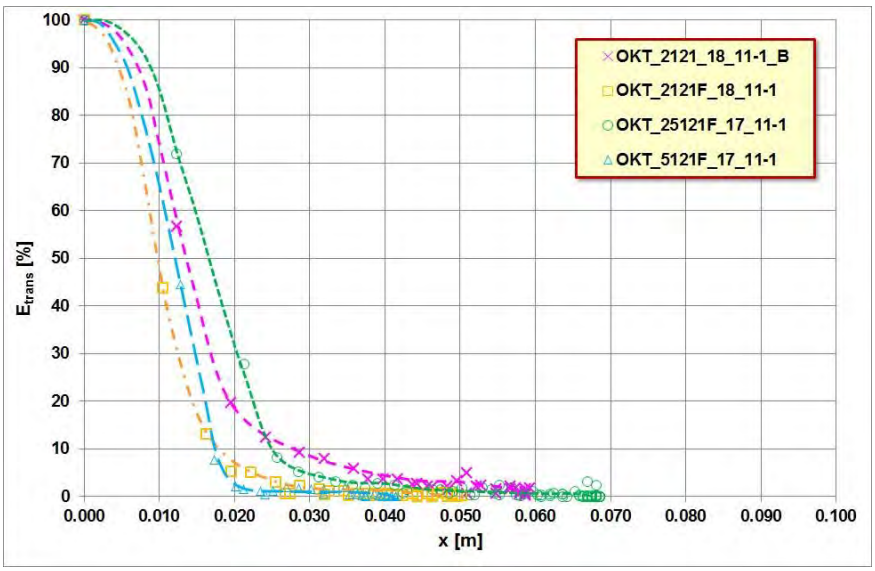

Fig. 3.57: Reduction of the standardized translational energy E_{trans} with horizontal movement x of block OKT for different embankment slope inclination and a crest to block ratio of approx. 1.1. Dashed lines are estimated mean values.

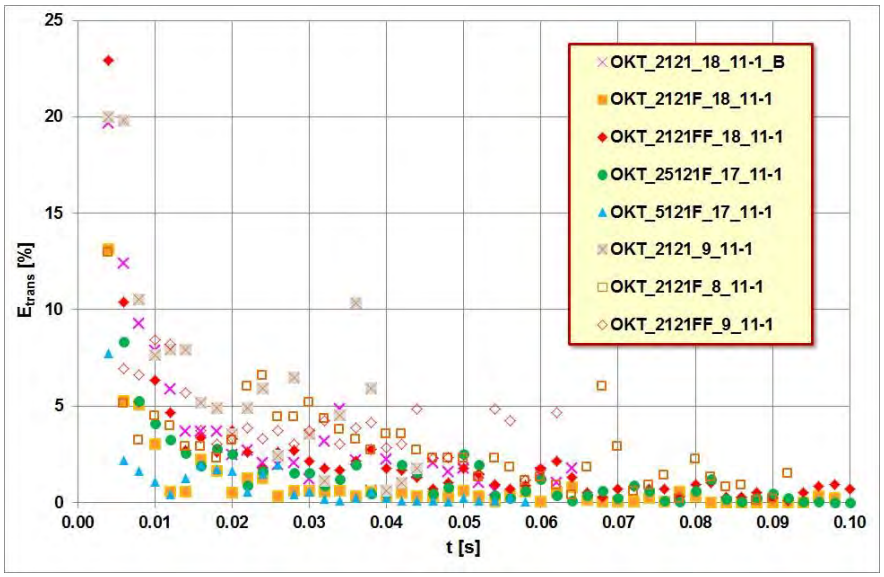

Fig. 3.58: Block OKT, standardized translational energy E_{trans} below the 25% level versus time t.

So the energy loss of translational block energy is much faster for non-rotating or low rotating blocks than for blocks with high rotation. This is the experimental confirmation of the thesis of Plassiard & Donzé (2009), that "the initial rotational kinetic energy favors an increase of the translational kinetic energy during impact". This statement of Plassiard & Donzé was based on results of numerical calculations using the Discrete Element Method (DEM).

3.5 Direct measurement of deceleration

Direct measurement of deceleration during the impact had been done with a triaxial acceleration sensor and a mini data logger placed in block GS (Fig. 2.2). The results of those measurements for the small crest to block diameter ratio of approx. 0.5 and the embankment cross section types 2121 and 2145 are presented in Figure 3.59.

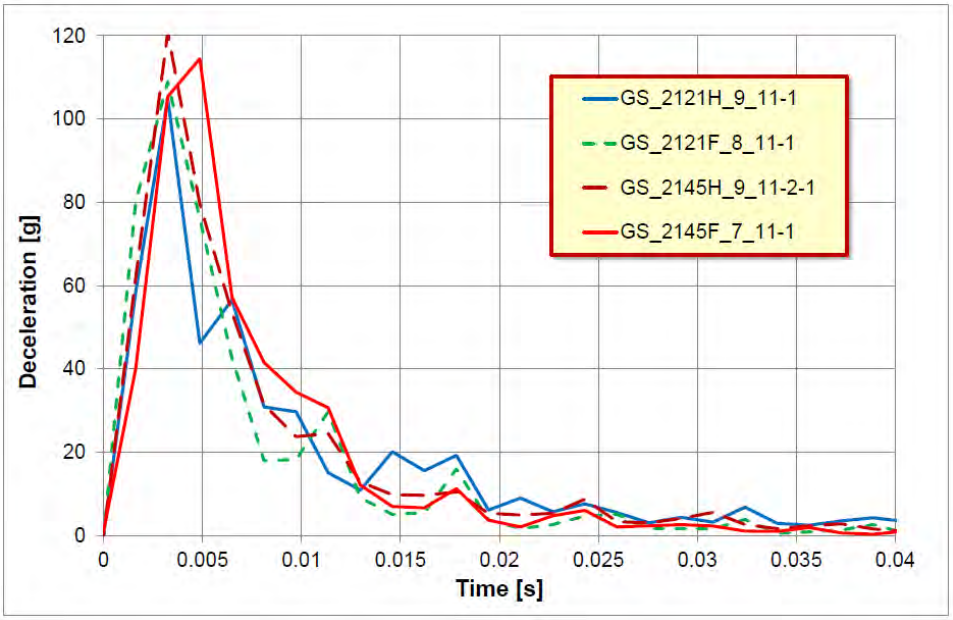

Fig. 3.59: Deceleration versus time of block GS for the small crest to block diameter ratio of approx. 0.5.

In all four tests with stones placed at the "uphill" slope the deceleration reached a maximum value, which is higher than 100g. For the embankments of type 2145 even deceleration values higher than 110g had been measured (121g for index H resp. 114g for index F). For the slender structures of embankment type 2121 smaller maximum values had been determined, 105g for index H resp. 109g for index F. So the maximum deceleration values for the two tests are very similar and the orientation of stones and therefore the roughness of the uphill slope seem to be of minor influence on the block deceleration. On the other hand the graph of test GS_2145F_7_11-1 in Fig. 3.59 differs in its shape in comparison to the other 3 graphs. The maximum value of deceleration is slightly shifted in time compared to the other three graphs and the graph has a broader shape.

Searching for explanation of the differences in the graphs of Fig. 3.59 the impact parameters had been checked. The translational velocity v of block GS before the impact is within the interval 6.5 m/s and 6.7 m/s in the four tests, i.e. the difference in block velocity is less than 4% and therefore may not explain the differences in the graphs. On the other hand the rotational energy in both tests of embankment type 2145 is approx. 15% higher than in both tests of embankment type 2121 (see Appendix C1). This may explain the differences of the maximum deceleration values in Fig. 3.59. The impact angle α in the three tests GS_2121H_9_11-1, GS_2121F_8_11-1 and GS_2145H_9_11-2-1 was determined to 12° resp. 13°. Only for test GS_2145F_7_11-1 a lower impact angle of 8° was determined. So this could be an indication that the impact angle affects the shape of the deceleration graph.

Fig. 3.60 shows the deceleration versus time graphs of block GS for the large crest to block diameter ratio of approx. 1.1 and embankment type 2121 for three cases:

a) without rockery at the slope,
b) with stones placed horizontally at the uphill slope and
c) with stones placed horizontally on both slopes of the embankment.

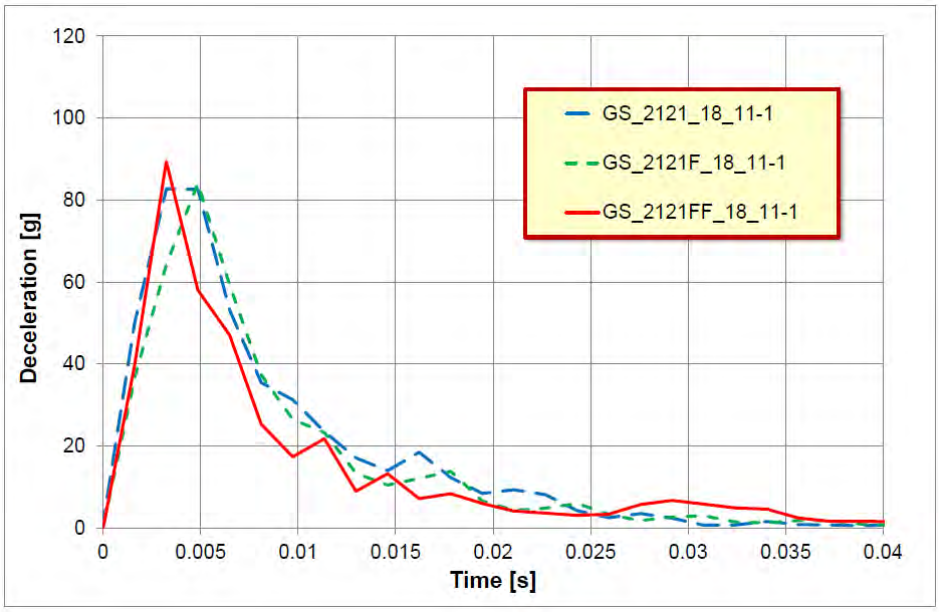

Fig. 3.60: Deceleration versus time of block GS for the large crest to block diameter ratio of approx. 1.1.

The maximum values of the graphs in Fig. 3.60 are very close together, but they are smaller in comparison to those in the graphs in Fig. 3.59 and did not exceed the 90g-level in all three tests. The translational velocities in the three tests had been determined to be in the interval 6.4 m/s to 7.1 m/s, which is in the same range as the velocities determined for the four tests mentioned before. The rotational energy is in the interval 19.7 Nm to 22.4 Nm, which is lower than in the tests shown in Fig. 3.59. So also in this case the smaller values for the deceleration maximum may be explained by differences in rotational energy. But the theory, that the deceleration will reach a larger value in case of a slope covered with stones instead made of pure soil, seems to be disproved due to the tests shown in Fig. 3.60. The maximum deceleration values are very similar for impacts on slopes with stone facing and on a slope made of pure soil. Due to the similarities of the graphs of the tests GS_2121F_18_11-1 and GS_2121_18_11-1 it may be deduced, that the stones placed horizontally and the roughness of the uphill slope seems to be of minor influence on the block deceleration.

Comparing the parameters of the tests presented in the Figures 3.59 and 3.60 for the embankment type 2121, additional to the rotational energy there is another parameter, the crest width, which significantly differs in the two small test series. The crest width in the tests of Fig. 3.59 is just approx. half of the crest width in the tests of Fig. 3.60. But the maximum value of deceleration received in the tests with a smaller crest width is higher than the values achieved for the tests with a larger crest width. This was not expected and therefore had to be checked.

Test	α [°]	E_{trans} [Nm]	E_{rot} [Nm]	E_{total} [Nm]	Deceleration [g]
GS_2121_18_11	14	141.0	22.4	163.5	82.7
GS_2121H_9_11	12	152.1	23.3	175.4	105.0
GS_2121F_8_11	12	149.7	23.6	173.3	108.9
GS_2121F_18_11	10	150.7	21.6	172.3	84.1
GS_2121FF_18_11	13	168.3	19.7	188.1	89.4

Table 3.10: Impact angle, energies and maximum deceleration values of tests done with embankment cross section type 2121.

To check, if an influence of the crest width on the block deceleration exists, results of tests done by Kister (2015) had been redrawn. In Fig. 3.61 the graphs of deceleration versus time of block GS for three different crest widths named as A, B and D for embankment type 2145 without rockery are presented.

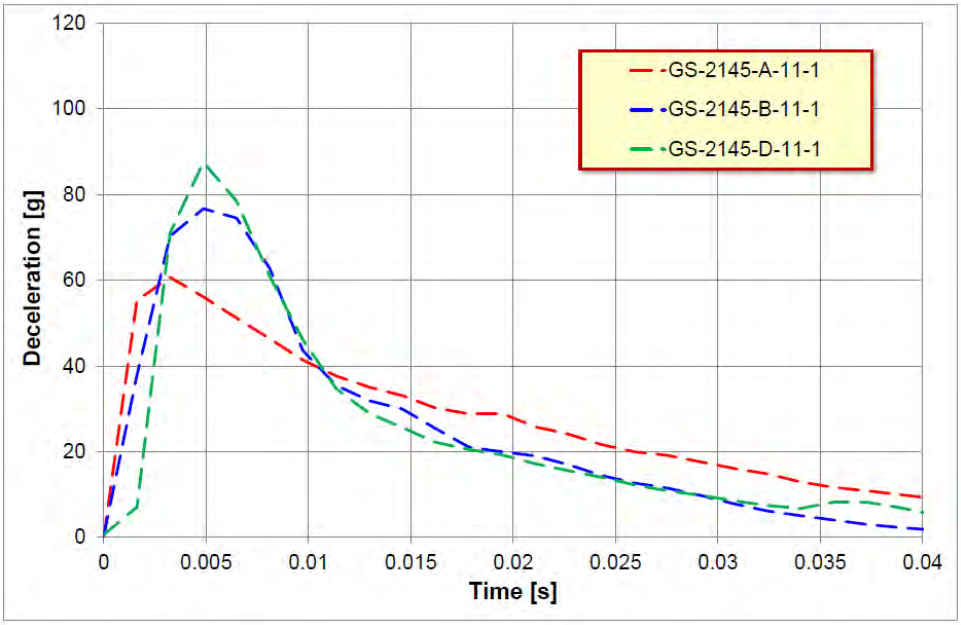

Fig. 3.61: Deceleration versus time of block GS for three different crest widths: A approx. 19 cm, B approx. 9.5 cm, C approx. 2.5 cm.

For the embankment with the largest crest width (index A) the smallest maximum value of deceleration had been achieved in Fig. 3.61. On the other hand, for the embankment with the smallest crest width (index D) the largest maximum value of deceleration had been achieved. The embankment with crest width type B (approx. 9.5 cm) lies in between the crest width types A (approx. 19 cm) and D (approx. 2.5 cm) and so the maximum value for deceleration does in the tests.

The translational velocities in the three tests are 6.3 m/s, 6.1 m/s and 6.1 m/s and therefore there is no large difference in the translational energies (104 Nm … 109 Nm). The rotational energies are in the interval 38.4 Nm (type D) and 44.3 Nm (type B). The rotational energy in the test with crest type A was 41.2 Nm, which lies in between the two other results. So the gradation in the graphs in Fig. 3.61 cannot be explained by differences in energy.

Also no correlation with the impact angle is visible, because only in test GS-2145-B-11-1 a larger value of 17° was determined for the impact angle. The impact angle in the tests GS-2145-A-11-1 and GS-2145-D-11-1 had been determined to 13°.

So there seems to be a really good chance for a correlation of crest width and block deceleration. To verify this, additional tests done by Kister (2015) had been redrawn.

Test	α [°]	E_{trans} [Nm]	E_{rot} [Nm]	E_{total} [Nm]	Deceleration [g]
GS-2145-A-01-1	19	86.1	41.1	127.2	82.3
GS-2145-A-11-1	13	109.4	41.2	150.5	60.7
GS-2145-B-01-1	19	75.1	48.4	123.5	88.6
GS-2145-B-11-1	17	105.8	44.3	150.1	76.7
GS-2145-D-01-1	21	83.4	42.2	125.6	71.9
GS-2145-D-11-1	13	104.4	38.4	142.8	87.5
GS_2145F_7_11	8	142.0	27.7	169.7	114.5
GS_2145H_9_11_2	13	145.8	26.7	172.5	120.8

Table 3.11: Impact angle, energies and maximum deceleration values of tests done with embankment cross section type 2145.

Fig. 3.62 shows results of impacts with block GS on an embankment of type 1111, i.e. a symmetric embankment with a slope inclination of approx. 1:1. The results of tests with crest width type A and type D are presented. The largest values of deceleration had been determined for the embankments with crest width type A, the largest crest width in this test series. For the smaller crest width type D the maximum values of deceleration are smaller than in the tests with crest type A. So these tests show a contradictory result in comparison to the tests shown in Fig. 3.61.

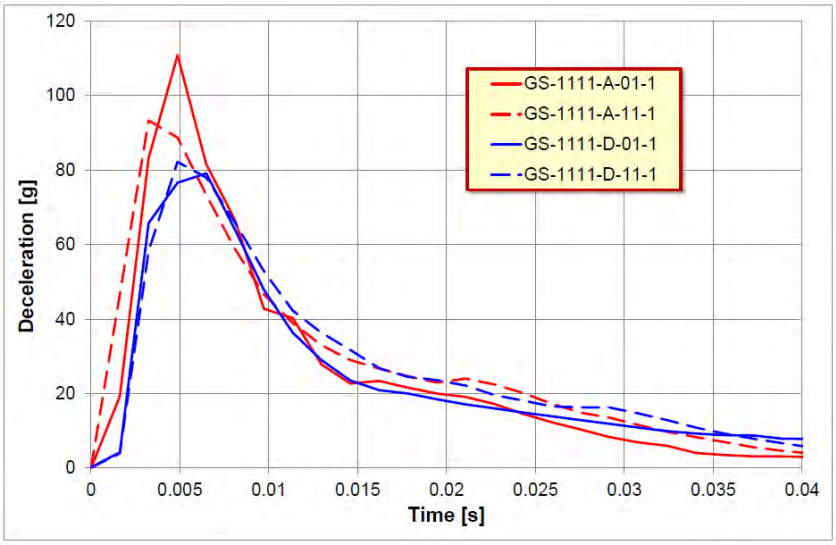

Fig. 3.62: Deceleration versus time of block GS for 2 different crest widths: A approx. 19 cm, C approx. 2.5 cm.

Test	α [°]	E_{trans} [Nm]	E_{rot} [Nm]	E_{total} [Nm]	Deceleration [g]
GS-1111-A-01-1	34	97.6	36.4	134.0	110.8
GS-1111-A-11-1	28	98.8	36.0	134.9	93.3
GS-1111-D-01-1	34	102.9	33.6	136.5	79.1
GS-1111-D-11-1	28	103.6	43.8	147.4	82.2

Table 3.12: Impact angle, energies and maximum deceleration values of tests done with embankment cross section type 1111.

The results of direct measurement of deceleration during the impact may be summarized as follows:

- The graph of deceleration versus time is characterized by a steep and asymmetric curve. With the used measurement device only a limited number of measurement points could be measured. So some details of the deceleration versus time graph may not be detected because of a limited resolution.
- The orientation of stones at the "uphill" slope and therefore the roughness of the "uphill" slope seem to be of minor influence on the block deceleration.
- The impact angle seems to have no influence on the shape of the deceleration versus time graph.
- To explain differences in the maximum value of deceleration the rotational energy of the block has to be taken into account.

Fig. 3.63 shows the total block energy versus the maximum deceleration value. Despite of the data scattering the graph shows increasing maximum deceleration values with increasing total block energy.

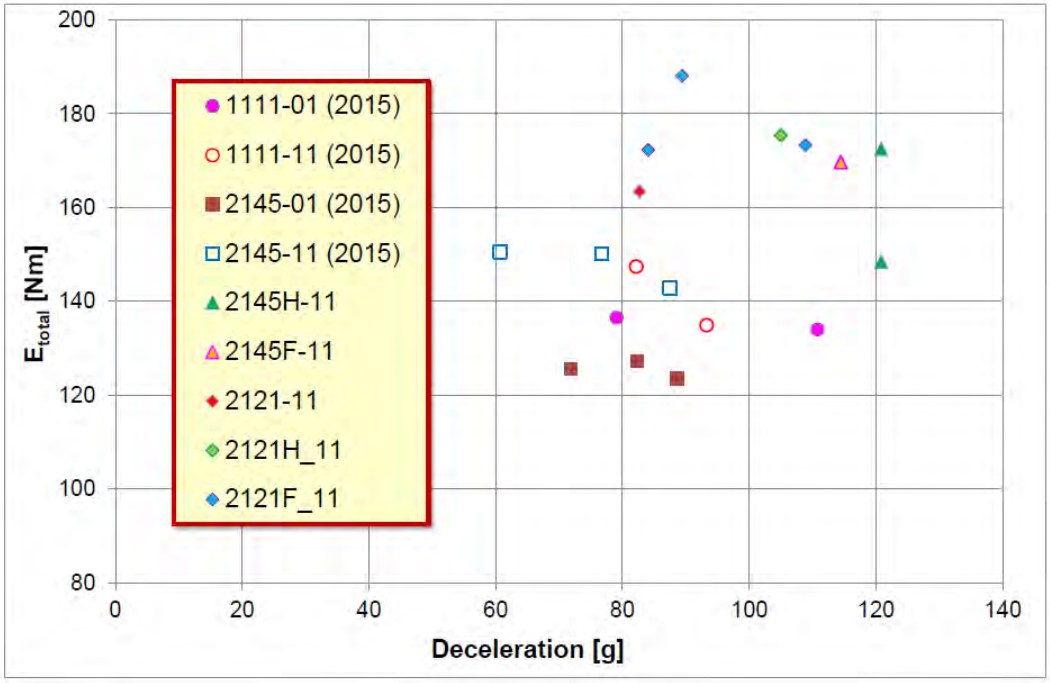

Fig. 3.63: Total block energy before impact versus maximum deceleration value.

3.6 Displacement inside the embankment due to impact

A few tests had been analyzed by the Particle Image Velocimetry method (PIV). This method is a kind of pattern recognition. For the analysis by the PIV method two pictures done at different time steps have to be compared. A time interval of 10 ms was used for these analyses. So time is known and the displacement of a selected area measured in pixels and characterized by a certain pattern can be determined by comparing the two pictures. With this method the velocity of an area with a certain pattern as well as the displacement can be determined. But to use the method successfully the pattern may be slightly deformed but not destroyed. The method and program used for these analyses are described in Kister (2015).

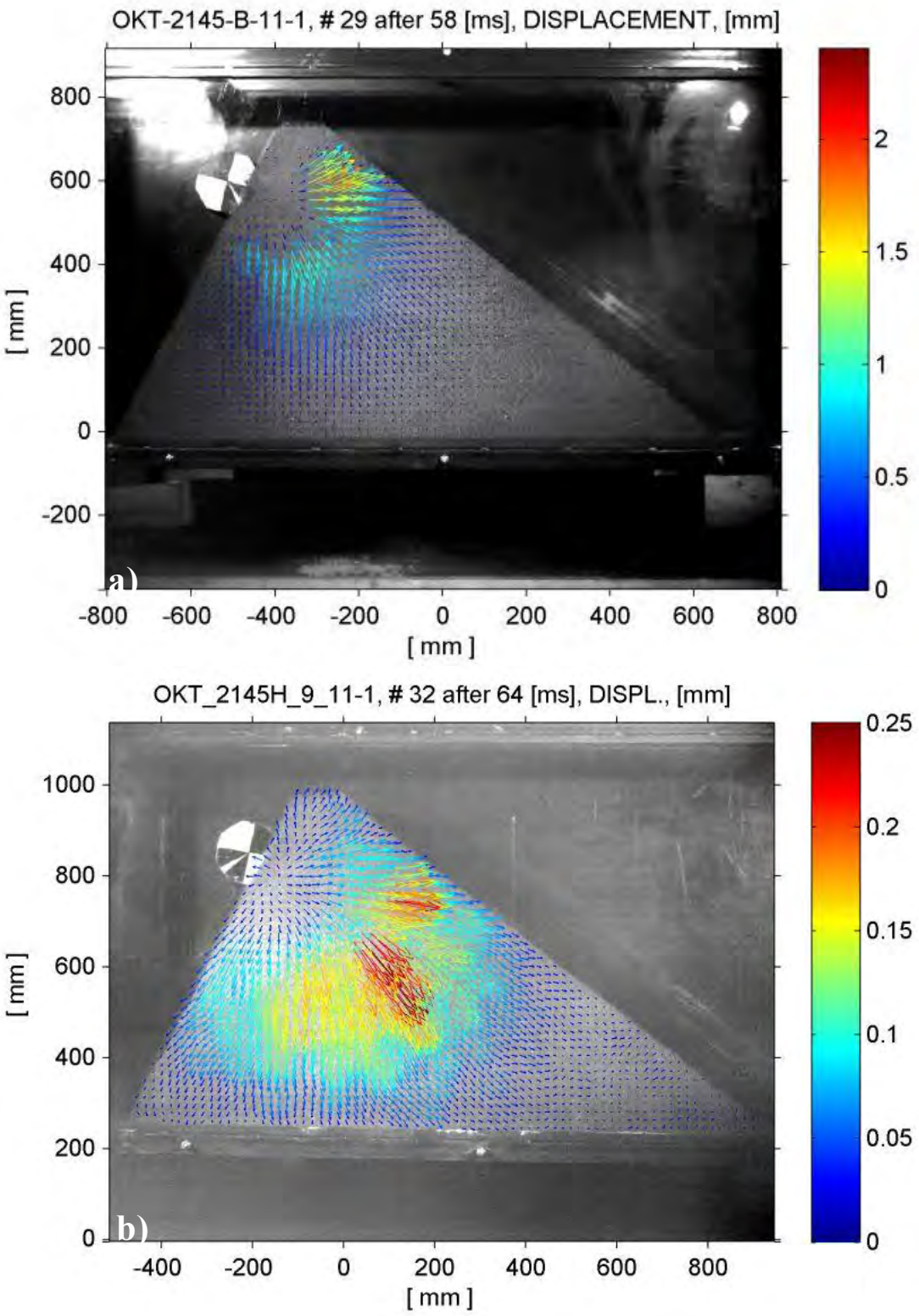

Fig. 3.64: Displacement field determined by PIV at a time 6 ms after the first contact of block and embankment, time interval: 10 ms: a) test OKT-2145-B-11-1 without stones on the "uphill" slope, b) test OKT_2145H_9_11-1 with stones placed parallel to the slope.

Fig. 3.64 shows the displacement field 6 ms after the first contact of block and embankment determined by PIV for the tests OKT-2145-B-11-1 and OKT_2145H_9_11-1. The test OKT-2145-B-11-1 is a test executed during the first test series (Kister, 2015) and the embankment was constructed without stones on the "uphill" slope. The index B in the test name is used for a crest width of approx. 9 cm. So the embankment geometry is the same as for test OKT_2145H_9_11-1 with stones placed parallel to the slope.

The PIV analysis of test OKT_2145H_9_11-1 led to significant smaller values for the displacements than the analysis done for test OKT-2145-B-11-1. So it is difficult to compare the two results because of the two different scales, which had to be used to present the data.

Additional to the difference of the size of displacements the two pictures in Fig. 3.64 show a significant difference in the alignment of the presented larger displacement arrows. The maximum displacements in test OKT-2145-B-11-1 are aligned more or less horizontally towards the "down-hill" slope, while the maximum displacements in test OKT_2145H_9_11-1 with stones placed parallel to the "uphill" slope show a downward direction.

In Fig. 3.65 the further evolution of the displacement field with time is presented for test OKT_2145H_9_11-1. While moving towards the "downhill" slope the values of the displacement field decrease. 28 ms after the contact block - embankment displacements are only visible in a narrow band at the level of the impacting block.

Fig. 3.66 shows the cumulated displacements of the test GS_2121HG_18_11-1 and the test GS_2121FG_18_11-1 determined by PIV at 58 ms after the contact block - embankment. For the slender structure of embankment type 2121 the areas showing the displacement field are looking similar, although in one case the rocks at the slope had been placed parallel to the slope (index H) and in the other the rocks had been placed horizontally (index F). But there is a small difference concerning the size of the displacements. Higher displacement values are achieved for the test with the stones placed parallel to the "uphill" slope, which may be an indication for a higher compaction of the embankment center in this test in comparison to the test with the stones placed horizontally.

Fig. 3.66 shows additional the displacements, which occur at the embankment's bottom at the "downhill" side for slender structures. But those displacements are small and did not impair the embankment's stability.

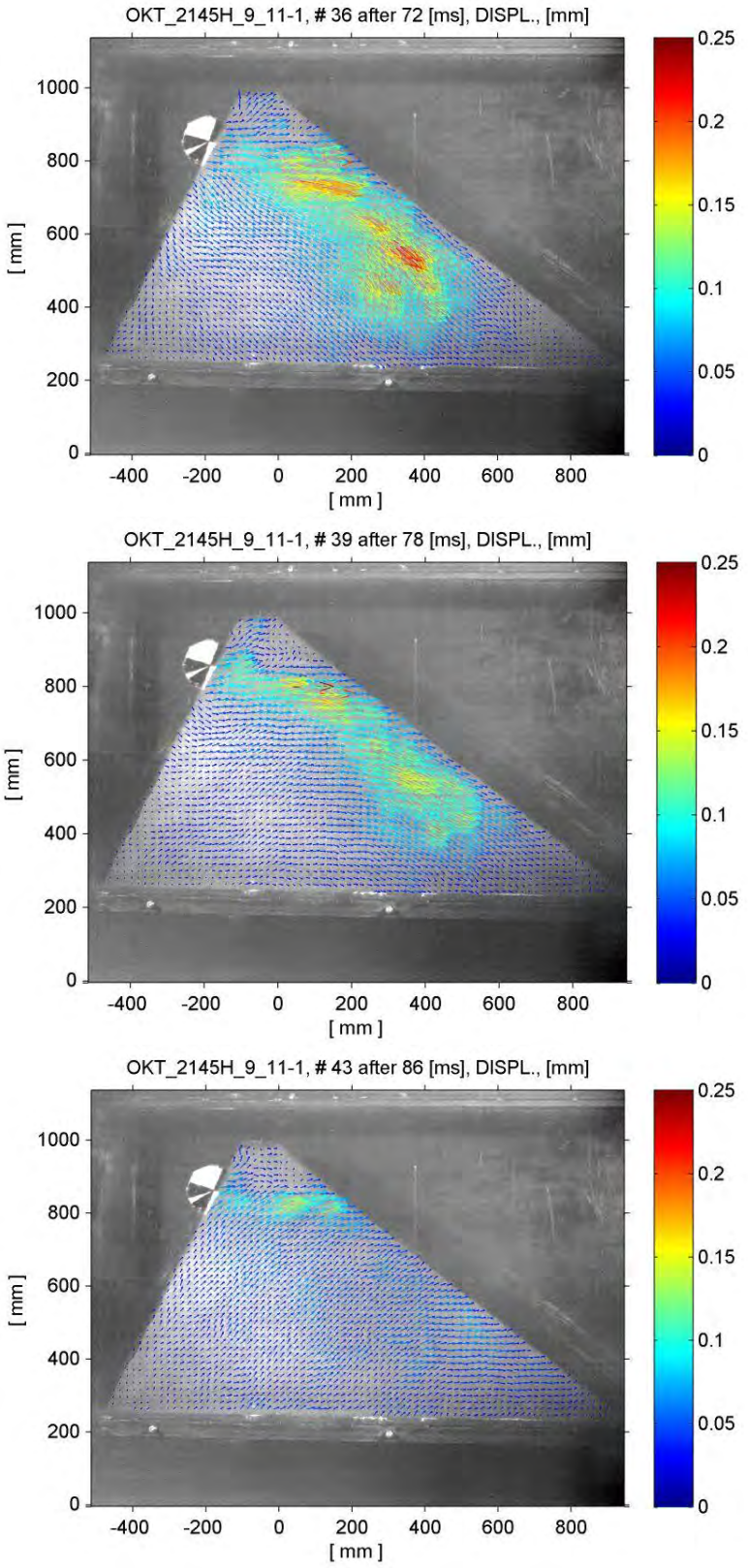

Fig. 3.65: Development of the displacement field determined by PIV of test OKT_2145H_9_11-1 : 14 ms, 20 ms and 28 ms after the first contact of block and embankment

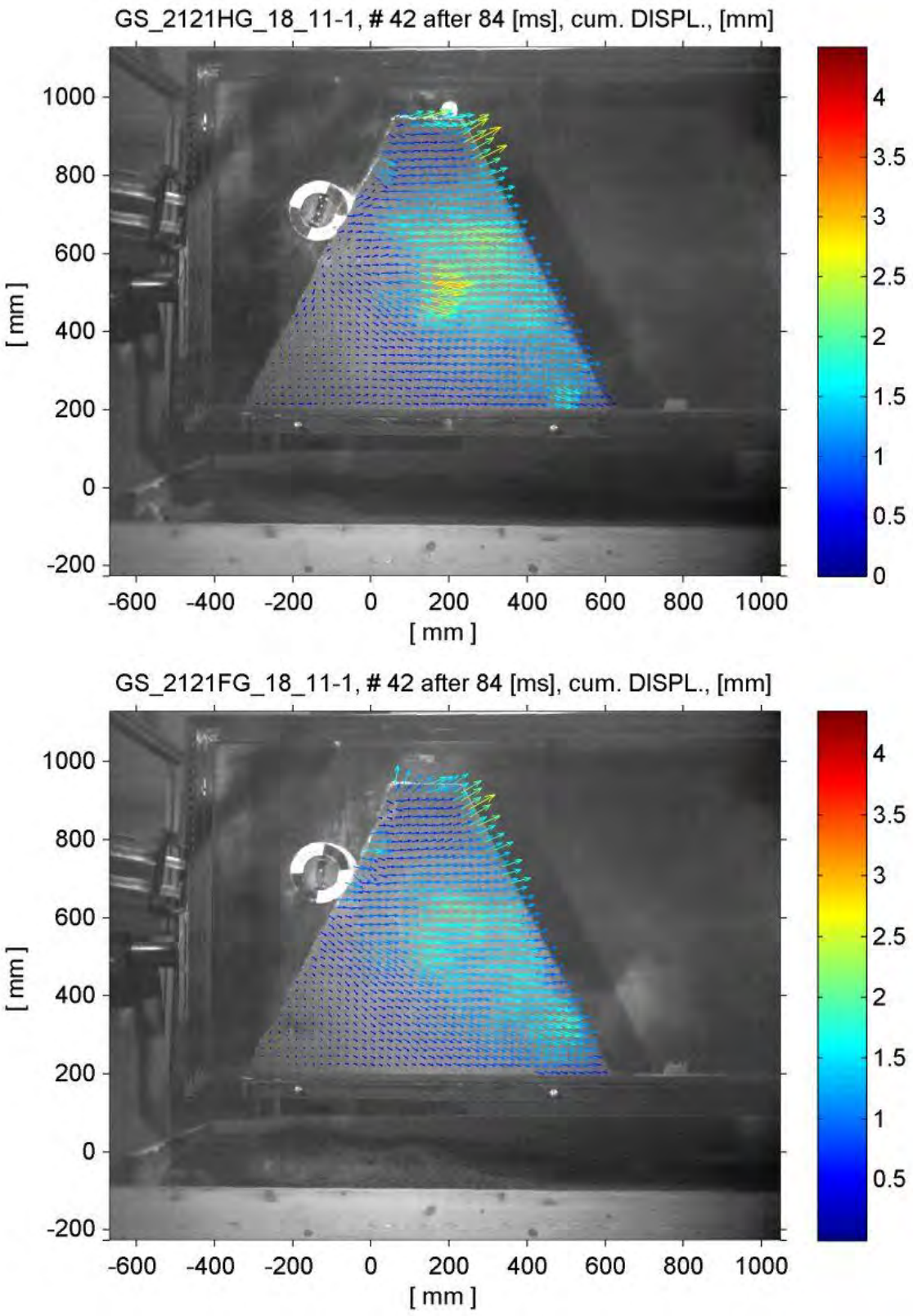

Fig. 3.66: Cumulated displacements determined by PIV: a) test GS_2121HG_18_11-1, b) test GS_2121FG_18_11-1.

4 Conclusions

The idea to combine rockfall protection embankments with natural stone masonry at the uphill side or sometimes at both sides is very common in Switzerland. This combination allows the construction of steep slopes and reduces thereby the place necessary for the embankment. Often material, which is around, can be used for the construction. Furthermore the removal of debris flow relicts is easy. But only little information is available on the behavior of such constructions in case of an impact by a block.

First studies on the influence of so called riprap or rockery at an embankment's surface have been done by Hofmann & Mölk (2012). But the two research reports which have been cited in their paper are not open to the public and the information given in their paper is very limited. So information concerning the roughness profile and the thickness of the used riprap is missing and only two statements are given as results of their tests:

- "Slope angles ≥ 50° require a freeboard of at least one-time the diameter of the sphere.
- After the impact, the sphere scarcely changes its height, whereas in the case of pure soil embankments and reinforced structures, it tends to jump or roll in the direction of the crest"

To check the experimental results of Hofmann & Mölk (2012) and to study the impact process of blocks impacting rockfall protection embankments with a rockery cover, small scale quasi-2D-experiments have been executed and analyzed at the HSLU during the project AERES. The results of this test series had been described in this report.

4.1 Influence of embankment's uphill slope inclination

To avoid an embankment made of pure soil (slope inclination ≤ 50°) will be surmounted by a block, the Austrian standard ONR 24810:2013 requires a freeboard of at least two block diameter. But the graph used for determining the design parameters according to Hofmann & Mölk (2012) and which is presented also in the appendix of ONR 24810:2013 limits the applicability of the diagram to a block rotational energy ≤ 1% for pure earth embankments (Fig. 4.1).

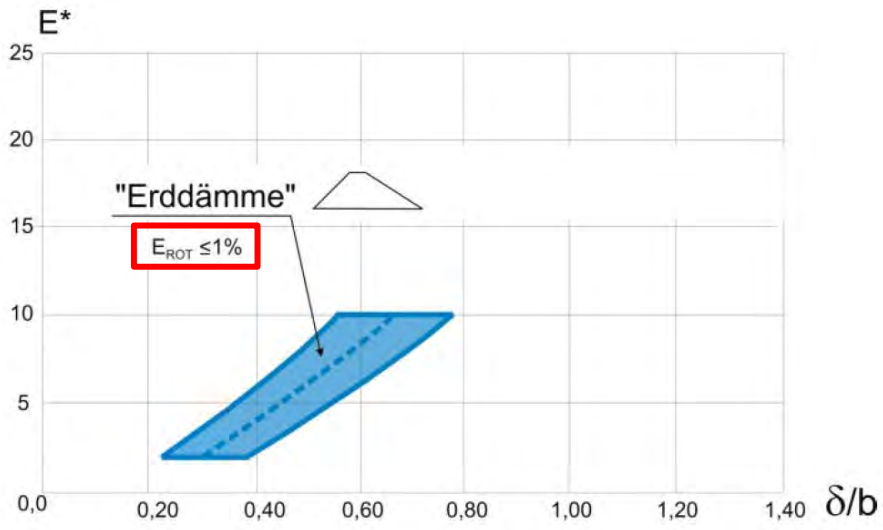

Fig. 4.1: Dimensionless illustration of the test results of Hofmann & Mölk (2012) received for pure earth embankments, relative impact energy E versus ratio of penetration depth δ and crest width b, rotational energy E_{ROT} is limited to ≤ 1%.*

On the other hand, in-situ tests done by Usiro et al. (2006) showed that the ratio of rotational to translational energy for natural blocks will be in the interval 0.025 to 0.2 respectively 2.5% to 20%, which is significantly higher than the energy limit given by Hofmann & Mölk (2012). Taking into account the results of Usiro et al. (2006) as well as the limit for the diagram presented in the appendix of ONR 24810:2013 no design parameters for the load case impact of natural blocks with real rotational energy on an embankment made of pure soil exist and therefore as a consequence the construction of pure earth embankments with an uphill slope inclination of about 1:1 or less should be omitted.

Kister (2015) showed test results of small-scale quasi-2D-experiments where, even in the case of edged blocks with no or only very low rotation, blocks move upward the embankment's slope during the impact process and reached the crest level, if the impact angle comes up to an appropriate value. Kister (2015) concludes out of this there is a good chance a block with a ratio of rotational to translational energy of 0.1 to 0.2 will surmount an embankment with slope inclination of 50° or less, even if a freeboard of two block diameters has been kept.

Two documented examples of existing rockfall protection embankments underpin the results and the statement presented by Kister (2015). The embankment Halteli-Talmatt, Canton Uri, was damaged during a larger event on 1st October 1983. The embankment, constructed with a slope inclination 1:1 at the uphill side, was neither punched through nor surmounted, but the impacting block reached the crest and caused some damage (Fig. 4.2). Schneider (1984) described the movement of the largest block as follows: "The block overcame the ditch with small jumps and hit the crest at the uphill side. The block produced a large impact crater and radial spreading shear joints, which penetrated the complete embankment. The block stayed at the crest for several hours and then fell down into the ditch." Fig. 4.2 shows the irregular shape of this block, which differs significantly from a sphere or a cylinder. According to Schneider the jumps of the block had been small before it hit the embankment and therefore the block could not directly hit the embankment's crest area because the ditch - crown vertical distance is more than 8 m.

Fig. 4.2: Impact at the embankment Halteli-Talmatt, Canton Uri. The embankment was neither punched through nor surmounted, but the impacting block reached the crest (Schneider, 1984)

The second example is the embankment Gretla, Canton Graubünden. This rockfall protection embankment was constructed in 2009 due to an event in 2008. The embankment was made of debris with a slope inclination of 2:3 on both sides. The ditch - crown vertical distance of this embankment is 5 m. The embankment was surmounted during events in 2009 and 2010 (2009: block size approx. 1.5 x 2 x 0.6 m^3, 2010: block size approx. 1.8 x 1.8 x 0.9 m^3). As a consequence a redesign of the embankment had been done and rockery with a batter 5:1 had been placed at the uphill slope. During a new event in 2011 the embankment Gretla, now with rockery, was able to stop 2 blocks with a volume of 4 m^3 resp. 6 m^3 (Fig. 4.3). Only a rock fragment with a mass of approx. 70 kg was spalled off during the event and reached the roadside behind the embankment (Nänni, 2011). So the redesign of the embankment with rockery in front of the embankment stood the test.

Fig. 4.3: Impacts of two blocks (4 m^3 resp. 6 m^3) in 2011 at embankment Gretla after redesign and implementation of rockery at the uphill slope (Photo: Tiefbauamt Graubünden). The rockery showed only minor damage.

To reduce the probability that an embankment will be surmounted by a block, it was suggested by Kister (2015) to design rockfall protection embankments in general with an uphill slope inclination of at least 60°. This is because the impact angle is essential for the impact process and the impact angle depends on the block trajectory as well as the inclination of the uphill slope of the embankment. But influencing the inclination of the uphill slope of an embankment is easier than influencing the block trajectory and a steep embankment slope will normally reduce the impact angle and with it an upward directed velocity component (Fig. 3.1).

But such a slope inclination of 60° or more cannot be constructed with pure soils. Additional measures have to be used to stabilize such steep slopes. Three different types of stabilization measures had been used in the past for the construction of steep slopes at rockfall protection embankments in Switzerland:

- Reinforcement of the soil structure using old tires
- Stabilization of the embankment slope / embankment body with geogrid reinforcement
- Stabilization of the embankment slope by putting rockery in front of the slope.

The use of old tires to create steep slopes at rockfall protection embankments was not very often executed in Switzerland. According to the interviews done during the project AERES, only two examples of rockfall protection embankments had been executed in Switzerland, where old tires had been used as supporting measure. Both embankments are located in Canton Lucerne. Unfortunately it was not possible to get information about the construction of these two embankments by the designer. A reason for the low spreading of this stabilization method may be the high effort for the construction.

The use of geogrid reinforcement for rockfall protection embankments is very new in Switzerland. Up to now only few embankments of this type have been constructed or are under construction in Switzerland. As an example the embankment Riemenstalden is shown in Fig. 4.4, which is mainly constructed to protect against snow avalanche, but also for protection of rockfalls.

Fig. 4.4: Embankment Riemenstalden, Canton Schwyz, constructed with geogrid reinforcement, (Photo: B. Kister, 2015)

The design of such embankments is mainly based on the experiments done by Professor Peila and his staff (see part A of the report). To fulfill the fitness for purpose of a rockfall protection embankment with geogrid reinforcement and a slope angle of at least 60°, Hofmann & Mölk (2012) stated: “For geogrid reinforced structures, a freeboard of 1.5 times the sphere diameter can be considered as being on the safe side.” This statement was also transferred to the standard ONR 24810:2013 and the applicability of the design diagram is limited to a block with a rotational energy $E_{ROT} \leq 15\%$ for embankments with geogrid reinforcement.

A common measure used in Switzerland to stabilize steep slopes of rockfall protection embankments is the use of riprap or rockery. According to the interviews done with employees of canton departments as well as with design engineers the rockery used in the past at the uphill slope of an embankment was constructed with a batter between 60° to 80°. But in general only less attention had been paid on the behavior of such natural stone walls during the impact of a block. The main reasons to use rockery was to limit the area, which is necessary for embankment construction and/or to stop rolling blocks.

In the project AERES small-scale quasi-2D-experiments had been done with embankments with stones placed parallel to the slope and stones placed horizontally. The batter of this "rockery" was chosen to be 2:1 (62.6°), 5:2 (68.6°) and 5:1 (79.5°) (Fig. 2.17). The experiments showed that rotating cylinders acting as impactors may surmount an embankment with batter 2:1, if the freeboard is less than 1 block diameter. For the "rough" rockery surface, where the stones had been placed horizontally, the climbing height of the hollow cylinder GS was 1.8 x the block diameter for the first impact and 1.55 x the block diameter for the second impact (Fig. 3.15). For the "smooth" rockery surface a smaller climbing height had been achieved. But for the first impact the climbing height was still 1.3 x the block diameter and for the second impact 1 x the block diameter (Fig. 3.14). According to these results a smooth rockery surface may help to reduce the climbing height of a block in comparison to a rough slope surface. But a slope with an inclination of 60° and equipped with rockery or riprap in general does not guarantee that a free board of 1.5 block diameter will be sufficient, if the block has the shape of a sphere or a cylinder and has rotational energy.

Also for a batter of 5:2 and with a rough slope surface the rotating cylinder was able to surmount the embankment. The freeboard in this test was chosen to be 0.6 x the block diameter, but the trajectory of the block in Fig. 3.18 allows the conclusion that even a freeboard of one block diameter would not be sufficient in this case. On the other hand an embankment with a batter of 5:1 and stones placed horizontally was able to stop the rotating cylinder (Fig. 3.20). The cylinder G showed still an upward movement in this test even though the impact angle was negative. But a freeboard of 0.4 x the block diameter was sufficient to avoid the embankment was surmounted by the block.

4.2 Influence of block rotation

As already shown by Kister (2015) the block rotation plays a very significant role in the impact process. This could be verified by the test series done during the AERES project and the results described before. Model embankments in the tests had been surmounted by cylinder G with rotation in most cases. But as already mentioned by Kister (2015) the test arrangement used in these tests led to a ratio of rotational to translational energy for cylinder G, which exceed the ratio of rotational to translational energy of natural blocks (see Usiro et al., 2006).

A ratio of rotational to translational energy, which is in the same range as for natural blocks, was achieved for the new cylinder GS with a steel lining (Fig. 3.5). For a freeboard of about 0.5 x the block diameter embankments with a batter of 2:1 had been surmounted by the block GS. This occurred irrespective to the construction of the slope with or without rockery. As already mentioned before the embankment with batter 2:1 and "rough" rockery surface was not surmounted by the block GS for a freeboard chosen to 1.9 x the block diameter.

On the other hand block OKT with no or only very low rotation was not able to surmount embankments with the same cross section in the tests. Block OKT with edges showed a significant different behavior. There was still an upward movement of the block OKT during the impact, but the climbing height was significant less. For slender structures, where the thickness of the embankment at the impact point was less than two times the block diameter, the embankment crest was damaged or even totally destroyed, but the block OKT was not able to surmount the embankment (Fig. 3.11). If the thickness of the embankments had been increased, there occurred still significant damage due to the first impact, but for embankments with rockery the penetration depth of the block was limited to less than the half block diameter (Fig. 3.13 c and d). Even for an embankment without rockery and for the second impact block OKT was not able to surmount the embankment and the penetration depth was less than one block diameter (Fig. 3.13 b).

4.3 Influence of block shape and freeboard

As already shown by Kister (2015) an impactor with edges (impactor OKT) may reach the crest level of an embankment with a slope inclination of approx. 1:1, even though the block rotation is very low and the freeboard was chosen to be two times the block diameter (Fig. 4.5). But this occurred for large impact angles. The test series done in the project AERES showed on the other hand, if the impact angle is small because of a steep slope of the embankment, the block OKT with no or low rotation was not able to surmount an embankment with a freeboard of about 0.8 x the block diameter.

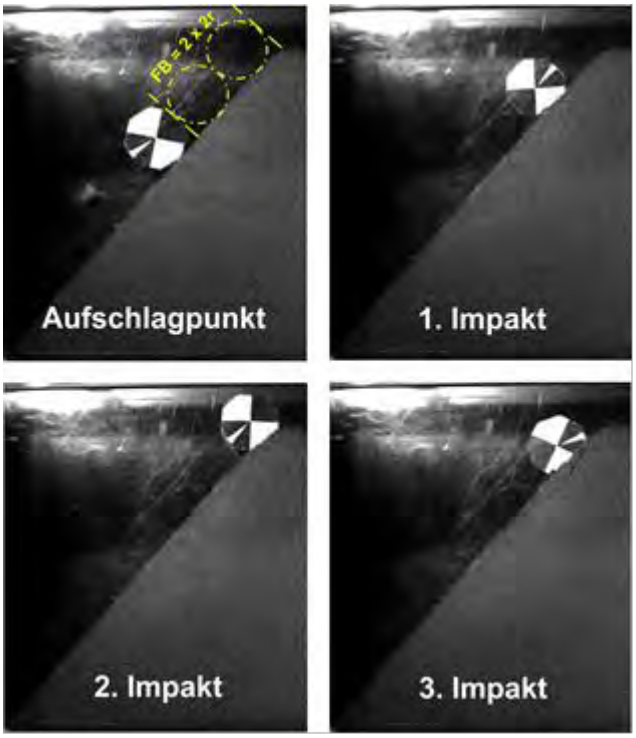

Fig. 4.5: Impact point and maximum climbing height for the first, second and third impact of impactor OKT onto a slope with inclination 1:1, rotational velocity of the block: 1.3 Hz (Kister, 2015).

On the other hand a ratio of rotational to translational energy, which is in the same range as for natural blocks and was achieved for the new cylinder GS with a steel lining, is not sufficient to avoid the embankment will be surmounted by a block. So also the shape of the block is of significant influence for the dimension of the freeboard.

Unfortunately with the existing experimental set-up it is not possible to increase the rotation of block OKT with edges or to define a special rotational block velocity. So the parameters block shape and block rotation are bound together for the existing experimental set-up and cannot be studied separately.

4.4 Embankments with rockery on both slopes

Sometimes in Switzerland rockfall protection embankments had been constructed with rockery on both slopes. As an example embankment Botegh, Canton Graubünden, is shown in Fig. 4.6. The reason for this type of construction very often is a very limited space for the construction of an embankment as shown for example in Fig. 4.6.

Fig. 4.6: Embankment Botegh, Canton Grisons, 2015 (Photo: Tiefbauamt Graubünden)

Some tests with model embankments of this type had been executed in the project AERES and the test results showed a probability for secondary rockfall at certain circumstances. Because no compression work will be done at the stones of the rockery, so these stones act approximately like a Newton pendulum and transfer the impact energy directly towards the soil behind the rockery. If the volume of soil between the two stone walls is small, the capability to dissipate energy by compression is very limited and a high quota of energy is transferred to the downhill rockery and may cause secondary rockfall (Fig. 4.7). The problem may be reduced, if the soil volume between the two stone walls has a horizontal extent of more than one block diameter (Fig. 3.13 d).

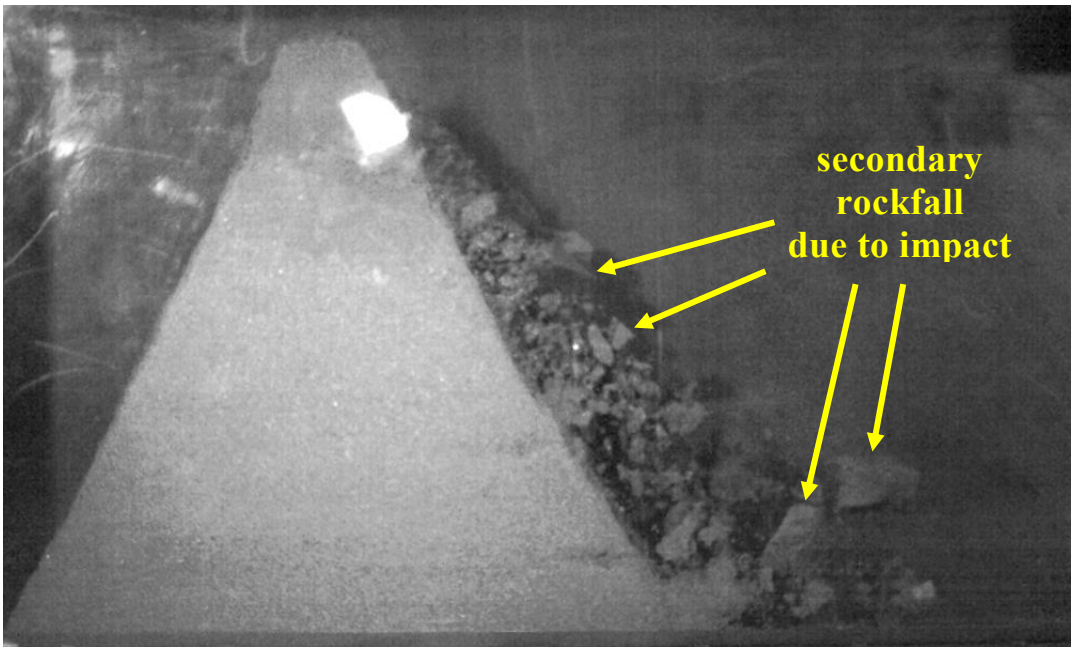

FIG. 4.7: Test OKT_2121FF_9_11-1: Secondary rockfall due to impact of block OKT, embankment was not surmounted by the block, but crest was destroyed.

To avoid the problem of secondary rockfall and construct nevertheless steep slopes at the downhill side of the embankment a construction with geogrid reinforcement is suggested. Such a construction prevents the downhill slope to act as a free boundary because the geogrids will bind back the embankment's soil material (see tests of Peila et al., 2007). Examples of such a construction with geogrids are shown in Fig. 4.8 and Fig. 4.9. With the existing experimental set-up it was not possible to do tests with such a type of embankment, because the lateral fixing of geogrids in a quasi-2D-model is not possible.

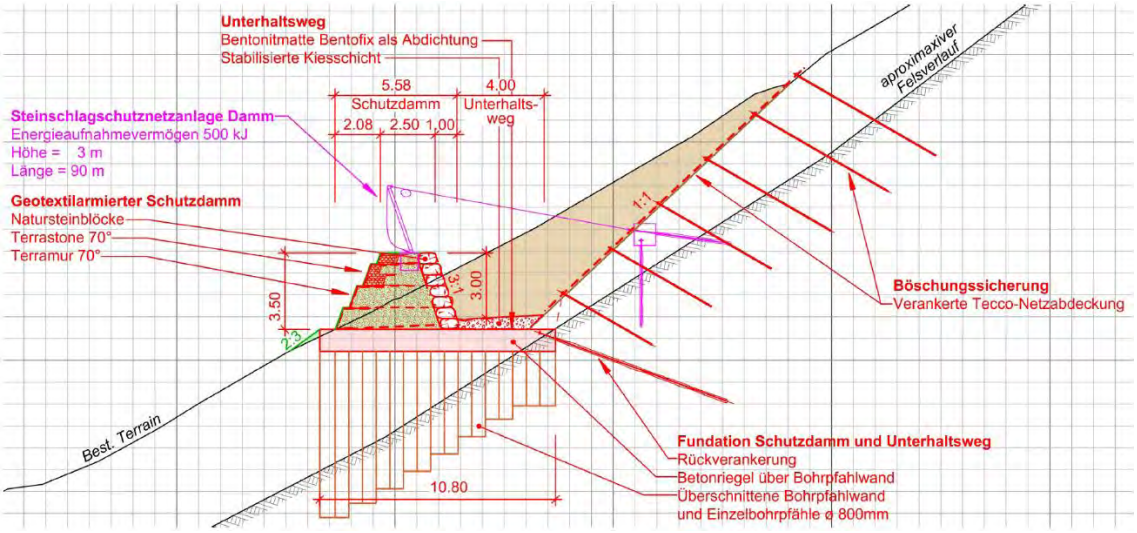

Fig. 4.8: Profile of the planned protection dam at Laugneri East with rockery at the uphill side and geogrid reinforcement and gabions at the downhill side of the embankment (Weggis, 2016).

Fig. 4.9: Example of an embankment constructed with geogrid reinforcement on both slopes nearby Lecco, Italy (Photos: B. Kister).

4.5 Dissipation of energy

The dissipation of energy has been studied by

- simple physical models (see for example Kister & Fontana, 2011)
- numerical calculations (see for example Ronco et al., 2009) and
- evaluation of experiments in the research project AERES.

According to those studies based on different methods and approaches at least 75% to 85% of the block total kinetic energy will be transformed into compression work, wave energy and heat when the block hits the embankment.

The evaluation of test data received in the project AERES showed that the main part of energy dissipation occurs during the first 6 ms of the impact process. During this period the block translational velocity is reduced to less than the half value for all three types of impactors (Table 3.7). Differences in loss of block velocity and block energy of the three used impactors mainly occur after the large drop of velocity and energy (Fig. 3.22).

A comparison of the velocity time diagram with the pictures made by the high-speed camera shows furthermore the heaviest damage at the embankment occurred at a time, when the translational energy was already dropped to a significant low level (G and GS: less than 15%, OKT: less than 5%, Figures 3.24, 3.25 and 3.26). It may be concluded due to this, that the heaviest damage is not directly produced by the block itself but by the wave, which is a product of the impact process.

4.6 General remarks

A rockfall protection embankment is a geotechnical structure and therefore in Switzerland it has to fulfill the requirements for structural safety for static load conditions as described in the standard specification SIA 267 and the standards referred in SIA 267. General remarks concerning the construction of an embankment can be found for example in Floss (2011) and had been described also by Kister (2015).

Additional the rockfall protection embankment has to withstand an impact of the design block. This means the embankment may be heavily damaged, but not punched-through by the design block in this load case. Up to now there is no standard specification available in Switzerland for this load case. To avoid that a rockfall protection embankment will be punched-through by a block, Kister (2015) suggested a thickness of the embankment at the impact point of at least three times the block diameter. This suggestion had been done due to the results of small and half scale impact tests on embankments made of pure soil. The test series described in this report was mainly based on embankments with rockery at the “uphill” slope. Because the density of stones is significantly higher than the density of soil, a lower embankment thickness at the impact point may be taken into account to achieve the same mass at the impact level of the embankment. On a physical view and taking into account that natural blocks hardly will receive translational velocities higher than 30 m/s, it seems to be unlikely a block will be able to punch-through an embankment, if the counteracting part of the embankment has a mass which is at least 2.5 times that one of the block. This does not mean that such a block will not be able to surmount the embankment due to its rotational energy, a large impact angle and a freeboard, which is undersized.

The fitness for purpose of a rockfall protection embankment is fulfilled, if the embankment will neither be punched-through nor the block will be able to surmount the embankment. The last requirement is much more complicated to fulfill than the former as shown before. Four main parameters have been found, which are dominating this process:

- the total block energy,
- the ratio of rotational to translational block energy,
- the impact angle, which is a function of block trajectory and slope inclination, and
- the shape of the block.

The experiments had shown that there are some interactions between these parameters, which could not be solved in detail with the existing experimental set-up. So for large impact angles (and slopes with low inclination) the edges of a block may help to move the block towards the crest level, because they act as a kind of crampon. On the other hand a block with edges but only low or no rotation will not be able to surmount an embankment's uphill slope, if the impact angle is small (and the embankment's slope is steep), even then a short freeboard of less than one block diameter has been chosen. Whereas a cylinder with steel lining and a ratio of rotational to translational energy like natural blocks exceeds the freeboard dimension given by Hofmann & Mölk (2012) for a slope with riprap significantly.

4.7 Need for further research

With the existing experimental set-up it is possible to produce rotating cylinders as impactors. With the steel lining placed on a cylinder it was possible to reduce the ratio of rotational to translational energy in such a way that the values are similar to those of natural blocks. But the experiments showed also a significant influence of the block shape. With the block OKT a block with edges had been used in the tests, but only with no or very low rotation. Several efforts had been undertaken to increase the rotation of the block OKT, but with no significant success.

The use of the Austrian standard ONR 24810:2013 is based on experiments with a small steel sphere and may induce large values for the freeboard which result in embankments with enormous heights (Fig. 1.2). The tests with block OKT showed that the freeboard for a block with edges will be less than for a sphere or a cylinder, if the impact occurs on a steep slope and with a small impact angle.

The full size tests done by Peila et al. (2007) and Mongiovì et al. (2014) had been executed with the same type of impactor as it is used for tests on rockfall net fences (Fig. 4.10). In both test series a funicular railway was used. But the use of a funicular railway to accelerate the impactor does not allow block rotation. So indeed in those tests a block with edges had been used, but without taking into account block rotation.

Fig. 4.10: Full size test done by Mongiovì et al. (2014): The block used for the tests complies with the ETAG 027 standard and has a total mass of 13'357 kg. The block was accelerated with a funicular railway therefore block rotation could not be taken into account.

Analyses of the movies made during the tests done by Peila et al. (2007) show additional an impact angle which is negative (Fig. 4.11). Therefore no velocity component parallel to the slope surface in upward direction is produced in those tests.

Fig. 4.11: Full size test done by Peila et al. (2007). Result of an analysis with the program Tracker of a movie presented by Tenax Geosynthetics. The test shows a negative impact angle.

So the significant question concerning the behavior of a block with edges and with a ratio of rotational to translational energy like natural blocks during the impact process is unsolved. And therefore the question concerning the dimension of the freeboard and by this the necessary height of a rockfall protection embankment could not be solved definitively up to now.

Therefore it is suggested to do tests with a more realistic block shape than a sphere or a cylinder for the impacting block and well defined ratios of rotational and translational energy. This may be able to clarify the question about a realistic freeboard and the fitness for purpose of a rockfall protection embankment. First tests for a new type of experimental set-up, which may fulfill the demands to use an impactor with the same shape as the impactors used for testing rockfall net fences as well as to adjust separately translation and rotation of such an impactor have been done at the HSLU.

References

- **Blovsky, S.:** Bewehrungsmöglichkeiten mit Geokunststoffen, PhD thesis, TU Wien, 2000
- **Floss, R.**: ZTVE-StB, Zusätzliche Technische Vertragsbedingungen und Richtlinien für Erdarbeiten im Strassenbau, Ausgabe 2009, Kommentar und Leitlinien mit Kompendium Erd- und Felsbau, 4. Auflage, Kirschbaum Verlag, Bonn, 2011
- **Hofmann, R., Mölk, M.:** Bemessungsvorschlag für Steinschlagschutzdämme. Geotechnik, Vol. 35, pp. 22-33, 2012
- **JRA, Japanese Road Association:** Japanese Rockfall Protection Handbook, 2000
- **Kälin, A.:** Steinschlagverbauung Wilerwald, Gurtnellen, Bauprojekt, Projektbasis und statische Berechnungen, 07.09.2006
- **Kister, B.:** Development of basics for dimensioning rock fall protection embankments in experiment and theory (in German, with abstracts in English and French), research project FEDRO 2012/003, FEDRO report 1524, 2015
- **Kister, B.; Fontana, O.**: On the evaluation of rock fall parameters and the design of protection embankments – a case study, Interdisciplinary Rockfall Workshop 2011, Innsbruck-Igls, 2011
- **Mongiovi, L. ; Bighignoli, M. ; Danzi, A. ; Recalcati, P. :** An impact test on a reinforced earth embankment. Proceedings of the interdisciplinary workshop on rockfall protection - Rocexs, Lecco, Italy, 2014
- **Nänni, C.:** Dokumentation des Felssturzes in Caltgeras vom 22.03.2011, Aktennotiz, Tiefbauamt Graubünden, Canton Gaubünden, 2011
- **ONR 24810:** Technischer Steinschlagschutz – Begriffe, Einwirkungen, Bemessung und konstruktive Durchbildung, Überwachung und Instandhaltung, ASI Austrian Standards Institute (Österreichisches Normungsinstitut), Ausgabe 15.01.2013.
- **Peila, D.; Oggeri, C.; Castiglia,C.:** Ground reinforced embankments for rockfall protection: design and evaluation of full scale tests, Landslides, 4, pp 255–265, 2007.
- **Plassiard, J.P.; Donzé, F.-V.:** Rockfall impact parameters on embankments: A Discrete Element Method Analysis, Structural Engineering International, 3, 2009.
- **Ronco, C.; Oggeri, C.; Peila, D.:** Design of reinforced ground embankments used for rockfall protection, Natural Hazards and Earth System Sciences, 9, 2009
- **Schneider, T. R.:** Der Felssturz von Bristen am 1. Oktober – 1983, Schweizer Ingenieur und Architekt, Heft 46, 102, 1984
- **Smith, D. D.; Duffy, J. D.:** Field tests and evaluation of rockfall restraining nets, Report No. CA/TL-90/05, Transportation Materials and Research, California Department of Transportation, Final Report, 1990
- **TRB, Transportation Research Board:** Estimating stiffness of subgrade and unbound materials for pavement design – a synthesis of highway practice, National Cooperative Highway Research Program, NCHRP Synthesis 382, 2008
- **Usiro, T.; Kusumoto, M.; Onishi, K.; Kinoshita, K.:** An experimental study related to rockfall movement mechanism, Doboku Gakkai Ronbunshu FVOL. 62, No. 2, pp 377-386, 2006
- **Weggis:** Risk management in the municipality of Weggis, Excursion Guide Weggis EX1, 13th Congress Interpraevent, 2016
- **Yoshida, H.:** Movement of boulders on slope and its simulation, in: Recent Studies on Rockfall Control in Japan, 1998

Appendix C1: Block data

Test	α [°]	v [m/s]	E_{trans} [Nm]	ω [1/s]	E_{rot} [Nm]
G_2121H_9_11	13	6.60	162.0	78.5	73.4
G_2145H_9_11	12	6.50	157.2	76.6	69.8
G_2145H_4K_11	13	6.88	176.2	80.0	76.3
G_2121F_8_11	14	6.08	134.7	80.9	76.3
G_2121_9_11	12	6.00	131.0	80.7	75.8
G_2121FF_9_11	9	6.25	142.2	80.1	74.8
G_2121F_9_11_G	14	5.70	118.3	76.3	67.8
GS_2145H_9_11	12	5.57	86.8	73.8	61.7
GS_2145F_7_11	8	6.48	142.0	43.6	27.7
GS_2145H_9_11_2	13	6.57	145.7	42.9	26.7
GS_2121H_9_11	12	6.71	152.1	40.0	23.3
GS_2121F_8_11	12	6.65	149.7	40.3	23.6
GS_2121F_18_11	10	6.68	150.7	38.5	21.6
GS_2121_18_11	14	6.46	141.0	39.3	22.4
GS_2121FF_18_11	13	7.06	168.3	36.8	19.7
GS_2121FF_18_11_B	10	6.89	160.5	36.8	19.7
GS_2121FG_18_11	14	6.92	161.8	38.5	21.6
GS_2121HG_18_11	15	6.75	154.1	36.3	19.2
OKT_2145H_9_11	14	6.17	128.7	9.9	1.0
OKT_2121H_7_11	14	6.14	127.7	0.0	0.0
OKT_2145H_6K_11	14	6.43	140.1	8.7	0.8
OKT_2121F_8_11	11	6.61	147.8	7.5	0.6
OKT_2121_9_11	13	6.56	142.8	10.2	1.1
OKT_2121FF_9_11	12	6.81	154.2	1.6	0.0
OKT_2121F_18_11	10	6.55	142.6	13.1	1.8
OKT_2121_18_11-B	13	6.63	145.8	10.9	1.2
OKT_2121FF_18_11	11	6.97	161.6	8.7	0.8
G_25121F_17_11	8	5.90	126.7	76.8	68.6
OKT_25121F_17_11	8	6.35	136.3	3.4	0.1
G_5121F_17_11	-4	5.97	129.7	79.0	72.8
OKT_5121F_17_11	-5	6.70	152.0	8.1	0.7

α: impact angle
v: mean value of translational block velocity just before impact
E_{trans}: translational block energy
ω: mean value of rotational block energy just before impact
E_{rot}: rotational block energy

Appendix C2

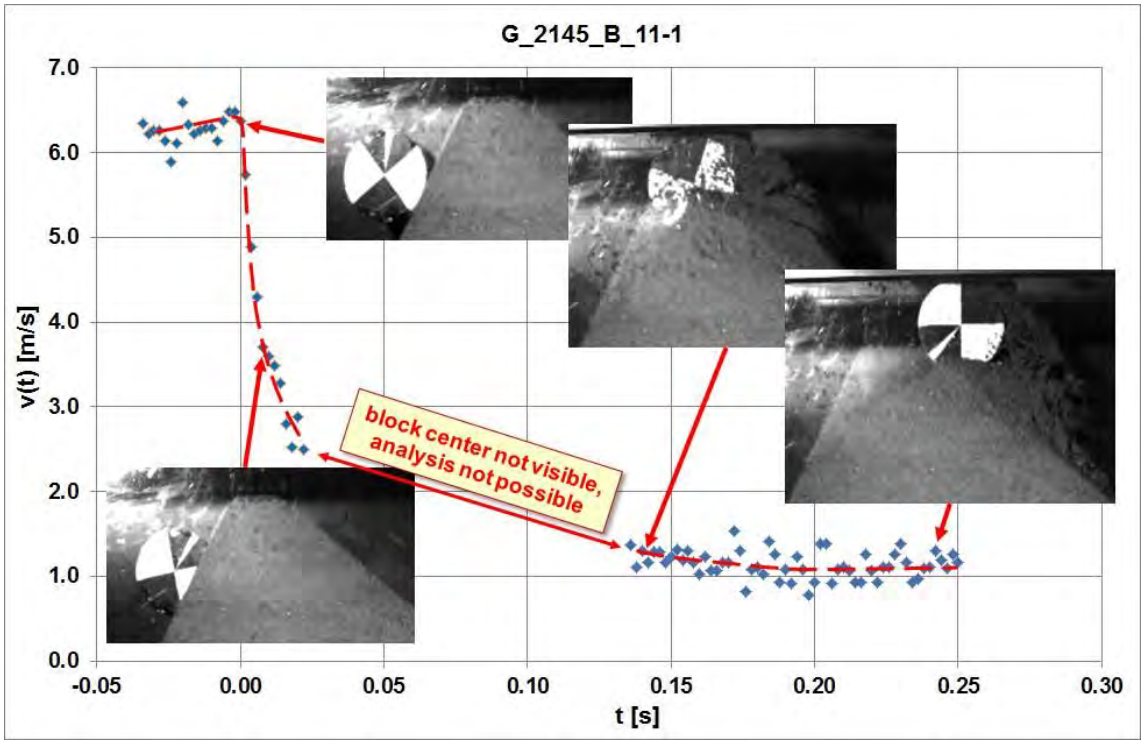

Fig. C2.1: Block deceleration in test G_2145_B_11-1, red line: assumed mean translational velocity.

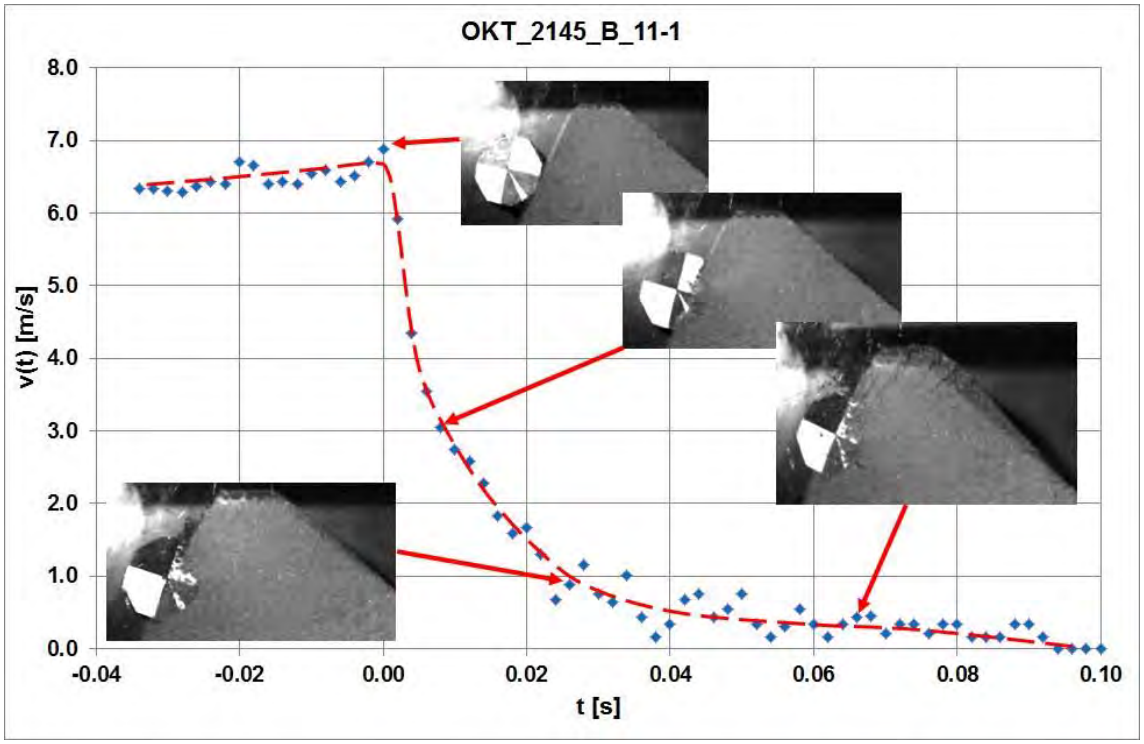

Fig. C2.2: Block deceleration in test OKT_2145_B_11-1, red line: assumed mean translational velocity.

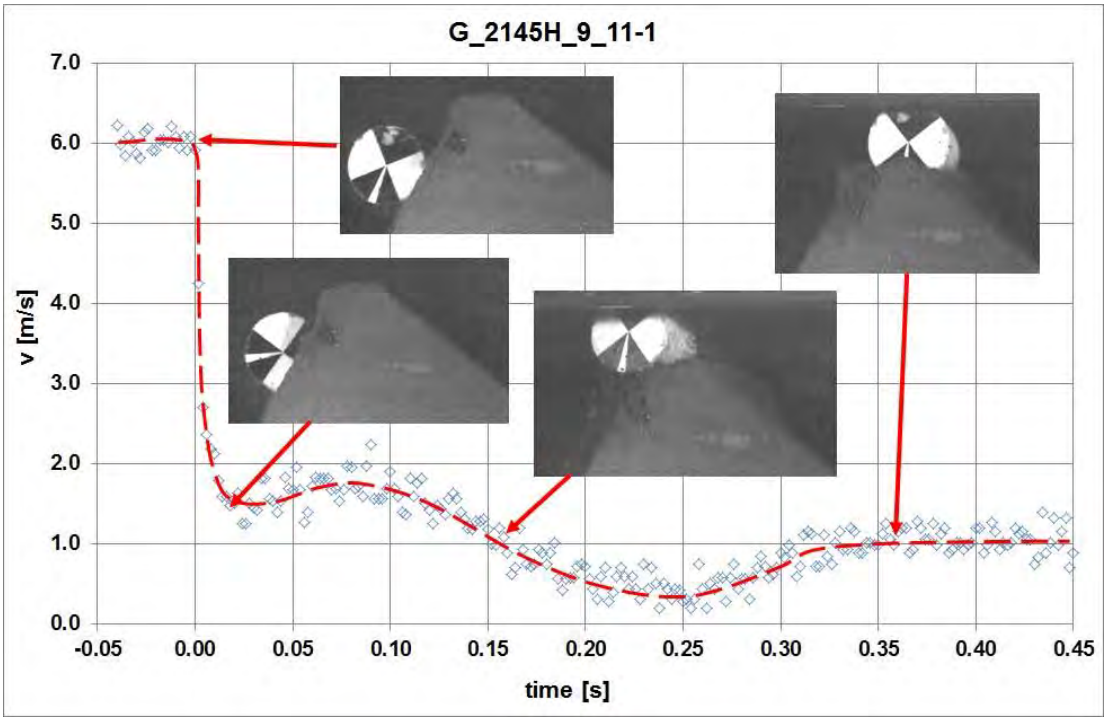

Fig. C2.3: Block deceleration in test G_2145H_9_11-1, red line: assumed mean translational velocity.

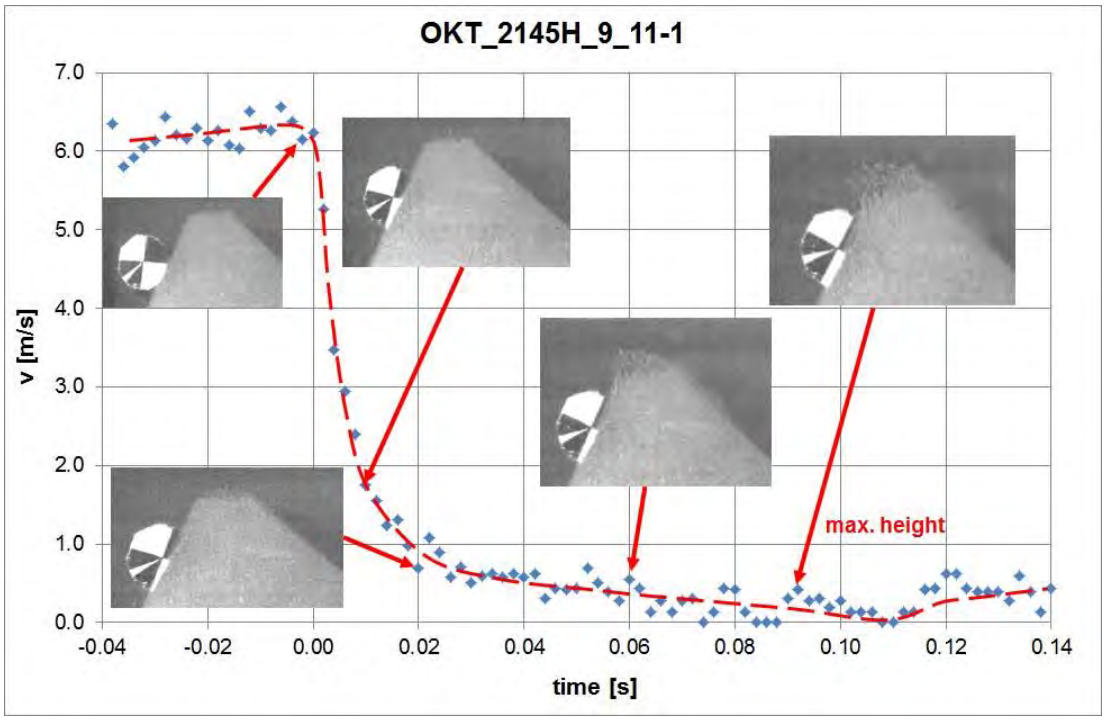

Fig. C2.4: Block deceleration in test OKT_2145H_9_11-1, red line: assumed mean translational velocity.

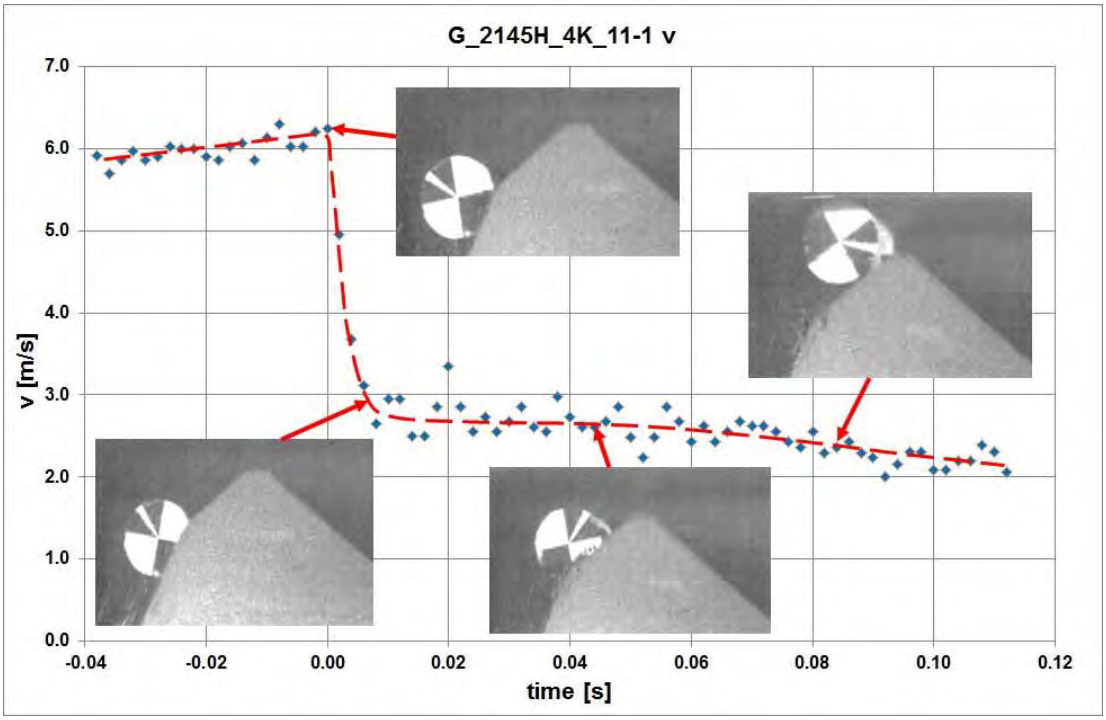

Fig. C2.5: Block deceleration in test G_2145H_4K_11-1, red line: assumed mean translational velocity.

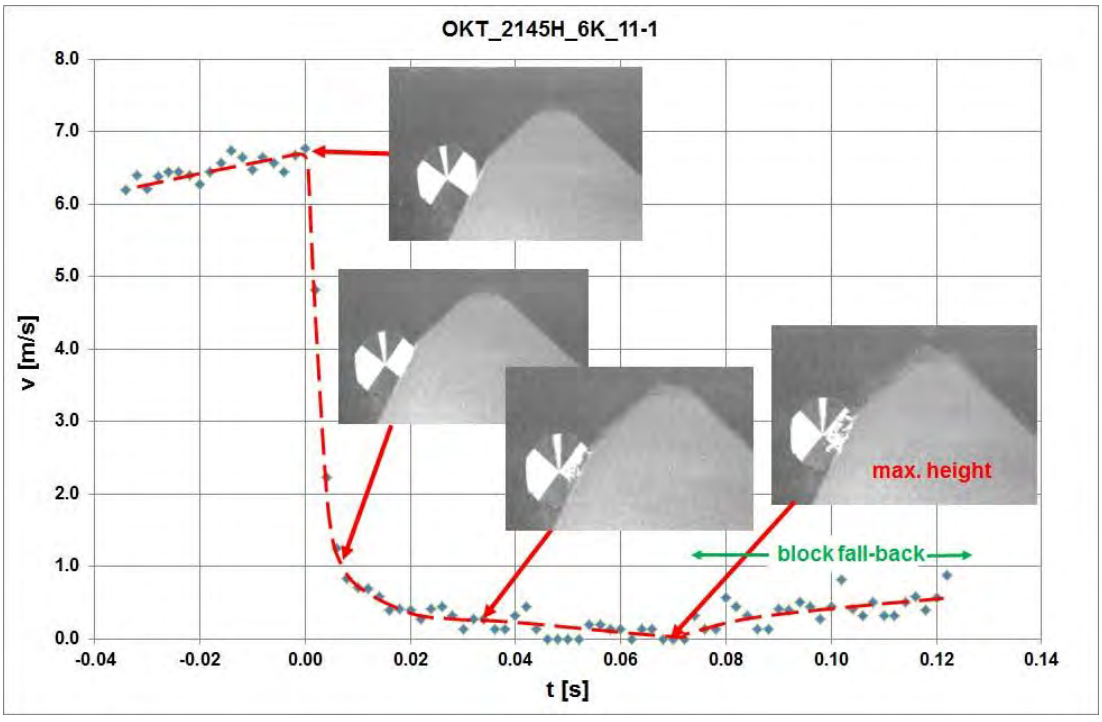

Fig. C2.6: Block deceleration in test OKT_2145H_6K_11-1, red line: assumed mean translational velocity.